Molecular characterization of paternal-defective fertilization mutants in *Arabidopsis thaliana*

Dissertation

der Mathematisch-Naturwissenschaftlichen Fakultät

der Eberhard Karls Universität Tübingen

zur Erlangung des Grades eines

Doktors der Naturwissenschaften

(Dr. rer. nat.)

vorgelegt von

Yingjing Miao

aus Shaanxi/China

Tübingen

2022

Gedruckt mit Genehmigung der Mathematisch-Naturwissenschaftlichen Fakultät der Eberhard Karls Universität Tübingen.

Tag der mündlichen Qualifikation:	12.12.2022
Dekan:	Prof. Dr. Thilo Stehle
1. Berichterstatter:	Dr. Martin Bayer
2. Berichterstatterin:	Prof. Dr. Marja Timmermans

Acknowledgments

My deepest gratitude first goes to my supervisor Dr. Martin Bayer for offering me the opportunity to work on such an intriguing topic in his group and for giving me guidance and support that helped me grow as a researcher throughout the years. I would like to express my gratitude to Prof. Dr. Gerd Jürgens for his inspiring insights in shaping this work.

I would like to convey my sincere gratitude to my TAC member Prof. Dr. Marja Timmermans, Prof. Dr. Susana Coelho, and Dr. Michael Borg for their continuous support during my PhD studies. Both their scientific and personal support is greatly appreciated.

I would like to thank the China Scholarship Council for financial support for the first three years of my stay. Thank Prof. Dr. Detlef Weigel for the generous hosting of the rest of my studies and for making it possible for me to finish my dissertation in the best possible way.

I would like to acknowledge colleagues who contributed to this work. I thank Agnes Henschen and Houming Chen for their help with the laborious plant work. I thank Sebastian Vorbrugg for his bioinformatics support. I thank Dr. Ziduan Han and Dr. Wen-sui Lo for their kind help with data analysis. I thank Christian Feldhaus and Aurora Panzera from the light microscopy facility for their technical support. I thank Dr. Felix Räsch for his comments and suggestions on the writing of this thesis.

I would like to thank current and former colleagues from the Bayer group, the Jürgens group, the Swart group, and the Department of Molecular Biology. Their company has made these far-from-home years a precious time that I look back on fondly.

My last thanks go to my family. Without their unconditional support, this thesis would not have been possible.

“问余何适，廓尔忘言。

华枝春满，天心月圆。”

Table of Contents

Abbreviations

Abbreviation	Definition
A	adenine
aa	amino acid
ACC	1-aminocyclopropane-1-carboxylic acid
ADK	adenosine kinase
Ado	adenosine
BAH	bromo-adjacent homology domain
BP	T-DNA/knock-out border primer
bp	base pair
C	cytosine
CALS5	CALLOSE SYNTHASE 5
Cas9	CRISPR-associated protein 9
CDC6	Cell Division Cycle 6
cDNA	complementary DNA
CDT1	Chromatin Licensing and DNA Replication Factor 1
Chr.	chromosome
CHS	CHALCONE SYNTHASE
COBL10	COBRA-LIKE PROTEIN 10
Col	*Arabidopsis thaliana* Columbia ecotype
CRISPR	clustered regularly interspaced short palindromic repeats
CTAB	cetyltrimethylammonium bromide
DAP	day(s) after pollination
DAPI	4′,6-diamidino-2-phenylindole
DAZ3	DUO1-ACTIVATED ZINC FINGER 3
DIC	differential interference contrast
DNA	deoxyribonucleic acid
easiRNAs	epigenetically activated small interfering RNAs
EC1	EGG CELL 1
ECS1	EGG CELL-SPECIFIC1
EMS	ethyl methane sulfonate
F1	first filial generation
F2	second filial generation
G	guanine
GPI	glycosylphosphatidylinositol
GUS	β-glucuronidase
H2AK119ub1	histone H2A monoubiquitylation at lysine119
H3K12ac	histone H3 acetylation at lysine 12

H3K27me0/3	histone H3 none/tri-methylation at lysine 27
H3K4me0/1/2/3	histone H3 none/mono/di/tri-methylation at lysine 4
H3K9me2/3	histone H3 di/tri-methylation at lysine 9
H3R2	histone H3 arginine 2
H4K20me0/2/3	histone H4 none/di/tri-methylation at lysine 20
HAP	hour(s) after pollination
HAP2	HAPLESS2
Hcy	homocysteine
HDG silencing	homology-dependent gene silencing
HOG1	HOMOLOGY-DEPENDENT GENE SILENCING 1
HTR12	HISTONE THREE RELATED 12
kb	kilobase
Ler	*Arabidopsis thaliana* Landsberg *erecta* ecotype
LP	left genomic primer
Mb	megabase
MCM	Minichromosome Maintenance Complex
Met	methionine
MGH3	MALE GAMETE HISTONE 3
mTP	mitochondria-targeted peptide
myr	N-myristoylation
MZT	maternal-to-zygotic transition
OC2	second outcross filial generation
ORC	origin of replication complex
PCR	polymerase chain reaction
PEGs	paternally expressed imprinted genes
PHD	plant homeodomain
pmd	paternal defective mutant
PRC2	POLYCOMB REPRESSIVE COMPLEX 2
pro	promoter
qRT-PCR	real-time quantitative reverse transcription PCR
RbFG	Rainbow Female Gametophyte marker
RbP	Rainbow Pollen marker
RNA	ribonucleic acid
RP	right genomic primer
RPM	reads per million
RT-PCR	reverse transcription PCR
SAH	S-adenosyl-L-homocysteine
SAHH	SAH hydrolase
SAM	S-adenosyl-L-methionine

sgRNA	single guide RNA
SNP	single nucleotide polymorphism
SR2200	SCRI Renaissance 2200
T	thymine
T-DNA	transfer-DNA
TEs	transposable elements
TFs	transcription factors
WT	wild type
ZGA	zygotic genome activation

Summary

In double fertilization of flowering plants, sperm cells rely on a vegetative cell to germinate a pollen tube which delivers them to the ovary, where one of the sperm cells fuses with an egg cell to form an embryo, and the other fuses with a central cell to form the nourishing endosperm. The *de novo* zygotic gene expression starts at the late karyogamy stage, followed by clearance of gametic transcripts, thus completing a maternal-to-zygotic transition. While our knowledge of pollen tube guidance and gametic interactions has grown considerably, the molecular signaling events orchestrating the onset of the zygotic genome activation remain elusive, especially those transmitted from the paternal side that has been suggested to be critical in initiating the zygotic program.

A powerful tool to reveal novel paternal genes in zygotic genome activation is a forward genetic screen. Next-generation sequencing-based bulked-segregant analysis has been widely used in identifying mutations in *Arabidopsis*. However, the laborious process of phenotypic analysis in preparing mapping populations limits the application of the classic bulked-segregant analysis to fertilization mutations. Here, we developed a semi-high throughput mapping-by-sequencing method for paternal-defective mutations. It allows mapping multiple mutants simultaneously with a limited workload. With this method, we corroborated the function of the known paternal genes, *CALS5*, *COBL10*, and *HAP2*, in pollen development, pollen tube guidance, and gametes fusion, respectively. We revealed a novel paternal gene encoding S-adenosyl-L-homocysteine hydrolase 2 (SAHH2) which is expressed in the vegetative cell of pollen. The loss-of-function mutants exhibited reduced male fertility with defective pollen tube elongation in the female transmitting tract, suggesting a role in preovular pollen tube guidance. Additionally, potential causative candidates were identified for further study. Taken together, this work offers a new approach and novel insights into understanding the paternal impact upon fertilization in *Arabidopsis*.

In addition, the Origin of Replication Complex (ORC) gene *ORC1b* was selected and characterized using a reverse genetic approach to reveal paternal factors in fertilization. ORC1b is a sperm nuclear protein enriched in chromocenters. The depletion of *ORC1b* in the T-DNA insertion allele *orc1b-1* and the knock-out allele *orc1b-2* led to reduced male fertility coupled with polytubey, defective gametic nuclear fusion, arrested embryo, and abnormal endosperm development. Furthermore, we isolated two mutant lines, *orc1b-1-as* and *orc1b-2-as*, that produced albino seeds with arrested embryo and endosperm in self-crossed siliques, which is presumably caused by disrupted genome integrity. Taken together, these results suggest that

ORC1 has additional functions apart from DNA replication in *Arabidopsis*. It acts as a paternal factor that contributes to gametes fusion, embryo/endosperm development, and genome integrity maintenance. These phenotypic analyses provide a solid basis for further deciphering the mechanism of *ORC1b*'s function in fertilization and offer new perspectives on the novel function of ORC genes in plants.

Furthermore, we constructed a set of fluorescent marker lines carrying several fluorescent marker cassettes labeling distinct cell structures of pollen and female gametophytes. These fluorescent marker cassettes can easily be introgressed into a mutant background by crossing and provide a powerful tool to study fertilization defects.

In summary, this thesis provides a novel mapping method and fluorescent marker lines for characterizing fertilization mutations. Assisted by these tools, several paternal contributed genes in fertilization have been studied. These results collectively further our understanding of the paternal contribution to fertilization in flowering plants.

Zusammenfassung

Bei der doppelten Befruchtung von Blütenpflanzen werden die Spermienzellen von der vegetativen Zelle, die den Pollenschlauch bildet, zum Ovarium gebracht. Dort befruchtet eine der Spermienzellen die Eizelle und die andere die Zentralzelle, die das nährende Endosperm bildet. Zygotische Genexpression beginnt im späten Karyogamie-Stadium, gefolgt vom Abbau gametischer Transkripte, wodurch ein Übergang von maternaler zu zygotischer Genexpression vollzogen wird. Während unser Wissen über Pollenschlauchanlockung und Interaktionen der Gameten in den letzten Jahren erheblich gewachsen ist, sind die molekularen Signalereignisse, die den Beginn der Aktivierung des zygotischen Genoms steuern, wenig erforscht. Insbesondere über Signale, die von der väterlichen Seite übertragen werden, und von denen angenommen wird, dass sie für die Initiierung des zygotischen Programms entscheidend sind, ist unser Wissen noch sehr begrenzt.

Um neue paternale Gene, die bei der Aktivierung des zygotischen Genoms eine wichtige Rolle spielen, aufzudecken, können genetische Screens ein wertvolles Werkzeug darstellen. Die auf *Next Generation Sequencing* basierende *Bulked-Segregant*-Analyse wurde häufig zur Identifizierung von Mutationen in *Arabidopsis* verwendet. Der mühsame Prozess der phänotypischen Analyse bei der Erstellung von Kartierungspopulationen schränkt jedoch die Anwendung der klassischen *Bulked-Segregant*-Analyse bei Befruchtungsmutationen ein. Hier haben wir eine *Mapping-by-Sequencing*-Methode mit mittelhohem Durchsatz für Mutationen mit paternalen Defekten entwickelt. Sie ermöglicht die gleichzeitige Kartierung mehrerer Mutanten mit begrenztem Arbeitsaufwand. Mit dieser Methode bestätigten wir die Funktion der bekannten paternalen Gene *CALS5*, *COBL10* und *HAP2* bei der Pollenentwicklung, Pollenschlauchführung bzw. Gametenfusion. Wir haben ein neues paternales Gen entdeckt, das für S-Adenosyl-L-Homocystein-Hydrolase 2 (SAHH2) kodiert. *SAHH2* wird in der vegetativen Pollenzelle exprimiert, und die Loss-of-Function-Mutanten zeigten eine reduzierte männliche Fertilität mit defektem Pollenschlauchwachstum. Darüber hinaus wurden potenziell ursächliche Kandidaten für weitere Studien identifiziert. Zusammengenommen bietet diese Arbeit einen neuen Ansatz und neue Einblicke in das Verständnis des väterlichen Einflusses auf die Befruchtung bei *Arabidopsis*.

Darüber hinaus wurde das *ORC1b*-Gen (Origin of Replication Complex) in einer revers-genetischen Studie für paternale Gene bei der Befruchtung charakterisiert. ORC1b ist ein Kernprotein der Spermienzellen, das in den Chromozentren lokalisiert ist. Verlust von ORC1b Funktion im T-DNA-Insertionsallel *orc1b-1* und im CRISPR *knock-out*-Allel *orc1b-2* führte zu

reduzierter männlicher Fertilität in Verbindung mit *polytubey*, defekter Karyogamy, gestörter Embryonalentwicklung und abnormaler Endospermbildung. Darüber hinaus identifizierten wir zwei mutante Linien, *orc1b-1-as* und *orc1b-2-as*, den weiße Samen in selbstgekreuzten Schoten produzierten, in denen das Embryo und Endospermwachstum zum Halt kommt. Dies ist vermutlich auf eine gestörte Genomintegrität zurückzuführen. Zusammengenommen legen diese Ergebnisse nahe, dass *ORC1b* neben der DNA-Replikation in *Arabidopsis* weitere Funktionen hat. Es wirkt als paternaler Faktor, der zur Gametenfusion, Embryo/Endosperm-Entwicklung und Aufrechterhaltung der Genomintegrität beiträgt. Diese phänotypischen Analysen bilden eine solide Grundlage für die weitere Entschlüsselung des Mechanismus der Funktion von *ORC1b* bei der Befruchtung und bieten neue Perspektiven auf die neuartige Funktion von *ORC*-Genen in Pflanzen.

Darüber hinaus haben wir eine Auswahl an fluoreszierender Markerlinien konstruiert, die mehrere Reportergen-Kassetten tragen, die unterschiedliche Zellstrukturen von Pollen und weiblichen Gametophyten markieren. Diese Fluoreszenz-Reportergene können durch Kreuzen leicht in einen mutanten Hintergrund eingeführt werden und bieten ein leistungsfähiges Werkzeug zur Untersuchung von Befruchtungsfehlern.

Zusammenfassend stellt diese Arbeit eine neuartige Kartierungsmethode und fluoreszierende Markerlinien zur Charakterisierung von Fertilisationsmutationen bereit. Mit Hilfe dieser Werkzeuge wurden mehrere paternale Gene bei der Befruchtung untersucht. Diese Ergebnisse fördern gemeinsam unser Verständnis des paternalen Beitrags zur Befruchtung bei Blütenpflanzen.

List of publications and contributions

Accepted publications

1. Kai Wang, Houming Chen, Marina Ortega-Perez, **Yingjing Miao**, Yanfei Ma, Agnes Henschen, Jan U. Lohmann, Sascha Laubinger, and Martin Bayer. (2021). Independent parental contributions initiate zygote polarization in *Arabidopsis thaliana*. *Current Biology*, *31*(21), 4810-4816.e5. https://doi.org/10.1016/j.cub.2021.08.033

   I contributed partially to generating transgenic lines, phenotypic analysis of early embryos by DIC imaging, data evaluation, and result interpretation.

2. Houming Chen, **Yingjing Miao**, Kai Wang, and Martin Bayer. (2021). Zygotic Embryogenesis in Flowering Plants. *Methods in Molecular Biology*, *2288*, 73–88. https://doi.org/10.1007/978-1-0716-1335-1_4

   I contributed to the publication collection and writing for the chapters titled "Early Steps of Axis Formation" and "Patterning Along the Apical-Basal Axis".

3. Daniel Slane, Cameron H. Lee, Martina Kolb, Craig Dent, **Yingjing Miao**, Mirita Franz-Wachtel, Steffen Lau, Boris Maček, Sureshkumar Balasubramanian, Martin Bayer, and Gerd Jürgens. (2020). The integral spliceosomal component CWC15 is required for development in *Arabidopsis*. *Scientific Reports*, *10*(1). https://doi.org/10.1038/s41598-020-70324-3

   I contributed to the expression pattern of genomic construct *gCWC15-3xGFP* during plant development by confocal microscopy and relative gene expression level analysis in mutant *cwc15* by real-time quantitative reverse transcription PCR.

4. Kai Wang, Houming Chen, **Yingjing Miao**, and Martin Bayer. (2020). Square one: zygote polarity and early embryogenesis in flowering plants. *Current Opinion in Plant Biology* (Vol. 53, pp. 128–133). https://doi.org/10.1016/j.pbi.2019.10.002

   I contributed to the publication collection and writing for the chapters titled "Early morphological changes" and "Zygotic gene expression".

Manuscripts ready for submission

5. **Yingjing Miao**, Sebastian Vorbrugg, Houming Chen, Agnes Henschen, Martin Bayer. A novel SNP-Ratio Mapping method for paternal-defective fertilization mutations.

   I contributed majorly to the experiment design, phenotypic analysis of the selected

paternal-defective mutants and T-DNA insertion mutants, DNA library preparation for Illumina sequencing, data analysis and interpretation, generating the rescue transgenic lines, figure preparation, and manuscript writing.

6. Kai Wang, **Yingjing Miao**, Marina Ortega-Perez, Houming Chen, Martin Bayer. A filament-like embryo system to study the suspensor-embryo transition.

   I contributed to the expression analysis of marker lines expressing *gWOX8Δ-nls-3xVenus* and *DR5:GFP* in zygotes, 1-cell embryos, 2-cell embryos, 8-cell embryos, early globular embryos, and late globular embryos of the transgenic line expressing *S4pro:SSP-YFP* by confocal microscopy and result interpretation.

7. Houming Chen, Feng Xiong, Yimin Hu, Kai Wang, **Yingjing Miao**, Daniel Slane, Rebecca Schwab, Thomas Laux, Martin Bayer. MAP Kinase 6-Dependent Activation of the bHLH Transcription Factor SCRM Promotes Polarization of the *Arabidopsis* Zygote.

   I contributed partially to the phenotypic analysis of early embryo development and stomata development in mutant *scrm* by DIC imaging and confocal microscopy.

1 Introduction

1.1 Gametogenesis in flowering plants

Flowering plants produce two types of spores, megaspores, and microspores, which after several mitoses give rise to female and male gametophytes. Taking *Arabidopsis thaliana* as an example, the female gametophyte develops in an ovule embedded inside the carpel. The megaspore undergoes three mitotic nuclear divisions thus forming a mature embryo sac containing seven cells: one egg cell at the micropyle, two synergid cells guarding the egg cell, one central cell with a 2n nucleus, and three antipodal cells sitting at the chalazal end (Yadegari and Drews 2004). The male gametophyte develops inside the anther of the stamen, where the microspore goes through two mitotic cell divisions to generate three-celled pollen with two sperm cells embraced in a big vegetative cell (Twell 2011).

The female and male gametes are endowed with distinct epigenetic modifications. In *Physcomitrella patens*, sporophytic genes are silenced in gametic differentiation, where the two *POLYCOMB REPRESSIVE COMPLEX 2* (*PRC2*) H3K27me3 writer genes, *FERTILIZATION INDEPENDENT ENDOSPERM* (*FIE*) and *CURLY LEAF* (*CLF*), repress some sporophyte-specific transcription factors in the gametophyte including *PpBELL1* (Okano et al. 2009; Horst et al. 2016; Mosquna et al. 2009). Analogous to this in *Arabidopsis* pollen development, the generative nucleus gradually loses chromatin accessibility among sporophytic-specific accessible chromatin regions. Transposable elements (TEs) are also silenced in the sperm nucleus by DNA methylation shaped by the small RNA-directed DNA methylation pathway (RdDM) with 24-nucleotide small interfering RNAs (siRNAs) derived from the surrounding nurse cell tapetum (Long et al. 2021) and the vegetative nucleus (Martínez et al. 2016). These non-cell-autonomously transcribed siRNAs target transposons thus maintaining genome integrity in the male germline. Sperm differentiation is linked to increased chromatin accessibility by removal of the repressive marker H3K27me3 at genes required for diploid-to-haploid transition, as well as at genes specifically expressed in re-initiation of the diploid life in the early embryo (Borg et al. 2020; 2021). In contrast to this, H3K27me3 is essential for maintaining vegetative cell fate, and H3K27me3 erasure results in vegetative cell fate shifting to the generative cell fate (Huang and Sun 2022). Compared with the sperm nucleus, the vegetative cell nucleus is highly diffused, and the depletion of the linker histone H1 and H3K9me2 gives rise to decondensation of the pericentromeric heterochromatin. The loose chromatin status further leads to the demethylation of pericentromeric DNA by the

gametophyte-specific DNA glycosylase DEMETER (DME), which allows transcription of TEs and epigenetically activated small interfering RNAs (easiRNAs) (He et al. 2019; Creasey et al. 2014). This DME-mediated demethylation is further associated with cis-regulatory elements that are presumably bound to pollen-expressed transcription factors involved in vegetative cell differentiation (Borg et al. 2021).

The epigenetic information of the female gametophyte is still obscurer. Unlike the egg cell, the central cell has decondensed chromatin and reduced repressive histone modifications (Pillot et al. 2010). Similar to the vegetative cell in pollen, the central cell shows a depletion of heterochromatin and the heterochromatic marker H3K9me2 (Pillot et al. 2010). DME-mediated demethylation is also active in the central cell. The demethylation preferentially targets TEs, which leads to the activation of siRNAs that are able to travel to the egg cell and silence their target genes (Ibarra et al. 2012).

1.2 Double fertilization in flowering plants

In flowering plants, the two sperm cells rely on the vegetative cell to form the pollen tube to deliver them to the ovary, where one of the sperm cells fuses with the egg cell to form an embryo and the other one fuses with the central cell to form the nourishing endosperm, respectively, thus achieving double fertilization (Johnson, Harper, and Palanivelu 2019). This process is coordinated by a series of signaling events between sporophytic and gametophytic cells as well as between the gametes themselves (Figure 1.1).

1.2.1 Pollen hydration and germination

After the dehiscence of an anther, pollen grains adhere to the surface of the pistil and initiate the process of self-pollination. Pollen grains are captured by the papilla cells, followed by hydration and formation of an adhesion zone consisting of the pollen coat components. Then, pollen undergoes polarity establishment and a pollen tube emerges at the germ pore near the adhesion site (Kandasamy, Nasrallah, and Nasrallah 1994). In *Brassicaceae*, pollen acceptance at the stigma is regulated by mechanisms of the stigma to reject incompatible pollen and allow the hydration of compatible ones (Watanabe, Suwabe, and Suzuki 2012). The hydration and germination of pollen on the stigma are regulated by molecules from both sides of pollen and papillae. Exo70A1 is a plasma-membrane-localized papillae protein involved in regulating polarized vesicle trafficking, and it delivers stigmatic components required for pollen hydration and germination in *Brassica napus* and *Arabidopsis* (Samuel et al. 2009). The level of phosphatidylinositol-4-phosphate (PI4P) is necessary for polarized secretion in plants, and it

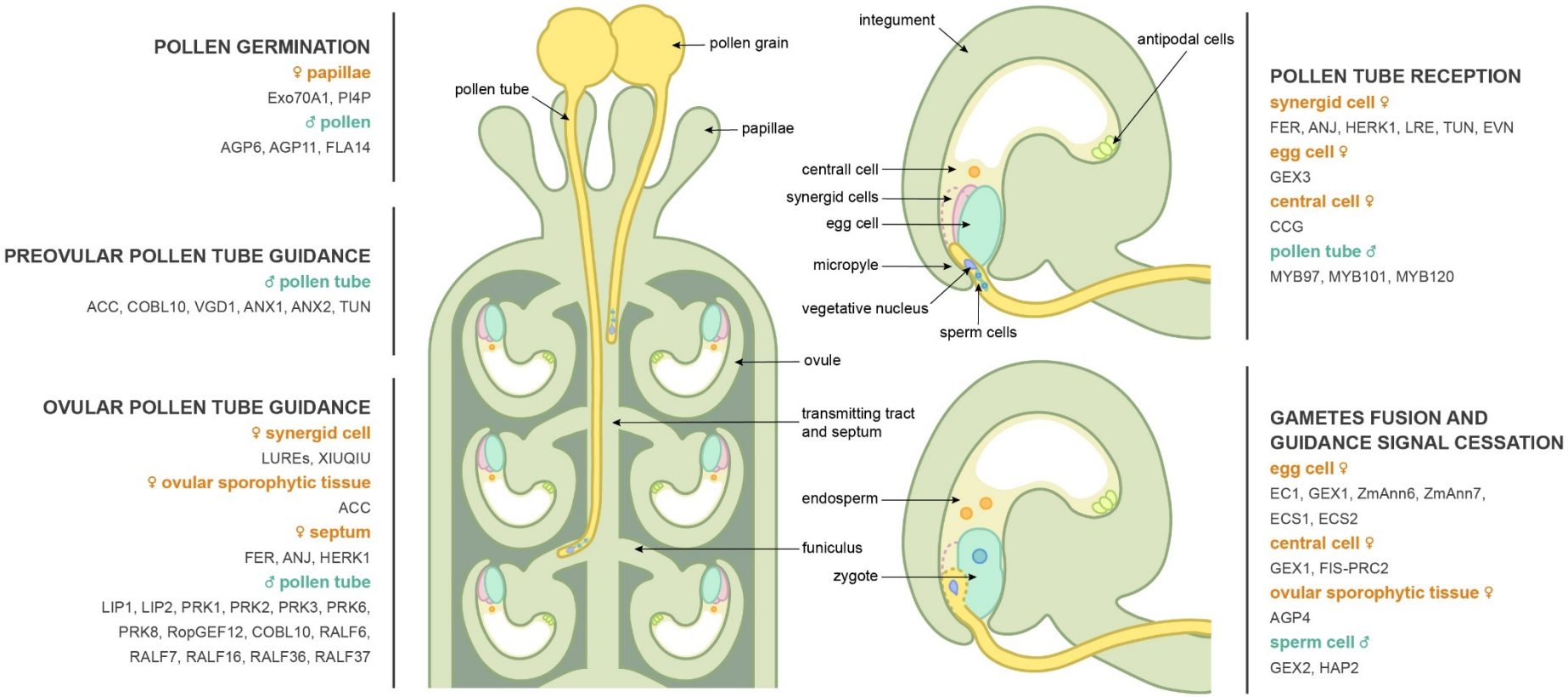

Figure 1.1 Schematic of double fertilization. The process of pollen germination, preovular pollen tube guidance, ovular pollen tube guidance, pollen tube reception, gametes fusion, and guidance signal cessation are represented in the diagrams. The factors contributed by different cells and tissues in each step are shown next to the diagrams.

is important for stigma-pollen interaction. An altered level of PI4P causes a reduced rate of pollen hydration on the stigma (Chapman and Goring 2011). Some pollen wall components, such as the arabinogalactan protein-encoding genes *AGP6*, *AGP11*, and *FLA14*, regulate water uptake in pollen germination (Coimbra et al. 2010; Miao et al. 2021). In the following, the pollen tube invades through the papilla cell and subsequently grows into the transmitting tissue of style, where it sets off on an intercellular journey (Kandasamy, Nasrallah, and Nasrallah 1994).

1.2.2 Preovular pollen tube guidance

Pollen tube elongation along the female transmitting tract is described as preovular guidance. It starts with pollen tubes invading through papilla cells toward the transmitting tract. Pollen tubes continue their growth in the transmitting tract until they emerge out of the septum toward the funiculus where they switch to ovular guidance (Higashiyama and Takeuchi 2015).

Pollen tubes perform tip-growth inside the maternal tissue, and the polarity is maintained by actin microfilament dynamics, polarized Ca^{2+} gradient, and membrane vesicle trafficking (Hepler, Vidali, and Cheung 2001). The ethylene precursor 1-aminocyclopropane-1-carboxylic acid (ACC) directly acts in pollen and stimulates pollen tube growth in tomato with or without ethylene perception (Althiab-Almasaud et al. 2021). COBL10 is a glycosylphosphatidylinositol (GPI)-anchored protein localized on the apical plasma membrane of the pollen tube. Mutations in *COBL10* cause compromised pollen tube growth in the transmitting tract with defective pollen tube wall deposition on the apical tip, suggesting its essential role as a paternal mediator of directional pollen tube growth (Sha Li et al. 2013). *VANGUARD1* (*VGD1*) encodes a pectin methylesterase specifically observed in pollen and pollen tube. It enhanced pollen tube growth in the transmitting tract probably by modifying pollen tube wall components thus mediating the interaction of the pollen tube with the female tissues (Jiang et al. 2005). *ANXUR1* (*ANX1*) and *ANX*2 are the sister genes of the maternal receptor-like kinase *FERONIA*, and the pollen tube of *anx1 anx2* mutants ruptures before the arrival at micropyle (Miyazaki et al. 2009). The expression of *ANX1* and *ANX*2 is disrupted in the mutant of *TURAN* (*TUN*), a uridine diphosphate-glycosyltransferase encoding gene. The mutant *tun* shows a defect in pollen tube growth and integrity, suggesting that misglycosylated ANX1 and ANX2 might be responsible for the pollen tube defect of *anx1 anx2* mutants (Lindner et al. 2015).

1.2.3 Ovular pollen tube guidance

Ovular guidance navigates pollen tubes to grow over the surface of the funiculus, target

ovule, and enter the micropyle, followed by pollen tube reception and sperm cell release inside the receptive synergid cell (Higashiyama and Takeuchi 2015).

Synergid cell signaling is essential for the emergence of the pollen tube out of the transmitting tract. LURE1.1 to LURE1.5 are peptides secreted by synergid cells that guide pollen tubes to emerge out of the septum toward ovules (Okuda et al. 2009). *LOST IN POLLEN TUBE GUIDANCE 1* (*LIP1*) and *2* (*LIP2*) represent two of the pollen tube receptor complex components in perceiving LURE1 signals (J. Liu et al. 2013). The pollen-specific receptor-like kinase 6 (PRK6) is another pollen tube receptor of LUREs, and it acts in cooperation with other PRK family receptors, PRK1, PRK3, and PRK8, in sensing the LURE1 attractants (Takeuchi and Higashiyama 2016). From the pollen side, PRK6 recruits the tip-growth machinery involving RopGEF12 in ovule targeting, which activates intracellular signaling components ROPs in various cellular responses (Takeuchi and Higashiyama 2016). Similarly, PRK2 also recruits RopGEF12 to maintain polar ROPs activity in pollen tubes (Zhang and McCormick 2007). LURE1-PRK6 signaling specifically accelerates pollen tube growth of conspecific pollen in reproductive isolation at both septum penetration and micropylar attraction, whereas another recently identified LURE-related peptide XIUQIU secreted from the synergid cells promotes pollen tube emergence at the septum in a non-species-specific manner (Zhong et al. 2019; M. Liu et al. 2021). The two preovular pollen tube guidance factors, ACC and COBL10, also take part in the ovular pollen tube guidance. ACC produced by the ovular sporophytic tissue stimulates transient Ca^{2+} elevation and promotes secretion of the pollen tube attractant LURE1.2, thereby acting as a maternally contributed molecule in pollen tube attraction independently of ethylene signaling (Mou et al. 2020). *COBL10* is involved in pollen-mediated ovular guidance, and the pollen tubes of *cobl10* mutant are defective in sensing ovular guidance cues (Sha Li et al. 2013).

The pollen tube reception at the micropyle is mediated by signaling from the synergid cell, egg cell, and central cell. *FERONIA* (*FER*), *ANJEA* (*ANJ*), and *HERCULES RECEPTOR KINASE 1* (*HERK1*) encode *Catharanthus roseus* RLK1-LIKE (CrRLK1L) receptor-like kinases that form a receptor complex on the membrane of the synergid cell which controls pollen tube reception at the micropyle (Escobar-Restrepo et al. 2007; Galindo-Trigo et al. 2020). *LORELEI* (*LRE*) is another synergid-expressed gene encoding a small plant-specific putative GPI-anchored protein on the plasma membrane, and mutation in *LRE* led to failed pollen tube reception with pollen tube overgrowth in the embryo sac (Capron et al. 2008). *TUN* and *EVAN* (*EVN*) function in protein N-glycosylation in synergid cells. Mutations in *TUN* and *EVN* lead to a similar pollen tube acceptance defect with overgrowth and failed pollen tube rupture

(Lindner et al. 2015). *GAMETE EXPRESSED 3 (GEX3)* accounts for the egg cell signal in pollen tube reception, and the loss-of-function mutant of *GEX3* showed non-fertilized ovules with pollen tubes on the funiculus that failed to enter the micropyle (Alandete-Saez, Ron, and McCormick 2008). *CENTRAL CELL GUIDANCE* (*CCG*) is the central cell-contributed factor in pollen tube reception. In *ccg* mutant ovules, pollen tubes were guided toward the ovule but failed to find the micropylar opening (Y. H. Chen et al. 2007). From the paternal side, MYB97, MYB101, and MYB120 are three pollen tube-expressed TFs function in pollen tube reception. The pollen tubes of the triple mutant exhibited a coiling structure inside the micropyle without pollen tube rupture and sperm discharge (Leydon et al. 2013).

1.2.4 Plasmogamy

Once the pollen tube ruptures and releases the sperms, interactions between proteins expressed on the surface of the male and female gametes are established, which enables cell recognition and adhesion, followed by the membrane fusion of the gametes (i.e. plasmogamy). *GAMETE EXPRESSED 2* (*GEX2*) encodes a sperm membrane protein that is required for the attachment of male and female gametes (Mori et al. 2014). The egg cell secrets small cysteine-rich EGG CELL 1 (EC1) which triggers the localization of the fusogen HAPLESS2 (HAP2) to the plasma membrane in the sperm cells and facilitates plasmogamy (Valansi et al. 2017; von Besser et al. 2006; S. N. Anderson et al. 2017; Dresselhaus, Sprunck, and Wessel 2016).

1.2.5 Karyogamy

Arabidopsis has adopted G2 karyogamy, in which sperm completes DNA synthesis prior to the deposition into an egg cell (Friedman 1999). The cell cycle of a sperm progresses alongside the process of pollination, which starts from the G1 phase in the mature pollen and achieves the S/G2 phase with 2C volume once the sperm reaches the ovule (Friedman 1999). Meanwhile, the egg cell stays in a quiescent status at the G0 phase and it is activated upon fertilization by the sperm cell (Peng et al. 2018). The male nucleus is transported in an F-actin-dependent manner during its migration toward the female nucleus. The actin filaments in the egg cell form a meshwork surrounding the nuclei and move the sperm nucleus to the egg nucleus through the convergence of the actin meshwork (Kawashima et al. 2014; Ohnishi and Okamoto 2015). Two annexin genes in maize, *ZmAnn6* and *ZmAnn7*, exhibit high and transient expression in both egg cells and early zygotes. They potentially link Ca^{2+} signaling to cytoskeleton dynamics and might be involved in cytoskeleton remodeling to set up the path for sperm nucleus transportation (J. Chen et al. 2017). After the attachment of the egg and the sperm

nuclei in rice, the egg chromatin unidirectionally migrates into the sperm nucleus, followed by decondensation of the sperm chromatin (Ohnishi and Okamoto 2015). *GAMETE EXPRESSED PROTEIN 1* (*GEX1*) is a nuclear membrane protein required for nuclear fusion in both fertilized eggs and central cells (Nishikawa et al. 2020). In *gex1-1* mutant seeds, the sperm nucleus failed in fusion with the central cell nucleus, resulting in abnormal endosperm proliferation and arrested embryo development shortly after the first zygotic cell division (Alandete-Saez et al. 2011; Nishikawa et al. 2020).

1.2.6 Polytubey block and fertilization recovery

Polytubey describes the simultaneous attraction of multiple pollen tubes to a single ovule (Beale, Leydon, and Johnson 2012). Polytubey block and fertilization recovery are established by coordinated signaling between the pollen tube, septum cells, synergid cells, the egg cell, the central cell, and the sporophytic cells of ovules, thus achieving maximum reproductive success. Polytubey block starts at the septum which involves the FER-ANJ-HERK1 receptor complex expressed in the female transmitting tract and septum (Zhong et al. 2022). The pollen tube-provided peptide ligands RAPID ALKANIZATION FACTOR 6 (RALF6), RALF7, RALF16, RALF36, and RALF37 interact with the septum-expressed FER-ANJ-HERK1 receptor complex coordinately in regulating polytubey block at the septum. When the pollen tube senses the attractants secreted by synergid cells and emerges out of the septum, it secrets RALFs to activate FER-ANJ-HERK1 signaling in the septum to block the emergence of a second pollen tube. Pollen tube acceptance and rupture in the receptive synergid cell leads to RALF signal fading, therefore releasing the pollen tube block at the septum. Once fertilization is achieved, the persistent synergid undergoes degeneration, which abolishes pollen tube attraction through an attractant outage (Zhong et al. 2022). Ethylene signaling induces the degeneration of the second synergid, and a constitutive ethylene response leads to premature synergid cell death (Völz et al. 2013). The aspartic endopeptidase genes *EGG CELL-SPECIFIC1* (*ECS1*) and *ECS2* are involved in the degradation of the attractant LURE1. These two proteases are exclusively expressed in the egg cell and their secretion is triggered upon the successful fertilization of the egg cell, which accounts for the contribution of the egg cell to polytubey block (Yu et al. 2021). The central cell contributes to polytubey block independently of the egg cell by employing the FERTILIZATION-INDEPENDENT SEED (FIS) class PRC2 (FIS-PRC2), implying a potential role of the chromatin-remodeling pathway in a second pollen tube avoidance (Maruyama et al. 2013). In addition, the integument-origin arabinogalactan protein AGP4/JAGGER regulates the elimination of the persistent synergid after fertilization (Pereira et al. 2016). In contrast, if the

gametic fusion failed, the fertilization recovery machinery is activated in the persistent synergid by the secretion of pollen attractants to trigger the emergence of a second pollen tube at the septum (Zhong et al. 2022).

1.3 Zygotic genome activation in *Arabidopsis*

Maternal-to-zygotic transition (MZT) describes the post-fertilization process in animals which constitutes of two major processes, the *de novo* zygotic genome activation (ZGA) and the clearance of maternal transcripts (Schier 2007; Tadros and Lipshitz 2009; Bai et al. 2018). MZT consists of two phases in animals: (i) maternally inherited transcripts and proteins regulate the early development of embryos; (ii) *de novo* transcription of the zygotic genome takes over the regulation of embryo development (Bai et al. 2018). This concept is adopted in flowering plants which exhibit a similar developmental process after fertilization (Baroux et al. 2008; Xin, Zhao, and Sun 2012). With growing knowledge of fertilization and early embryogenesis in flowering plants, the MZT in flowering plants is distinguished from animals by equal parental contribution to the zygote transcriptome and early activation timing of zygotic genome (P. Zhao et al. 2022).

1.3.1 Timing of zygotic genome activation

In worms, echinoderms, amphibians, fishes, and insects, ZGA takes place after the cleavage period (Baroux et al. 2008). However, in mammals, the zygotic genome is transcriptionally activated in the later zygotic to the two-cell stage (Sha, Zhang, and Fan 2019). In the fern species *Marsilea vestita*, polyadenylated mRNA from maternal origin supports the early embryo until the 16-cell stage (Kuligowski, Ferrand, and Chenou 1991). In contrast, transcription of the zygotic genome occurs at the zygote stage in higher plants. Transcriptome profiling in rice observed large-scale changes in zygotes (S. N. Anderson et al. 2017), which is in line with the identification of 3605 induced genes in zygotes at 12 hours after pollination (12 HAP) in maize (J. Chen et al. 2017). In *Arabidopsis*, the transcriptional inhibitor α-amanitin has been used to block *de novo* transcription to define the ZGA timing. Zygotes treated at 8 HAP failed in cell elongation and polarity establishment, while zygotes treated at 14 HAP elongated and performed asymmetrical division (P. Zhao et al. 2019). These results give rise to the assumption that, in contrast to animals, the maternal-inherited transcripts are not sufficient to orchestrate the development of the early embryo in *Arabidopsis*. Taken together, ZGA in higher plants occurs much earlier than in animals, and the *de novo* transcription of the zygotic genome is required for polarity establishment and first cell division of zygotes.

1.3.2 Transcriptional regulation of zygotic genome activation

Current knowledge about ZGA is still limited, but the identification of a few key transcription factors (TFs) outlines a transcriptional regulation network in initiating the zygotic program. In *Drosophila*, a maternally transmitted zinc-finger protein Zelda is found to be a key TF that can bind to the cis-regulatory heptamer motif of 75% early transcribed genes in the embryo, and mutants lacking Zelda failed to activate genes essential for differentiation, sex determination, and pattern formation (Liang et al. 2008). In plants, the evolutionarily conserved homeodomain TFs have been suggested to be regulators in ZGA. In the unicellular alga *Chlamydomonas reinhardtii*, the two homeodomain TFs, the KNOX protein GAMETE SPECIFIC MINUS1 (GSM1) and the BELL protein GAMETE SPECIFIC PLUS1 (GSP1), act as factors contributed by the minus and plus gametes, respectively, in a two-component system that forms heterodimer upon fertilization and thus initiates a zygotic transcriptional program (Lee et al. 2008; Sekimoto 2017). The ortholog of KNOX in *Marchantia polymorpha*, *MpKNOX1*, is shown to be preferentially transcribed in the egg cell and translocated to both the male and female pronuclei after fertilization (Hisanaga et al. 2021). The mutant *mpknox1* showed defects in karyogamy at the nuclear membrane fusion step, indicating that egg-derived *MpKNOX1* regulates the expression of genes that are required for nuclear membrane fusion. Consistent with the heterodimer function mode in algae, the paternal-derived *MpBELL3/4* contribute to the pronuclear translocation of *MpKNOX1* after fertilization, thus achieving ZGA (Hisanaga et al. 2021). In contrast, in the other bryophyte model plant *Physcomitrella patens*, the BELL/KNOX proteins showed diverged functions in egg cell morphology, alternation of generations, and sporophyte development (Horst et al. 2016; Ortiz-Ramírez et al. 2017; Singer and Ashton 2007; Sakakibara et al. 2013). Along with gene duplication and neofunctionalization as land plants evolved, the ancestral role of BELL/KNOX proteins in ZGA shifted towards meristem maintenance (Hay and Tsiantis 2010; Meng et al. 2020). In flowering plants, the TF-encoding gene *BABY BOOM* (*BBM*) induces embryogenesis in somatic cells in *Arabidopsis* (Horstman et al. 2017). Its paternally provided orthologue *BBML1* in rice is involved in the activation of *de novo* gene expression. Over-expression of *BBML1* in the egg cell led to proliferation without fertilization (Khanday et al. 2019), while suppression of the function of *BBML1* in zygotes resulted in a developmental arrest, suggesting that *BBML1* possesses an important role in initiating zygotic development (Rahman et al., 2019).

1.3.3 Epigenetic regulation of zygotic genome activation

Changes in chromatin histone content, chromatin structure, and transcription factors

appear to regulate the availability of the genome for transcription in the early embryo. The sperm genome is highly condensed in order to maintain its chromatin stability during the long journey to the egg cell. In *Arabidopsis*, histone 3 (H3) variants contributed by both the sperm and the egg cell nuclei are removed from the zygote chromatin and are replaced by *de novo* synthesis of H3 variants in a replication-independent manner (Ingouff et al. 2010). These changes in nucleosome composition enable transcription and expression from the paternal-inherited chromatin.

Genomic imprinting shaped by asymmetric DNA methylation between parental genomes contributes to biased parental gene expression. Up to date, imprinting is mainly found in the proliferation of endosperm in plants. It is shown that in the interploidy crossing, the increased activity of paternally expressed imprinted genes (PEGs) in the endosperm of triploid seeds causes failed cellularization of the endosperm, which further leads to a compromised embryo in short of sucrose supply (Wolff et al. 2015; Morley-Smith et al. 2008; Hehenberger, Kradolfer, and Köhler 2012). This paternal-regulated triploid barrier establishment is caused by an increased abundance of easiRNAs from 2n pollen, which negatively interferes with the repression of PEGs in the endosperm (Martinez et al. 2018).

The paternal genome expression in the embryo is epigenetically regulated by some maternal components. The maternal SUVH4 histone methyltransferase *KRYPTONITE* (*KYP*) and the maternal-inherited RdDM pathway components suppress the transcription of many paternal alleles, and their progressive depletion during the development of embryos may lead to a gradual activation of the paternal genome (Autran et al. 2011).

1.3.4 Parental contributions to the early embryo

Opinions concerning parental contributions to the early embryo on the transcriptional level were divided (Autran et al. 2011; Nodine and Bartel 2012). Recent transcriptomic profiling of hybrid zygotes and early embryos derived from a reciprocal cross between Columbia (Col) and Landsberg *erecta* (Ler) ecotypes in *Arabidopsis* settled this dispute by showing that both parents contribute equally to the transcriptomes of elongated zygotes and early embryos (P. Zhao et al. 2019; 2020). However, despite the equal transcriptional contribution, the parental control of early embryo development is biased, with the basal cell lineage showing a strong maternal effect (P. Zhao et al. 2020). Certain parent-of-origin genes exhibit a strong impact on zygotic and embryonic development. *BBML1* in rice is a paternal-transmitted gene in the activation of the *de novo* gene expression in zygotes (Khanday et al. 2019). *SHORT SUSPENSOR* (*SSP*) is a paternal-transmitted gene that promotes polarity establishment in zygote and suspensor

development (Bayer et al. 2009). Corresponding to *SSP* from the paternal side, two maternal-derived TF encoding genes, *HOMEODOMAIN GLABROUS 11* (*HDG11*) and *HDG12*, contribute to the regulation of the polarity change and asymmetric division in zygotes (Ueda et al. 2017).

1.3.5 Maternal transcripts clearing

To finalize the MZT the maternally contributed RNAs have to be degraded. In *Drosophila*, Zelda and the Zelda-activated microRNA *miR309* target maternally deposited transcripts and trigger the large-scale degradation of maternal transcripts (Bushati et al. 2008; Liang et al. 2008). In accordance with this, transcriptome profiling in *Arabidopsis* revealed that transcript abundance largely differs between the egg and zygote, with thousands of transcripts showing a decreased level in zygotes (P. Zhao et al. 2019). The elimination of maternal transcripts in endosperm seems to be essential for its proliferation. The sperm-transmitted *miR159* promotes endosperm nuclear division by degradation of *MYB33* and *MYB65* transcripts in the fertilized central cell (Y. Zhao et al. 2018). The regulatory mechanisms involved in maternal transcripts clearance in the zygote are yet to be discovered

2 Objectives and aims

In flowering plants, a successful double-fertilization is achieved by the coordination of a series of signaling events between sporophytic and gametophytic cells as well as between the gametes themselves (recently reviewed in Johnson, Harper, and Palanivelu 2019; Dresselhaus, Sprunck, and Wessel 2016). With knowledge growing on pollen tube guidance and gametic interactions, the molecular signaling events orchestrating zygotic genome activation remain to be discovered. Despite the equal transcripts contribution from both parental sides in the early embryo (P. Zhao et al. 2020), certain paternal-of-origin genes exhibit a strong impact on zygotic and embryonic development, such as *SSP* in *Arabidopsis* (Bayer et al. 2009) and *BBML1* in rice (Khanday et al. 2019). Therefore, the overall aim of this thesis was to reveal novel paternal-contributed genes in fertilization and zygotic genome activation.

Aim 1: Perform a forward genetic screen for paternal-defective fertilization mutants in *Arabidopsis*

Forward genetic screen is a powerful tool to reveal novel genes. The forward genetic screen for paternal-defective fertilization mutants in an EMS-induced mutant population had been performed by the host lab. The first aim was to re-screened the already available candidates. Phenotyping of the mutant plants was based on crossings to wild type plants as pollen donors and subsequent microscopic analysis of the resulting seeds. Mutants that showed paternal defects ranging from pollen tube function, gamete fusion, and zygotic genome activation were selected and subjected to causative variant mapping.

Aim 2: Tailor a mapping-by-sequencing method for identifying paternal-defective fertilization mutations

Sequencing-based bulked-segregant analysis has been widely used to identify causative genes in forward genetic screen. However, this approach is poorly suited to identifying variants with fertilization defects due to the depletion of homozygous parents and the laborious phenotypic work required. The second aim of the thesis was to develop a mapping-by-sequencing method that is specifically tailored to identify causative genes underlying paternal fertilization defects of the mutants obtained from the forward genetic screen in Aim 1.

Aim 3: Characterize an Origin of Replication Complex gene *ORC1b* in fertilization

ORC1b encodes an Origin of Replication Complex gene that is expressed highly in proliferating tissues including sperm cells and developing embryos (Diaz-Trivino et al. 2005; P. Zhao et al. 2019; Borges et al. 2008), suggesting a potential role as a paternal gene in fertilization. The third aim of this thesis was to use the reverse genetic approach to study the

function of *ORC1b* in fertilization. A T-DNA insertion mutant allele *orc1b-1* and a knock-out allele *orc1b-2* generated by the CRISPR-Cas9 system were used to characterize the function of *ORC1b*.

Aim 4: Design fluorescent marker lines to assist phenotypic analysis of fertilization-defective mutants

Fertilization and early embryo development in *Arabidopsis* occur inside the embryo sac that is deeply embedded inside the sporophytic tissue, which makes it challenging to obtain phenotypic information on a cellular and sub-cellular level. Therefore, the fourth aim of this thesis was to design a set of fluorescent marker lines to assist phenotypic analysis during fertilization. Several fluorescent proteins were introduced into specific cell structures in pollen and female gametophyte to visualize the fertilization process.

Taken together, this thesis aimed to provide novel methods and new insights into understanding the paternal contribution to fertilization in flowering plants.

3 A novel mapping-by-sequencing method for paternal-defective fertilization mutations

Forward genetic screen assisted by sequencing-based bulked-segregant analysis has been widely used to discover novel genes. However, this approach is poorly suited to the identification of variants with fertilization defects in plants due to the depletion of homozygous parents and the laborious phenotypic work required. Here, we describe a semi-high-throughput mapping-by-sequencing method that is specifically tailored to identify genes underlying paternal fertilization defects. This approach enables the mapping of multiple mutants simultaneously with a limited workload. We employed this method to capture a set of both known and novel paternal genes in fertilization. Taken together, this study greatly enhances our ability to discover novel signaling mechanisms in fertilization and offers new insights into understanding the paternal contribution to fertilization in flowering plants.

3.1 Introduction

In flowering plants, the pair of sperm cells rely on the vegetative cell to form the pollen tube to deliver them to the ovary. Here, one of the sperm cells fuses with the egg cell to form an embryo and the other one fuses with the central cell to form the nourishing endosperm, thus achieving double-fertilization. Successful fertilization depends on a series of signaling events performed synergistically between sporophytic and gametophytic cells as well as between the gametes themselves (Dresselhaus, Sprunck, and Wessel 2016). Pollen is captured by papilla cells on the surface of the pistil, followed by pollen hydration and germination of a pollen tube, which invades through the female transmitting tract towards ovules (Kandasamy, Nasrallah, and Nasrallah 1994). The synergid cell-secreted peptides LURE1s are perceived by the pollen tube receptor complex components, the pollen-specific receptor-like kinase PRK6, LIP1, and LIP2, hence guiding the pollen tube to emerge out of the septum (Okuda et al. 2009; Takeuchi and Higashiyama 2016). *FER*, *ANJ*, and *HERK1* encode CrRLK1L receptor-like kinases that form a receptor complex on the membrane of the synergid cell and control pollen tube reception at the micropyle (Escobar-Restrepo et al. 2007; Galindo-Trigo et al. 2020). In addition, the egg cell expressed *GEX3* and the central cell expressed *CCG* also contribute to pollen tube guidance at the micropyle (Y. H. Chen et al. 2007). *MYB97*, *MYB101*, and *MYB120* are three transcription factor genes in pollen tubes that serve as pollen components in pollen tube rupture and sperm release (Leydon et al. 2013). *GEX2* encodes a sperm membrane protein, which is required for attachment between male and female gametes (Mori et al. 2014). The egg cell secreted small

cysteine-rich EC1 triggers the localization of the fusogen protein HAP2 (Valansi et al. 2017; von Besser et al. 2006) to the plasma membrane in sperm cells and facilitates plasmogamy (S. N. Anderson et al. 2017; Dresselhaus, Sprunck, and Wessel 2016). The egg cell stays in a quiescent status at the G0 phase and it is activated upon fertilization with the sperm cell (Peng et al. 2018). GEX1 is a nuclear membrane protein required for sperm nuclear fusion in both fertilized egg cells and central cells (Nishikawa et al. 2020). In *gex1-1* mutant seeds, deficiency in sperm nuclear fusion in the central cell caused abnormal endosperm proliferation, and embryo development was arrested shortly after the first zygotic cell division (Alandete-Saez et al. 2011; Nishikawa et al. 2020).

MZT describes the post-fertilization process in animals which constitutes two major processes: the *de novo* ZGA and the clearance of maternal transcripts (Schier 2007; Tadros and Lipshitz 2009; Bai et al. 2018). Current knowledge about zygotic activation is still limited, but the identification of several key TFs outlines a transcriptional regulation network in initiating the zygotic program as described in chapter 1. With more high-quality transcriptomic data available in recent years, we have gained a better understanding of the transcripts that shape the development of zygotes and early embryos, but the molecular signaling events orchestrating the onset of the zygotic program remain to be discovered.

Forward genetic screen is a powerful tool to reveal novel genes, which could be adopted in identifying molecules involved in ZGA. The exemption of prior assumptions and the unbiased selection among the whole genome in a forward genetic screen is instrumental for capturing key players in biological processes that are barely understood. The nature of single nucleotide polymorphism (SNP) among genomes of different *Arabidopsis* ecotypes is essential for the identification of the causative genes behind phenotypic variations. Map-based cloning (also known as positional cloning) is the traditional PCR-based marker detection method to identify the genetic basis of a mutant phenotype based on the linkage to genetic markers whose physical location in the genome is known (Jander et al. 2002). With more than 50,000 genetic markers available, it is possible to reach a 40-kb resolution, though phenotypic and genotypic analysis of each individual in a fine-mapping population of 3,000 to 4,000 plants is recommended (Jander et al. 2002). Bulked-segregant analysis, which involves phenotype-based separation of two populations each containing individuals showing mutant or WT-like phenotypes, has drastically reduced the number of PCR reactions required to establish genome linkage of mutations (Lukowitz, Gillmor, and Scheible 2000). However, the laborious work of verifying all the candidate genes in a broad genetic interval is hindering the efficiency of map-based cloning. The development of whole-genome sequencing-based bulked-segregant analysis

has rendered the mapping approach faster and more affordable. It is able to provide genotypic information on a variant-level resolution rather than an interval-level resolution in map-based cloning. Nonetheless, due to the requirement of identifying homozygous mutants in an F2 mapping population for these methods, they cannot be used to identify lethal and poorly transmitted variants. Utilization of SNP-ratio mapping has lifted the restriction of lethal mutations and managed to map gametophyte lethal mutations, where the causative variant segregates by 1:1 while the phenotype-unlinked variants segregate by 1:3 in the second backcross progenies (Lindner et al. 2012). However, it still requires phenotyping of segregated individual plants in the second backcross population (Lindner et al. 2012), which is not feasible for high-throughput mapping of hard-to-score phenotypes, such as subtle fertilization defects and hypomorphic mutations.

To address this limitation, we tailored a semi-high throughput mapping-by-sequencing method based on SNP-ratio mapping that allows the identification of paternal-defective mutations with a limited phenotyping workload of a few individual plants. Adopting this method, we corroborated several known paternal genes involved in pollen development, pollen tube guidance, and gametes interaction. We also revealed a novel paternal gene, *SAHH2*, which we showed to be involved in pollen tube guidance in the female transmitting tract. Additionally, a list of potential causative candidates was generated for further study. The identification of these variants demonstrates the power of our improved mapping method to elucidate the paternal impact on fertilization in flowering plants.

3.2 Results

3.2.1 Phenotypic characterization of the paternal-defective mutants

Using a forward genetic screen, we examined 3500 ethyl methane sulfonate (EMS)-mutated M2 plants in Ler for paternal fertilization defects. Phenotyping based on crossings to wild type plants and subsequent microscopic analysis of the resulting seeds was performed to screen for paternal-defective mutations. The paternal defects during the fertilization process ranged from pollen germination, pollen tube growth, pollen tube reception, gamete fusion, and zygotic development to early embryo development. These defects converged in a seed abortion phenotype with a reduced seed set rate, which serves as an indicator in the mutant screen. Pollen from mutants was obtained and crossed to WT pistils. The resulting siliques were dissected and the seed set pattern was recorded: (i) a completely failed seed set indicates defects in pollen development or pollen tube germination rather than in fertilization, which was ruled out in the screen; (ii) a basal part seed abortion in siliques indicates defects in pollen tube elongation and

guidance; (iii) a randomly distributed seed abortion in siliques indicates that the mutated pollen behaves comparably to WT pollen at pollen tube reception, and the defects rather reside in gametes fusion, zygotic genome activation, or early embryo/endosperm development. Furthermore, an early abortion of the defective seeds in siliques suggests a failure in fertilization, whereas a late abortion of defective seeds that manage to expand to the size of WT or a smaller size than WT suggests a misregulation in the embryo or/and endosperm development. These traits of the seed set enable the capture of paternal defects at certain steps during fertilization. More subtle phenotypes were characterized by light microscopy of ovules after fertilization assisted by clearing and staining techniques. Altogether, 19 mutants displaying paternal defects during fertilization were selected and named *paternal-defective mutant 1-19* (*pmd1-19*). These mutants were further subjected to mapping as described below.

3.2.2 Design of the mapping approach

Generating F2 mapping populations for fertilization-defective mutations is rendered problematic by the difficult-to-score phenotypes. Segregation distortion can occur without losing seed set such as in the context of pollen competition. Furthermore, hand pollination makes the seed set phenotype variable with full or limited pollination, which makes scoring by counting misleading and prone to observe bias. Rather than phenotypically sorting each individual in F2, we decided to leverage the reduced paternal transmission of the mutants. In our mapping strategy (Figure 3.1 A), each paternal-defective mutant in Ler was crossed to Col-0 as the maternal parent to generate the heterozygous F1 with 50% Ler genome. A single F1 mutant was selected to outcross to Col-0 as the pollen donor to generate the outcross 2 (OC2) population. The male gametes carrying the mutation failed in fertilization, thus abolishing the transmission to the resulting OC2 population. Therefore, we generated a wildtype pool with a 25% Ler genome. There are two optional approaches to generating mutant pools. The first involved self-crossing of the EMS mutant in Ler, and the second involved self-crossing of the selected F1 plant which resulted in the F2 population with equal parental genome contribution. These two approaches were both used in this study and their mapping efficiency will be compared in the following sections. Approximately 1000 seedlings of each mapping population were pooled for sequencing. Segregation distortion of Ler SNP frequency at the region of the causative mutation was expected in the wildtype pool OC2 due to the abolished transmission, and the candidate interval would be determined accordingly. A causative variant in the candidate interval would be identified in the corresponding mutant pool M or F2 (Figure 3.1 B). As a control to avoid natural genome bias, an OC2 pool generated from Ler-0 and Col-0 was adopted.

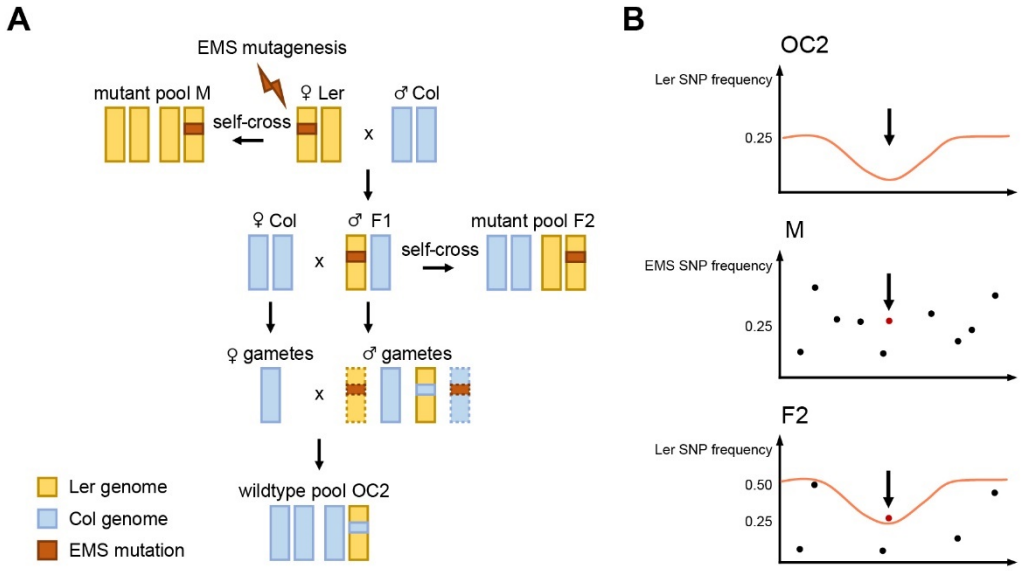

Figure 3.1 Crossing and mapping scheme of the novel mapping-by-sequencing method for paternal-defective fertilization mutations. (A) Crossing combinations for generating the mapping populations. Drawings of single chromosome pairs were used as representatives for the full genome. The chromosomes outlined by dashed lines indicate the infertility of the gametes. EMS mutant in Ler background was self-crossed to generate the M population, and the EMS mutant was outcrossed to Col-0 as the maternal parent to generate the heterozygous F1. Single F1 mutant was selected to outcross to Col-0 as the pollen donor to generate the OC2 population. This single F1 mutant was self-crossed to generate the F2 population. **(B)** The mapping strategy to reveal the paternal-defective mutation. Ler SNP frequency of the OC2 and F2 populations was adopted to map the candidate interval. The EMS SNP analysis in M and F2 populations revels the causative mutation. Ler SNP frequency is indicated by orange curves, the candidate interval is indicated by arrows, and the causative mutation is indicated by red dots.

As shown in the mapping workflow (Figure 3.2), sequencing results of each mapping population were subjected to the control mapping module, the interval mapping module, the causative variant mapping module, or the interval and causative variant mapping module accordingly. The Col-Ler variants generated by the control mapping module from the control OC2 were adopted to perform variant filtering in the interval mapping process. The candidate interval determined by interval mapping in OC2 was further employed for causative variant mapping in M or F2. In the OC2 mapping population, the SNPs in the flanking region of the causative variant would exhibit a rather low frequency since they have been co-selected due to genetic linkage. These SNPs are prone to be excluded with standard settings in variant detection for their similarity to the spurious variation caused by sequencing artifacts. Therefore, we adjust the observation thresholds with an alternate fraction of 0.01 instead of 0.05 by default in the genetic variant detector (Garrison and Marth 2012) to preserve these valuable low-frequency SNPs. In analyzing the causative variants generated from the M and F2 populations, the variant annotation and SNP effect prediction were performed. The SNPs located in the non-coding region were filtered out, and typical EMS-induced GC-to-AT nucleotide change, as well as

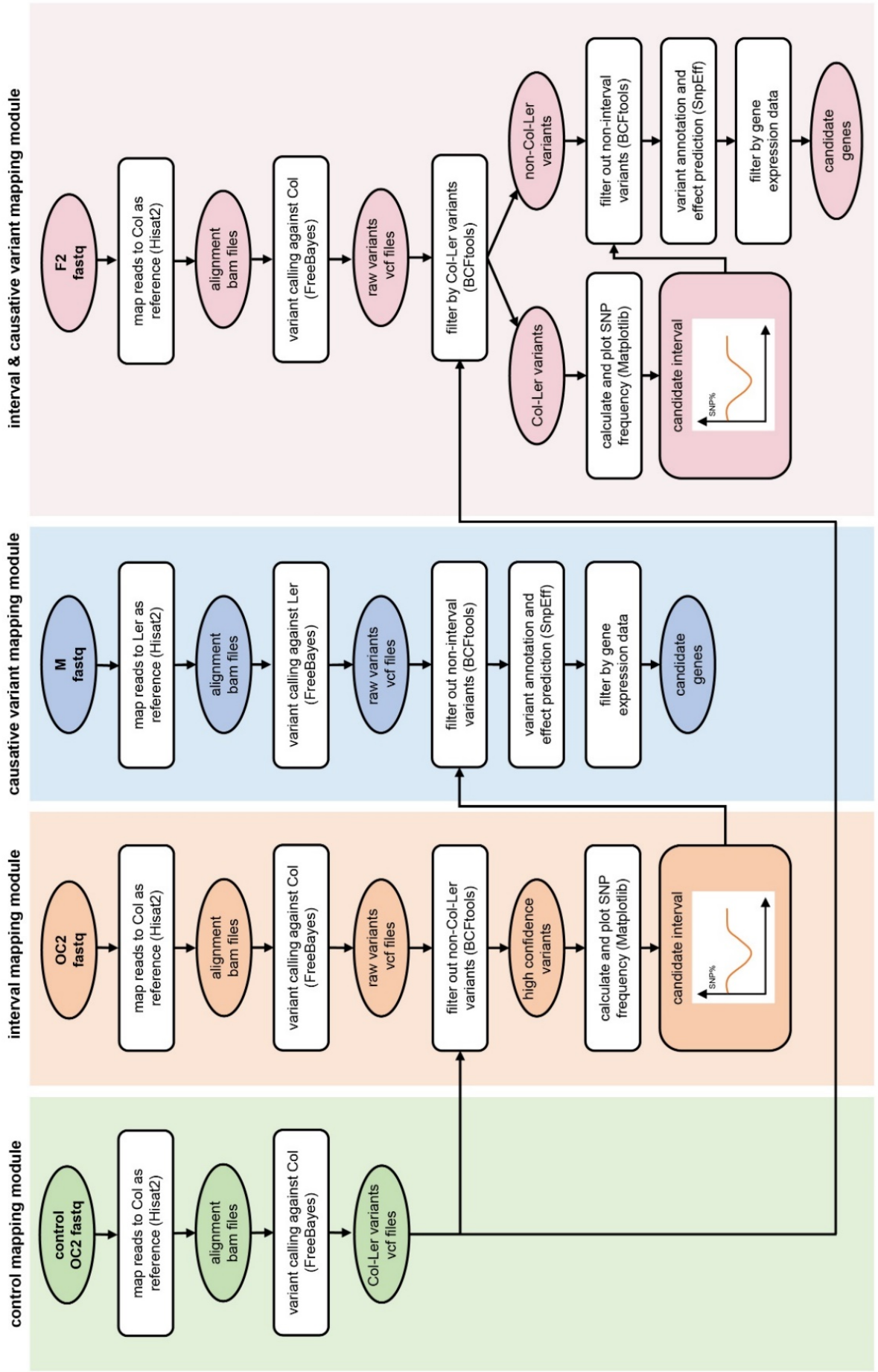
control mapping module
control OC2 fastq
map reads to Col as reference (Hisat2)
alignment bam files
variant calling against Col (FreeBayes)
Col-Ler variants vcf files
interval mapping module
OC2 fastq
map reads to Col as reference (Hisat2)
alignment bam files
variant calling against Col (FreeBayes)
raw variants vcf files
filter out non-Col-Ler variants (BCFtools)
high confidence variants
calculate and plot SNP frequency (Matplotlib)
candidate interval
SNP%
causative variant mapping module
M fastq
map reads to Ler as reference (Hisat2)
alignment bam files
variant calling against Ler (FreeBayes)
raw variants vcf files
filter out non-interval variants (BCFtools)
variant annotation and effect prediction (SnpEff)
filter by gene expression data
candidate genes
interval & causative variant mapping module
F2 fastq
map reads to Col as reference (Hisat2)
alignment bam files
variant calling against Col (FreeBayes)
raw variants vcf files
filter by Col-Ler variants (BCFtools)
non-Col-Ler variants
Col-Ler variants
filter out non-interval variants (BCFtools)
calculate and plot SNP frequency (Matplotlib)
variant annotation and effect prediction (SnpEff)
candidate interval
SNP%
filter by gene expression data
candidate genes

Figure 3.2 Mapping workflow. The sequencing result of each mapping population was proceeded to the control mapping module (green), the interval mapping module (orange), the causative variant mapping module (blue), and the interval & causative variant mapping module (pink) accordingly. The Col-Ler variants generated by the control mapping module from the control OC2 was adopted to perform variant filtering in interval mapping. The candidate interval determined by interval mapping was further employed for causative variant filtering. In each module, nodes with a colored background represent important input/result files, whereas nodes with white background represent the main analysis steps and the tools used.

insertion-deletion mutations (InDels) with relatively high impact effect types, were included, such as missense variants, frameshift variants, stop gained variants, start lost variants, and intron splicing-related variants. The candidate gene list was further filtered according to the available transcriptome data of pollen and sperms (Borges et al. 2008; Loraine et al. 2013).

3.2.3 Mapping-by-sequencing reveals causative variants

First, the control OC2 pool generated from Ler-0 and Col-0 was analyzed and the Ler SNP frequency was calculated and plotted against their chromosomal position (Figure 3.3 A). As expected, the overall Ler SNP frequency was around 25% along the genome. Ler SNP frequency in the centromeric regions displayed a rather noisy pattern, probably due to the poor reads assembly at the highly repetitive centromeric regions. In addition, a small fluctuation at the end of Chr. 1 was observed in the control OC2, as well as all the other OC2 and F2 mapping populations, which might be caused by a bias introduced during crossing or sampling.

The sequencing results revealed promising segregation distortions in 7 out of the 19 OC2 mapping populations (Table S3.1). The mutant *pdm7* exhibited a segregation distortion on Chr. 2 in its OC2 sequencing result, while the distortion was missing in F2. This was probably due to the dependency of the segregation distortion on some environmental factors. Since the reduced transmission appeared to be not stable in *pdm7*, the mutant was excluded for further analysis. Taking mutant *pdm1* as an example, the Ler SNP frequency dropped down on the right arm of Chr. 4 in both OC2 and F2 (Figure 3.3 A). To investigate which one of OC2 and F2 fits better for defining the candidate interval, the distribution of Ler SNPs identified on Chr. 4 in OC2 and F2 of *pdm1* was plotted against their chromosomal position (Figure 3.3 B). In theory, the Ler SNPs frequency should drop from 50% to 25% in the causative interval in F2, while ideally all the Ler SNPs should be preserved. In line with this, more Ler SNPs were identified in F2 (2581.05 per Mb) than in OC2 (429.05 per Mb). The Ler SNPs in F2 were equally distributed along the chromosome, while in OC2, the Ler SNPs number was reduced in the flanking region of the causative mutation due to genetic linkage, which largely affected the determination of the causative interval as shown in Figure 3.3 C. The stretched Ler SNP frequency plot of Chr. 4 in OC2 exhibited a rather noisy plot pattern, whereas F2 showed a

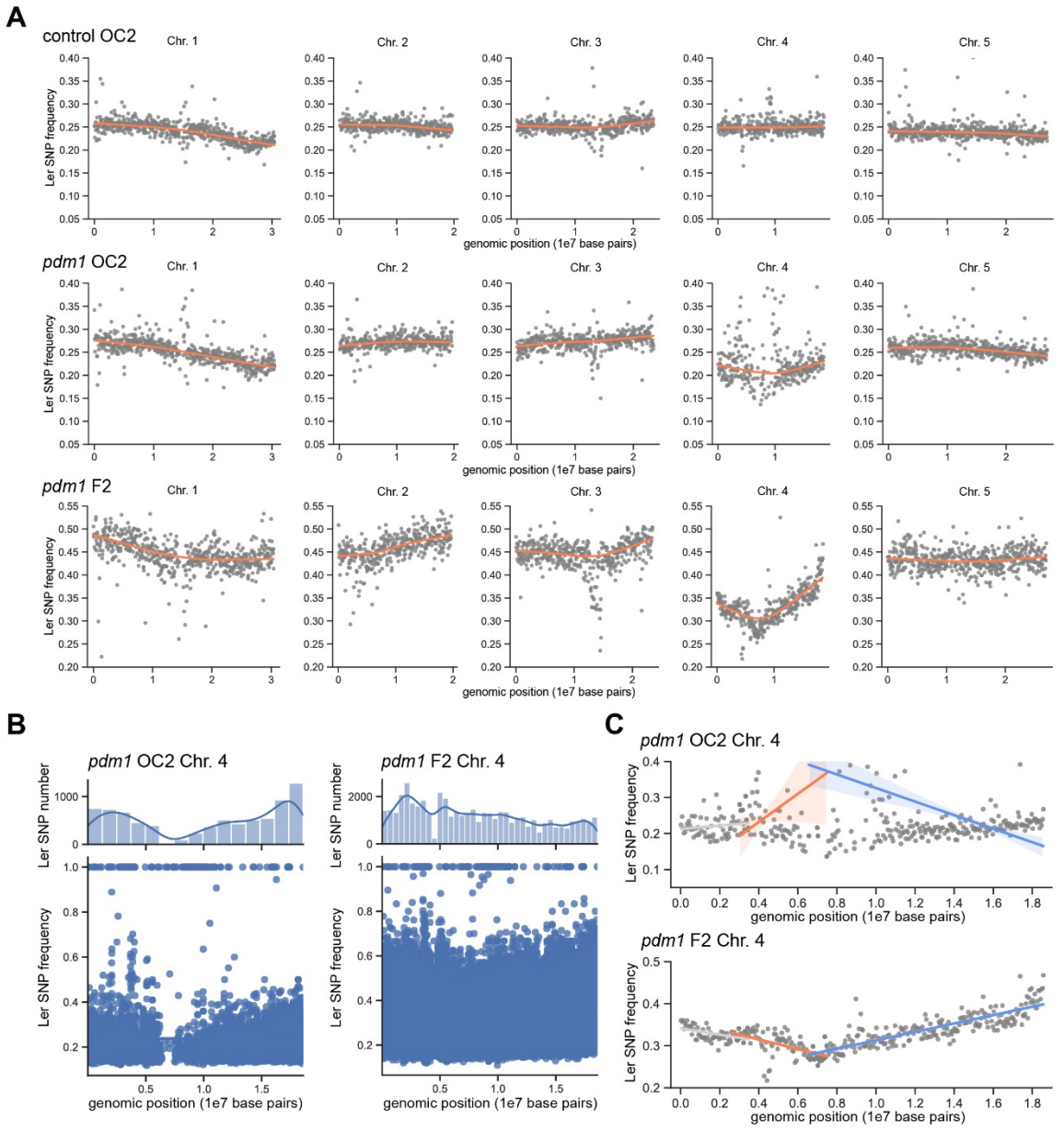

Figure 3.3 Comparison of the mapping results for OC2 and F2 populations. (A) Ler SNP frequency plots of control OC2, *pdm1* OC2, and *pdm1* F2. The five panels per row represent five chromosomes. Each grey dot indicates the average frequency per 50 kb. Orange lines indicate LOWESS (locally weighted scatterplot smoothing) regression lines fitted to the plots. The control OC2 exhibited 25% Ler SNP frequency along the genome. Significant Ler SNP frequency distortions were observed on Chr. 4 in both *pdm1* OC2 and *pdm1* F2. **(B)** The distribution of Ler SNPs identified on Chr. 4 in *pdm1* OC2 and *pdm1* F2. Each blue dot indicates a Ler SNP. The histone grams above indicate the number of Ler SNPs on Chr. 4. Blue lines indicate the distribution tendency of Ler SNPs. **(C)** Stretched Ler SNP frequency plots of Chr. 4 in *pdm1* OC2 and *pdm1* F2. Each grey dot indicates the average frequency per 50 kb. Linear regression lines were fitted to the distorted chromosome arm from the left side (indicated by the orange line) and the right side (indicated by the blue line), leaving the left chromosome arm aside (indicated by the grey line).

considerably improved resolution (Figure 3.3 C). Fitting linear regression lines to the distorted chromosome arm from the left side and the right side enabled us to define the chromosomal position with the lowest Ler SNP frequency, thus narrowing down the causative interval size.

Finally, a causative interval of 2 Mb (at the genome position of 6-8 Mb) flanking the point with the lowest Ler SNP frequency was selected for causative variant mapping in the mutant pool of *pdm1*.

Candidate intervals of *pdm1-6* obtained from the interval mapping module were subjected to the candidate variant mapping module, and a candidate gene list was generated. Four genes on the candidate list were further verified to be the causative genes for the paternal defects (detailed information see Table S3.2.), and they will be described below.

3.2.4 Identification of causative variants in known paternal genes

We identified the causative variants for the *pdm1* and *pdm2* which reside in pollen genes that have been characterized during fertilization in previous literature. These mutant alleles will be briefly described in this subsection.

A reading frameshift mutation caused by a single thymine deletion in the coding sequence of *HAP2* on chromosome 4 (Chr. 4) was found in mutant *pdm1* (hereafter referred to as *hap2-3/+*, Figure 3.4 A). The known *HAP2* mutant allele, *hap2-2/+*, was used as a control to confirm the causative mutation (von Besser et al. 2006). The mutant *hap2-3/+* showed a reduced seed set rate in self-crossed siliques (68.80% ± 10.38% b), which is similar to the self-crossed seed set rate of *hap2-2/+* (65.48% ± 10.49% b). When crossed to WT as the pollen donor, *hap2-3/+* showed reduced paternal fertility with a seed set rate of 62.12% ± 6.80% b (vs 93.73% ± 4.00% a in WT) (Figure 3.4 C). WT ovules fertilized by *hap2-3/+* pollen 24 HAP were dissected out and stained with Renaissance staining. It was observed that in some ovules more than one pollen tube entered the micropyle, which is referred to as polytubey. Polytubey occurred with an elevated frequency of 32.21% ± 6.00%, whereas the frequency derived from WT pollen was 9.06% ± 3.82%.

To characterize the cause of the paternal-induced polytubey phenotype in *hap2-3/+*, Rainbow Pollen marker (RbP) was introduced into *hap2-3/+*. The resulting mutant was crossed to Rainbow Female Gametophyte marker (RbFG) and ovules at 24 HAP were dissected out and stained with Renaissance staining for microscopy. As shown in Figure 3.4 B, the vsfGFP-0 signal on the egg cell membrane was still observable, suggesting that the egg cell failed in fertilization. The absence of the mScarlet signal in the synergid cells suggests that the maternal machinery for fertilization recovery was activated, which was proved by the arrival of the second pollen tube. The sperm cells were attached to the egg cell membrane, and the colocalization of the mRuby2 signal on the sperm membrane and MGH3-NeonGreen in the sperm nuclei indicated a failure in plasmogamy. These phenotypes resembled the gamete fusion

defects of mutants with disrupted *HAP2* as described previously (Beale, Leydon, and Johnson 2012; von Besser et al. 2006). To confirm that the single thymine deletion in HAP2 was the cause of the reduced paternal fertility of *pdm1*/*hap2-3*/+, a rescue assay was performed by introducing HAP2-mScarlet into *hap2-3*/+. The resulting lines restored the fertility defect, producing a replete seed set in the self-crossed siliques (Figure 3.2 C, D). Taken together, *pdm1*/*hap2-3*/+ harbors a single thymine deletion in *HAP2* and represents a newly discovered *hap2* allele that produces defective pollen giving rise to gametic fusion failure.

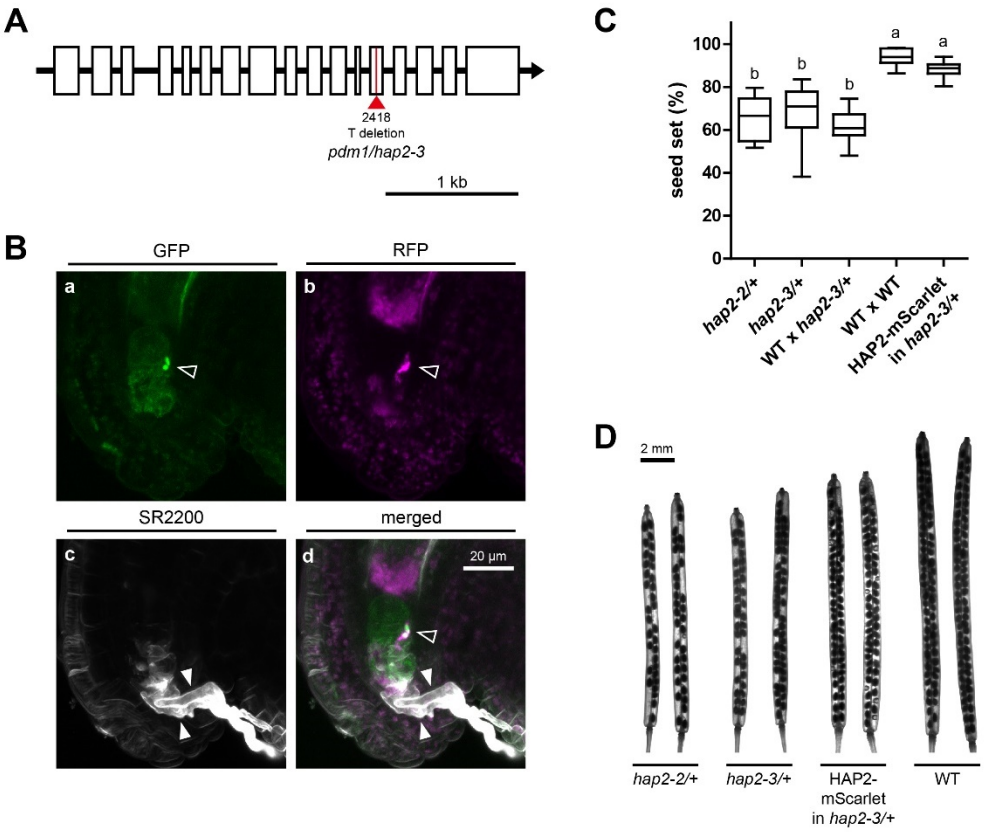

Figure 3.4 Phenotypic analysis of *pdm1* and its rescue line. (A) The causative variant of *pdm1* is a frameshift deletion located in *HAP2* (hereafter referred to as *hap2-3*/+). Boxes indicate exons, arrow indicates gene direction, red line indicates the deletion mutation, and numbers below indicate the nucleotide position. **(B)** SR2200 staining of Rainbow Female Gametophyte (RbFG, expressing *proEC1.2en-EC1.1:myr-vsfGFP-0* and *proMYB98:mTP-mScarlet*) ovules fertilized by *pdm1* pollen labeled by Rainbow Pollen marker (RbP, expressing *proHTR12:HTR12-mCherry*, *proMGH3:MGH3-NeonGreen* and *proDAZ3:myr-mRuby2*) at 24 HAP. (a) GFP channel detecting vsfGFP-0 on the membrane of the unfertilized egg cell and NeonGreen in the sperm nuclei. (b) RFP channel detecting mScarlet in the synergid mitochondria, mRuby2 on the sperm membrane, and mCherry on the sperm centromeres. (c) DAPI channel detecting SR2200 signal on the cell perimeter. (d) Merged image of all the channels. White arrowheads indicate the arrival of two pollen tubes, hollow arrowheads indicate the unfused sperm cells. **(C)** Seed set rate of *hap2-2*/+, *hap2-3*/+ and the rescue line HAP2-mScarlet in *hap2-3*/+. Letters above boxes refer to individual groups in a one-way ANOVA with a post hoc Tukey test ($p < 0.05$). **(D)** Cleared siliques of *hap2-2*/+, *hap2-3*/+, and the rescue line HAP2-mScarlet in *hap2-3*/+.

Our mapping method is capable of detecting multiple mutations as we were able to show in mutant *pdm2*. Two segregation distortions were detected on Chr. 2 and Chr. 3 in mutant *pdm2*,

and G-to-A mutation in the coding regions of *CALLOSE SYNTHASE 5* (*CALS5*) and *COBRA-LIKE PROTEIN 10* (*COBL10*) were found on Chr. 2 and Chr. 3, respectively (Figure 3.5 A, B). These two mutant alleles are named *cals5-6* and *cobl10-5* after the existing alleles. In order to verify the causative mutations by rescue assay, two fluorescent protein-tagged rescue cassettes expressing *CALS5-mScarlet* and *COBL10-YPet* driven by their native promoters were introduced into WT and were further introgressed into mutants by crossing. The rescue lines exhibited decent fluorescent signals in WT, with both CALS5-mScarlet and COBL10-YPet visible in the vegetative cell of mature pollen (Figure 3.5 C). *CALS5* is required for exine wall formation of pollen grains, pollen tube wall deposition, and callose plug formation in an elongating pollen tube (Dong et al. 2005; Abercrombie et al. 2011). In line with this, the glutamic acid-to-lysine mutation in the glucan synthase domain at position 1662 of the amino acid sequence of CALS5 in *cals5-6* led to abolished pollen development, which is similar to that in the T-DNA allele *cals5-2* as indicated by Alexander staining in Figure 3.5 D, suggesting that this single amino acid plays a major role in its protein function. Introducing CALS5-mScarlet into *cals5-6* rescued the pollen development defect and produced healthy-looking pollen grains inside the anther (Figure 3.5 D). The causative gene on Chr.3, *COBL10*, is known to mediate directional pollen tube growth (Sha Li et al. 2013). Correspondingly, the observed threonine-to-isoleucine mutation at position 169 of the amino acid sequence of COBL10 in *cobl10-5/+* caused malfunction of the pollen tube, leading to a reduced seed set rate in self-crossed siliques (58.35% ± 7.11% c), which was even lower than the seed set rate of the T-DNA allele *cobl10-2/+* (72.49% ± 14.63% b). The seed abortion was observed primarily in the basal part of the siliques in *cobl10-5/+*, which mirrored the seed set pattern in *cobl10-2/+* (Figure 3.5 F), reinforcing its role in pollen tube growth and directional guidance. Introducing COBL10-YPet into *cobl10-5* restored the seed set defect in the self-crossed siliques, giving out a seed set rate of 92.32% ± 2.18% a (vs 94.39% ± 3.47% a in WT) (Figure 3.5 E), reassuring that *COBL10* was the causative gene for the malfunctioned pollen.

These causative mutations in genes with known functions demonstrate that our mapping method is capable of mapping both single and multiple EMS-induced mutations in the *Arabidopsis* genome. A novel paternal candidate gene derived from this mapping method will be presented in the following subsection.

3.2.5 *SAHH2* is a novel paternal gene in pollen tube guidance

Segregation distortion was observed on Chr. 3 in *pdm3* (Figure 3.6 A), and a C-to-T transition mutation caused a glycine-to-serine mutation at position 25 in the amino acid

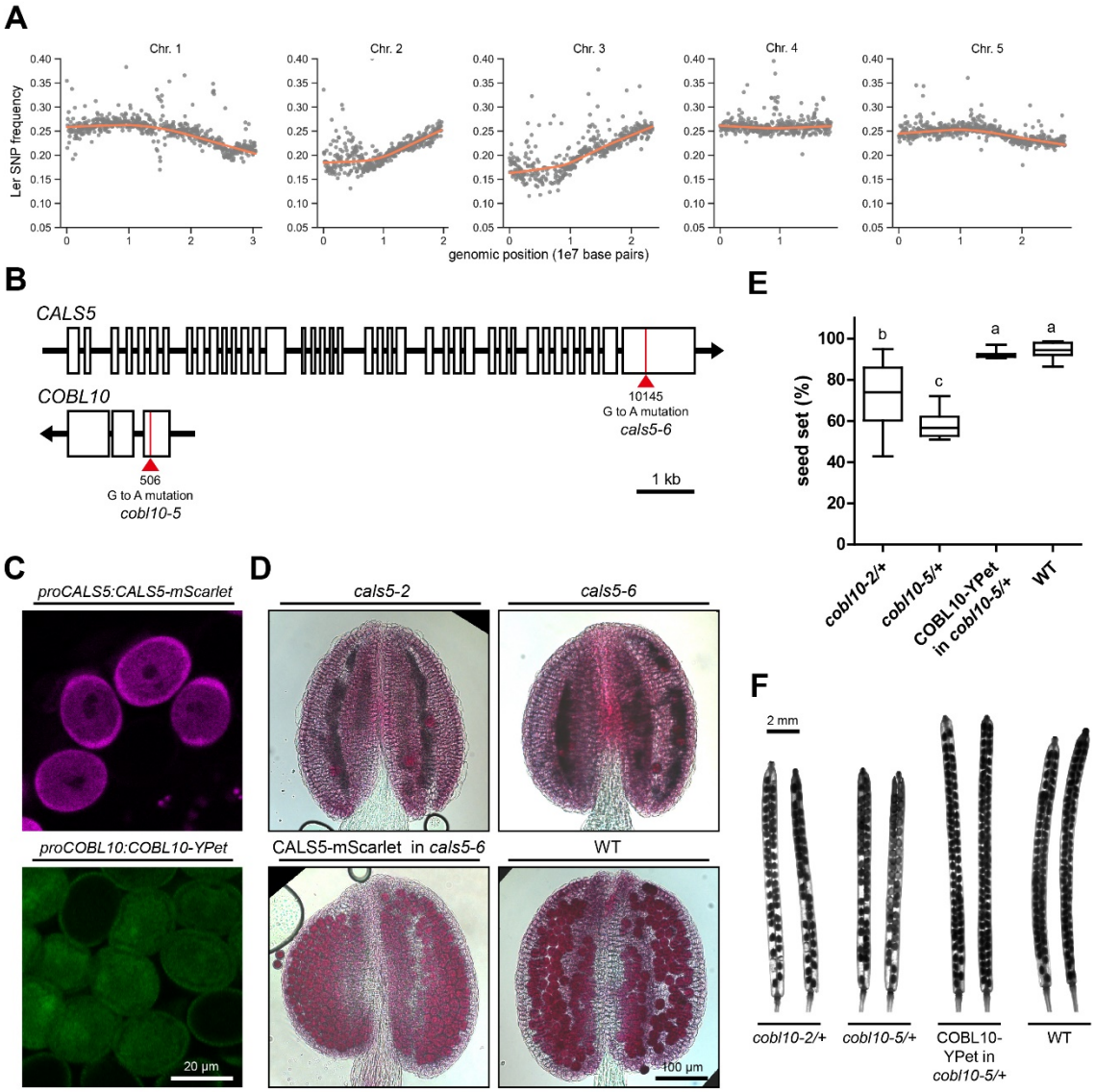

Figure 3.5 Phenotypic analysis of *pdm2* and its rescue lines. (A) Ler SNP frequency plot of *pdm2* OC2. The five panels represent five chromosomes. Each grey dot indicates the average frequency per 50 kb. Orange lines indicate LOWESS (locally weighted scatterplot smoothing) regression lines fitted to the plots. Significant Ler SNP frequency distortions were observed on Chr. 2 and Chr. 3. **(B)** The causative variants of *pdm2* located in *CALS5* and *COBL10* (hereafter referred to as *cals5-6* and *cobl10-5*, respectively). Boxes indicate exons, arrows indicate gene direction, red lines indicate the mutations, and numbers below indicate nucleotide positions. **(C)** Expression of *CALS5-mScarlet* and *COBL10-YPet* in mature pollen driven by their native promoters. **(D)** Alexander staining of anthers of *cals5-2*, *cals5-6*, and the rescue line CALS5-mScarlet in *cals5-6* before anthesis. **(E)** Seed set rate of *cobl10-2*/+, *cobl10-5*/+, and the rescue line COBL10-YPet in *cobl10-5*/+. Letters above boxes refer to individual groups in a one-way ANOVA with a post hoc Tukey test ($p < 0.05$). **(F)** Cleared siliques of *cobl10-2*/+, *cobl10-5*/+, and the rescue line COBL10-YPet in *cobl10-5*/+.

sequence of the novel paternal gene, S-adenosyl-L-homocysteine hydrolase 2 (SAHH2), was identified, which is referred to as *sahh2-1* hereafter. SAHH2 is a key enzyme for the maintenance of cellular transmethylation potential (C. H. Li et al. 2008), however, its role in fertilization remains unknown. Three additional loss-of-function mutant alleles each carrying a

T-DNA insertion in the *SAHH2* gene locus, *sahh2-2*, *sahh2-3*, and *sahh2-4*, were used to support the functional characterization of *SAHH2* in fertilization (Figure 3.6 B).

It has been shown that SAHH2 fused to a β-glucuronidase (GUS) was specifically expressed in anthers of the floral organ (C. H. Li et al. 2008). To investigate the expression pattern of *SAHH2* inside the male gametes, a reporter cassette expressing *proSAHH2:SAHH2-YPet* was introduced into WT. The fluorescent signal was observed in both the vegetative cytoplasm and the vegetative nuclei, whereas the signal was missing in sperm cells (Figure 3.4 C panel a). The expression of *SAHH2* in fertilization was investigated by pollinating WT pistil with pollen from the reporter line. A distinct SAHH2-YPet signal was observed in the pollen tube at the micropyle at 24 HAP, suggesting *SAHH2-YPet* was expressed during the whole process of pollen tube growth and reception (Figure 3.4 C panel b-c).

Male fertility was reduced in the *sahh2* alleles. When crossed to WT as pollen donors, *sahh2-1*, *sahh2-2*, *sahh2-3*, and *sahh2-4* all exhibited reduced paternal fertility, displaying seed set rate of 65.46% ± 17.55% b in *sahh2-1*, 67.22% ± 10.17% b in *sahh2-2*, 63.81% ± 15.49% b in *sahh2-3*, and 65.47% ± 10.95% b in *sahh2-4*, while the seed set rate derived from WT pollen was 94.10% ± 3.16% a. (Figure 3.6 D). To check the maternal fertility of *sahh2-2*, WT pollen was pollinated to *sahh2-2* and the seed set was checked at 3 DAP. The resulting seed set (91.00% ± 4.10% a) showed no difference from WT, suggesting that maternal fertility of *sahh2-2* was not affected. The seed abortion was primarily observed in the basal part of the siliques as shown in Figure 3.6 E. Compromised pollen viability would be a possible reason for reduced fertilization in siliques. Therefore, Alexander staining was used to check pollen viability. The staining results demonstrated that all four mutant alleles produced viable pollen with a healthy appearance (Figure S3.1). To investigate if the aborted seeds in the basal part were caused by failed pollen tube attraction to ovules, *sahh2-1* and *sahh2-2* pollen were crossed to WT pistil, and the growth of pollen tubes inside the transmitting tract inside the pistils at 24 HAP was indicated by aniline blue staining, which stains callose on the pollen tube wall (Figure 3.6 F). A comparable amount of *sahh2-1*, *sahh2-2,* and WT pollen germinated on the stigma, suggesting that pollen germination was not affected. However, only a few pollen tubes of *sahh2-1* and *sahh2-2* were observed in the lower half of the transmitting tract, leaving most of the ovules in the basal part unfertilized. In contrast, a considerable number of WT pollen tubes penetrated down the transmitting tract to the bottom of the pistil. These observations are suggesting that the reduced pollen tube growth in the female transmitting tract was the main cause of the seed abortion in the basal part of the siliques.

A rescue assay was conducted to verify the causative gene. The functional reporter cassette

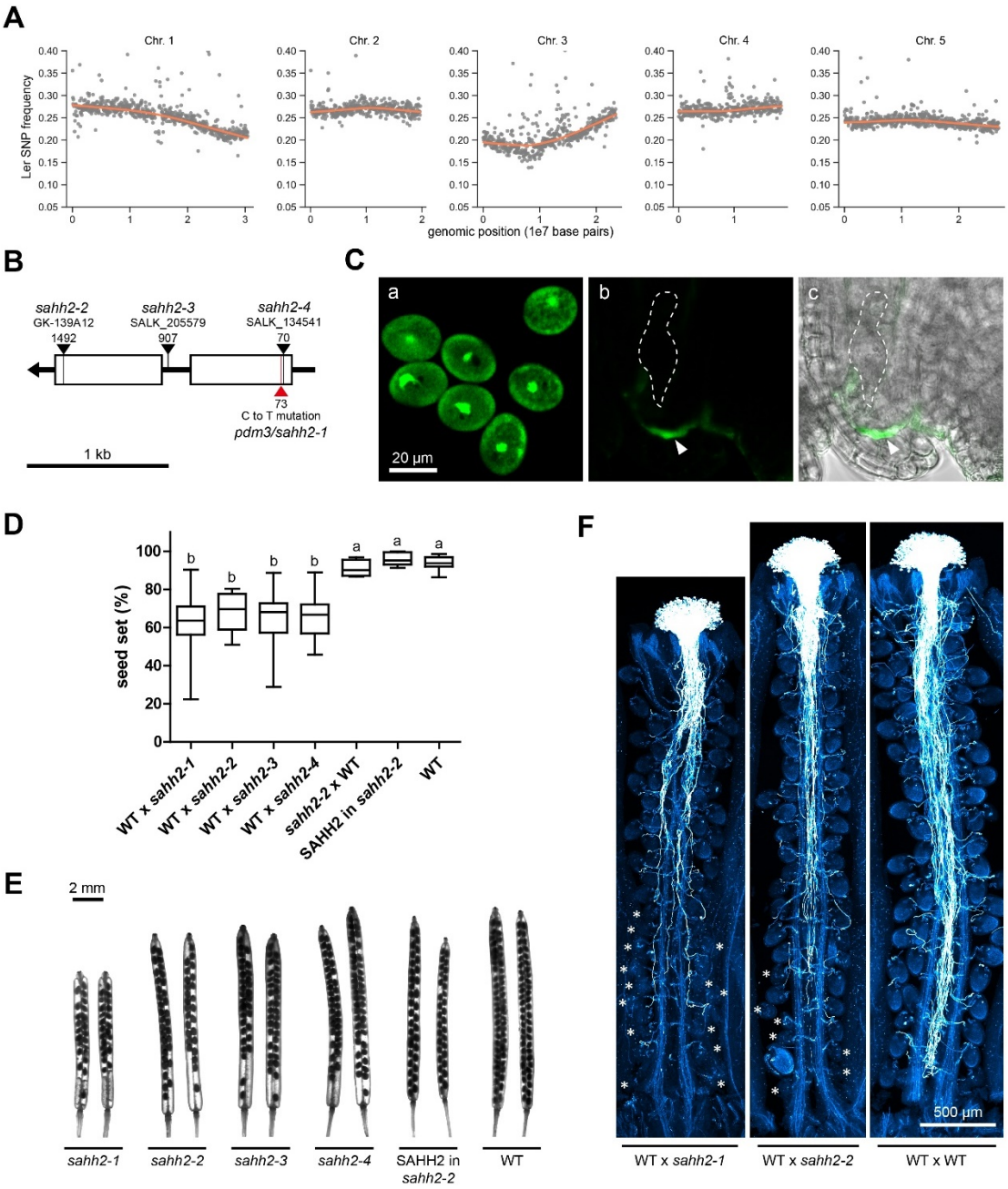

Figure 3.6 Phenotypic analysis of *pdm3*, its T-DNA insertion alleles, and rescue lines. (A) Ler SNP frequency plot of *pdm3* OC2. The five panels represent five chromosomes. Each grey dot indicates the average frequency per 50 kb. Orange lines indicate LOWESS (locally weighted scatterplot smoothing) regression lines fitted to the plots. Significant Ler SNP frequency distortions were observed on Chr. 3. **(B)** The causative variant of *pdm3* located in *SAHH2* (hereafter referred to as *sahh2-1*). Boxes indicate exons, arrow indicates gene direction, red line indicates the causative mutation, black lines indicate T-DNA insertion sites of the T-DNA insertion alleles, and numbers indicate nucleotide positions. **(C)** Expression of *SAHH2-YPet* driven by its native promoter. (a) Signal of SAHH2-YPet was observed in the vegetative cells and vegetative nuclei of mature pollen. (b) Signal of SAHH2-YPet was observed in the pollen tube at the micropyle in the WT ovule pollinated by pollen expressing *proSAHH2:SAHH2-YPet* at 24 HAP. (c) Merged image of YPet channel and bright field channel of the ovule in (b). Pollen tubes are indicated by arrowheads. The early zygotes are outlined by dashed lines. **(D)** Seed set rate of *sahh2-1*, *sahh2-2*, *sahh2-3*, and *sahh2-4* crossings and the rescue line. Letters above boxes refer to individual groups in a one-way ANOVA with a post hoc Tukey test ($p < 0.05$). **(E)** Cleared siliques of *sahh2-1*, *sahh2-2*, *sahh2-3*, *sahh2-4*, and the rescue line. **(F)** Aniline staining image of *sahh2-1* and *sahh2-2* pollen tubes in WT pistils at 24 HAP. WT pollen was adopted as a control. Asterisks indicate ovules without pollen tube arrival.

expressing *proSAHH2:SAHH2-YPet* failed to restore the fertility defects in both *sahh2-1* and *sahh2-2* (data not shown). Whereas introducing the tag-free rescue cassette expressing *proSAHH2:SAHH2* into *sahh2-2* restored the fertility defect, producing a wild-like seed set (Figure 3.6 D, E). Thus, we assume that SAHH2 is either sensitive to C-terminal tagging, or that the additional YPet hampered its normal function in pollen.

Taken together, we identified a novel pollen gene, *SAHH2*, involved in paternal fertility regulation. It is expressed in the vegetative cell of pollen, and the loss-of-function mutants show reduced male fertility with defective pollen tube guidance in the transmitting tract.

3.2.6 Potential causative genes for further study

The mutants *pdm4*, *pdm5,* and *pdm6* demonstrated paternal defects in pollen tube reception, embryo development, and endosperm proliferation, respectively. Here, the phenotypic characterization, mapping results, and potential candidate variants are described.

The mutant *pdm4* showed reduced fertility when crossed to WT as a pollen donor, resulting in a seed set rate of 70.03% ± 12.54% (vs 94.19% ± 3.20% in WT) (Figure 3.7 A). Seed abortion occurred early after fertilization without ovule expansion. To further investigate the cause of failed fertilization, *pdm4* pollen was crossed to the RbFG marker, and ovules at 24 HAP were

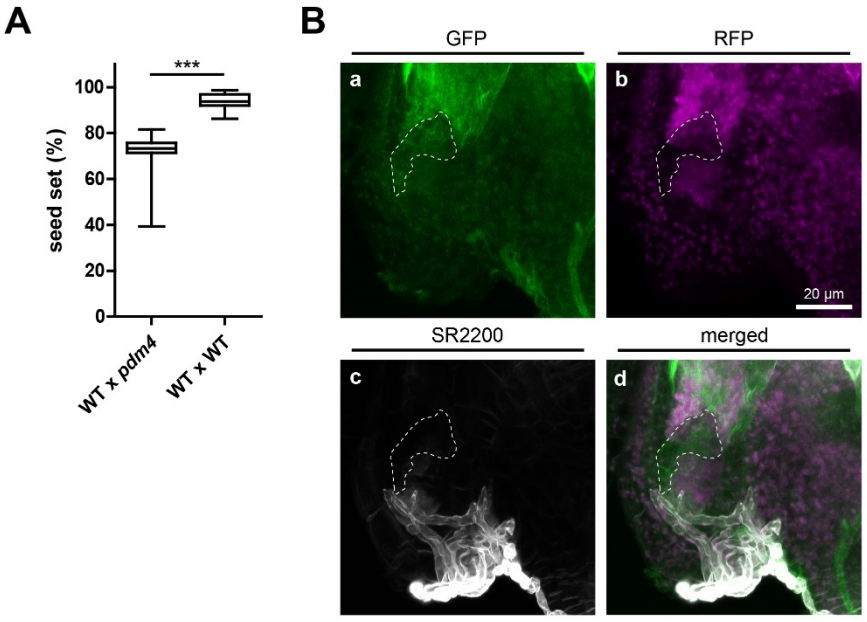

Figure 3.7 Phenotypic analysis of *pdm4*. (A) Seed set rate of *pdm4* crossed to WT as a pollen donor. ***: P<0.001, Student's t-test. **(B)** SR2200 staining of the Rainbow Female Gametophyte (RbFG, expressing *proEC1.2en-EC1.1:myr-vsfGFP-0* and *proMYB98:mTP-mScarlet*) ovules fertilized by *pdm4* pollen at 24 HAP. (a) GFP channel detecting vsfGFP-0 on the membrane of the unfertilized egg cell. (b) RFP channel detecting mScarlet in the synergid mitochondria. (c) DAPI channel detecting SR2200 signal on the pollen tube perimeter. (d) Merged image of all the channels. The unfertilized egg cell is outlined by dashed lines. *pdm4* pollen tubes lost directional guidance at micropyle of ovules.

dissected out and stained by SR2200. Pollen tube arrival was observed in the majority of the ovules, suggesting that ovular pollen tube guidance was not affected. However, in these ovules showing fertilization failure, pollen tubes lost directional guidance and showed random overgrowth at the micropyle (Figure 3.7 B). Taken together, *pdm4* shows a paternal-derived defect in pollen tube reception at the micropyle.

The mutant *pdm5* produced a reduced seed set when crossed to WT as a pollen donor. The resulting siliques showed a seed set rate of 76.30% ± 16.07% (vs 94.19% ± 3.20% in WT) (Figure 3.8 A) with aborted seeds randomly distributed in the siliques. To characterize the fertilization defects, WT ovules fertilized by *pdm5* pollen were dissected out, cleared by Hoyer's solution, and imaged by DIC microscopy (Figure 3.8 B). At 1 DAP, when the WT-like embryo was at the one-cell stage (Figure 3.8 B panel d), the development of zygotes in the defective ovules was delayed and remained not elongated (Figure 3.8 B panel a-c). At 2 DAP, the WT-like embryo reached the 8-cell stage (Figure 3.8 B panel h), whereas the defective

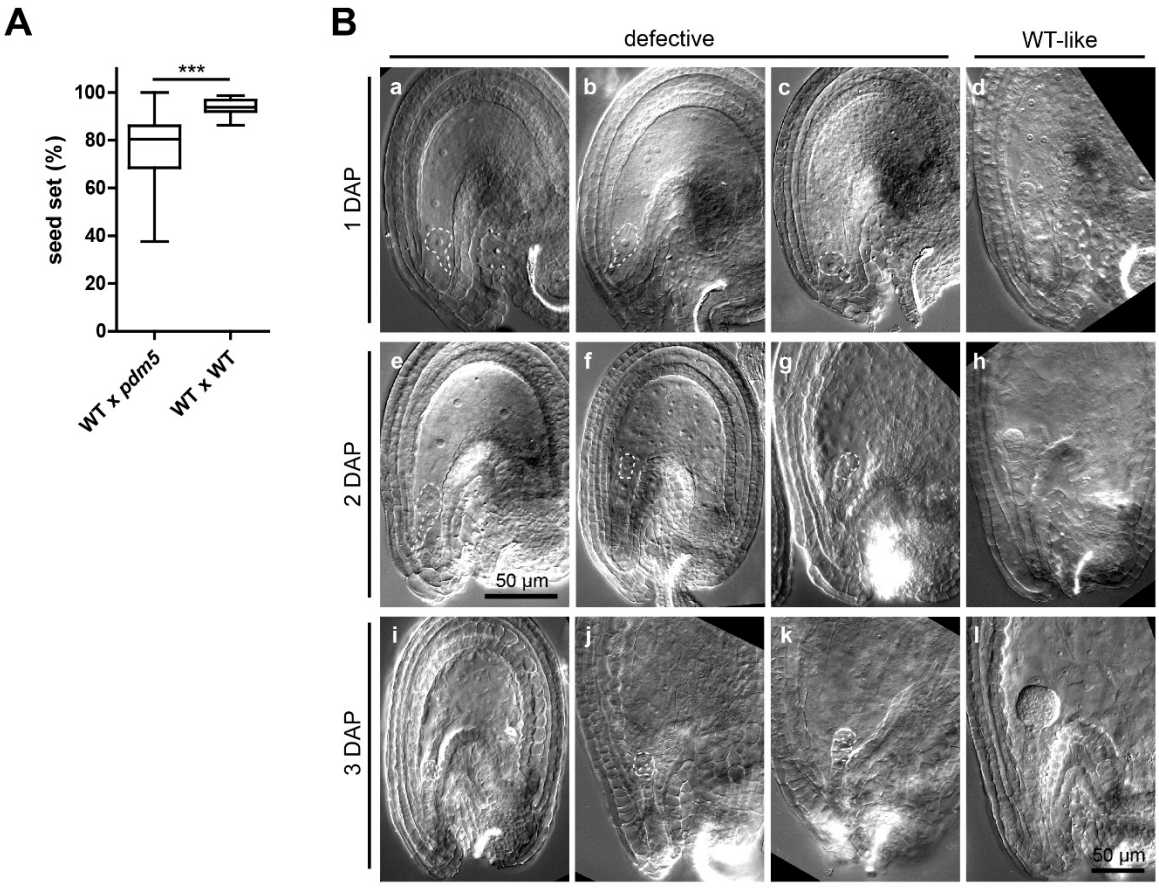

Figure 3.8 Phenotypic analysis of *pdm5*. (A) Seed set rate of *pdm5* crossed to WT as a pollen donor. ***: P<0.001, Student's t-test. **(B)** Hoyer's solution clearing and DIC imaging of WT ovules fertilized by *pdm5* pollen at 1 DAP (a-d), 2 DAP (e-h), and 3 DAP (i-l). Delayed embryo development and aberrant cell divisions are outlined by dashed lines. Panel a-e and panel f-l share the same scale bar, respectively. Embryo development was delayed and aberrant cell divisions were observed in ovules fertilized by *pdm5* pollen.

ovules were at the elongated zygote stage or one-cell stage (Figure 3.8 B panel e-f), and oblique embryonic cell division was also observed (Figure 3.8 B panel g). At 3 DAP, the WT-like embryo reached the globular stage (Figure 3.8 B panel h), while some of the defective ovules exhibited a smaller size with embryos just finishing the first cell division of the embryo proper (Figure 3.8 B panel i). The other defective ovules expanded to the size of WT but showed irregular cell divisions in the embryos (Figure 3.8 B panel j-k). In summary, *pdm5* exhibited paternal-induced embryo development delay and aberrant cell division in the embryos.

The mutant *pdm6* showed reduced fertility when crossed to WT as a pollen donor, resulting in a seed set rate of 73.24% ± 18.21% (vs 94.19% ± 3.20% in WT) (Figure 3.9 A). Seed abortion occurred early after fertilization, and the arrested ovules exhibited shriveled integuments. To characterize embryo development after fertilization, WT ovules fertilized by *pdm6* pollen at 3 DAP were dissected out, cleared by Hoyer's solution, and imaged by DIC microscopy. At 3 DAP, the wild-like ovule was at the globular stage (Figure 3.9 B panel d), while in the defective ovules, endosperm proliferation was compromised (Figure 3.9 B panel a-c). The lacking of endosperm development was presumably the reason for the shriveled integuments. In addition,

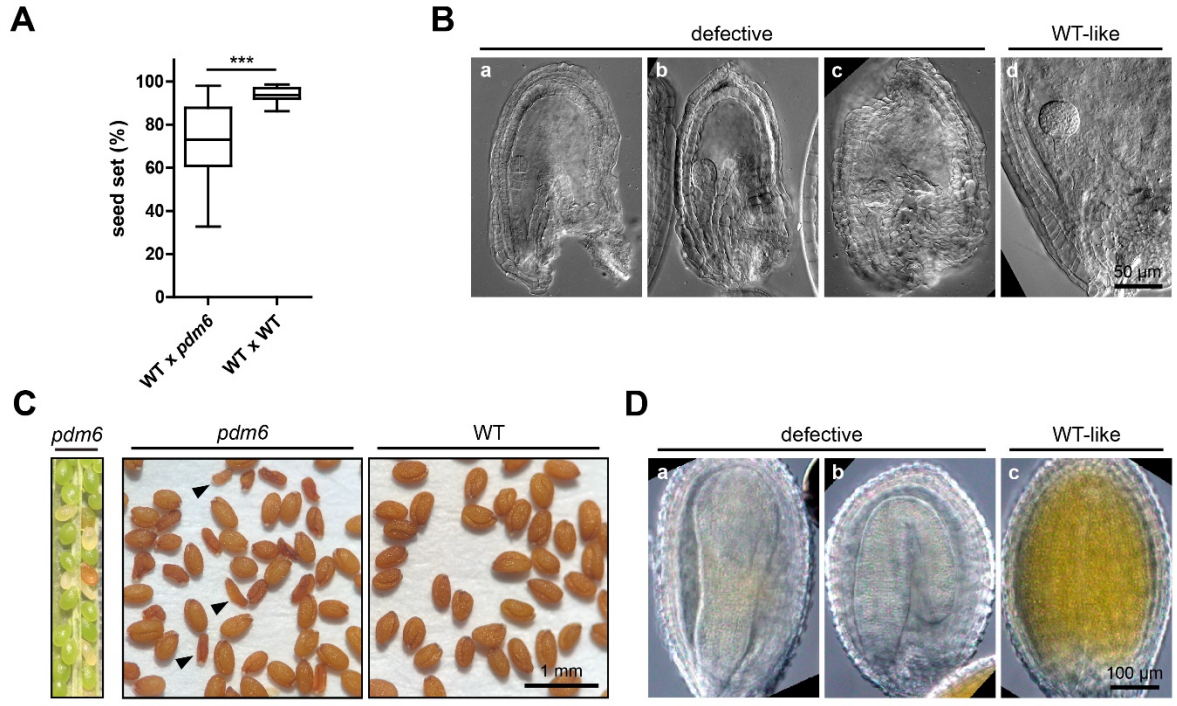

Figure 3.9 Phenotypic analysis of *pdm6*. (A) Seed set rate of *pdm6* crossed to WT as a pollen donor. ***: P<0.001, Student's t-test. **(B)** Hoyer's solution clearing and DIC imaging of WT ovules fertilized by *pdm6* pollen at 3 DAP. **(C)** Albino seeds were observed in *pdm6* self-crossed siliques and they showed a wizened appearance at the mature stage. Some of the aberrant seeds are indicated by black arrowheads. **(D)** Hoyer's solution clearing and DIC imaging of albino seeds from *pdm6* self-crossed siliques at mature green stage. Endosperm development was compromised in ovules fertilized by *pdm6* pollen, and *pdm6* produced aberrant seeds with arrested embryos when self-crossed.

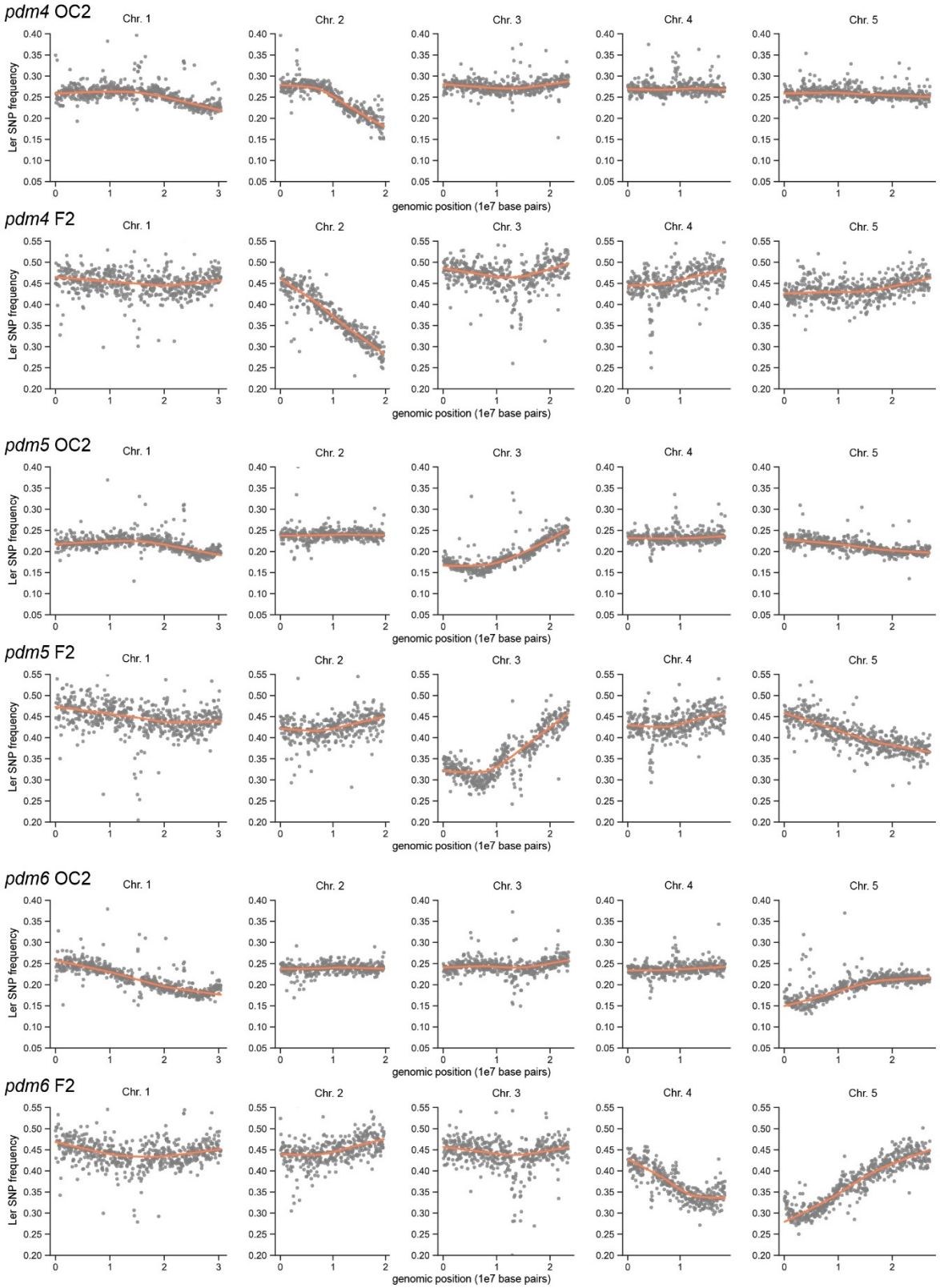

Figure 3.10 Mapping results for OC2 and F2 populations of *pdm4*, *pdm5*, and *pdm6*. Ler SNP frequency plots of OC2 and F2 populations of *pdm4*, *pdm5*, and *pdm6*. The five panels per row represent five chromosomes. Each grey dot indicates the average frequency per 50 kb. Orange lines indicate LOWESS (locally weighted scatterplot smoothing) regression lines fitted to the plots. Ler SNP frequency distortions were observed on Chr. 2 in both *pdm4* OC2 and *pdm4* F2; Chr. 3 in both *pdm5* OC2 and *pdm5* F2; Chr. 5 in both *pdm6* OC2 and *pdm6* F2, and additional Ler SNP frequency distortion was observed on Chr. 4 in *pdm6* F2.

pdm6 produced albino seeds in the self-crossed siliques, resulting in aberrant seeds with a wizened shape at the mature stage (Figure 3.9 C). The embryo development was checked in these albino seeds by Hoyer's solution clearing and DIC microscopy. At the green mature stage, the WT-like embryo turned green and the cotyledons bent (Figure 3.9 D panel c). While in the albino seeds, embryos stayed colorless and displayed defects in cotyledon bending (Figure 3.9 D panel a). Some cotyledons bent to the side (Figure 3.9 D panel b) but were still much shorter than the WT-like embryo. Taken together, *pdm6* pollen is defective in fertilizing the central cell, resulting in a compromised endosperm, and an additional recessive mutation in *pdm6* causes late-stage embryo arrest.

The mapping results revealed segregation distortions in the OC2 and F2 mapping populations of the three mutants mentioned above (Figure 3.10). The segregation distortion for *pdm4*, *pdm5,* and *pdm6* was on the right arm of Chr. 2, the left arm of Chr. 3, and the left arm of Chr. 5 in both OC2 and F2, respectively. Additional segregation distortion was found on the right arm of Chr. 4 in *pdm6* F2, which might be derived from a recessive mutation in the genome. Stretched plots were drawn and linear regression lines were drawn to help define the causative intervals of these chromosomes with segregation distortions (Figure 3.11). Based on this, a causative interval of 2 Mb was selected for causative variant mapping in *pdm4* (Chr. 2: 18-20 Mb), *pdm5* (Chr. 3: 6-8 Mb), and *pdm6* (Chr. 4: 13-15 Mb; Chr. 5: 2-4 Mb).

A candidate variant list was generated by the causative variant mapping module with F2 as an input (Table 3.1). The G-to-A mutation with the SNP effect of "stop gained" was identified

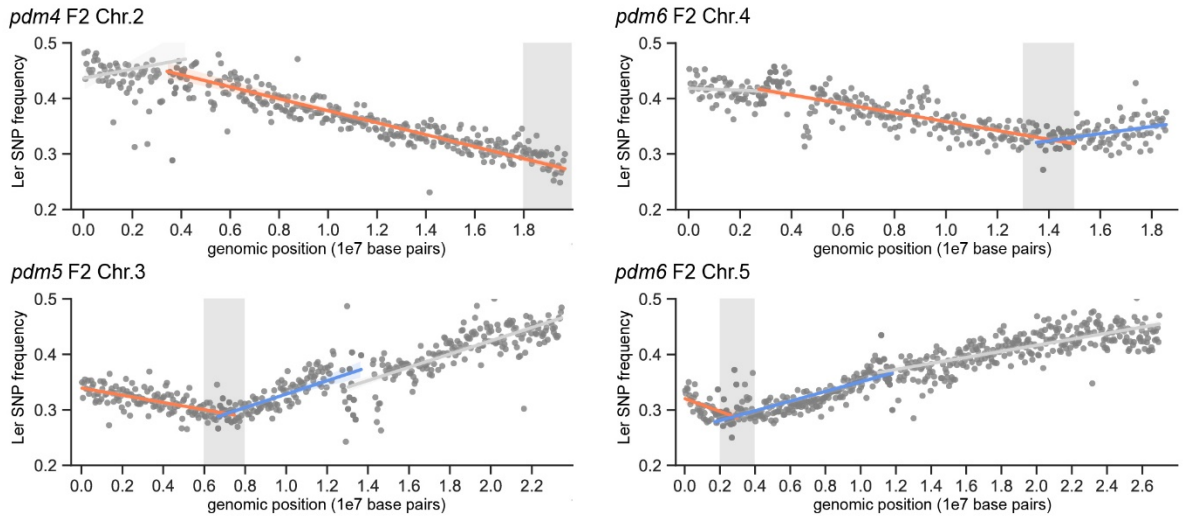

Figure 3.11 Candidate intervals and candidate variants for *pdm4*, *pdm5*, and *pdm6*. Stretched Ler SNP frequency plots of Chr. 2 in *pdm4* F2, Chr. 3 in *pdm5* F2, Chr. 4 and Chr.5 in *pdm6* F2. Each grey dot indicates the average frequency per 50 kb. Linear regression lines were fitted to the distorted chromosome arm from the left side (indicated by the orange line) and the right side (indicated by the blue line), leaving the other chromosome arm aside (indicated by the grey line). Grey shadows indicate the 2-Mb candidate intervals.

in the candidate interval on Chr. 4 in *pdm6*. The mutation locates in a WD repeat protein-encoding gene *TANMEI/EMB2757* (*TAN*) required for embryo development. The T-DNA allele *tan-1* displayed similar albino seeds with embryonic lethality as described previously (Yamagishi et al. 2005). Thus, we presume that *TAN* is the causative gene for the segregation distortion on Chr. 4 in *pdm6*. The potential causative genes responsible for these above-described intriguing phenotypes in *pdm4*, *pdm5,* and *pdm6* still need to be further investigated.

Table 3.1 The candidate variant list for *pdm4*, *pdm5*, and *pdm6*

Mutant	SNP position	Reference	Variant	SNP effect	Gene	Other name
pdm4	Chr. 2:19077275	G	A	missense variant	AT2G46480	*GAUT2*
	Chr. 2:19570391	G	A	missense variant	AT2G47780	*LDAP2*
pdm5	Chr. 3:6764304	AGTCGGGG	AGTTGGGC	missense variant	AT3G19510	*HAT3.1*
	Chr. 3:7046790	C	T	missense variant	AT3G20190	*PRK4*
	Chr. 3:7403856	C	T	missense variant	AT3G21110	*PUR7*
pdm6	Chr. 4:13846064	CTTCC	CTCC	frameshift variant	AT4G27760	*FEY*
	Chr. 4:14108366	G	A	splice donor variant & intron variant	AT4G28540	*CKL6*
	Chr. 4:14278822	G	A	missense variant	AT4G28950	*ROP9*
	Chr. 4:14503107	G	A	missense variant	AT4G29550	
	Chr. 4:14604550	G	A	stop gained	AT4G29860	*TAN*
	Chr. 5:1572305	C	T	missense variant	AT5G05310	
	Chr. 5:3040955	C	T	missense variant	AT5G09790	*ATXR5*
	Chr. 5:3248371	G	A	stop gained	AT5G10330	*HPA1*

3.3 Discussion

3.3.1 The novel mapping-by-sequencing method enables the identification of paternal-defective mutations

Whole-genome sequencing-based bulked-segregant analysis has been widely utilized in revealing mutations in forward genetic screens. It requires crossing of a mutant to a WT plant in a different genome background as a reference and isolation of homozygous individuals for sequencing. Sequencing enables the identification of a candidate interval with a decreased reference allele frequency and the causative variation with a frequency of 100% in the candidate interval (Schneeberger et al. 2009). However, the classic bulked-segregant analysis is not applicable to map gametophyte lethal mutations, since it is impossible to obtain homozygotes. Therefore, SNP-ratio mapping is used in mapping lethal mutations, which discriminates background variation from causal mutations thus identifying a genomic region that contains the causative (Lindner et al. 2012). Based on the SNP-ratio mapping, we tailored a semi-high throughput mapping-by-sequencing method specific for paternal-defective mutations. The

bottleneck for mapping these paternal-defective mutations lies in the phenotypic analysis of the difficult-to-score phenotypes. To isolate enough mutant individual plants with fertilization defects in the F2 population for pooling, a series of laborious work is required, such as pollination of WT plants with mutant pollen and clearing and/or staining-based microscopy.

To address this limitation, we leveraged the paternal lethality of the mutants to do the phenotype sorting. The heterozygous F1 is obtained by pollinating mutants in Ler with Col-0 pollen. Phenotyping work in the whole mapping process is only required at this step to select a single mutant in F1. In principle, the mutation segregates by 1:1 in F1, so, one mutant plant should be easily obtained in every two plants. This F1 mutant is either self-crossed to generate F2 or outcrossed to Col-0 as a pollen donor to generate OC2. In the resulting F2, the causative variant segregates by 1:3 while the phenotype-unlinked variants segregate by 1:1. In the resulting OC2, the causative variant is fully ruled out and the phenotype-unlinked variants segregate by 1:3. These discriminations in SNP-ratio of the causative variant and the unlinked variants allow the identification of a candidate interval.

Since F2 possesses both segregation distortion as in OC2 and causative variant as in M, we compared the mapping efficiency between OC2 and F2 in candidate interval mapping. More Ler SNPs were identified in F2 than in OC2, and the Ler SNPs positions in F2 showed a relatively more even distribution, which offers a better data basis for a less-noisy plot with a clearer tendency (Figure 3.3 B-C). This is probably due to the limited sequencing coverage (35-fold on average in *pmd1* OC2), which makes it impossible to distinguish variants with a frequency lower than 2.86% that are co-selected with the causative variant. In contrast to this, a 1:3 SNP ratio is easily distinguished in F2 with similar coverage (29-fold on average in *pmd1* F2). However, a self-crossed population may generate additional segregation distortions, such as the additional segregation distortion on the Chr. 4 in *pmd6 F2* (Figure 3.10), due to some other possibly existing recessive mutations or sporophytic mutations, which would tremendously hinder defining the candidate interval. Therefore, combining OC2 with F2 is necessary to achieve efficient and precise mapping. Furthermore, F2 serves better as a mutant pool than M in causative variant mapping, even though they share the same causative variant ratio of 1:3. One needs to be careful when applying candidate intervals identified in the Col genome to M in Ler genome for causative variant mapping, considering the existence of genome position difference and large-scale inversions. F2 allows interval mapping and variant mapping using Col as a reference in the same sequencing dataset, which is accurate and time-saving. Thus, using a combination of F2 and OC2 is recommended. Tools involved in this mapping method are all well-developed and widely used, and data analysis does not require

advanced statistical methods.

With this method, we identified 8 candidate intervals in 19 mutants. Reasons for some mutants showing no segregation distortions might be (i) these are epigenetic alleles with no difference on a sequence level; (ii) these are mutations on a chromosome level such as large-scale inversions which cannot be detected by short-reads sequencing; (iii) the paternal penetrance of the mutations is partially abolished when crossed to Col; (iv) or simply mistakes during F1 phenotyping. Segregation distortion was observed on Chr. 2 in *pmd7* OC2 but absent in *pmd7* F2, which is presumably caused by the instability of the mutant defect, such as high sensitivity to environmental factors or poor heritability. The additional segregation distortion observed on Chr. 4 in *pmd6* F2 suggests that recessive mutations causing abolished fertility could also be detected using this mapping method. Candidate variants were mapped in the 6 candidate intervals related to paternal defects in fertilization. With the assistance of SNP effect prediction and available transcriptome data of pollen and sperms, the candidate number for each mutant shrank to a few (Table S3.1), which requires a low workload in confirmation of the causative gene. The detection of deletion mutations in the candidate variant mapping in *pdm1* emphasizes the need for an advanced variant detection that takes InDels into consideration since these atypical mutations can be selected in screen. Collectively, this mapping method is capable to perform semi-high throughput mapping of paternal-defective mutations with a limited workload in mapping, data analysis, and the follow-up work in causative variants confirmation. With good sequence information available, this method could also be transferred to a wide range of other easy-to-propagate species.

In this screen, among four of the identified candidate genes, three have been characterized in previous studies. These known paternal-defective genes nicely confirm our improved mapping method. A novel paternal gene *SAHH2* was revealed using the mapping method, which will be discussed in the following section. We did not reveal any novel candidate genes in ZGA as initially intended. This might be a limitation of the non-biased screen, which is not sensitive enough to capture subtle defects during the short time window of fertilization and zygotic activation. To address this question, an advanced screen method involving a sensitized background with specific markers will be required.

3.3.2 *SAHH2* is essential for preovular pollen tube guidance

In plant fertilization, pollen germinates on the stigma, and pollen tubes invade through papilla cells toward the transmitting tract, which is later attracted to ovules for gametes fusion (Johnson, Harper, and Palanivelu 2019). Pollen tubes perform tip-growth in the female

transmitting tract, and their polarity is maintained by actin microfilament dynamics, polarized Ca^{2+} gradient, and membrane vesicle trafficking (Hepler, Vidali, and Cheung 2001). Several mutants with altered pollen wall deposition showed defective preovular pollen tube guidance, such as mutations in *COBL10* (Sha Li et al. 2013) and *VGD1* (Jiang et al. 2005). In this study, we identified a novel pollen gene *SAHH2* involved in pollen tube growth in the transmitting tract. *SAHH2* encodes a key enzyme for the maintenance of cellular transmethylation potential (Rocha et al. 2005). It is expressed in the pollen vegetative cell and pollen tube (Figure 3.4 C). The loss-of-function mutants exhibited reduced male fertility with a reduced seed setting rate in the basal part of the siliques (Figure 3.4 D, E). Pollen development is not affected in the *sahh2* mutant alleles (Figure S3.1), while pollen tubes germinated from *sahh2-1* and *sahh2-2* showed reduced growth in the female transmitting tract (Figure 3.4 F), suggesting a compromised peovular pollen tube guidance.

SAHH functions in the methyl cycle as described previously (Figure 3.12, Moffatt and Weretilnyk 2001). S-adenosyl-L-methionine (SAM) is the major source of methyl groups for biological transmethylation reactions. When the methyl group of SAM is transferred to acceptors, S-adenosyl-L-homocysteine (SAH) is generated, which inhibits methyltransferases and transmethylation reactions. SAHH catalyzes SAH into adenosine (Ado) and homocysteine (Hcy) in a reversible manner. The continuous removal of the products Hcy and Ado is a prerequisite to drive the reaction toward SAH hydrolysis. The product Ado is converted into AMP by adenosine kinase (ADK), and Hcy is converted into methionine (Met), which is further

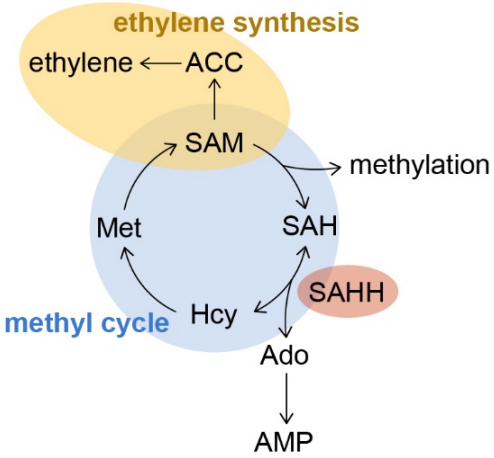

Figure 3.12 Methyl cycle and ethylene synthesis. SAM serves as a methyl donor and produces SAH after transmethylation reactions. SAHH catalyzes the repressive product SAH into Ado and Hcy in a reversible manner. Ado and Hcy are converted into AMP and Met, respective, to promote the hydrolysis reaction. Met is further salvaged by SAM synthetase which generates SAM for further transmethylation reactions. Additionally, SAM serves as substrate for ACC and ethylene synthesis (Moffatt and Weretilnyk 2001).

catalyzed by SAM synthetase into SAM for further transmethylation reactions. In addition, SAM also serves as a substrate for the synthesis of the ethylene precursor 1-aminocyclopropane-1-carboxylic acid (ACC) and ethylene (Moffatt and Weretilnyk 2001).

The two paralogues of SAHH in *Arabidopsis*, SAHH1 and SAHH2, share a 96% identity in their amino acid sequences (Rocha et al. 2005), suggesting they might have highly similar functions. The GUS-fused reporter lines showed that SAHH1 was observed in cotyledon, root, leaf, and floral organs but depleted in anthers, while SAHH2 was exclusively found in anthers, hypocotyl, and trichomes (C. H. Li et al. 2008). These exclusive expression patterns of *SAHH1* and *SAHH2* suggest that these two paralogues might diverge in expression patterns rather than in biological function.

Existing knowledge of *SAHH1* might hint at the role of *SAHH2* in pollen tube elongation. *SAHH1*, also known as *HOMOLOGY-DEPENDENT GENE SILENCING 1* (*HOG1*), was first identified in the restoration of homology-dependent gene silencing (HDG silencing) (Furner, Sheikh, and Collett 1998). HDG silencing is a phenomenon frequently observed when introducing transgenes into the genome leading to gene silencing and/or silencing of its homologous endogenous genes (Meyer and Saedler 1996). The *CHALCONE SYNTHASE* (*CHS*) is induced when exposed to strong light or high sucrose leading to anthocyanin biosynthesis and a purple appearance. Introducing another copy of *CHS* into WT impaired its anthocyanin biosynthesis by hypermethylation at endogenous *CHS*, but mutation in *HOG1* demethylated *CHS* locus and reactivates its expression (Furner, Sheikh, and Collett 1998). The SAM:SAH ratio decreased in *hog1-1* and genome-wide demethylation of CpG sites was observed (Rocha et al. 2005). In addition, the two important enzymes for the non-CG DNA methylation pathway, *SUVH*, and *CMT3*, are susceptible to the perturbations in SAHH1 activity, and the disruption of SAHH1 expression caused depletion of the H3K9me2-guided non-CG DNA methylation (Mull, Ebbs, and Bender 2006). The *hog1-7* allele reduced the centromeric-localized H3K9me2, whereas most DNA methylation at the chromocenters was maintained, suggesting a novel role of *SAHH1* in chromatin modification (Baubec et al. 2010). In line with this, the majority of the up-regulated genes in *hog1-1* are located in the pericentromeric heterochromatin with one-third annotated as transposons (Jordan et al. 2007). Collectively, these findings suggest that a proper function of *SAHH1* is required for maintaining DNA methylation and histone modification in gene silencing, which is presumably achieved by modulating cytosine methyltransferase and histone methyltransferase activity via tuning the SAM:SAH ratio.

It has been shown that chromatin accessibility shaped by DNA methylation in the vegetative nucleus is important for pollen tube function. The vegetative cell nucleus exhibits

increased chromatin accessibility in regions containing genes that are unique for pollen functions, and DME-mediated DNA demethylation is significantly associated with genes upregulated in growing pollen tubes (Borg et al. 2021). In line with this, the mutant *dme/+* showed reduced male fertility, and the pollen tubes lost orientation in the transmitting tract forming aberrant trajectories (Khouider et al. 2021). This raises the possibility that misregulated DNA methylation status at genes indispensable for pollen tube function could be the cause of the defective pollen tube behavior in *sahh2* mutants. Thus, it would be worth exploring if *SAHH2* plays a similar role to *SAHH1* in maintaining DNA methylation and histone modification.

Further evidence for the role of *SAHH1* resides in ACC signaling. *sahh1* produces short roots with less root hair, and the defect can be restored by applying all the precursors in the methyl cycle involved in ethylene synthesis, including Hcy, SAM, and ACC, implying that *SAHH1* might also affect ethylene-related pathways (Wu et al. 2009). ACC is capable of acting independently of ethylene in signal transduction in fertilization. ACC produced by ovular sporophytic tissue stimulates transient Ca^{2+} elevation and promotes secretion of the pollen tube attractant LURE1.2 in pollen tube attraction (Mou et al. 2020). It also directly acts in pollen and stimulates pollen tube growth in tomato with or without ethylene perception (Althiab-Almasaud et al. 2021). To investigate if the pollen tube defects in *sahh1* alleles were caused by a shortage of ACC, flower buds before anthesis were treated with ACC (5 μM) and Hcy (300 μM), and the seed set rate of the resulting siliques was recorded. The seed set rate in these siliques after treatment appeared to be no different from the mock control in both *sahh2-1* and *sahh2-2* (Figure S3.2). It was difficult to evaluate if the chemicals penetrated through the tissue layers and arrived at the cells where they were supposed to function. These results might be improved by performing the chemical treatment assay directly on pollen germination media containing ACC, Hcy, or SAM which serves as the direct substitute for ACC synthesis.

In conclusion, we developed a semi-high-throughput mapping-by-sequencing method for paternal-defective mutations with a limited workload. With this method, we corroborate three known paternal genes including *HAP2*, *CALS5*, and *COBL10* in fertilization. A novel paternal gene, *SAHH2*, was identified and further characterized to function in preovular pollen tube guidance in the female transmitting tract. This discovery hints at the importance of maintaining transmethylation potential in pollen tube function. Taken together, this study offers both a new mapping approach and novel insights into understanding the paternal impact on fertilization in flowering plants.

3.4 Materials and methods

3.4.1 Plant materials and growth conditions

The T-DNA insertion lines *hap2-2* (SALK_152706) (von Besser et al. 2006), *cals5-2* (SALK_026354) (Dong et al. 2005), *cobl10-2* (SAIL_1306_E02) (Sha Li et al. 2013) have been described previously. The *sahh2-2* (GK-139A12) (Rosso et al. 2003) allele in Col-0 background carries a T-DNA insertion in the second exon, the *sahh2-3* (SALK_205579) allele in Col-0 background carries a T-DNA insertion in the intron, and the *sahh2-4* (SALK_134541) allele in Col-0 background carries a T-DNA insertion in the first exon. The allele-specific genotyping primers are listed in Table S3.5.

Insertion lines were provided by the Nottingham *Arabidopsis* Stock Center (NASC) (Scholl, May, and Ware 2000). The Rainbow Pollen marker and Rainbow Female Gametophyte marker used in this study are described in chapter 5. Plants used in this study were grown under long-day conditions as described previously in (Babu et al. 2013).

3.4.2 EMS-induced mutagenesis in *Arabidopsis*

The EMS-mutagenized M2 Ler population for a forward genetic screen for paternal effect mutations used in this study was described in (Babu et al. 2013).

3.4.3 Plasmid construction

For the construction of binary vectors *proMGH3:HAP2-mScarlet,* the coding sequence of *HAP2* was amplified from cDNA of Col-0 inflorescence and cloned into the binary vector *pGIIk* containing the *MGH3* expression cassette using ligation-based molecular cloning. For the *proCALS5:CALS5-mScarlet* expression vector, the promoter sequence starting from 2093 bp upstream of the start codon and the full-length genomic sequence was amplified and cloned into the binary vector *pMB3300* containing *mScarlet-tNos* using In-Fusion® Snap Assembly. For the *proCOBL10:COBL10-YPet* expression vector, the promoter sequence starting from 1254 bp upstream of the start codon and the full-length genomic sequence were amplified and cloned into the binary vector *pMB1300* containing *YPet-tNos* using In-Fusion® Snap Assembly. For the *proSAHH2:SAHH2-YPet* expression vector, the promoter sequence starting from 2161 bp upstream of the start codon and the full-length genomic sequence were amplified and cloned into the binary vector *pMB1300* containing *YPet-tNos* using In-Fusion® Snap Assembly. For the *proSAHH2:SAHH2* expression vector, the promoter sequence starting from 2161 bp upstream of the start codon and the full-length genomic sequence was amplified and cloned into the binary vector *pMB3300* containing *tNos* using In-Fusion® Snap Assembly. All the

expression vectors were transformed into Col-0 or mutants by Agrobacterium-mediated transformation via floral dip as previously described (Clough and Bent 1998).

3.4.4 Phenotypic analysis of mutants

Hoyer's solution clearing of ovules

Ovules were dissected and cleared in Hoyer's solution as described previously in (Bayer et al. 2009). Cleared samples were examined by DIC microscopy with Zeiss Axio Imager.Z1 microscope equipped with an AxioCam HRc camera.

Fluorescence and confocal laser scanning microscopy

Mature pollen was mounted in 10% glycerol for microscopy. Ovules at 24 HAP were dissected out and stained by SR2200 as described previously in (Musielak et al. 2016). Confocal scanning microscopy was performed with Zeiss LSM780NLO.

Aniline blue staining of pollen tubes in pistils

Pollen grains were collected from freshly opened flowers and pollinated to pistils emasculated 24 h earlier. Pistils were excised at 24 HAP and proceeded to fixation and aniline blue staining as described previously in (Zhong et al. 2022). Pistils after staining were mounted in 10% glycerol and examined with Zeiss LSM780NLO.

Pollen viability staining

Anthers before anthesis were collected in Carnoy's fixative for 2 h and stained with the simplified Alexander staining as described in (Peterson, Slovin, and Chen 2010). Images were taken with a Zeiss Axio Imager.Z1 microscope equipped with an AxioCam HRc camera.

Silique clearing

Mature siliques were fixed and cleared as described in (Pereira et al. 2016). Images were taken with a Zeiss Axio Zoom.V16 microscope equipped with a Prime BSI Express sCMOS camera.

3.4.5 DNA preparation for library preparation

Seeds of the mapping populations were sowed out on 1/2 MS media with 0.1% agar, pH 5.7, and the whole seedlings were collected before the proliferation of a true leaf. Seedlings were grounded with mortar and pestle in liquid nitrogen. About 500 mg of plant powder was collected and subjected to CTAB DNA preparation as described previously (Healey et al. 2014).

3.4.6 Illumina sequencing and data preprocessing

DNA libraries were prepared with the NEBNext® Ultra II FS DNA Library Prep Kit for Illumina and the NEBNext® Multiplex Oligos for Illumina (Index Primers Set 1). The quality

of libraries was accessed by Agilent 2100 Bioanalyzer with the Agilent High Sensitivity DNA Kit. Every 10 libraries were pooled and sequenced in one lane in HiSeq 3000 platform in-house. Raw sequencing reads were assembled to TAIR10 (Giraut et al. 2011) or Ler-1 genome (Schneeberger et al. 2011) by Hisat2 (Kim et al. 2019); non-reference SNPs were analyzed by FreeBays (Garrison and Marth 2012); SNP frequency was plotted in Matplotlib (Hunter 2007); SNP effect prediction was annotated by SnpEff (Cingolani et al. 2012).

3.5 Supplementary information

Table S3.1 The mapping results for the paternal-defective mutants in this study

Mutant		Candidate interval		Number of candidate variant
M2 plant	Name	OC2	F2	
9-30	*pdm1*	Chr. 3: 6-8 Mb	Chr. 3: 6-8 Mb	2
10A13	*pdm2*	Chr. 2: 4.5-6.5 Mb; Chr. 3: 6-8 Mb	-	1; 3
7D74	*pdm3*	Chr. 3: 7.5-9.5 Mb	-	1
3B67	*pdm4*	Chr. 2: 18-20 Mb	Chr. 2: 18-20 Mb	2
10A22	*pdm5*	Chr. 3: 6-8 Mb	Chr. 3: 6-8 Mb	3
10A43	*pdm6*	Chr. 5: 2-4 Mb	Chr. 4: 13-15 Mb; Chr. 5: 2-4 Mb	5; 3
5C13	*pdm7*	Chr. 2: 17.5-19.5 Mb	0	-
2-25	*pdm8*	0	-	-
2A80	*pdm9*	0	0	-
3A38	*pdm10*	0	-	-
3E15	*pdm11*	0	0	-
4-60	*pdm12*	0	0	-
7A29	*pdm13*	0	-	-
7B2	*pdm14*	0	-	-
7D43	*pdm15*	0	-	-
8A35	*pdm16*	0	-	-
8C48	*pdm17*	0	-	-
10A32	*pdm18*	0	-	-
10A69	*pdm19*	0	-	-

Table S3.2 Verified causative SNP list

Mutant	SNP position	Reference	Variant	SNP effect	Gene	Other name
pdm1	Chr. 4:7065707	CTTTTAAG	CTTTAAA	frameshift variant and missense variant	AT4G11720	*HAP2*
pdm2	Chr. 2:5451611	G	A	missense variant	AT2G13680	*CALS5*
	Chr. 3:7254133	G	A	missense variant	AT3G20580	*COBL10*
pdm3	Chr. 3:8648733	C	T	missense variant	AT3G23810	*SAHH2*

Figure S3.1 Alexander staining of *sahh2-1*, *sahh2-2*, *sahh2-3*, and *sahh2-4* anthers before anthesis. Pollen viability of *sahh2-1*, *sahh2-2*, *sahh2-3*, and *sahh2-4* exhibited no difference from WT.

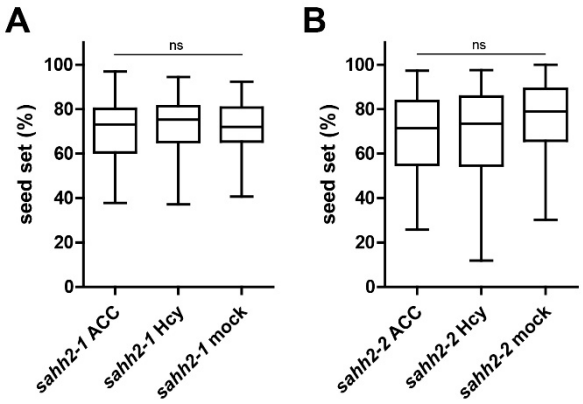

Figure S3.2 ACC and Hcy treatment of *sahh2-1* and *sahh2-2* flower buds before anthesis. (A) Seed set rate of the resulting siliques of *sahh2-1* flower buds after ACC and Hcy treatment. **(B)** Seed set rate of the resulting siliques of *sahh2-2* flower buds after ACC and Hcy treatment. "ns" indicates "not significant" in a one-way ANOVA with a post hoc Tukey test.

Table S3.3 Specific genotyping primers for *sahh2* mutant alleles

Mutant allele		Primer sequence	PCR product length
sahh2-2	LP	5'-TTCCATTCGTTTCAAGGTTTG-3'	LP+RP: 1034 bp in WT; none in mutant BP+RP: none in WT; ~600 bp in mutant
	BP	5'-ATAATAACGCTGCGGACATCTACATTTT-3'	
	RP	5'-TTCTGACCCTTGAGGATGTTG-3'	
sahh2-3	LP	5′-ACTCTGTCACCAAGAGCAAGG-3'	LP+RP: 1109 bp in WT; none in mutant BP+RP: none in WT; ~600 bp in mutant
	BP	5′-ATTTTGCCGATTTCGGAAC-3'	
	RP	5′-CAATATTTGGTCACACGCATC-3'	
sahh2-4	LP	5′-TTTAGTGACGAACATCCGATG-3'	LP+RP: 1030 bp in WT; none in mutant BP+RP: none in WT; ~600 bp in mutant
	BP	5′-ATTTTGCCGATTTCGGAAC-3'	
	RP	5′-ACCCCAGTCAAGAGCTCTCTC-3'	

4 ORC1b is a sperm nuclear protein required for fertilization

4.1 Introduction

DNA replication sets up the basis for cell division and it starts at hundreds or thousands of separate sites called origins of replication. Origin licensing is the first step in DNA replication. This process is conserved in eukaryotes and involves the recruitment of four crucial groups of proteins including the Origin of Replication Complex (ORC), Minichromosome Maintenance 2-7 Complexes (MCM2-7), Cell Division Cycle 6 (CDC6), and Chromatin Licensing and DNA Replication Factor 1 (CDT1) (Makarova and Koonin 2013).

The ORC consists of six proteins called ORC1-ORC6 which form a hetero-hexametric protein complex to bind to DNA and histones as a scaffold where origin licensing takes place during late mitosis and the G1 phase. ORC1-ORC5 together with CDC6 share conserved AAA+ folds which include Walker A and Walker B ATP-binding domains for ATP-dependent DNA encirclement and Sensor-1 and Sensor-2 motifs for facilitating ATP hydrolysis as well as a carboxy (C)-terminal winged-helix (WH) DNA-binding domain (Iyer et al. 2004; Duncker, Chesnokov, and McConkey 2009; Speck et al. 2005). Crystallographic studies in *Drosophila* showed that CDC6 assembles into the ORC hexametric complex together with ORC1-ORC5 forming a two-layered six-subunit ring of AAA+ ATPase and WH domains around DNA. The resulting complex in turn recruits the MCM2–7 replicative helicase and its associated CDT1 chaperone via the WH ring layer (Bleichert, Botchan, and Berger 2015). ORC6 shows less similarity with other ORC members, and it does not contribute to the hexameric protein complex, but rather mediates the interaction with CDT1 and loads MCM2-7 onto DNA (S. Chen, De Vries, and Bell 2007). Later in the S phase, cyclin-dependent kinases (CDKs) promote the origin firing and MCM activation, thereby establishing directional replisomes (Yeeles et al. 2015).

DNA replication does not occur simultaneously along the genome, instead, it is temporally programmed in a fine-tuned manner. In mice and humans, euchromatin replicates during the early and the middle S phase and heterochromatin replicates in the late S phase. These early and late replication regions form compartments that differ in nuclease accessibility, transcriptional activity, and epigenetic modifications (Woodfine et al. 2004; Yaffe et al. 2010; Pope et al. 2014; Kirstein et al. 2021). It is confirmed that *Arabidopsis* shares similar features in DNA replication, where chromosome arms tend to replicate early while pericentromeric regions replicate late (Wheeler et al. 2020; Concia et al. 2018). In the early S phase, early

replication activity is in line with an open chromatin structure while strong initiation is depleted in the condensed centromeric and pericentromeric regions, implying that the temporal replication is probably modulated by chromatin accessibility (Wheeler et al. 2020; Concia et al. 2018). Profiling of newly synthesized DNA in *Arabidopsis* further linked replication origins to the specific epigenetic environment which is correlated with a higher GC content, but a lower CG methylation, and is enriched in histone H2A.Z, H3K4me2, H3K4me3, and acetylated H4K5, but depleted in H3K4me1 and H3K9me2 (Costas et al. 2011).

It is critical to ensure each origin of replication only fires once. Re-replication gives rise to double-strand DNA breaks, which in turn, triggers DNA damage response, causing a cell cycle arrest and apoptosis (Arias and Walter 2007). In *Arabidopsis*, DNA methylation and histone modification markers are responsible for the repression of re-replication. Mutations of the H3K27 monomethyltransferase genes, *ATXR5* and *ATXR6*, result in re-replication in heterochromatin and activation of transposable elements (Jacob et al. 2010). Loss of DNA methylation suppressed the re-replication phenotype of *atxr5/6* (Stroud et al. 2012). Furthermore, introducing a mutation in a DNA repairing gene, *TONSOKU* (*TSK*), into an *atxr5/6* mutant suppressed the replication and transcriptional de-repression of heterochromatin (Davarinejad et al. 2022). Mutations in TSK cause loss of gene silencing and altered heterochromatin organization, suggesting its role in the maintenance of epigenetic states (Takeda et al. 2004). TSK recognizes H3K27me0 on the newly synthesized copies of the replication-coupled H3 variant H3.1 and repairs broken replication forks. ATXR5/6 specifically mediate the monomethylation at H3K27 to prevent the binding of TSK on mature DNA, ensuring heterochromatin stability and silencing (Davarinejad et al. 2022). In contrast to this, the human copy of TSK, TONSOKU-LIKE (TONSL), interacts with H4K20me0 to achieve DNA repairing via its ankyrin repeat domain (ARD) which is lacking in the plant TSK (Saredi et al. 2016). Interestingly, the crystal structure of the ARD reveals a surface aromatic cage that resembles the tri-methylated lysine binding pocket of the plant homeodomain (PHD) (Gao et al. 2009), suggesting that the PHD might take over the H4K20me0 interaction of ARD in plants.

Among the 6 ORCs, ORC1 is arresting for its additional bromo-adjacent homology (BAH) domain at the N-terminus (Schmidt and Bleichert 2020). BAH is an evolutionarily conserved motif that appears in proteins involved in DNA methylation, DNA replication, and transcriptional regulation (Callebaut, Courvalin, and Mornon 1999). The BAH of ORC1 in budding yeast contributed to several distinct functions of ORC1 within and beyond DNA replication: (1) Genome-wide analyses in budding yeast indicate that BAH contributes to the

recognition of the most replication origins and the stable association of ORC1 with chromatin (Müller et al. 2010). (2) The BAH in yeast ORC1 is highly related to SIR3, a transcriptional silencing regulator of the mating-type loci, and the deletion of BAH in yeast ORC1 led to a dramatic reduction of mating efficiency, indicating a function in transcriptional silencing (Bell et al. 1995). (3) ORC1 binds nucleosomes across the genome irrespective of the chromatin accessibility and the binding is essential to maintain the integrity of ribosomal RNA genes (rDNA) borders during meiosis (De Ioannes et al. 2019). In humans, a mutation in the ORC1 BAH domain has been implicated in the primordial dwarfism Meier-Gorlin syndrome (MGS) (Bicknell et al. 2011). The human ORC1 BAH domain specifically recognizes H4K20me2 which is enriched in the replication origin, and the disrupted recognition in the mutant impairs ORC chromatin loading and cell-cycle progression. In addition, human ORC1, but not the mutant with impaired H4K20me2 binding, restored the MGS-like phenotype in zebrafish *orc1* mutants, suggesting an H4K20me2 effector role of ORC1 in DNA replication via its BAH domain (Kuo et al. 2012).

Plant ORC1 proteins possess a plant homeodomain (PHD), a small zinc finger structural fold, embedded in BAH forming a plant-specific fused BAH-PHD cassette (Sisi Li et al. 2016). PHD acts as a histone modification reader in a sequence-dependent manner for H3K4me3, H3K4me0, H3R2, as well as H3K12ac, to promote both gene expression and repression (R. Sanchez and Zhou 2011). PHD is not confined to the plant kingdom as the name may suggest, instead, it was shown that misregulation of PHD fingers in humans is associated with several cancers in the prerequisite of H3K4me2/3 recognition (Park et al. 2022). PHD always presents in proteins in a multisubunit either with PHD copies or with other effectors, which together mediate a high specificity for modification recognition and biological readout (Mellor 2006; Musselman and Kutateladze 2011). There are only four BAH-PHD cassette-containing proteins found in the *Arabidopsis* genome. This uncommon hybrid domain is probably endowed with the ability to recognize certain chromatin configurations via the distinct reader combination. SHORT LIFE (SHL) and EARLY BOLTING IN SHORT DAYS (EBS) are two of the BAH-PHD-containing proteins that share a similar function as a replacement of animal POLYCOMB REPRESSIVE COMPLEX 1 (PRC1) in the context of polycomb-mediated gene silencing (Z. Li et al. 2018). In animals, PRC2 catalyzes H3K27me3 at the target sites which is read and interpreted by PRC1 for further addition of ubiquityl moiety to histone H2A at Lys119 (H2AK119ub1), leading to chromatin compaction and gene silencing (Blackledge, Rose, and Klose 2015). In the absence of PRC1, plants recruit EBS and SHL to form a complex together with EMBRYONIC FLOWER 1 (EMF1) for reading and effecting the H3K27me3 mark and

mediating genome-wide transcriptional repression through their BAH domain (Z. Li et al. 2018). In the meanwhile, EBS and SHL can also read H3K4me2/3 through their PHD fingers. In the chromatin-mediated repression of floral initiation, SHL and EBS bind to the regulatory regions of the floral integrator *SUPPRESSOR OF OVEREXPRESSION OF CO1* (*SOC1*) and *FLOWERING LOCUS T* (*FT*), respectively, via the recognition of H3K4me2/3. The binding prevents a high level of H3 acetylation in the regulatory region, which in turn maintains an inactive chromatin configuration for transcriptional repression (López-González et al. 2014).

The other two BAH-PHD-containing genes in *Arabidopsis* are the two ORC1 homologs, *ORC1a* and *ORC1b*. With the 87% sequence identity throughout the entire sequence and 88% sequence identity within the BAH-PHD region of ORC1a and ORC1b, however, they diverge in a different expression pattern, with *ORC1a* expressed exclusively in endoreplicating tissues and *ORC1b* in proliferating cells (Diaz-Trivino et al. 2005). The activity of *ORC1b* promoter indicated by GUS-fusion expression was observed strongly in proliferating tissues including shoot, root meristem, anther, and developing embryos (Diaz-Trivino et al. 2005). *ORC1a* and *ORC1b* each contain an E2F binding site in the promoter and the expression is regulated by the RBR/E2F pathway (Diaz-Trivino et al. 2005). The opinions on the epigenetic binding capacity of the BAH-PHD cassette in ORC1a and ORC1b are divergent. A pull-down assay from *Arabidopsis* extracts showed that ORC1b was able to pull down H3K4me3 whereas no binding to H3K9me3, H4K20me3, and the unmodified histones H3 or H4 was detected. Plants expressing ORC1b with a mutated PHD which reduced its H3K4me3 interaction resulted in impaired binding of ORC1b to the promoters of its targeted genes followed by reduced transcriptional activity (M. D. L. P. Sanchez and Gutierrez 2009). On the contrary, the isolated BAH-PHD cassette of ORC1b exhibited a strong preference for the unmodified H3 N-terminal peptide in an isothermal titration calorimetry (ITC) assay. This was further supported by structural studies revealing that the BAH-PHD specifically recognizes the unmodified H3 tail by clamping the histone target from the opposing sides with the two domains in a sandwich manner (Sisi Li et al. 2016). However, binding of ORC1b BAH-PHD to unmodified H3 tails seems unlikely related to DNA replication since *Arabidopsis* replication origins are characterized by H3K4me2/3 marks (Costas et al. 2011), suggesting an additional role of *ORC1b* outside of the origin licensing complex.

With such a versatile potential of the BAH-PHD cassette in reading and effecting multiple epigenomic modifications, the function of *ORC1* within and/or beyond DNA replication in plants is still elusive. The absence of phenotypic characterization of the loss-of-function mutants of *ORC1* in *Arabidopsis* is hampering our understanding of its biological function.

Whether *ORC1* is endowed with additional roles independently of the other ORC subunits in epigenetic regulation needs to be further addressed. Here, by characterizing the expression pattern and the phenotypes of loss-of-function mutants of *ORC1b*, we show that ORC1b preferentially localizes to the centromeric area in the sperm nucleus. Furthermore, the depletion of *ORC1b* expression led to reduced fertility with defective gametic nuclear fusion and arrested embryo and endosperm development. These phenotypic analyses provided a solid basis for further deciphering the mechanism of *ORC1b* function in fertilization and seed development. Hypophyses of the potential role of *ORC1b* in plant reproduction are discussed.

4.2 Results

4.2.1 ORCs show diverse expression abundance

As qPCR analysis of ORCs' relative transcript level suggested, ORCs are differentially expressed in different plant tissues in *Arabidopsis* (Diaz-Trivino et al. 2005). ORCs appear preferentially in proliferating tissues, with *ORC4*, *ORC5*, and *ORC6* showing a higher expression level, while the transcript abundance is much lower for *ORC1a*, *ORC1b*, *ORC2*, and *ORC3* (Diaz-Trivino et al. 2005). To study the expression pattern of ORCs during reproduction, available transcriptomic data of *Arabidopsis* pollen, egg cell, zygote, and embryo was checked (Loraine et al. 2013; P. Zhao et al. 2019). We observed that the expression abundance of ORCs also diverges in pollen (Figure 4.1 A), egg cell, and embryo (Figure 4.1 B). In pollen, ORC6 showed a higher-level expression than the other ORCs. *ORC1a* expression was much lower than *ORC1b*. Reverse transcriptase (RT)-PCR was carried out with cDNA prepared from WT pollen RNA to confirm the presence of *ORC1a* and *ORC1b* in the male gamete. *ORC1b* transcripts were more abundant in pollen but no *ORC1a* transcripts were detected (Figure 4.1C). In egg cell and embryo, *ORC1a* and *ORC1b* were much less expressed than the other subunits. It is worth noting that *ORC1a* and *ORC1b* were expressed in a complementary manner. *ORC1a* was expressed in egg cell but absent in zygote and early embryo, while *ORC1b* was absent in egg cell but appeared in the spherical zygote (Zy14) and early embryo (Figure 4.1 B).

4.2.2 ORC1b is enriched in the sperm nucleus

A functional reporter line expressing *proORC1b:ORC1b-YPet* was generated, and the centromere-specific histone 3 variant *HTR12* (*CENH3*) reporter line expressing *proHTR12:HTR12-mCherry* was introduced into it. ORC1b-YPet expression was observed in the nucleus of the microspore, the generative nucleus of the bicellular microspore, and the nucleus of the sperm cell in mature pollen and germinating pollen tube but not in the vegetative

nucleus (Figure 4.1 D). The ORC1b-YPet signal was not uniformly distributed in the nucleus, instead, it preferentially colocalized with centromeres marked by HTR12-mCherry. During the development process of pollen, the ORC1b-YPet signal appeared to be gradually confined to the centromeric region, with less signal observed in the non-centromeric area in mature pollen (Figure 4.1 D).

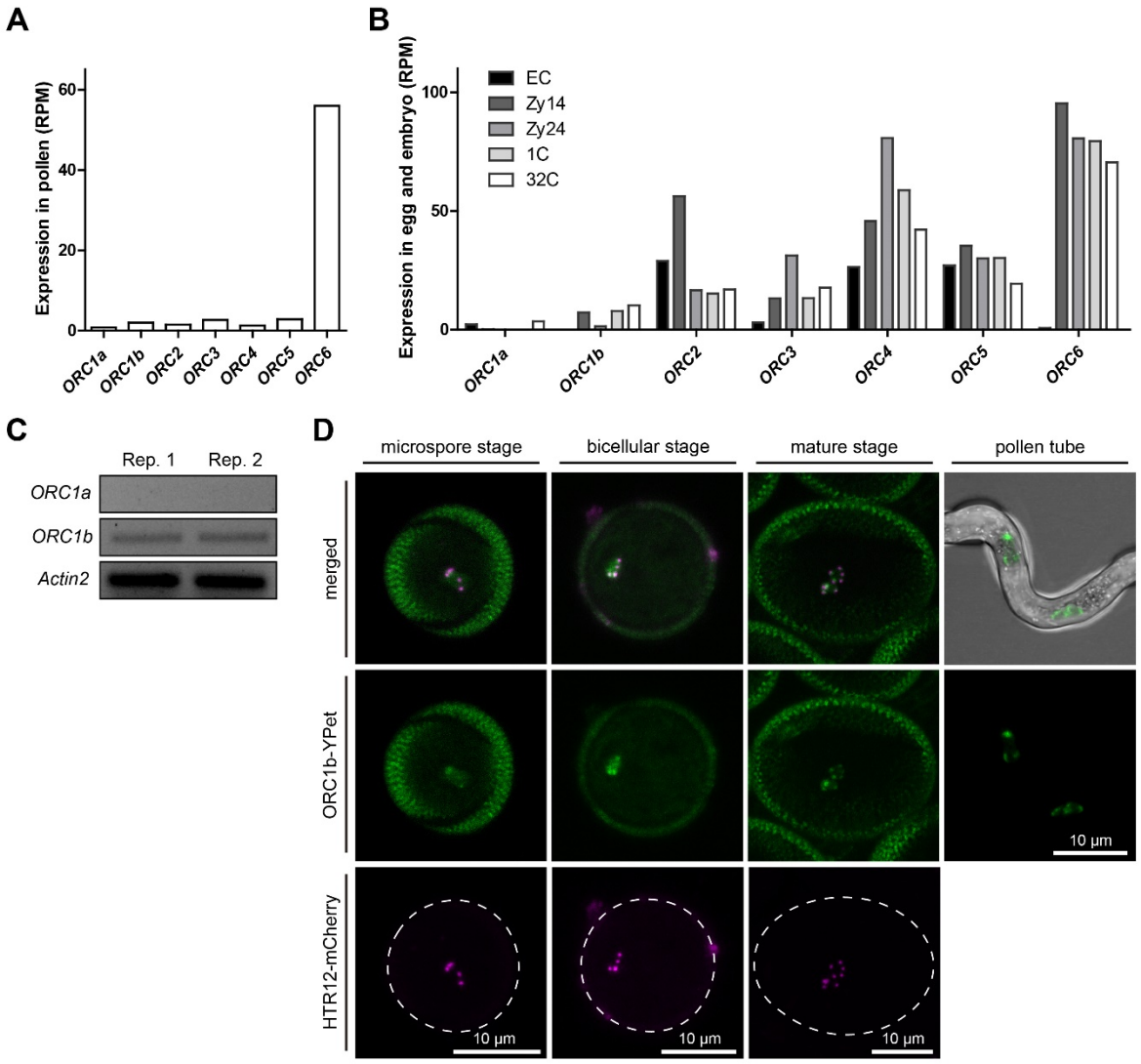

Figure 4.1 The expression pattern of ORCs. (A) The relative expression level of ORCs in pollen in reads per million (RPM) (Loraine et al. 2013). **(B)** The relative expression level of ORCs in the egg cell, zygote, and early embryo in RPM (P. Zhao et al. 2019). EC, egg cells; Zy14, spherical zygotes; Zy24, elongated zygotes; 1C, one-cell embryos; 32C, 32-cell embryos. **(C)** RT-PCR of *ORC1a* and *ORC1b* in WT pollen. *Actin2* was used as control. 30 reaction cycles were adopted. Rep. 1 and Rep. 2 indicate two PCR reaction replications. **(D)** ORC1b-YPet expression in the reporter line expressing *proORC1b*:*ORC1b-YPet* and *proHTR12:HTR12-mCherry*. Dashed lines in HTR12-mCherry panels indicate the pollen periphery.

4.2.3 *ORC1b* loss-of-function mutants show reduced fertility

To investigate the function of *ORC1a* and *ORC1b* in reproduction, T-DNA insertion alleles

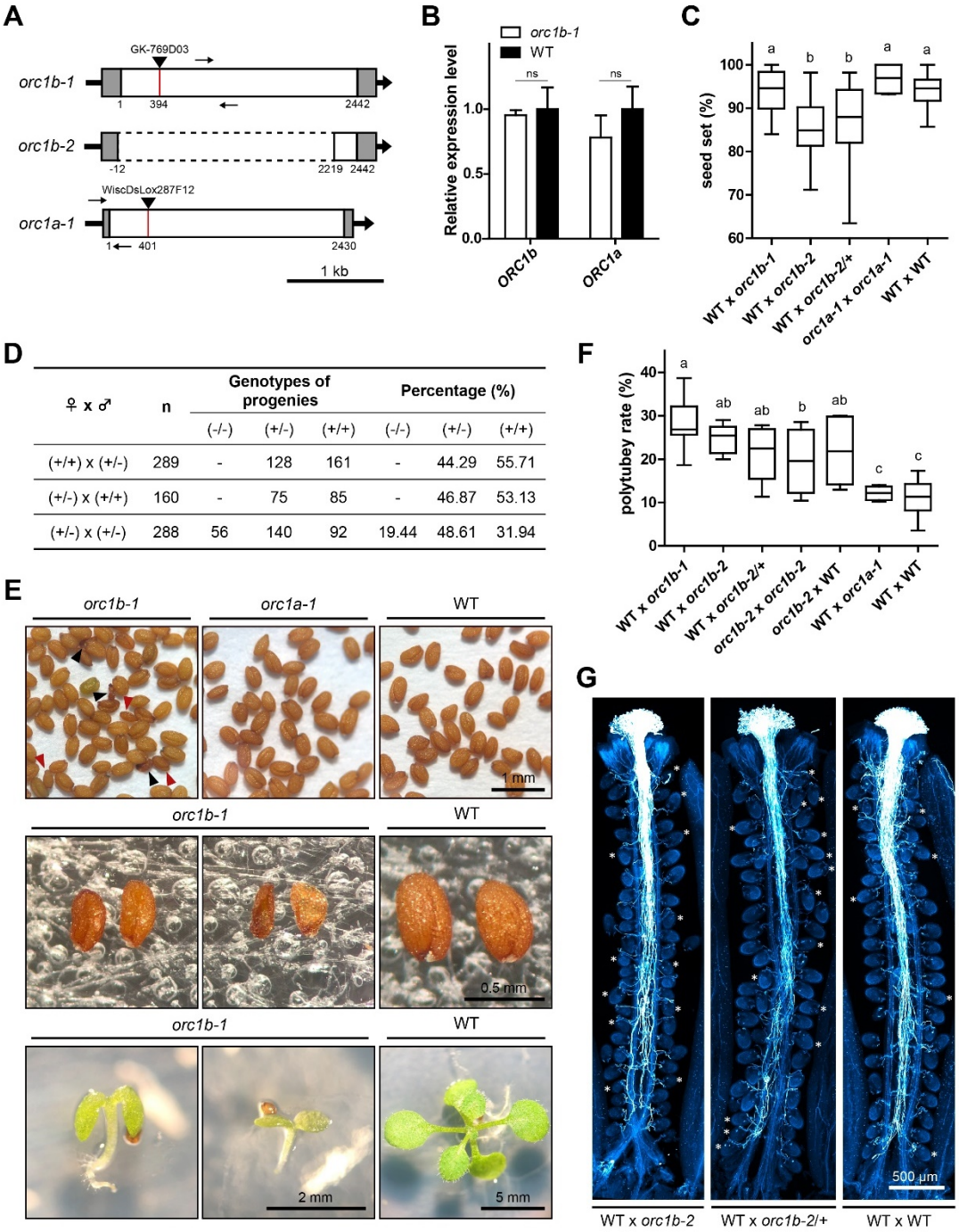

Figure 4.2 *ORC1b* loss-of-function mutants show reduced fertility. (A) Schematic representation of *orc1b-1*, *orc1b-2*, and *orc1a-1* mutant alleles. White boxes represent exons, grey boxes indicate UTRs, and the black arrows indicate gene directions. The red lines indicate the positions of T-DNA insertions in the two genes. Oligo nucleotide primers used for RT-PCR are indicated by small arrows on the sides. The dashed white box represents the deletion in the CRISPR-Cas9 modified allele. The numbers below indicate the nucleotide position. **(B)** The relative expression level of *ORC1a* and *ORC1b* in *orc1b-1* pollen. The expression values were normalized to WT which was set as 1. "ns" indicates "not significant" in Student's T-test. **(C)** The seed set rate of *orc1b-1*, *orc1b-2*, and *orc1b-2/+* when crossed to WT as the pollen donors at 3 DAP, and the seed set rate in the self-crossed siliques of *orc1a-1*. Letters above boxes refer to individual groups in a one-way ANOVA with a post hoc Tukey test ($p < 0.05$). **(D)** The transmission rate of *orc1b-2* allele, n represents the number of progenies genotyped. **(E)** Aberrant seeds were observed in *orc1b-1* and the seeds showed poor germination. **(F)** Polytubey rate of crossing combinations between *orc1b-1*, *orc1b-2*, *orc1b-2/+*, *orc1a-1* and WT. **(G)** Aniline staining image of *orc1b-2* and *orc1b-2/+* pollen tubes in WT pistils at 24 HAP. Asterisks indicate ovules which showed polytubey.

orc1a-1, *orc1b-1*, and a CRISPR-Cas9 knock-out allele *orc1b-2* with a 2231-bp out-of-frame deletion were phenotypically characterized (Figure 4.2 A). A qPCR analysis was carried out to check *ORC1a* and *ORC1b* expression in *orc1b-1* pollen. The relative transcript level of the *ORC1b* fragment on the 3' side of the T-DNA insertion was not significantly reduced. It could be possible that fragments are still partially transcribed. The change in *ORC1a* expression level was not significant compared to WT pollen (Figure 4.2 B).

The sperm-specific expression pattern of *ORC1b* suggests that it might play a potential role in sperm function during fertilization. To address if paternal disruption of *ORC1b* affects fertilization, *orc1b* mutants were crossed to WT as pollen donors and the seed set in siliques at 3 DAP was checked (Figure 4.2 C). When crossed to WT as a pollen donor, *orc1b-1* gave out a mostly full seed set (93.82% ± 5.67% a) similar to WT (93.94% ± 3.96% a), while the seed set rate of *orc1b-2* (85.54% ± 6.82% b) and *orc1b-2/+* (87.08% ± 8.89% b) was significantly reduced. In addition, *orc1a-1* (96.78% ± 3.73% a) showed no fertility defect when it was self-crossed (Figure 4.2 C). These results showed that the absence of *ORC1b* led to malfunctioned pollen which failed in fertilization, while the disruption of *ORC1a* expression did not affect fertility.

Though *orc1b-1* pollen gave out a seed set similar to WT pollen in siliques at 3 DAP, some aberrant seeds were observed at the mature stage in self-crossed seeds, while *orc1a-1* seeds showed no observable difference from WT. As shown in Figure 4.2 E, two different kinds of aberrant seeds were found in *orc1b-1*, with some showing a smaller size than WT seeds and others showing a wizened appearance. To test if these aberrant seeds are viable or not, they were carefully put on a 1/2 MS media for seed germination. After 12 days of incubation, the wizened seeds were not capable to germinate at all, since they mostly bore nothing inside the seed coat. Most of the seeds with a smaller size germinated, but the seedlings arrested at the cotyledon stage with a short root, and some seedlings even failed to produce a root (Figure 4.2 E). 11 out of 32 of these defective seedlings survived in soil and showed no difference to *orc1b-1* plants germinated from normal-looking seeds.

To address the transmission rate of the *orc1b-2* allele with reduced fertility, a reciprocal cross between *orc1b-2/+* and WT was performed and the genotypes of F1 progenies were checked (Figure 4.2 D). When crossed to WT as a pollen donor, the paternal *orc1b-2* allele segregation was distorted, with 44.29% of F1 individuals carrying *orc1b-2/+*. Interestingly, when *orc1b-2/+* was crossed to WT as the maternal parent, the *orc1b-2* allele also showed slightly reduced transmission, with 46.86% of F1 individuals carrying *orc1b-2/+*, even though *ORC1b* transcripts were not found in the egg cell (Figure 4.1 B, Zhao et al. 2019). Consistent

with both reduced paternal and maternal transmission rates, the self-crossed progenies of *orc1b-2/+* showed more severe segregation distortion, giving out a ratio of (31.94% WT) : (48.61% *orc1b-2/+*) : (19.44% *orc1b-2*). These observations indicate that both parental transmission rates of *orc1b-2* are reduced, and they additively affect the allele segregation of their progenies.

To investigate if the cause of the reduced paternal fertility in *orc1b* mutants resides in the pollen tube function or the sperm function, the directional guidance of *orc1b* pollen tube to ovules was checked. Pollen grains from *orc1b-1*, *orc1b-2*, and *orc1b-2/+* were crossed to WT, and ovules at 24 hours after pollination (24 HAP) were dissected out and stained with Renaissance staining. Pollen tubes germinated from *orc1b-1*, *orc1b-2*, and *orc1b-2/+* pollen all managed to arrive at the micropyle, suggesting a normal function in ovular pollen tube guidance and pollen tube reception. In some ovules, more than one pollen tube entered the micropyle, which is referred to as polytubey. The polytubey rates of WT × *orc1b-1* (28.31% ± 6.00% a), WT × *orc1b-2* (24.62% ± 3.40% ab), and WT × *orc1b-2/+* (21.46% ± 6.49% ab) are significantly higher than that of WT × *orc1a-1* (12.13% ± 1.63% c) and WT × WT (10.97% ± 4.16% c) (Figure 4.2 F). Aniline blue which stains callose, one of the main components on the pollen tube wall, was used to observe pollen tube growth in the female transmitting tract. In pistils at 24 HAP, a comparable amount of *orc1b-2*, *orc1b-2/+,* and WT pollen germinated on the stigma, and pollen tube elongation along the transmitting tract showed no difference between them (Figure 4.2 G). An increased polytubey rate was also observed in pistils when pollinated with *orc1b-2* and *orc1b-2/+* pollen, and the second-pollen tube arrival happened randomly in pistils. Taken together, these results suggest that the paternal fertility defect resides after pollen tube reception and the defect triggers the second pollen tube attraction.

In accordance with the reduced maternal transmission rate, *orc1b-2* also showed an increased polytubey rate when crossed as the maternal parent (Figure 4.2 F). Both *orc1b-2* × *orc1b-2* (19.53% ± 7.59% b) and *orc1b-2* × WT (21.95% ± 7.87% ab) crossing combinations showed an increased polytubey rate, implying that *ORC1b* might also function maternally in pollen tube attraction.

4.2.4 *ORC1b* loss-of-function mutants exhibited paternal defects in karyogamy

The polytubey phenotype is triggered by the failure of establishing the pollen tube block at the septum or triggered by fertilization recovery (Zhong et al. 2022). To characterize the cause for paternal-induced polytubey phenotype in *orc1b-1*, Rainbow Pollen marker (RbP) was introduced into *orc1b-1* and the resulting mutant line is referred to as *orc1b-1*-RbP. As shown in Figure 4.3 A, the *orc1b-1*-RbP pollen showed a healthy-looking appearance, suggesting that

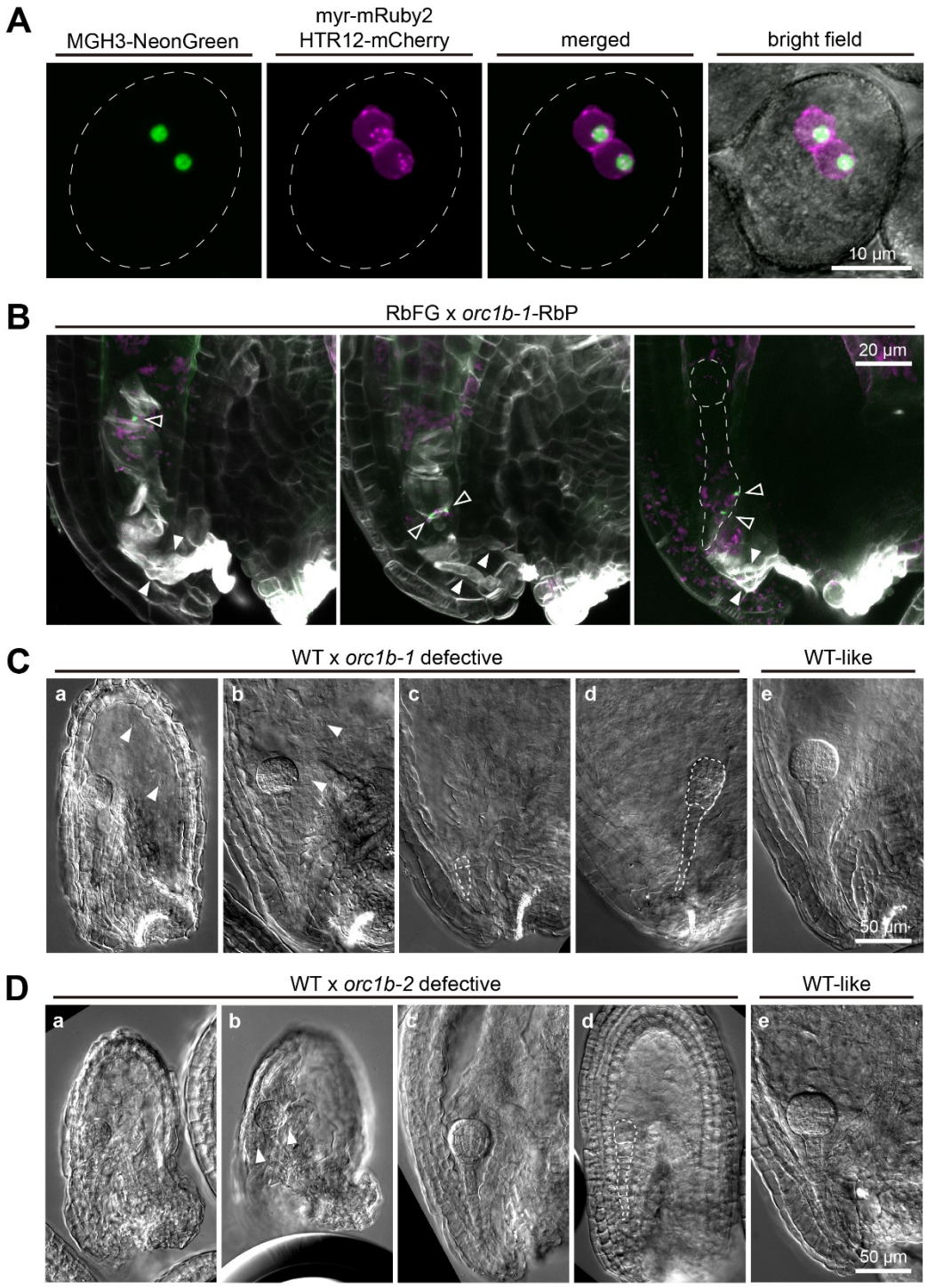

Figure 4.3 *ORC1b* loss-of-function mutants exhibit paternal defects in karyogamy, embryo, and endosperm development. (A) Fluorescent signals expressed in Rainbow Pollen marker (RbP, expressing *proHTR12:HTR12-mCherry*, *proMGH3:MGH3-NeonGreen* and *proDAZ3:myr-mRuby2*) in *orc1b-1*. The sperm nucleus is labeled by NeonGreen, the sperm membrane is labeled by mRuby2, and the sperm centromeres are labeled by mCherry. **(B)** SR2200 staining of Rainbow Female Gametophyte marker (RbFG, expressing *proEC1.2en-EC1.1:myr-vsfGFP-0* and *proMYB98:mTP-mScarlet*) ovules fertilized by *orc1b-1*-RbP at 24 HAP. White filled arrowheads indicate the arrival of pollen tubes, hollow arrowheads indicate the unfused sperm nuclei. The developing embryo is outlined by dashed lines. **(C)** Hoyer's solution clearing and DIC imaging of WT ovules fertilized by *orc1b-1* pollen at 3 DAP. Arrowheads indicate endosperm nuclei of uneven sizes. Aberrant embryos are outlined by dashed lines. **(D)** Hoyer's solution clearing and DIC imaging of WT ovules fertilized by *orc1b-2* pollen at 3 DAP. White arrowheads indicate endosperm nuclei of uneven sizes. Aberrant embryos are outlined by dashed lines.

the disrupted *ORC1b* expression did not affect the cytological development of pollen. Then, *orc1b-1*-RbP pollen was crossed to Rainbow Female Gametophyte marker (RbFG) and ovules at 24 HAP were dissected out and stained with Renaissance staining for microscopy (Figure 4.3 B). The GFP signal on the egg cell membrane (*proEC1.2en-EC1.1:myr-vsfGFP-0*) was no longer observable, suggesting that the egg cell was fertilized. The absence of the mScarlet signal in the synergid cells (*proMYB98:mTP-mScarlet*) showed that the maternal machinery for pollen tube attraction was already abolished. Extra sperm cells were observed in the ovules with polytubey, and the second pollen tube burst and released the sperm cells since the sperms were no longer wrapped inside the pollen tube. Interestingly, some sperm nuclei carrying MGH3-NeonGreen localized at the basal part of the developing embryo without the presence of the mRuby2 signal on the sperm membrane, suggesting that plasmogamy between sperm and egg cell was achieved, but these sperm nuclei failed to fuse the egg nuclei. Taken together, *orc1b-1*-RbP sperm showed failure in gametic nuclei fusion, and the polytubey phenotype was probably triggered by fertilization recovery rather than failed pollen tube block.

In addition to the fertilization defects in *orc1b-1*, the paternal effect of *orc1b-1* on the early embryo and endosperm development 3 days after pollination (3 DAP) was characterized by Hoyer's solution clearing and DIC imaging (Figure 4.3 C). Consistent with the absence GFP signal on the egg cell membrane in the crossing of RbPF × *orc1b-1*-RbP at 24HAP, the ovules at 3 DAP were all fertilized with developing embryos inside the embryo sac. But a small number of ovules showed delayed embryo development (Figure 4.3 C panel c) or aberrant cell division in the embryo proper (Figure 4.3 C panel d). Some others showed defects in endosperm development, including failed endosperm with unexpanded seed coat (Figure 4.3 C panel a)and abnormal endosperm with uneven nuclear size (Figure 4.3 C panel b). Similar defects were also observed when *orc1b-2* pollen was crossed to WT (Figure 4.3 D).

Collectively, loss-of-function mutants of *ORC1b* exhibit paternal defects in gametic nuclear fusion, early embryo development, and endosperm development.

4.2.5 *ORC1b* loss-of-function mutants produce albino seeds with aberrant embryos and/or endosperm

In the self-crossed siliques of *orc1b-2* at late developmental stages, about 9% of albino seeds with normal or smaller sizes were observed. To investigate the development of embryo and endosperm inside these albino seeds, seeds from siliques at the development phase of the torpedo stage, the linear cotyledon stage, and the mature green stage were dissected out, cleared by Hoyer's solution, and imaged by DIC microscopy. As shown in Figure 4.4, some early-

arrested ovules with shriveled integuments (Figure 4.4 E, J, O) and late-stage seed abortion with failed embryo and/or endosperm development were observed. At the torpedo stage, in the defective ovules, the embryo development retarded at the globular stage (Figure 4.4 D) or the heart stage (Figure 4.4 B, C), and the endosperm nuclei accumulated around the periphery of the embryo sac. At the linear cotyledon stage, the delayed embryos seemly were not able to catch up. The seed coat expanded together with the development of the endosperm, but the endosperm nuclei clumped around the peripheric area without going through cellularization (Figure 4.4 H, I). At the mature green stage, embryos were arrested at the heart stage in the albino seeds of normal size (Figure 4.4 M). Some delayed embryos managed to get to the torpedo stage but were arrested for the absence of a proper endosperm (Figure 4.4 N).

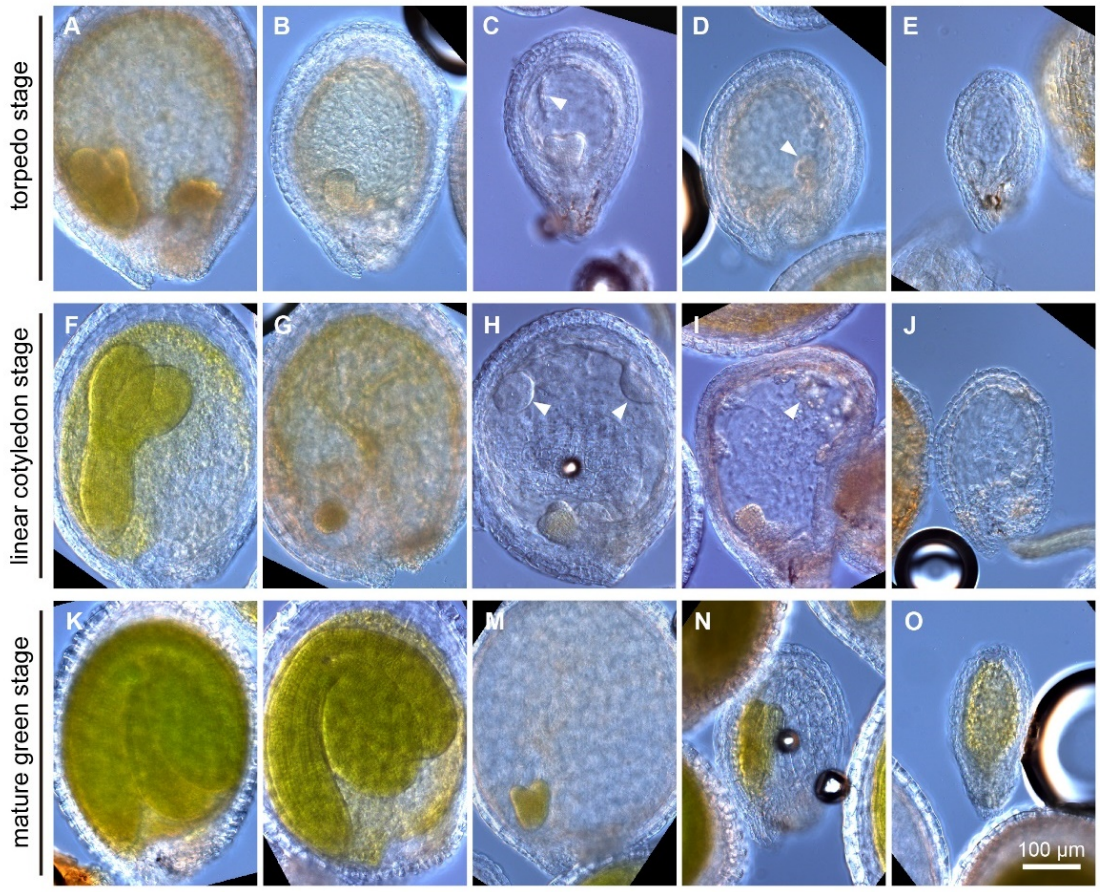

Figure 4.4 Mutant *orc1b-2* produced albino seeds with an arrested embryo or endosperm. Hoyer's solution clearing and DIC imaging of abnormal seeds from silique at the torpedo stage **(A-E)**, the linear cotyledon stage **(F-J)**, and the mature green stage **(K-O)**. Arrowheads indicate the abnormal accumulation of the endosperm nuclei.

It is worth noting that a single offspring of *orc1b-2*, produced 31.48% ± 2.77% albino seeds in the mature siliques, which is much more than the other mutant individuals (about 9%). This single offspring is referred to as *orc1b-2-albino seeds* (*orc1b-2-as*) hereafter. These albino seeds appeared no different from others at early embryonic development stages, but are

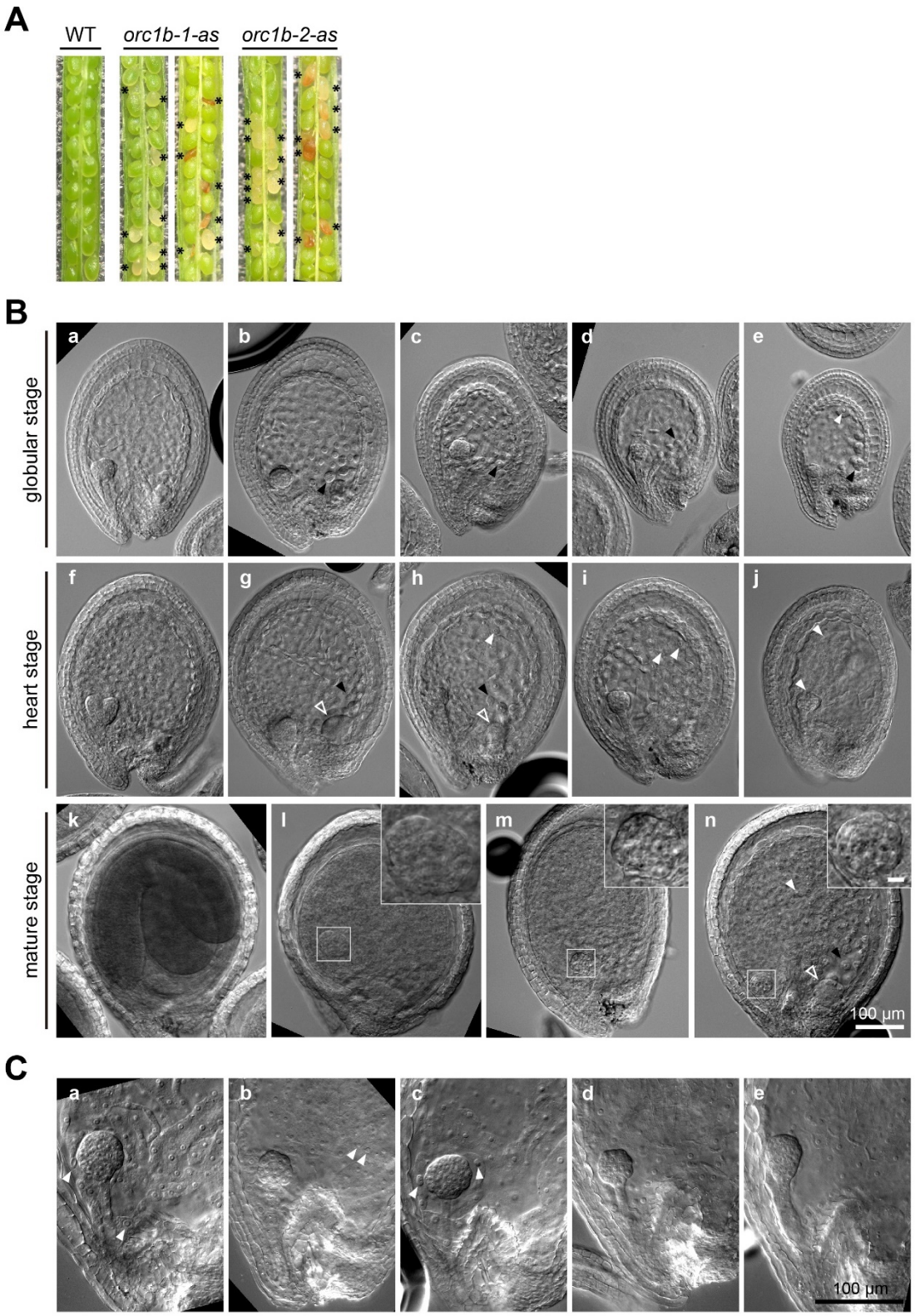

Figure 4.5 Two *ORC1b* loss-of-function mutant lines induced albino seeds. (A) Albino seeds in the self-crossed siliques of *orc1b-1-as*, *orc1b-2-as* and WT. Asterisks indicate albino seeds. **(B)** Hoyer's solution clearing and DIC imaging of abnormal seeds from silique of *orc1b-2-as* at the globular stage, the heart stage, and the mature stage. White filled arrowheads indicate the uneven size of endosperm nuclei, white hollow arrowheads indicate the over-accumulated chalazal endosperm, black filled arrowheads indicate irregular cellularization, and white boxes in panel i-n indicate the magnified embryo proper. **(C)** Hoyer's solution clearing and DIC imaging of abnormal seeds from silique of *orc1b-1-as* at the heart stage. Arrowheads indicate the uneven size of endosperm nuclei.

distinguished from the rest at the maturation stage. While normal seeds began the accumulation of chloroplasts and chlorophyll (greening of the embryo), these defective seeds stayed colorless (Figure 4.5 A). Along with seed maturation, the advanced accumulation of tannins in the seed coat turned these albino seeds brown, indicating that the seed coat development was not abolished. Later in the mature silique, these abnormal seeds collapsed and ended up with a wizened appearance (Figure 4.5 A). The formation of these albino seeds was tracked at the development phase of the globular stage, the heart stage, and the mature stage by Hoyer's solution clearing and DIC microscopy (Figure 4.5 B). In contrast to the WT-like seeds (Figure 4.5 B panels a, f, k), embryonic development was arrested at the globular stage and the shape of the embryos deformed at the mature stage, forming a clump of turgid cells (Figure 4.5 B panels i-n). Abnormal development of endosperm was seen to coincide with arrested embryos. Variable endosperm abnormalities were observed, including uneven endosperm nuclear sizes (Figure 4.5 B panels e, h-j, n) and over-accumulated chalazal endosperm (Figure 4.5 B panels g, h, n). In addition, a cloudy structure formed around some endosperm nuclei, especially in the area close to the chalazal end, which might arise from the irregular cellularization (Figure 4.5 B panels b-e, g, h, n).

Since only one single plant from *orc1b-2* mutants exhibited the over-production of albino seeds, we cannot rule out the possibility that the phenotype was triggered by non-genetic disruptions. Hence, we investigated the inheritance of the phenotype in progenies of *orc1b-2-as*. The 8 out of 16 progenies of *orc1b-2-as* produced 29.88% ± 6.58% albino seeds in the self-crossed siliques similar to the mother plant, indicating that the albino seed defect was inheritable. The segregation of the phenotype implied that the phenotype is independent of the *ORC1b* genotype. Interestingly, these abnormal seeds were only seen in self-crossed siliques, but not in out-crossed siliques when the mutant was crossed to WT as the pollen donor, suggesting that it is not a paternal defect. These observations suggest that the over-production of albino seeds in *orc1b-2-as* is genetically inheritable, and it is probably caused by an additional genetic disruption independent of *orc1b-2*.

Taking the CRISPR-Cas9 knock-out background of *orc1b-2*, the phenotype of over-produced albino seeds could be an off-target effect. In this case, the segregation of the phenotype independent of the *orc1b-2* genotype would be plausible. To investigate if the phenotype is triggered by *ORC1b* depletion or not, we searched for a similar phenotype in the T-DNA insertion allele *orc1b-1*. We found a single mutant of the *orc1b-1* allele also produced an increased number of albino seeds (24.47% ± 7.49%) (Figure 4.5 A), which is referred to as *orc1b-1-albino seeds* (*orc1b-1-as*) hereafter. In the albino seeds of *orc1b-1-as*, the embryos

showed more dramatic cell division defects, leading to an unordered tumor-like pattern (Figure 4.5 C). The abnormal endosperm proliferation with uneven nuclear sizes was also observed (Figure 4.5 C panels a-c). The phenotype of over-produced albino seeds in *orc1b-1-as* also segregated by 1:1 despite the *ORC1b* genotype. Since both the knock-out allele and T-DNA insertion allele showed an over-production of albino seeds, it is more likely to be a genetic disruption induced by mutations in *ORC1b* rather than an off-targeting effect.

The phenotype of albino seeds with arrested embryos in *orc1b-1-as* and *orc1b-2-as* is reminiscent of the embryos produced by mutant *meristem unstructured-1* (*mun-1*). *MUN* encodes a kinetochore complex protein localized at the centromere with HTR12, and *mun-1* exhibits chromosome segregation defects and DNA aneuploidy (Shin et al. 2018). To check if the genome integrity is disrupted on a chromosome level in *orc1b-2-as*, the RbP marker was introduced into the mutant. HTR12-mCherry signal on the sperm centromeres revealed the centromere number in mutant pollen. Only four centromeres were observed in some sperms (Figure 4.6 A-C), whereas five centromeres were observed in the others (Figure 4.6 D). These observations suggest that the genome integrity of *orc1b-2-as* is disrupted.

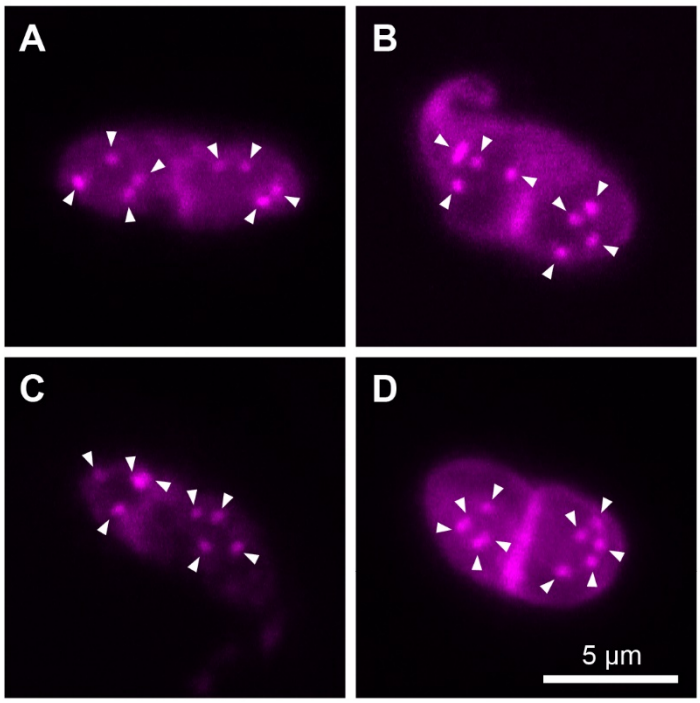

Figure 4.6 Mutant sperms labeled by Rainbow Pollen (RbP) marker cassettes. Mutant sperms with four centromeres observed **(A)-(C)**. Mutant sperms with five centromeres observed **(D)**. Signals of myr-mRuby2 on the sperm membrane and HTR12-mCherry on the sperm centromeres were detected. Arrowheads indicate centromeres labeled by HTR12-mCherry.

4.3 Discussion

4.3.1 *ORC1b* is dispensable for DNA replication during microspore development

ORC consists of six proteins named ORC1-ORC6 which form a hetero-hexametric protein complex for DNA binding as the cryo-electron microscopy (cryo-EM) structure of DNA-bound ORC in *Drosophila* showed (Schmidt and Bleichert 2020). Contrary to the synergistic working mode of the 6 ORC subunits, their expression abundance dramatically diverges, with *ORC1a*, *ORC1b*, *ORC2*, and *ORC3* showing a lower expression level compared to the others (Diaz-Trivino et al. 2005). In a solved crystal structure of *Drosophila* ORC·DNA·CDC6, ORC1 and ORC2 represent each end of the ring structure while CDC6 is in between to close the ring (Schmidt and Bleichert 2020). Even though mutants lacking ORC4 or ORC5 are not viable, the complex lacking ORC1 or ORC2 still retains the ability of origin licensing, indicating the complex is more tolerant of missing the open ends than being segmented (Bell 2017). In this study, ORC1b-YPet expression was observed in the generative nuclei in pollen throughout microspore development (Figure 4.1 D), whereas the mutant allele *orc1b-2* produced healthy-looking pollen which managed to complete two mitoses (Figure 4.3 A). These observations suggest that *ORC1b* is dispensable for DNA replication in *Arabidopsis*. The additional function of *ORC1b* independent of its classic role in origin licensing will be discussed in the following sections.

4.3.2 *ORC1b* loss-of-function mutants exhibit gametic transmission distortions

ORC1b loss-of-function mutants showed reduced fertility and the reciprocal cross between *orc1b-2/+* and WT had both reduced paternal (44.29%) and maternal (46.86%) transmission rates. The expected segregation ratio of the self-crossed *orc1b-2/+* based on the parental transmission rates was 29.60% (+/+) : 49.64% (+/-) : 20.76% (-/-), which fits the segregation ratio obtained from genotyping of *orc1b-2/+* self-crossed progenies (Figure 4.7 A, B). In the reciprocal cross between *orc1b-2* and WT, polytubey was observed in *orc1b-2* as both paternal and maternal parents (Figure 4.2 F), suggesting that a fertilization recovery machinery could be triggered by both *orc1b-2* male and female gametes. A model for parental transmission of *orc1b-2* mutant allele is shown in Figure 4.7 C. As shown in the model, when crossing *orc1b-2/+* to WT as a pollen donor, failed sperm-egg cell fertilization with the mutant sperm triggers the attraction of another pollen tube by the persistent synergid cell. The egg cell has a second chance to meet a WT pollen, and this fertilization recovery machinery raises the WT progeny number by 6%. When crossing *orc1b-2/+* to WT as a maternal parent, some mutant egg cells

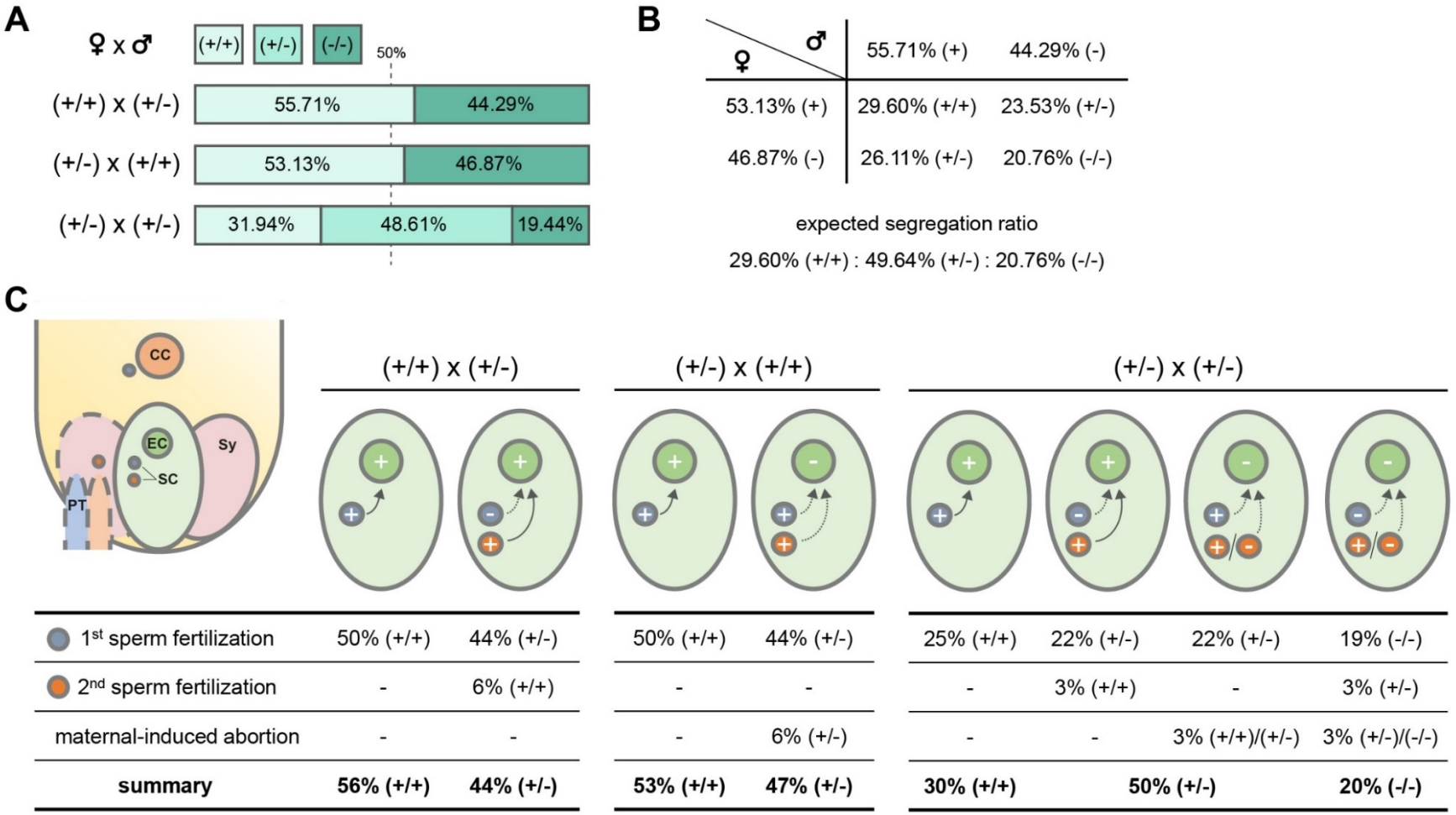

Figure 4.7 Parental Transmission of *orc1b-2* mutant allele. (A) The segregation ratio obtained from genotyping PCR of the progenies in the reciprocal crossings between *orc1b-2/+* and WT. **(B)** The expected segregation ratio of the self-crossed *orc1b-2/+* based on parental transmission rates. **(C)** A model for parental transmission of *orc1b-2* mutant allele. When cross *orc1b-2/+* to WT as a pollen donor, failed fertilization with mutant sperms triggers fertilization recovery machinery and raises the WT progeny number by 6%. When cross *orc1b-2/+* to WT as a maternal parent, failed fertilization with mutant egg cells results in a 6% seed abortion and a 3% reduction in the female transmission rate. When *orc1b-2/+* is self-crossed, the reduced gametic transmission additively affects the segregation of the progenies, resulting a segregation ratio of 30% (+/+) : 50% (+/-) : 20% (+/+). EC, egg cell; CC, central cell; Sy, synergid; PT, pollen tube; SC, sperm cell.

fail in fertilization. The fertilization recovery machinery is triggered but could not complement the maternal defects, resulting in a 6% seed abortion which further leads to a 3% reduction in the female transmission rate. When *orc1b-2/+* is self-crossed, the reduced gametic transmission additively affects the segregation of the progenies, leading to a segregation ratio of 30% (+/+) : 50% (+/-) : 20% (+/+). How the depletion of *ORC1b* causes the transmission distortions of both male and female gametes will be discussed below.

4.3.3 *ORC1b* is involved in sperm-egg cell nuclear fusion

orc1b-2 pollen triggered polytubey when crossed to WT (Figure 4.2 F, G). Combined with the failure in sperm-egg cell nuclear fusion (Figure 4.3 B), it seems that in the polytubey ovules, plasmogamy between the first sperm and the egg cell was accomplished but the following karyogamy failed, leading to activation of fertilization recovery and the attraction of the second pollen tube. Concerning the function of ORCs in origin licensing in DNA replication, it would be possible that the karyogamy failure is caused by the unsynchronized cell cycle between the sperm and the egg cell.

In rice, the cell cycle of a rice egg cell is estimated as the G1 phase with 1C DNA volume, and the genome replication progresses after karyogamy to reach the 4C volume in zygotes 6–10 h after gamete fusion (Sukawa and Okamoto 2018). In contrast, *Arabidopsis* has adopted G2 karyogamy, in which sperm cells complete DNA synthesis prior to the deposition into an egg cell (Friedman 1999). The cell cycle of sperm progresses along the process of pollination. It starts from the G1 phase in mature pollen and achieves the S/G2 phase with 2C volume once arrived at the ovule (Friedman 1999). The egg cell stays in a quiescent status at G0 and is activated upon fertilization by the sperm cell (Peng et al. 2018). The synchronizing signals exchanged between the male and female gametes are not yet understood. *ORC1b* transcripts are missing in the egg cell but appear in the spherical zygote and early embryo (P. Zhao et al. 2019), which fits a paternal transmitted expression in a manner similar to *SHORT SUSPENSOR* (*SSP*), the parent-of-origin regulator for the asymmetric first division in the early embryo (Bayer et al. 2009). We propose that *ORC1b* acts as the paternal factor carried over by the sperm in switching on the S-phase progression in the egg cell, where nuclear fusion is delayed because of the unsynchronized cell cycle of the two gametes when *ORC1b* is absent from the sperm. It has been shown in tobacco that pollination accelerates the S-phase progression in the egg cell, while in the absence of fertilization, the synchronization of the cell cycle of the egg cell is still completed but delayed for more than a day (Weterings and Russell 2004). Similarly, in *Arabidopsis*, the expression of *AtTMPK*, a thymidylate kinase gene activated during the G1/S-

phase transition, was observed in the unfertilized embryo sac at 44 h after emasculation (Ronceret et al. 2008). The autonomous catch-up of the G1/S-phase transition in the egg cell could explain that *orc1b-1* and *orc1b-2* pollen still produced embryos when crossed with WT (Figure 4.3 C, D). In this scenario, the incompatible cell cycle causes the karyogamy delay of the first sperm and triggers polytubey for fertilization recovery. Then, the egg cell starts S-phase progression autonomously and rescued karyogamy without the paternal signal. In addition, *ORC1b* seems not required for this autonomous synchronization of cell cycle in the egg cell, since *orc1b-2* self-crossed ovules showed increased polytubey (19.53% ± 7.59%) but with a mostly-full seed set (84.05% ± 7.83%) (Figure 4.2 C, F).

4.3.4 *ORC1b* is involved in sperm-central cell nuclear fusion

When *orc1b-1* and *orc1b-2* were crossed to WT as pollen donors, in some ovules the integument expansion failed with arrested seed coat development and uneven endosperm nuclear size, while the embryo appeared to be normal (Figure 4.3 C panel a; D panel a, b). It has been shown previously that endosperm goes through early syncytial development, cellularization, and degeneration autonomously together with a normal seed coat initiation independent of the embryo development, as observed in the single-fertilization mutant *dmp8/9* seeds without an embryo (Xiong, Wang, and Sun 2021). On the contrary, single fertilization leading to embryo only is not sufficient to initiate the development of surrounding integument, as observed in the *dmp8/9* seeds and *kokopelli* (*kpl*) seeds containing only embryos, where seed coat development was abolished and the integument began to degenerate at the globular stage (Xiong, Wang, and Sun 2021). Seed coat initiation is regulated by the crosstalk between the integument and the endosperm by a dosage-sensitive polycomb signaling pathway. Polycomb group (PcG) proteins represent conserved gene-silencing machinery that forms the PRC2 which acts as an H3K27me3 writer (Derkacheva and Hennig 2014). EMBRYONIC FLOWER2 (EMF2) and VERNALIZATION2 (VRN2) are two sporophytic PcG proteins that suppress seed coat development in the absence of fertilization. The type I MADS-box transcription factor AGL62 activates a mobile signal upon fertilization to relieve PcG repression in the integuments and to initiate seed coat formation (Roszak and Köhler 2011). In the ovules with arrested seed coat development from siliques of WT × *orc1b-1* and WT × *orc1b-2,* the failed endosperm proliferation seems to account for the failure in the seed coat. The abnormal endosperm failed to alleviate the PRC2 suppression of seed coat development, leading to the deformation of the integument at the globular stage.

A similar phenotype with uneven sizes of the endosperm nuclei is observed in the mutants

of two immunoglobulin binding protein genes (BiP) *BIP1* and *BIP2*, as well as the two ER-resident J-protein genes *P58IPK* and *ERdj3A* that are required for polar nuclear-membrane fusion in female gametophyte development. The double mutants *bip1 bip2* and *erdj3a p58ipk* produce polar nuclei closely attached without fusion (Maruyama et al. 2014; Maruyama, Endo, and Nishikawa 2010). These unfused polar nuclei are defective in sperm nuclear fusion, leading to aberrant endosperm proliferation with irregular nucleus size and retarded paternal gene expression, emphasizing that a proper nuclear fusion between sperm and central cell is critical for endosperm proliferation (Maruyama et al. 2020). The arrested endosperm proliferation in the ovules fertilized by *orc1b-1/2* pollen with only a few nuclei of uneven size could be a consequence of failed sperm-central cell nuclear fusion, and the large-sized nuclei could be derived from the autonomous division of the polar nucleus, while the small size nuclei could be the unfused sperm nucleus (Figure 4.3 C panel a, D panel b). In addition, the uneven size of the endosperm nuclei was also seen in the ovules with a normal seed coat development. As shown in Figure 4.3 C panel b, a few endosperm nuclei were extra-large at the micropylar area while the rest appeared to be normal. The function of the endosperm seemed to be not disturbed since the seed coat expanded as planned. It could be that polytubey brought an extra pair of sperm, one of which fused with the egg cell and the other one accidentally fused with one of the 3n endosperm nuclei that are already dividing.

The endosperm defects were more dramatic at late stages in the self-crossed ovules of *orc1b-2* (Figure 4.4). Some ovules failed in seed coat development with no endosperm proliferation (Figure 4.4 E, J, N, O). In some of the ovules of normal size, the seed coat expanded together with the development of the endosperm, but the endosperm nuclei clumped around the peripheric area without going through cellularization (Figure 4.4 C, D, H, I). In earlier studies, the failure in endosperm cellularization could be triggered by pollination with pollen donors of higher ploidy. In the interploidy crossings, the increased activity of paternally expressed imprinted genes (PEGs) in the endosperm of triploid seeds causes failed cellularization of endosperm, which further leads to a compromised embryo in short sucrose supply (Wolff et al. 2015; Morley-Smith et al. 2008; Hehenberger, Kradolfer, and Köhler 2012). *ADMETOS* (*ADM*), *SUVH7*, *PEG2*, and *PEG9* are four of these PEGs, and the suppression of pectin hydrolysis in *adm*, *suvh7*, *peg2*, and *peg9* promotes cell wall formation and cellularization in the endosperm (Wolff et al. 2015; Kradolfer et al. 2013). This paternal-regulated triploid barrier establishment is also found to be regulated by easiRNAs in a dosage-sensitive manner during interploidy hybridizations. The increased abundance of easiRNAs from 2n pollen negatively interferes with the repression of some PEGs in the endosperm correlated

with reduced CHH methylation. And the triploid barrier was partially broken in the loss of the plant-specific RNA polymerase IV which suppressed easiRNA formation and restored small-RNA-directed DNA methylation at transposable elements (TEs) (Martinez et al. 2018). The failed endosperm cellularization in the *orc1b-2* self-crossed ovules nicely mimicked the triploid seeds produced by 2n pollen. We suspect that, with the arrival of the extra pollen tube in *orc1b-2*, more than one sperm could fuse with the central cell, leading to an over-dosage of the paternal easiRNAs similar to that in the 2n pollen, which further interferes with the gene suppression and compromises the endosperm cellularization. It was shown that ORC1b binding correlates with increased H4K20me3 in the proximal promoter region of ORC1 targets (M. D. L. P. Sanchez and Gutierrez 2009). In human cells, H4K20me3 facilitates the origin licensing and selection of active initiation sites in late-replicating heterochromatin domains (Brustel et al. 2017; Kirstein et al. 2021). H4K20me3 also crosstalks to DNA methylation in heterochromatin formation, where DNA methyltransferase 1 (DNMT1) specifically recognizes H4K20me3 via its BAH and reinforces DNA methylation (Ren et al. 2021). Taken together with the co-localization of ORC1b-YPet with centromeric regions, this suggests a potential role of *ORC1b* in genomic integrity and stability in the heterochromatin area. Whether the absence of ORC1b binding causes misregulation of TEs and easiRNAs in the sperms still needs to be explored.

The potential causes for these abnormalities observed in endosperm development still require more experimental proof. The *orc1b-2*-RbP and the central cell marker line expressing *proAGL80:HTR12-YPet*, which marks the central cell and endosperm nucleus, could be adopted to characterize nuclear fusion and endosperm proliferation in *orc1b-2* in detail. If the misbehaved *orc1b-2* pollen induced a similar paternal-induced misregulation of PEGs and TEs, could be further checked by transcription level characterizations, such as qPCR, RNA sequencing, or *in situ* hybridization.

4.3.5 *ORC1b* is involved in genome integrity maintenance

In the self-crossed siliques of two *orc1b* mutant individuals, *orc1b-1-as* and *orc1b-2-as*, nearly one-third of ovules were abnormal with albino appearance (Figure 4.5 A). These abnormal ovules showed a normal layered seed coat structure and normal accumulation of tannins at the mature stage, suggesting that the crosstalk between endosperm proliferation and seed coat development was not abolished. Though endosperm proliferation was not arrested, the endosperm nuclei showed some abnormalities such as uneven nuclear size and irregular cellularization (Figure 4.5 B). The presence of the dramatic phenotype in both the knock-out allele and T-DNA insertion allele confirmed that it was induced by *ORC1b* depletion, and

segregation of the phenotype in *orc1b-2-as* progenies in the same homozygous mutant background implied it to be independent of *ORC1b* genotype.

Interestingly, these albino seeds with embryo and endosperm defects are reminiscent of the defects in the mutants of *MCM2-7* genes. MCM2-7 complex acts as a DNA helicase and is recruited to replication origins by the ORC in coordination with CDT1 and CDC6 (Makarova and Koonin 2013). All the *mcm2-7* mutants showed a maternal effect with defects in embryo patterning, endosperm nuclear size, and endosperm cellularization (Holding and Springer 2002; Herridge, Day, and Macknight 2014). Specific reduction of *MCM5* and *MCM7* expression in the endosperm using artificial microRNAs resulted in an upregulation of genes in DNA damage response, indicating that genome integrity was disrupted when MCMs were depleted. And the enlarged endosperm nuclear size could be a consequence of the activation of the ATAXIA TELANGIECTASIA MUTATED (ATM)-dependent DNA damage response (Herridge, Day, and Macknight 2014). Mutation in *MUN,* a kinetochore complex protein gene colocalized with HTR12 at the centromere, causes chromosome segregation defects and DNA aneuploidy. The mutant also produces defective seeds with arrested embryos (Shin et al. 2018). The epigenetic alterations of centromeres, such as mutations in the centromere-specific histone variant *CENH3* and the centromere licensing factor *KNL2*, have been shown to result in chromosome segregation errors, genome elimination, and lethality (Ravi et al. 2011; Marimuthu et al. 2021; Ahmadli et al. 2022). These previous findings might explain the over-produced albino seed phenotype observed in *orc1b-1-as* and *orc1b-2-as*. With the multilateral potential of ORC1b BAH-PHD domain in reading and writing histone modifications, mutations in *ORC1b* might alter the epigenetic environment in the centromeric area, therefore leading to a similar defect in chromosome segregation and genome elimination. In this scenario, the mutation in *ORC1b* disrupted centromere integrity, and it caused a rare case of single chromosome elimination during cell division in *orc1b-1-as* and *orc1b-2-as*. It would explain that the albino seed phenotype did not co-segregate with the *ORC1b* genotype. In good agreement with this, in *orc1b-2-as* pollen labeled by the centromere marker HTR12-mCherry, only four centromeres were observed in some sperm nuclei, whereas five centromeres should be observed in a WT sperm nucleus (Figure 4.6). The 1:1 segregation ratio of the over-production of albino seeds in *orc1b-2-as* progenies suggest it to be a gametic lethal mutation. The abnormal seeds were not seen in out-crossed siliques when *orc1b-2-as* was adopted as a pollen donor, implying the abnormal seeds are attributed to the maternal parent. These observations suggest that the maternal parent is more sensitive to the unintact genome.

To further confirm the nuclear content in *orc1b-2-as*, a flow cell cytometry assay was

performed to measure the nuclear content of nuclei prepared from the cotyledons of *orc1b-2-as* seedlings. Despite the heavy contamination from the cell fragments, the nuclear signal of *orc1b-2-as* was slightly reduced than that in WT (data not shown). However, the resolution was not adequate to distinguish the signal reduction in an aneuploid genome with single chromosome depletion. Since the phenotype of albino seeds is segregating in *orc1b-2-as*, half of the *orc1b-2-as* seedlings harbor an aneuploid genome with 9 chromosomes, resulting in a 5% reduction of nuclear content in the nuclei samples prepared from cotyledons of *orc1b-2-as* seedlings. It is recommended to repeat the flow cell cytometry assay with nuclei extracted from pollen in the following work. In this way, we would have the privilege to sample after phenotyping and extract nuclei only from mutants that produce albino seeds, which presumably results in a 20% reduction of nuclear content.

Human ORC1 was shown to function in the centrosomes in cell division. Cyclin A promotes ORC1 localization to centrosomes where ORC1 prevents cyclin E-dependent re-duplication of both centrioles and centrosomes in the cell division cycle, suggesting the additional role of ORC1 in controlling the copy number of centriole and centrosome (Hemerly et al. 2009). Land plants have lost centrosomes and utilize microtubule-organizing centers (MTOCs) as replacements for centrosomes in initiating spindle bipolarity and orientation (reviewed in Yi and Goshima 2018). The B1-type cyclin, CYCB1;2, coupled with CDKB2;2 can phosphorylate an MT-nucleation factor GIP1 in orchestrating mitotic microtubule networks (Romeiro Motta et al. 2022). Whether ORC1b keeps the ability to interact with these cyclins in establishing MTOCs during mitosis needs to be further addressed.

In conclusion, ORC1b is a sperm nuclear protein required for fertilization. Disruption of *ORC1b* expression causes reduced fertility, defective gametic nuclear fusion, arrested embryo, and abnormal endosperm development. The characterization of the inheritable phenotype of over-production of albino seeds in two independent single mutant lines suggests a potential role of *ORC1b* in genome integrity maintenance. These phenotypic analyses provide a solid basis for further deciphering the mechanism of *ORC1b*'s function in fertilization. Collectively, this study offers new perspectives on additional roles of ORC genes independent of origin licensing in plants and furthers our understanding of the paternal contribution to fertilization in flowering plants.

4.4 Materials and methods

4.4.1 Plant materials and growth conditions

These mutant alleles *orc1a-1* (WiscDsLox287F12) (Woody et al. 2007) and *orc1b-1* (GK-

769D03) (Rosso et al. 2003) in Col-0 background each carry a T-DNA insertion in the coding region. The mutant allele *orc1b-2* was generated by the in-house CRISPR-Cas9 knockout vector expressing sgRNA1 (5′-GCCATTGATGGTGTAAGCTA-3’) and sgRNA2 (5′-ACGATACTGTCGTTGCCACT-3’) in Col-0 background. The transgene-free *orc1b-2* mutants were selected and subjected to phenotypic analysis. The allele-specific genotyping primers are listed in Table 4.1.

Insertion lines were provided by the Nottingham *Arabidopsis* Stock Center (NASC) (Scholl, May, and Ware 2000). The Rainbow Pollen (RbP) and Rainbow Female Gametophyte (RbFG) marker lines used in this study were described in chapter 5. Plants used in this study were grown under long-day conditions as described previously in (Babu et al. 2013).

Table 4.1 Specific genotyping primers for *orc1* mutant alleles

Mutant allele		Primer	PCR product length
orc1a-1	LP	5′-TTTACGAGAATTTGCACCACC-3’	LP+RP: 1204 bp in WT; none in mutant BP+RP: none in WT; ~600 bp in mutant
	BP	5′-TCCTCGAGTTTCTCCATAATAATGT-3’	
	RP	5′-CCTTCTGCGTCACCATCTTAG-3’	
orc1b-1	LP	5′-CCTCACAACTTCTCGATCCAACTCTC-3’	LP+RP: 2660 bp in WT; none in mutant BP+RP: none in WT; ~600 bp in mutant
	BP	5′-ATAATAACGCTGCGGACATCTACATTTT-3’	
	RP	5′-GAGCAAAAACCTTCAAATCCC-3’	
orc1b-2	LP	5′-CGCCTTAGCAAACTCGATCC-3’	LP+RP: 3492 bp in WT; 126 bp in mutant BP+RP: 1001 bp in WT; none in mutant
	BP	5′-ATTGGGTCATTTCCCAGATCGA-3’	
	RP	5′-CCTCACAACTTCTCGATCCAACTCTC-3’	

4.4.2 Plasmid construction

For the construction of the CRISPR-Cas9 destination binary vector, sgRNA1 and sgRNA2 were integrated into two shuffle-in vectors containing *AtU6* promoter and sgRNA scaffold by overlapping PCR reactions, and the two sgRNA expression units were assembled into destination *pMB3300* vector containing *proEC1.2en-EC1.1:pcoCas9* and *proAt2S3:mCherry*. For the construction of the *proORC1b:ORC1b-YPet* binary vector, the promoter sequence starting from 2147 bp upstream of the start codon and the full-length genomic sequence of *ORC1b* were amplified and cloned into the binary vector *pMB3300* containing *YPet-tNos*. All the fragments were cloned into vectors using In-Fusion® Snap Assembly according to the manufacturer’s instructions. All the expression vectors were transformed into Col-0 by Agrobacterium-mediated transformation via floral dip as previously described (Clough and

Bent 1998).

4.4.3 Pollen RNA preparation and quantitative PCR

400 freshly opened flowers from orc1b-1 and WT were collected into 2-mL tubes on ice, respectively. 1 mL 0.3 M mannitol was added into the 2-mL tubes and vortexed for 1 min to release pollen from anthers. The suspensions were collected into new 2-mL tubes and centrifuged at 5000 rpm for 2 min to pellet pollen. Total RNA was extracted from orc1b-1 and WT pollen using the QIAGEN RNeasy® Plant Mini Kit cDNA was synthesized using the Thermo Scientific RevertAid First Strand cDNA Synthesis Kit. RT-PCR was performed using Thermo Scientific DreamTaq PCR Master Mix (2x) with 30 reaction cycles. qRT-PCR was performed using NEB Luna® Universal (RT)-qPCR Reagents. All the reagents were used according to the manufacturers' recommendations. The primers used are listed in Table 4.2. *Actin2* was used as a control.

Table 4.2 Primers for quantitative PCR in *orc1b-1* pollen

Gene		Primer	PCR product length
ORC1a	LP	5′-CCTTCTGCGTCACCATCTTAG-3'	144 bp
	RP	5′-TGAGGAGGAGTGAGTGAAGTTG-3'	
ORC1b	LP	5′-CGCATAATCTGAAACGAGAGC-3'	248 bp
	RP	5′-AACCTCCTCCTCCTTCCTACC-3'	
Actin2	LP	5′-TGTGCCAATCTACGAGGGTTT-3'	137 bp
	RP	5′-TTTCCCGCTCTGCTGTTGT-3'	

4.4.4 Phenotypic analysis of mutants

Hoyer's solution clearing of ovules

Ovules were dissected and cleared in Hoyer's solution as described previously in (Bayer et al. 2009). Cleared samples were examined by DIC microscopy with Zeiss Axio Imager.Z1 microscope equipped with an AxioCam HRc camera.

Fluorescence and confocal laser scanning microscopy

Pollen grains at different developmental stages were mounted in 10% glycerol for microscopy. Mature pollen was collected and germinated as described previously (Vogler et al. 2014). Sperm cells inside the germinating pollen tube were imaged after 6 h on pollen germination media. Ovules at 24 HAP were dissected out and stained by SR2200 as described previously in (Musielak et al. 2016). Confocal scanning microscopy was performed with Zeiss LSM780NLO.

Aniline blue staining of pollen tubes in pistils

Pollen grains were collected from freshly opened flowers and pollinated to pistils emasculated 24 h earlier. Pistils were excised at 24 HAP and proceeded to fixation and aniline blue staining as described previously (Zhong et al. 2022). Pistils after staining were mounted in 10% glycerol and examined with Zeiss LSM780NLO.

Seeds gemination

The mutant seeds were put on a 1/2 MS media plate with 0.1% agar, pH 5.7, and incubated for 12 days under long-day conditions the same as the plants used in this study. Seeds and seedlings were observed with a dissecting microscope with an external camera.

5 Fluorescent marker lines assist phenotypic characterization of fertilization-defective mutants

Plant fertilization involves the coordination of a series of male and female cells and tissues which work in a fine-tuned system. Light microscopy in combination with a variety of whole-mount staining and clearing methods for pollen tubes, female gametes, and early embryos inside ovules is widely utilized in phenotypic analysis in plant reproduction. However, the deep embedding of the generative cells inside the integument cell layers with a low opacity makes it challenging to obtain phenotypic information on a cellular or sub-cellular level. Therefore, introducing fluorescent proteins into specific cells and tissues would be instrumental in visualizing the fertilization process. Here, we constructed a set of transgenic marker lines each carrying several fluorescent marker cassettes that are expressed in either pollen or female gametophytes. These fluorescent marker cassettes are genetically linked in two lines which can be easily introgressed into a mutant background by crossing. A combination of the fluorescent signals from both parental sides enables versatile analyses of fertilization defects within one single crossing.

5.1 Results

5.1.1 Rainbow Pollen marker cassettes

In earlier attempts of the host lab to construct the integrated transgenic cassettes expressing quadruple fluorescent markers, transgenic silencing was frequently observed resulting in one or two fluorescent markers being absent. The female gametophyte seemed to be intolerant of the over-expressed fluorescent proteins, giving rise to a homozygous transgenic plant with reduced maternal fertility when pollinated by WT pollen (data not shown). According to these observations, we redesigned the fluorescent markers to minimize the number of transgenic cassettes but still offer enough information for addressing fertilization defects. For Rainbow Pollen (RbP) marker cassettes, three fluorescent proteins driven by cell-specific promotors were integrated into *Arabidopsis* to label several cell structures in the male gametes by genomic transgene. The fluorescent markers expressed in the pollen of RbP are shown in Figure 5.1. The chromatin in the sperm nuclei was labeled by the sperm-specific histone 3 variant MALE GAMETE HISTONE 3 (MGH3) (Okada et al. 2005) fused with NeonGreen under the control of its native promoter (Figure 5.1 A). The sperm membrane was labeled by mRuby2 fused with the membrane localization signal N-myristoylation (Resh 1999) driven by the promoter of the

sperm-specific gene *DUO1-ACTIVATED ZINC FINGER 3* (*DAZ3*) (Borg et al. 2011). The sperm centromeres were stained by mCherry fused with the centromere-identifying histone 3 variant HISTONE THREE RELATED 12 (HTR12) (Talbert et al. 2002) driven by its endogenous promoter (Figure 5.1 B). The two red fluorescent proteins can be easily distinguished from each other by their unique membrane-specific and centromere-specific localization during fertilization, even though they share the same excitation and emission spectrum. Using this system, after the discharge of sperms from the pollen tube, the integration of the myr-mRuby2 signal on the egg cell membrane would be observed once plasmogamy is achieved. The migration of the sperm nucleus inside the egg cell would be indicated by the nuclear signals MGH3-NeonGreen and HTR12-mCherry. The signals would expand shortly after nuclear fusion and become invisible in the zygote due to the removal of the sperm-inherited MGH3 during chromatin remodeling, which is considered a sign of successful activation of the zygote program (Ingouff et al. 2007).

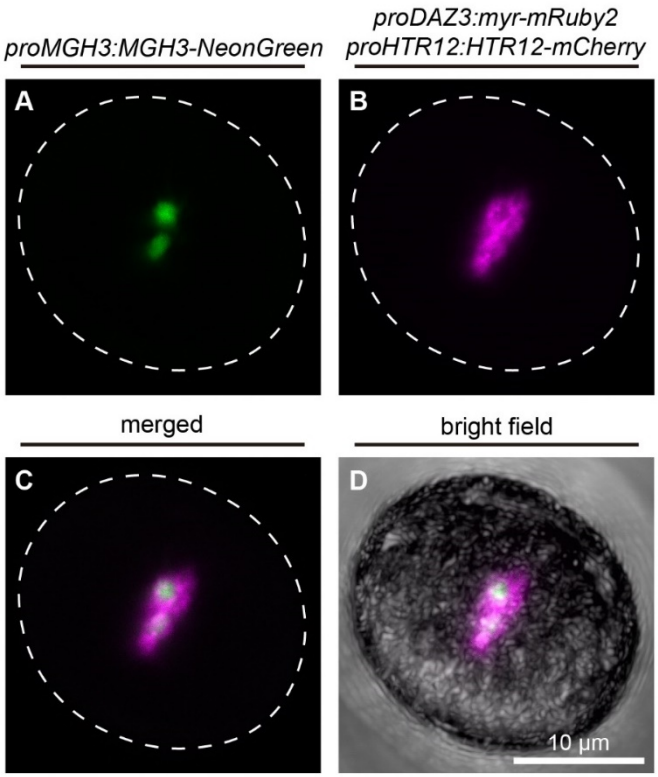

Figure 5.1 Rainbow Pollen (RbP) marker cassettes. (A) Expression of *MGH3-NeonGreen* in the sperm nuclei. **(B)** Expression of *myr-mRuby2* on the sperm membrane and *HTR12-mCherry* in the sperm centromeres. **(C)** Merged image of the GFP and RFP channel. **(D)** Merged image of the GFP, RFP, and the bright field channel. The dashed lines indicate the pollen periphery.

5.1.2 Rainbow Female gametophyte cassette

For Rainbow Female Gametophyte (RbFG) marker cassettes, three fluorescent proteins

driven by cell-specific promotors were integrated into *Arabidopsis* to label different cell structures in the female gametophyte by genomic transgene. The fluorescent markers expressed in RbFG ovules stained by SCRI Renaissance 2200 (SR2200) are shown in Figure 5.2. The egg cell membrane was marked by myr-vsfGFP-0 driven by the promoter of the egg cell-specific gene *EGG CELL 1* (*EC1*) fused with the *EC1.2* enhancer (*proEC1.2en-EC1.1*) which was shown to exhibit a much higher efficiency (Z. P. Wang et al. 2015). This promoter offers the additional benefit of indicating successful fertilization due to the silencing of *EC1* in the early zygote. The synergid cells were indicated by mScarlet signal in the mitochondria driven by the *MYB98* promoter which is exclusively active in the synergid cells (Punwani, Rabiger, and Drews 2007). Mitochondrial targeting was achieved by incorporating the first 22 aa of Cytochrome c oxidase subunit IV (ScCOX4) from budding yeast (*Saccharomyces cerevisiae*) (Köhler et al. 1997) into the mScarlet sequence. A homozygous marker line was obtained with stable expression of the fluorescent proteins, and the female fertility showed no difference from WT (data not shown). This dual-color marker can be used to monitor pollen tube reception, the fusion of the persisting synergid cell with the central cell after fertilization as well as the onset of the zygotic program.

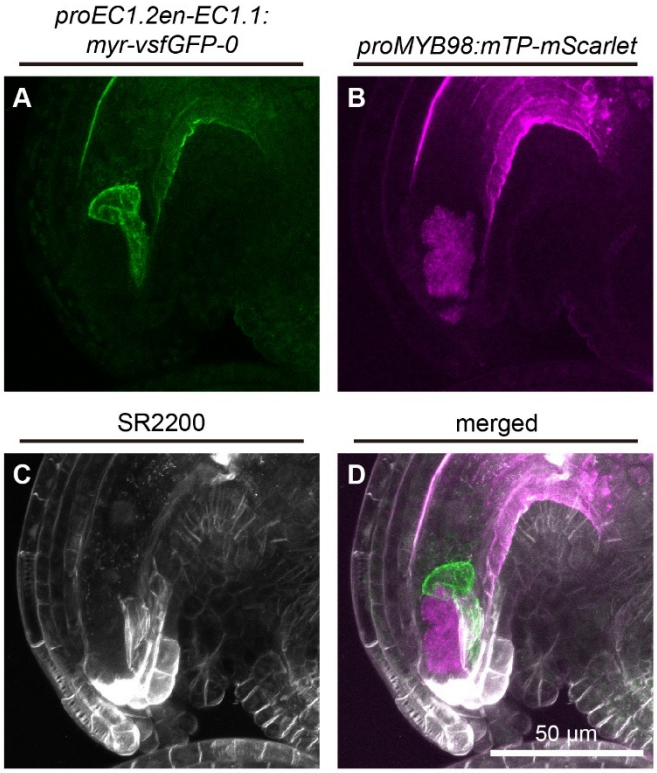

Figure 5.2 Rainbow Female Gametophyte (RbFG) marker cassettes. (A) Expression of *myr- vsfGFP-0* on the egg cell membrane. **(B)** Expression of *mTP-mScarlet* in the mitochondria of the synergid cells. **(C)** SR2200 staining indicates the cell perimeter of the ovule. **(C)** Merged image of the GFP channel, RFP channel, and the DAPI channel used for SR2200 staining signals.

5.1.3 Single female gametophyte marker lines

Due to the sensitivity of the female gametophyte to certain levels of over-expressed fluorescent proteins that we observed while creating the marker line, only the necessary maker cassettes were included in the current RbFG marker line. To make full use of the additionally designed female gametophyte marker cassettes, a bunch of single female gametophyte marker cassettes was cloned into empty *pMB3300* binary vectors and introduced into plants separately. These marker lines include two egg cell membrane makers expressing *myr-mTFP1* driven by the promoter of the egg cell-specific gene *EGG CELL-SPECIFIC1* (*ECS1*) (Yu et al. 2021) (Figure 5.3 A) and *myr-vsfGFP-0* driven by *proEC1.2en-EC1.1* (Figure 5.3 B). Furthermore, we obtained a synergid marker line expressing *mTP-mScarlet* in the mitochondria driven by the promoter of the synergid cell-specific gene *MYB98* (Punwani, Rabiger, and Drews 2007) (Figure 5.3 C), and a central cell/endosperm marker expressing *HTR12-YPet* driven by the promoter of the central cell/endosperm-specific gene *AGL80* (Portereiko et al. 2006) (Figure 5.3 D). Lastly, we also made a zygote/embryo marker expressing *RanGAP1WPP-superfolderGFP* on the nuclear envelope driven by the *S4* promoter which was shown to be active in the zygote/embryo (Slane et al. 2014) (Figure 5.3 E), where the nuclear envelope localization is achieved by incorporating the N-terminal WPP domain of RanGAP1, a small GTPase involved in nuclear transport and nuclear envelope assembly (Jeong et al. 2005).

5.2 Discussion

The fertilization process in *Arabidopsis* occurs deep inside the female tissue, which hinders the phenotypic characterization of the fertilization defective mutants. Hoyer's solution clearing (L. E. Anderson 1954) of dissected ovules combined with DIC imaging allows the observation of embryo and endosperm development as shown in recent publications from the host lab (Neu et al. 2019; K. Wang et al. 2021). However, not much information on gametic interaction during fertilization could be obtained. SR2200 stains all the cell perimeter of ovules which helps identify most cell types including the pollen tube, while the cells need to be fixed (Musielak et al. 2016). The fluorescent marker lines developed in this study constitute a versatile toolbox that allows the subtle characterization of pollen development, female gametophyte development, gametic interaction, gametes fusion, embryonic development, and endosperm proliferation. The broad spectrum of fluorescent proteins in this toolbox offers various channel combinations for crossing either to mutants labeled by other marker lines or crossing to transgenic lines expressing target genes fused to fluorescent proteins. Most importantly, these marker lines are eligible for live imaging, which enables the capture of subtle

events that arise within a short time window.

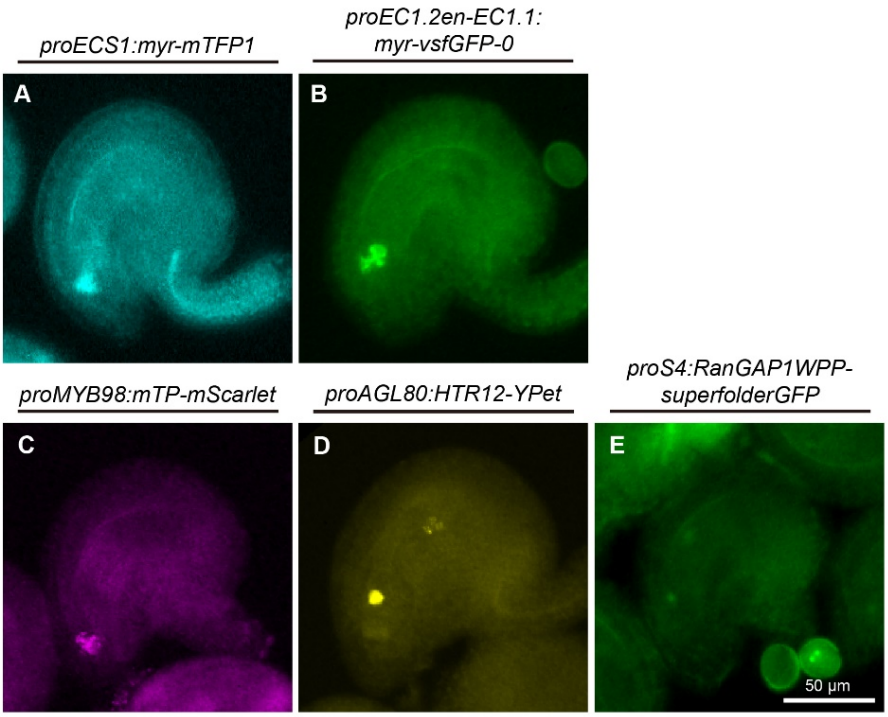

Figure 5.3 Single female gametophyte marker cassettes. (A) Female gametophyte marker expressing *myr-mTFP1* on the egg cell membrane. **(B)** Female gametophyte marker expressing *myr-vsfGFP-0* on the egg cell membrane. **(C)** Female gametophyte marker expressing *mTP-mScarlet* in the mitochondria of the synergid cells. **(D)** Female gametophyte marker expressing *HTR12-YPet* in the nuclei of the central cell and the antipodal cells. **(E)** Female gametophyte marker expressing *RanGAP1WPP-superfolderGFP* on the nuclear envelope of the zygote.

5.3 Materials and methods

5.3.1 Plant material and growth conditions

Arabidopsis thaliana Col-0 was used for transgenic transformation in this study. All plants used were grown under long-day conditions as described previously (Babu et al. 2013).

5.3.2 Plasmid construction

For the construction of RbP marker expression vector, *proHTR12:HTR12-mCherry*, *proMGH3:MGH3-NeonGreen,* and *proDAZ3:myr-mRuby2* sequences were synthesized. For the construction of RbFG marker expression vector, *proEC1.2en-EC1.1:myr-vsfGFP-0* and *proMYB98:mTP-mScarlet* sequences were synthesized. For construction of the single female gametophyte markers expression vectors, the *proECS1:myr-mTFP1, proEC1.2en-EC1.1:myr-vsfGFP-0*, *proMYB98:mTP-mScarlet, proAGL80:HTR12-YPet* and *proS4:RanGAP1WPP-superfolderGFP* sequences were synthesized. All the fragments were cloned into empty binary vector *pMB3300* using In-Fusion® Snap Assembly according to the manufacturer's instructions, respectively. All the expression vectors were transformed into Col-0 by Agrobacterium-

mediated transformation via floral dip as previously described (Clough and Bent 1998).

5.3.3 Microscopic analysis of pollen and ovules

Mature pollen grains of RbP were mounted in 10% glycerol. Ovules of RbFG were dissected from pistils 1 day after emasculation and stained by SR2200 as described previously (Musielak et al. 2016). These samples were imaged by confocal scanning microscopy with Zeiss LSM780NLO. Ovules of the single female gametophyte marker lines were dissected, mounted in 10% glycerol, and examined by Zeiss Axio Imager.Z1 microscope equipped with an AxioCam HRc camera.

6 References

Abercrombie, Jason M., Brian C. O'Meara, Andrew R. Moffatt, and Joseph H. Williams. 2011. "Developmental Evolution of Flowering Plant Pollen Tube Cell Walls: Callose Synthase (CalS) Gene Expression Patterns." *EvoDevo* 2 (1): 14. https://doi.org/10.1186/2041-9139-2-14.

Ahmadli, Ulkar, Manikandan Kalidass, Lucie Crhak Khaitova, Joerg Fuchs, Maria Cuacos, Dmitri Demidov, Sheng Zuo, et al. 2022. "High Temperature Increases Centromere-Mediated Genome Elimination Frequency in Arabidopsis Deficient in CenH3 or Its Assembly Factor KNL2." *BioRxiv*, March, 2022.03.24.485459. https://doi.org/10.1101/2022.03.24.485459.

Alandete-Saez, Monica, Mily Ron, Samuel Leiboff, and Sheila McCormick. 2011. "Arabidopsis Thaliana GEX1 Has Dual Functions in Gametophyte Development and Early Embryogenesis." *Plant Journal* 68 (4): 620–32. https://doi.org/10.1111/j.1365-313X.2011.04713.x.

Alandete-Saez, Monica, Mily Ron, and Sheila McCormick. 2008. "GEX3, Expressed in the Male Gametophyte and in the Egg Cell of Arabidopsis Thaliana, Is Essential for Micropylar Pollen Tube Guidance and Plays a Role during Early Embryogenesis." *Molecular Plant* 1 (4): 586–98. https://doi.org/10.1093/mp/ssn015.

Althiab-Almasaud, Rasha, Huguette Sallanon, Caren Chang, and Christian Chervin. 2021. "1-Aminocyclopropane-1-Carboxylic Acid Stimulates Tomato Pollen Tube Growth Independently of Ethylene Receptors." *Physiologia Plantarum* 173 (4): 2291–97. https://doi.org/10.1111/ppl.13579.

Anderson, Lewis E. 1954. "Hoyer's Solution as a Rapid Permanent Mounting Medium for Bryophytes." *The Bryologist* 57 (3): 242. https://doi.org/10.2307/3240091.

Anderson, Sarah N., Cameron S. Johnson, Joshua Chesnut, Daniel S. Jones, Imtiyaz Khanday, Margaret Woodhouse, Chenxin Li, Liza J. Conrad, Scott D. Russell, and Venkatesan Sundaresan. 2017. "The Zygotic Transition Is Initiated in Unicellular Plant Zygotes with Asymmetric Activation of Parental Genomes." *Developmental Cell* 43 (3): 349-358.e4. https://doi.org/10.1016/j.devcel.2017.10.005.

Arias, Emily E., and Johannes C. Walter. 2007. "Strength in Numbers: Preventing Rereplication via Multiple Mechanisms in Eukaryotic Cells." *Genes and Development* 21 (5): 497–518. https://doi.org/10.1101/gad.1508907.

Autran, Daphné, Célia Baroux, Michael T. Raissig, Thomas Lenormand, Michael Wittig, Stefan Grob, Andrea Steimer, et al. 2011. "Maternal Epigenetic Pathways Control Parental Contributions to Arabidopsis Early Embryogenesis." *Cell* 145 (5): 707–19. https://doi.org/10.1016/j.cell.2011.04.014.

Babu, Yashodar, Thomas Musielak, Agnes Henschen, and Martin Bayer. 2013. "Suspensor Length Determines Developmental Progression of the Embryo in Arabidopsis." *Plant Physiology* 162 (3): 1448–58. https://doi.org/10.1104/pp.113.217166.

Bai, Shun, Kaiqiang Fu, Huiqi Yin, Yiqiang Cui, Qiuling Yue, Wenbo Li, Le Cheng, et al. 2018. "Erratum: Sox30 Initiates Transcription of Haploid Genes during Late Meiosis and Spermiogenesis in Mouse Testes (Development (Cambridge) (2018) 145 (Dev164855) DOI: 10.1242/Dev.164855)." *Development (Cambridge)* 146 (11).

https://doi.org/10.1242/DEV.161471.

Baroux, C., D. Autran, C. S. Gillmor, D. Grimanelli, and U. Grossniklaus. 2008. “The Maternal to Zygotic Transition in Animals and Plants.” *Cold Spring Harbor Symposia on Quantitative Biology* 73: 89–100. https://doi.org/10.1101/sqb.2008.73.053.

Baubec, Tuncay, Huy Q. Dinh, Ales Pecinka, Branislava Rakic, Wilfried Rozhon, Bonnie Wohlrab, Arndt von Haeseler, and Ortrun Mittelsten Scheid. 2010. “Cooperation of Multiple Chromatin Modifications Can Generate Unanticipated Stability of Epigenetic States in Arabidopsis.” *Plant Cell* 22 (1): 34–47. https://doi.org/10.1105/tpc.109.072819.

Bayer, Martin, Tal Nawy, Carmela Giglione, Mary Galli, Thierry Meinnel, and Wolfgang Lukowitz. 2009. “Paternal Control of Embryonic Patterning in Arabidopsis Thaliana.” *Science* 323 (5920): 1485–88. https://doi.org/10.1126/science.1167784.

Beale, Kristin M., Alexander R. Leydon, and Mark A. Johnson. 2012. “Gamete Fusion Is Required to Block Multiple Pollen Tubes from Entering an Arabidopsis Ovule.” *Current Biology* 22 (12): 1090–94. https://doi.org/10.1016/j.cub.2012.04.041.

Bell, Stephen P. 2017. “Rethinking Origin Licensing.” *ELife* 6 (January). https://doi.org/10.7554/eLife.24052.

Bell, Stephen P., Jay Mitchell, Jess Leber, Ryuji Kobayashi, and Bruce Stillman. 1995. “The Multidomain Structure of Orc1 p Reveals Similarity to Regulators of DNA Replication and Transcriptional Silencing.” *Cell* 83 (4): 563–68. https://doi.org/10.1016/0092-8674(95)90096-9.

Besser, Kiera von, Aubrey C. Frank, Mark A. Johnson, and Daphne Preuss. 2006. “Arabidopsis HAP2 (GCS1) Is a Sperm-Specific Gene Required for Pollen Tube Guidance and Fertilization.” *Development* 133 (23): 4761–69. https://doi.org/10.1242/dev.02683.

Bicknell, Louise S., Ernie M.H.F. Bongers, Andrea Leitch, Stephen Brown, Jeroen Schoots, Margaret E. Harley, Salim Aftimos, et al. 2011. “Mutations in the Pre-Replication Complex Cause Meier-Gorlin Syndrome.” *Nature Genetics* 43 (4): 356–60. https://doi.org/10.1038/ng.775.

Blackledge, Neil P., Nathan R. Rose, and Robert J. Klose. 2015. “Targeting Polycomb Systems to Regulate Gene Expression: Modifications to a Complex Story.” *Nature Reviews Molecular Cell Biology* 16 (11): 643–49. https://doi.org/10.1038/nrm4067.

Bleichert, Franziska, Michael R. Botchan, and James M. Berger. 2015. “Crystal Structure of the Eukaryotic Origin Recognition Complex.” *Nature* 519 (7543): 321–26. https://doi.org/10.1038/nature14239.

Borg, Michael, Lynette Brownfield, Hoda Khatab, Anna Sidorova, Melanie Lingaya, and David Twella. 2011. “The R2R3 MYB Transcription Factor DUO1 Activates a Male Germline-Specific Regulon Essential for Sperm Cell Differentiation in Arabidopsis.” *Plant Cell* 23 (2): 534–49. https://doi.org/10.1105/tpc.110.081059.

Borg, Michael, Yannick Jacob, Daichi Susaki, Chantal LeBlanc, Daniel Buendía, Elin Axelsson, Tomokazu Kawashima, et al. 2020. “Targeted Reprogramming of H3K27me3 Resets Epigenetic Memory in Plant Paternal Chromatin.” *Nature Cell Biology* 22 (6): 621–29. https://doi.org/10.1038/s41556-020-0515-y.

Borg, Michael, Ranjith K. Papareddy, Rodolphe Dombey, Elin Axelsson, Michael D. Nodine,

David Twell, and Frédéric Berger. 2021. “Epigenetic Reprogramming Rewires Transcription during the Alternation of Generations in Arabidopsis.” *ELife* 10 (January): 1–66. https://doi.org/10.7554/eLife.61894.

Borges, Filipe, Gabriela Gomes, Rui Gardner, Nuno Moreno, Sheila McCormick, José A. Feijó, and Jörg D. Becker. 2008. “Comparative Transcriptomics of Arabidopsis Sperm Cells.” *Plant Physiology* 148 (2): 1168–81. https://doi.org/10.1104/pp.108.125229.

Brustel, Julien, Nina Kirstein, Fanny Izard, Charlotte Grimaud, Paulina Prorok, Christelle Cayrou, Gunnar Schotta, et al. 2017. “Histone H4K20 Tri-methylation at Late-firing Origins Ensures Timely Heterochromatin Replication.” *The EMBO Journal* 36 (18): 2726–41. https://doi.org/10.15252/embj.201796541.

Bushati, Natascha, Alexander Stark, Julius Brennecke, and Stephen M. Cohen. 2008. “Temporal Reciprocity of MiRNAs and Their Targets during the Maternal-to-Zygotic Transition in Drosophila.” *Current Biology* 18 (7): 501–6. https://doi.org/10.1016/j.cub.2008.02.081.

Callebaut, Isabelle, Jean Claude Courvalin, and Jean Paul Mornon. 1999. “The BAH (Bromo-Adjacent Homology) Domain: A Link between DNA Methylation, Replication and Transcriptional Regulation.” *FEBS Letters* 446 (1): 189–93. https://doi.org/10.1016/S0014-5793(99)00132-5.

Capron, Arnaud, Mathieu Gourgues, Lissiene S. Neiva, Jean Emmanuel Faure, Frederic Berger, Gabriela Pagnussat, Anjali Krishnan, et al. 2008. “Maternal Control of Male-Gamete Delivery in Arabidopsis Involves a Putative GPI-Anchored Protein Encoded by the Lorelei Gene.” *Plant Cell* 20 (11): 3038–49. https://doi.org/10.1105/tpc.108.061713.

Chapman, Laura A., and Daphne R. Goring. 2011. “Misregulation of Phosphoinositides in Arabidopsis Thaliana Decreases Pollen Hydration and Maternal Fertility.” *Sexual Plant Reproduction* 24 (4): 319–26. https://doi.org/10.1007/s00497-011-0172-1.

Chen, Junyi, Nicholas Strieder, Nadia G. Krohn, Philipp Cyprys, Stefanie Sprunck, Julia C. Engelmann, and Thomas Dresselhaus. 2017. “Zygotic Genome Activation Occurs Shortly after Fertilization in Maize.” *Plant Cell* 29 (9): 2106–25. https://doi.org/10.1105/tpc.17.00099.

Chen, Shuyan, Milan A. De Vries, and Stephen P. Bell. 2007. “Orc6 Is Required for Dynamic Recruitment of Cdt1 during Repeated Mcm2-7 Loading.” *Genes and Development* 21 (22): 2897–2907. https://doi.org/10.1101/gad.1596807.

Chen, Yan Hong, Hong Ju Li, Dong Qiao Shi, Li Yuan, Jie Liu, Rajini Sreenivasan, Ramarmurthy Baskar, Ueli Grossniklaus, and Wei Cai Yang. 2007. “The Central Cell Plays a Critical Role in Pollen Tube Guidance in Arabidopsis.” *Plant Cell* 19 (11): 3563–77. https://doi.org/10.1105/tpc.107.053967.

Cingolani, Pablo, Adrian Platts, Le Lily Wang, Melissa Coon, Tung Nguyen, Luan Wang, Susan J. Land, Xiangyi Lu, and Douglas M. Ruden. 2012. “A Program for Annotating and Predicting the Effects of Single Nucleotide Polymorphisms, SnpEff: SNPs in the Genome of Drosophila Melanogaster Strain W1118; Iso-2; Iso-3.” *Fly* 6 (2): 80–92. https://doi.org/10.4161/FLY.19695/SUPPL_FILE/KFLY_A_10919695_SM0001.ZIP.

Clough, Steven J., and Andrew F. Bent. 1998. “Floral Dip: A Simplified Method for Agrobacterium-Mediated Transformation of Arabidopsis Thaliana.” *Plant Journal* 16 (6): 735–43. https://doi.org/10.1046/j.1365-313X.1998.00343.x.

Coimbra, Sílvia, Mário Costa, Marta Adelina Mendes, Ana Marta Pereira, João Pinto, and Luís Gustavo Pereira. 2010. "Early Germination of Arabidopsis Pollen in a Double Null Mutant for the Arabinogalactan Protein Genes AGP6 and AGP11." *Sexual Plant Reproduction* 23 (3): 199–205. https://doi.org/10.1007/s00497-010-0136-x.

Concia, Lorenzo, Ashley M. Brooks, Emily Wheeler, Gregory J. Zynda, Emily E. Wear, Chantal LeBlanc, Jawon Song, et al. 2018. "Genome-Wide Analysis of the Arabidopsis Replication Timing Program." *Plant Physiology* 176 (3): 2166–85. https://doi.org/10.1104/pp.17.01537.

Costas, Celina, Maria De La Paz Sanchez, Hume Stroud, Yanchun Yu, Juan Carlos Oliveros, Suhua Feng, Alberto Benguria, et al. 2011. "Genome-Wide Mapping of Arabidopsis Thaliana Origins of DNA Replication and Their Associated Epigenetic Marks." *Nature Structural and Molecular Biology* 18 (3): 395–400. https://doi.org/10.1038/nsmb.1988.

Creasey, Kate M., Jixian Zhai, Filipe Borges, Frederic Van Ex, Michael Regulski, Blake C. Meyers, and Robert A. Martienssen. 2014. "MiRNAs Trigger Widespread Epigenetically Activated SiRNAs from Transposons in Arabidopsis." *Nature* 508 (7496): 411–15. https://doi.org/10.1038/nature13069.

Davarinejad, Hossein, Yi Chun Huang, Benoit Mermaz, Chantal LeBlanc, Axel Poulet, Geoffrey Thomson, Valentin Joly, et al. 2022. "The Histone H3.1 Variant Regulates TONSOKU-Mediated DNA Repair during Replication." *Science* 375 (6586): 1281–86. https://doi.org/10.1126/science.abm5320.

Derkacheva, Maria, and Lars Hennig. 2014. "Variations on a Theme: Polycomb Group Proteins in Plants." *Journal of Experimental Botany* 65 (10): 2769–84. https://doi.org/10.1093/jxb/ert410.

Diaz-Trivino, Sara, María del Mar Castellano, María de la Paz Sanchez, Elena Ramirez-Parra, Bénédicte Desvoyes, and Crisanto Gutierrez. 2005. "The Genes Encoding Arabidopsis ORC Subunits Are E2F Targets and the Two ORC1 Genes Are Differently Expressed in Proliferating and Endoreplicating Cells." *Nucleic Acids Research* 33 (17): 5404–14. https://doi.org/10.1093/nar/gki854.

Dong, Xiaoyun, Zonglie Hong, Muthuswamy Sivaramakrishnan, Magdy Mahfouz, and Desh Pal S. Verma. 2005. "Callose Synthase (CalS5) Is Required for Exine Formation during Microgametogenesis and for Pollen Viability in Arabidopsis." *Plant Journal* 42 (3): 315–28. https://doi.org/10.1111/j.1365-313X.2005.02379.x.

Dresselhaus, Thomas, Stefanie Sprunck, and Gary M. Wessel. 2016. "Fertilization Mechanisms in Flowering Plants." *Current Biology* 26 (3): R125–39. https://doi.org/10.1016/j.cub.2015.12.032.

Duncker, Bernard P., Igor N. Chesnokov, and Brendan J. McConkey. 2009. "The Origin Recognition Complex Protein Family." *Genome Biology* 10 (3): 214. https://doi.org/10.1186/gb-2009-10-3-214.

Escobar-Restrepo, Juan Miguel, Norbert Huck, Sharon Kessler, Valeria Gagliardini, Jacqueline Gheyselinck, Wei Cai Yang, and Ueli Grossniklaus. 2007. "The Feronia Receptor-like Kinase Mediates Male-Female Interactions during Pollen Tube Reception." *Science* 317 (5838): 656–60. https://doi.org/10.1126/science.1143562.

Friedman, William E. 1999. "Expression of the Cell Cycle in Sperm of Arabidopsis: Implications for Understanding Patterns of Gametogenesis and Fertilization in Plants and

Other Eukaryotes." *Development* 126 (5): 1065–75. https://doi.org/10.1242/dev.126.5.1065.

Furner, Ian J., Mazhar A. Sheikh, and Clare E. Collett. 1998. "Gene Silencing and Homology-Dependent Gene Silencing in Arabidopsis: Genetic Modifiers and DNA Methylation." *Genetics* 149 (2): 651–62. https://doi.org/10.1093/genetics/149.2.651.

Galindo-Trigo, Sergio, Noel Blanco-Touriñán, Thomas A DeFalco, Eloise S Wells, Julie E Gray, Cyril Zipfel, and Lisa M Smith. 2020. " Cr RLK 1L Receptor-like Kinases HERK 1 and ANJEA Are Female Determinants of Pollen Tube Reception ." *EMBO Reports* 21 (2). https://doi.org/10.15252/embr.201948466.

Gao, Tiyu, Robert E. Collins, John R. Horton, Xing Zhang, Rongguang Zhang, Arunkumar Dhayalan, Raluca Tamas, Albert Jeltsch, and Xiaodong Cheng. 2009. "The Ankyrin Repeat Domain of Huntingtin Interacting Protein 14 Contains a Surface Aromatic Cage, a Potential Site for Methyl-Lysine Binding." *Proteins: Structure, Function and Bioinformatics* 76 (3): 772–77. https://doi.org/10.1002/prot.22452.

Garrison, Erik, and Gabor Marth. 2012. "Haplotype-Based Variant Detection from Short-Read Sequencing," July. https://doi.org/10.48550/arxiv.1207.3907.

Giraut, Laurène, Matthieu Falque, Jan Drouaud, Lucie Pereira, Olivier C. Martin, and Christine Mézard. 2011. "Genome-Wide Crossover Distribution in Arabidopsis Thaliana Meiosis Reveals Sex-Specific Patterns along Chromosomes." *PLOS Genetics* 7 (11): e1002354. https://doi.org/10.1371/JOURNAL.PGEN.1002354.

Hay, Angela, and Miltos Tsiantis. 2010. "KNOX Genes: Versatile Regulators of Plant Development and Diversity." *Development* 137 (19): 3153–65. https://doi.org/10.1242/dev.030049.

He, Shengbo, Martin Vickers, Jingyi Zhang, and Xiaoqi Feng. 2019. "Natural Depletion of H1 in Sex Cells Causes DNA Demethylation, Heterochromatin Decondensation and Transposon Activation." *ELife* 8 (May). https://doi.org/10.7554/eLife.42530.001.

Healey, Adam, Agnelo Furtado, Tal Cooper, and Robert J. Henry. 2014. "Protocol: A Simple Method for Extracting next-Generation Sequencing Quality Genomic DNA from Recalcitrant Plant Species." *Plant Methods* 10 (1): 1–8. https://doi.org/10.1186/1746-4811-10-21.

Hehenberger, Elisabeth, David Kradolfer, and Claudia Köhler. 2012. "Endosperm Cellularization Defines an Important Developmental Transition for Embryo Development." *Development* 139 (11): 2031–39. https://doi.org/10.1242/dev.077057.

Hemerly, Adriana S., Supriya G. Prasanth, Khalid Siddiqui, and Bruce Stillman. 2009. "Orc1 Controls Centriole and Centrosome Copy Number in Human Cells." *Science* 323 (5915): 789–93. https://doi.org/10.1126/science.1166745.

Hepler, P. K., L. Vidali, and A. Y. Cheung. 2001. "Polarized Cell Growth in Higher Plants." *Annual Review of Cell and Developmental Biology* 17 (November): 159–87. https://doi.org/10.1146/annurev.cellbio.17.1.159.

Herridge, Rowan P., Robert C. Day, and Richard C. Macknight. 2014. "The Role of the MCM2-7 Helicase Complex during Arabidopsis Seed Development." *Plant Molecular Biology* 86 (1–2): 69–84. https://doi.org/10.1007/s11103-014-0213-x.

Higashiyama, Tetsuya, and Hidenori Takeuchi. 2015. "The Mechanism and Key Molecules

Involved in Pollen Tube Guidance." *Annual Review of Plant Biology* 66: 393–413. https://doi.org/10.1146/annurev-arplant-043014-115635.

Hisanaga, Tetsuya, Shota Fujimoto, Yihui Cui, Katsutoshi Sato, Ryosuke Sano, Shohei Yamaoka, Takayuki Kohchi, Frédéric Berger, and Keiji Nakajima. 2021. "Deep Evolutionary Origin of Gamete-Directed Zygote Activation by Knox/ Bell Transcription Factors in Green Plants." *ELife* 10 (September). https://doi.org/10.7554/eLife.57090.

Holding, David R., and Patricia S. Springer. 2002. "The Arabidopsis Gene PROLIFERA Is Required for Proper Cytokinesis during Seed Development." *Planta* 214 (3): 373–82. https://doi.org/10.1007/s00425-001-0686-0.

Horst, Nelly A., Aviva Katz, Idan Pereman, Eva L. Decker, Nir Ohad, and Ralf Reski. 2016. "A Single Homeobox Gene Triggers Phase Transition, Embryogenesis and Asexual Reproduction." *Nature Plants* 2 (2): 1–6. https://doi.org/10.1038/nplants.2015.209.

Horstman, Anneke, Mengfan Li, Iris Heidmann, Mieke Weemen, Baojian Chen, Jose M. Muino, Gerco C. Angenent, and Kim Boutiliera. 2017. "The BABY BOOM Transcription Factor Activates the LEC1-ABI3-FUS3-LEC2 Network to Induce Somatic Embryogenesis." *Plant Physiology* 175 (2): 848–57. https://doi.org/10.1104/pp.17.00232.

Huang, Xiaorong, and Meng-Xiang Sun. 2022. "H3K27 Methylation Regulates the Fate of Two Cell Lineages in Male Gametophytes." *The Plant Cell* 34 (8). https://doi.org/10.1093/plcell/koac136.

Hunter, John D. 2007. "Matplotlib: A 2D Graphics Environment." *Computing in Science and Engineering* 9 (3): 90–95. https://doi.org/10.1109/MCSE.2007.55.

Ibarra, Christian A., Xiaoqi Feng, Vera K. Schoft, Tzung Fu Hsieh, Rie Uzawa, Jessica A. Rodrigues, Assaf Zemach, et al. 2012. "Active DNA Demethylation in Plant Companion Cells Reinforces Transposon Methylation in Gametes." *Science* 337 (6100): 1360–64. https://doi.org/10.1126/science.1224839.

Ingouff, Mathieu, Yuki Hamamura, Mathieu Gourgues, Tetsuya Higashiyama, and Frédéric Berger. 2007. "Distinct Dynamics of HISTONE3 Variants between the Two Fertilization Products in Plants." *Current Biology* 17 (12): 1032–37. https://doi.org/10.1016/j.cub.2007.05.019.

Ingouff, Mathieu, Svenja Rademacher, Sarah Holec, Lucija Šoljić, Nie Xin, Anne Readshaw, Shi Hui Foo, Benoît Lahouze, Stefanie Sprunck, and Frédéric Berger. 2010. "Zygotic Resetting of the HISTONE 3 Variant Repertoire Participates in Epigenetic Reprogramming in Arabidopsis." *Current Biology* 20 (23): 2137–43. https://doi.org/10.1016/j.cub.2010.11.012.

Ioannes, Pablo De, Victor A. Leon, Zheng Kuang, Miao Wang, Jef D. Boeke, Andreas Hochwagen, and Karim Jean Armache. 2019. "Structure and Function of the Orc1 BAH-Nucleosome Complex." *Nature Communications* 10 (1): 1–11. https://doi.org/10.1038/s41467-019-10609-y.

Iyer, Lakshminarayan M., Detlef D. Leipe, Eugene V. Koonin, and L. Aravind. 2004. "Evolutionary History and Higher Order Classification of AAA+ ATPases." *Journal of Structural Biology* 146 (1–2): 11–31. https://doi.org/10.1016/j.jsb.2003.10.010.

Jacob, Yannick, Hume Stroud, Chantal Leblanc, Suhua Feng, Luting Zhuo, Elena Caro,

Christiane Hassel, Crisanto Gutierrez, Scott D. Michaels, and Steven E. Jacobsen. 2010. "Regulation of Heterochromatic DNA Replication by Histone H3 Lysine 27 Methyltransferases." *Nature* 466 (7309): 987–91. https://doi.org/10.1038/nature09290.

Jander, Georg, Susan R. Norris, Steven D. Rounsley, David F. Bush, Irena M. Levin, and Robert L. Last. 2002. "Arabidopsis Map-Based Cloning in the Post-Genome Era." *Plant Physiology* 129 (2): 440–50. https://doi.org/10.1104/pp.003533.

Jeong, Sun Yong, Annkatrin Rose, Jomon Joseph, Mary Dasso, and Iris Meier. 2005. "Plant-Specific Mitotic Targeting of RanGAP Requires a Functional WPP Domain." *Plant Journal* 42 (2): 270–82. https://doi.org/10.1111/j.1365-313X.2005.02368.x.

Jiang, Lixi, Shu Lan Yang, Li Fen Xie, Ching San Puah, Xue Qin Zhang, Wei Cai Yang, Venkatesan Sundaresan, and De Ye. 2005. "VANGUARD1 Encodes a Pectin Methylesterase That Enhances Pollen Tube Growth in the Arabidopsis Style and Transmitting Tract." *Plant Cell* 17 (2): 584–96. https://doi.org/10.1105/tpc.104.027631.

Johnson, Mark A., Jeffrey F. Harper, and Ravishankar Palanivelu. 2019. "A Fruitful Journey: Pollen Tube Navigation from Germination to Fertilization." *Annual Review of Plant Biology* 70: 809–37. https://doi.org/10.1146/annurev-arplant-050718-100133.

Jordan, Nicholas David, Jonathan Paul West, Andrew Bottley, Mazhar Sheikh, and Ian Furner. 2007. "Transcript Profiling of the Hypomethylated Hog1 Mutant of Arabidopsis." *Plant Molecular Biology* 65 (5): 571–86. https://doi.org/10.1007/s11103-007-9221-4.

Kandasamy, Muthugapatti K., June B. Nasrallah, and Mikhail E. Nasrallah. 1994. "Pollen-Pistil Interactions and Developmental Regulation of Pollen Tube Growth in Arabidopsis." *Development* 120 (12): 3405–18. https://doi.org/10.1242/dev.120.12.3405.

Kawashima, Tomokazu, Daisuke Maruyama, Murat Shagirov, Jing Li, Yuki Hamamura, Ramesh Yelagandula, Yusuke Toyama, and Frédéric Berger. 2014. "Dynamic F-Actin Movement Is Essential for Fertilization in Arabidopsis Thaliana." *ELife* 3: 1–18. https://doi.org/10.7554/eLife.04501.

Khanday, Imtiyaz, Debra Skinner, Bing Yang, Raphael Mercier, and Venkatesan Sundaresan. 2019. "A Male-Expressed Rice Embryogenic Trigger Redirected for Asexual Propagation through Seeds." *Nature* 565 (7737): 91–95. https://doi.org/10.1038/s41586-018-0785-8.

Khouider, Souraya, Filipe Borges, Chantal LeBlanc, Alexander Ungru, Arp Schnittger, Robert Martienssen, Vincent Colot, and Daniel Bouyer. 2021. "Male Fertility in Arabidopsis Requires Active DNA Demethylation of Genes That Control Pollen Tube Function." *Nature Communications* 12 (1): 1–10. https://doi.org/10.1038/s41467-020-20606-1.

Kim, Daehwan, Joseph M. Paggi, Chanhee Park, Christopher Bennett, and Steven L. Salzberg. 2019. "Graph-Based Genome Alignment and Genotyping with HISAT2 and HISAT-Genotype." *Nature Biotechnology 2019 37:8* 37 (8): 907–15. https://doi.org/10.1038/s41587-019-0201-4.

Kirstein, Nina, Alexander Buschle, Xia Wu, Stefan Krebs, Helmut Blum, Elisabeth Kremmer, Ina M. Vorberg, et al. 2021. "Human ORC/MCM Density Is Low in Active Genes and Correlates with Replication Time but Does Not Delimit Initiation Zones." *ELife* 10 (Mcm): 1–30. https://doi.org/10.7554/eLife.62161.

Köhler, Rainer H., Warren R. Zipfel, Watt W. Webb, and Maureen R. Hanson. 1997. “The Green Fluorescent Protein as a Marker to Visualize Plant Mitochondria in Vivo.” *Plant Journal* 11 (3): 613–21. https://doi.org/10.1046/j.1365-313X.1997.11030613.x.

Kradolfer, David, Philip Wolff, Hua Jiang, Alexey Siretskiy, and Claudia Köhler. 2013. “An Imprinted Gene Underlies Postzygotic Reproductive Isolation in Arabidopsis Thaliana.” *Developmental Cell* 26 (5): 525–35. https://doi.org/10.1016/j.devcel.2013.08.006.

Kuligowski, Janine, Michèle Ferrand, and Eliane Chenou. 1991. “Stored MRNA in Early Embryos of a Fern Marsilea Vestita: A Paternal and Maternal Origin.” *Molecular Reproduction and Development* 30 (1): 27–33. https://doi.org/10.1002/mrd.1080300104.

Kuo, Alex J., Jikui Song, Peggie Cheung, Satoko Ishibe-Murakami, Sayumi Yamazoe, James K. Chen, Dinshaw J. Patel, and Or Gozani. 2012. “The BAH Domain of ORC1 Links H4K20me2 to DNA Replication Licensing and Meier-Gorlin Syndrome.” *Nature* 484 (7392): 115–19. https://doi.org/10.1038/nature10956.

Lee, Jae Hyeok, Huawen Lin, Sunjoo Joo, and Ursula Goodenough. 2008. “Early Sexual Origins of Homeoprotein Heterodimerization and Evolution of the Plant KNOX/BELL Family.” *Cell* 133 (5): 829–40. https://doi.org/10.1016/j.cell.2008.04.028.

Leydon, Alexander R., Kristin M. Beale, Karolina Woroniecka, Elizabeth Castner, Jefferson Chen, Casie Horgan, Ravishankar Palanivelu, and Mark A. Johnson. 2013. “Three MYB Transcription Factors Control Pollen Tube Differentiation Required for Sperm Release.” *Current Biology* 23 (13): 1209–14. https://doi.org/10.1016/j.cub.2013.05.021.

Li, Chun Hong, Nan Yu, Shi Min Jiang, Xiao Xia Shangguan, Ling Jian Wang, and Xiao Ya Chen. 2008. “Down-Regulation of S-Adenosyl-L-Homocysteine Hydrolase Reveals a Role of Cytokinin in Promoting Transmethylation Reactions.” *Planta* 228 (1): 125–36. https://doi.org/10.1007/s00425-008-0724-2.

Li, Sha, Fu Rong Ge, Ming Xu, Xin Ying Zhao, Guo Qiang Huang, Liang Zi Zhou, Jia Gang Wang, et al. 2013. “Arabidopsis COBRA-LIKE 10, a GPI-Anchored Protein, Mediates Directional Growth of Pollen Tubes.” *Plant Journal* 74 (3): 486–97. https://doi.org/10.1111/tpj.12139.

Li, Sisi, Zhenlin Yang, Xuan Du, Rui Liu, Alex W. Wilkinson, Or Gozani, Steven E. Jacobsen, Dinshaw J. Patel, and Jiamu Du. 2016. “Structural Basis for the Unique Multivalent Readout of Unmodified H3 Tail by Arabidopsis ORC1b BAH-PHD Cassette.” *Structure* 24 (3): 486–94. https://doi.org/10.1016/j.str.2016.01.004.

Li, Zicong, Xing Fu, Yizhong Wang, Renyi Liu, and Yuehui He. 2018. “Polycomb-Mediated Gene Silencing by the BAH–EMF1 Complex in Plants.” *Nature Genetics* 50 (9): 1254–61. https://doi.org/10.1038/s41588-018-0190-0.

Liang, Hsiao Lan, Chung Yi Nien, Hsiao Yun Liu, Mark M. Metzstein, Nikolai Kirov, and Christine Rushlow. 2008. “The Zinc-Finger Protein Zelda Is a Key Activator of the Early Zygotic Genome in Drosophila.” *Nature* 456 (7220): 400–403. https://doi.org/10.1038/nature07388.

Lindner, Heike, Sharon A. Kessler, Lena M. Müller, Hiroko Shimosato-Asano, Aurélien Boisson-Dernier, and Ueli Grossniklaus. 2015. “TURAN and EVAN Mediate Pollen Tube Reception in Arabidopsis Synergids through Protein Glycosylation.” *PLoS Biology* 13 (4): e1002139. https://doi.org/10.1371/journal.pbio.1002139.

Lindner, Heike, Michael T. Raissig, Christian Sailer, Hiroko Shimosato-Asano, Rémy Bruggmann, and Ueli Grossniklaus. 2012. "SNP-Ratio Mapping (SRM): Identifying Lethal Alleles and Mutations in Complex Genetic Backgrounds by next-Generation Sequencing." *Genetics* 191 (4): 1381–86. https://doi.org/10.1534/genetics.112.141341.

Liu, Jingjing, Sheng Zhong, Xinyang Guo, Lihong Hao, Xiaolin Wei, Qingpei Huang, Yingnan Hou, et al. 2013. "Membrane-Bound RLCKs LIP1 and LIP2 Are Essential Male Factors Controlling Male-Female Attraction in Arabidopsis." *Current Biology* 23 (11): 993–98. https://doi.org/10.1016/j.cub.2013.04.043.

Liu, Meiling, Zhijuan Wang, Saiying Hou, Lele Wang, Qingpei Huang, Hongya Gu, Thomas Dresselhaus, Sheng Zhong, and Li Jia Qu. 2021. "AtLURE1/PRK6-Mediated Signaling Promotes Conspecific Micropylar Pollen Tube Guidance." *Plant Physiology* 186 (2): 865–73. https://doi.org/10.1093/PLPHYS/KIAB105.

Long, Jincheng, James Walker, Wenjing She, Billy Aldridge, Hongbo Gao, Samuel Deans, Martin Vickers, and Xiaoqi Feng. 2021. "Nurse Cell-Derived Small RNAs Define Paternal Epigenetic Inheritance in Arabidopsis." *Science* 373 (6550). https://doi.org/10.1126/science.abh0556.

López-González, Leticia, Alfonso Mouriz, Laura Narro-Diego, Regla Bustos, José Miguel Martínez-Zapater, Jose A. Jarillo, and Manuel Piñeiro. 2014. "Chromatin-Dependent Repression of the Arabidopsis Floral Integrator Genes Involves Plant Specific PHD-Containing Proteins." *Plant Cell* 26 (10): 3922–38. https://doi.org/10.1105/tpc.114.130781.

Loraine, Ann E., Sheila McCormick, April Estrada, Ketan Patel, and Peng Qin. 2013. "RNA-Seq of Arabidopsis Pollen Uncovers Novel Transcription and Alternative Splicing." *Plant Physiology* 162 (2): 1092–1109. https://doi.org/10.1104/pp.112.211441.

Lukowitz, Wolfgang, C. Stewart Gillmor, and Wolf Rüdiger Scheible. 2000. "Positional Cloning in Arabidopsis. Why It Feels Good to Have a Genome Initiative Working for You." *Plant Physiology* 123 (3): 795–805. https://doi.org/10.1104/pp.123.3.795.

Makarova, Kira S., and Eugene V. Koonin. 2013. "Archaeology of Eukaryotic DNA Replication." *Cold Spring Harbor Perspectives in Biology* 5 (11): a012963. https://doi.org/10.1101/cshperspect.a012963.

Marimuthu, Mohan P.A., Ravi Maruthachalam, Ramesh Bondada, Sundaram Kuppu, Ek Han Tan, Anne Britt, Simon W.L. Chan, and Luca Comai. 2021. "Epigenetically Mismatched Parental Centromeres Trigger Genome Elimination in Hybrids." *Science Advances* 7 (47): 1151. https://doi.org/10.1126/sciadv.abk1151.

Martínez, Germán, Kaushik Panda, Claudia Köhler, and R. Keith Slotkin. 2016. "Silencing in Sperm Cells Is Directed by RNA Movement from the Surrounding Nurse Cell." *Nature Plants* 2 (4): 1–8. https://doi.org/10.1038/NPLANTS.2016.30.

Martinez, German, Philip Wolff, Zhenxing Wang, Jordi Moreno-Romero, Juan Santos-González, Lei Liu Conze, Christopher Defraia, R. Keith Slotkin, and Claudia Köhler. 2018. "Paternal EasiRNAs Regulate Parental Genome Dosage in Arabidopsis." *Nature Genetics* 50 (2): 193–98. https://doi.org/10.1038/s41588-017-0033-4.

Maruyama, Daisuke, Toshiya Endo, and Shuh Ichi Nishikawa. 2010. "BiP-Mediated Polar Nuclei Fusion Is Essential for the Regulation of Endosperm Nuclei Proliferation in Arabidopsis Thaliana." *Proceedings of the National Academy of Sciences of the United*

States of America 107 (4): 1684–89. https://doi.org/10.1073/pnas.0905795107.

Maruyama, Daisuke, Yuki Hamamura, Hidenori Takeuchi, Daichi Susaki, Moe Nishimaki, Daisuke Kurihara, Ryushiro D. Kasahara, and Tetsuya Higashiyama. 2013. "Independent Control by Each Female Gamete Prevents the Attraction of Multiple Pollen Tubes." *Developmental Cell* 25 (3): 317–23. https://doi.org/10.1016/j.devcel.2013.03.013.

Maruyama, Daisuke, Tetsuya Higashiyama, Toshiya Endo, and Shuh Ichi Nishikawa. 2020. "Fertilization-Coupled Sperm Nuclear Fusion Is Required for Normal Endosperm Nuclear Proliferation." *Plant and Cell Physiology* 61 (1): 29–40. https://doi.org/10.1093/pcp/pcz158.

Maruyama, Daisuke, Masaya Yamamoto, Toshiya Endo, and Shuh Ichi Nishikawa. 2014. "Different Sets of ER-Resident J-Proteins Regulate Distinct Polar Nuclear-Membrane Fusion Events in Arabidopsis Thaliana." *Plant and Cell Physiology* 55 (11): 1937–44. https://doi.org/10.1093/pcp/pcu120.

Mellor, Jane. 2006. "It Takes a PHD to Read the Histone Code." *Cell* 126 (1): 22–24. https://doi.org/10.1016/j.cell.2006.06.028.

Meng, Lingyan, Xiaomei Liu, Congfen He, Biyao Xu, Yaxuan Li, and Yingkao Hu. 2020. "Functional Divergence and Adaptive Selection of KNOX Gene Family in Plants." *Open Life Sciences* 15 (1): 346–63. https://doi.org/10.1515/biol-2020-0036.

Meyer, P., and H. Saedler. 1996. "Homology-Dependent Gene Silencing in Plants." *Annual Review of Plant Physiology and Plant Molecular Biology* 47 (1): 23–48. https://doi.org/10.1146/annurev.arplant.47.1.23.

Miao, Yingjing, Jiashu Cao, Li Huang, Youjian Yu, and Sue Lin. 2021. "FLA14 Is Required for Pollen Development and Preventing Premature Pollen Germination under High Humidity in Arabidopsis." *BMC Plant Biology* 21 (1): 1–19. https://doi.org/10.1186/s12870-021-03038-x.

Miyazaki, Saori, Takashi Murata, Nami Sakurai-Ozato, Minoru Kubo, Taku Demura, Hiroo Fukuda, and Mitsuyasu Hasebe. 2009. "ANXUR1 and 2, Sister Genes to FERONIA/SIRENE, Are Male Factors for Coordinated Fertilization." *Current Biology* 19 (15): 1327–31. https://doi.org/10.1016/j.cub.2009.06.064.

Moffatt, Barbara A., and Elizabeth A. Weretilnyk. 2001. "Sustaining S-Adenosyl-L-Methionine-Dependent Methyltransferase Activity in Plant Cells." *Physiologia Plantarum* 113 (4): 435–42. https://doi.org/10.1034/j.1399-3054.2001.1130401.x.

Mori, Toshiyuki, Tomoko Igawa, Gen Tamiya, Shin Ya Miyagishima, and Frédéric Berger. 2014. "Gamete Attachment Requires GEX2 for Successful Fertilization in Arabidopsis." *Current Biology* 24 (2): 170–75. https://doi.org/10.1016/j.cub.2013.11.030.

Morley-Smith, Edward R., Marilyn J. Pike, Kim Findlay, Walter Köckenberger, Lionel M. Hill, Alison M. Smith, and Stephen Rawsthorne. 2008. "The Transport of Sugars to Developing Embryos Is Not via the Bulk Endosperm in Oilseed Rape Seeds." *Plant Physiology* 147 (4): 2121–30. https://doi.org/10.1104/pp.108.124644.

Mosquna, Assaf, Aviva Katz, Eva L. Decker, Stefan A. Rensing, Ralf Reski, and Nir Ohad. 2009. "Regulation of Stem Cell Maintenance by the Polycomb Protein FIE Has Been Conserved during Land Plant Evolution." *Development* 136 (14): 2433–44. https://doi.org/10.1242/dev.035048.

Mou, Wangshu, Yun Ting Kao, Erwan Michard, Alexander A. Simon, Dongdong Li, Michael M. Wudick, Michael A. Lizzio, José A. Feijó, and Caren Chang. 2020. “Ethylene-Independent Signaling by the Ethylene Precursor ACC in Arabidopsis Ovular Pollen Tube Attraction.” *Nature Communications* 11 (1): 1–11. https://doi.org/10.1038/s41467-020-17819-9.

Mull, Lori, Michelle L. Ebbs, and Judith Bender. 2006. “A Histone Methylation-Dependent DNA Methylation Pathway Is Uniquely Impaired by Deficiency in Arabidopsis S-Adenosylhomocysteine Hydrolase.” *Genetics* 174 (3): 1161–71. https://doi.org/10.1534/genetics.106.063974.

Müller, Philipp, Sookhee Park, Erika Shor, Dana J. Huebert, Christopher L. Warren, Aseem Z. Ansari, Michael Weinreich, Matthew L. Eaton, David M. MacAlpine, and Catherine A. Fox. 2010. “The Conserved Bromo-Adjacent Homology Domain of Yeast Orc1 Functions in the Selection of DNA Replication Origins within Chromatin.” *Genes and Development* 24 (13): 1418–33. https://doi.org/10.1101/gad.1906410.

Musielak, Thomas, Patrick Bürgel, Martina Kolb, and Martin Bayer. 2016. “Use of SCRI Renaissance 2200 (SR2200) as a Versatile Dye for Imaging of Developing Embryos, Whole Ovules, Pollen Tubes and Roots.” *Bio-Protocol* 6 (18). https://doi.org/10.21769/bioprotoc.1935.

Musselman, Catherine A., and Tatiana G. Kutateladze. 2011. “Handpicking Epigenetic Marks with PHD Fingers.” *Nucleic Acids Research* 39 (21): 9061–71. https://doi.org/10.1093/nar/gkr613.

Neu, Ancilla, Emily Eilbert, Lisa Y. Asseck, Daniel Slane, Agnes Henschen, Kai Wang, Patrick Bürgel, et al. 2019. “Constitutive Signaling Activity of a Receptor-Associated Protein Links Fertilization with Embryonic Patterning in Arabidopsis Thaliana.” *Proceedings of the National Academy of Sciences of the United States of America* 116 (12): 5795–5804. https://doi.org/10.1073/pnas.1815866116.

Nishikawa, Shuh Ichi, Yuki Yamaguchi, Chiharu Suzuki, Ayaka Yabe, Yuzuru Sato, Daisuke Kurihara, Yoshikatsu Sato, Daichi Susaki, Tetsuya Higashiyama, and Daisuke Maruyama. 2020. “Arabidopsis GEX1 Is a Nuclear Membrane Protein of Gametes Required for Nuclear Fusion During Reproduction.” *Frontiers in Plant Science* 11 (October): 1518. https://doi.org/10.3389/fpls.2020.548032.

Nodine, Michael D., and David P. Bartel. 2012. “Maternal and Paternal Genomes Contribute Equally to the Transcriptome of Early Plant Embryos.” *Nature* 482 (7383): 94–97. https://doi.org/10.1038/nature10756.

Ohnishi, Yukinosuke, and Takashi Okamoto. 2015. “Karyogamy in Rice Zygotes: Actin Filament-Dependent Migration of Sperm Nucleus, Chromatin Dynamics, and de Novo Gene Expression.” *Plant Signaling and Behavior* 10 (2): 1–4. https://doi.org/10.4161/15592324.2014.989021.

Okada, Takashi, Makoto Endo, Mohan B. Singh, and Prem L. Bhalla. 2005. “Analysis of the Histone H3 Gene Family in Arabidopsis and Identification of the Male-Gamete-Specific Variant AtMGH3.” *Plant Journal* 44 (4): 557–68. https://doi.org/10.1111/j.1365-313X.2005.02554.x.

Okano, Yosuke, Naoki Aono, Yuji Hiwatashi, Takashi Murata, Tomoaki Nishiyama, Takaaki Ishikawa, Minoru Kubo, and Mitsuyasu Hasebe. 2009. “A Polycomb Repressive

Complex 2 Gene Regulates Apogamy and Gives Evolutionary Insights into Early Land Plant Evolution." *Proceedings of the National Academy of Sciences of the United States of America* 106 (38): 16321–26. https://doi.org/10.1073/pnas.0906997106.

Okuda, Satohiro, Hiroki Tsutsui, Keiko Shiina, Stefanie Sprunck, Hidenori Takeuchi, Ryoko Yui, Ryushiro D. Kasahara, et al. 2009. "Defensin-like Polypeptide LUREs Are Pollen Tube Attractants Secreted from Synergid Cells." *Nature* 458 (7236): 357–61. https://doi.org/10.1038/nature07882.

Ortiz-Ramírez, Carlos, Erwan Michard, Alexander A. Simon, Daniel S.C. Damineli, Marcela Hernández-Coronado, Jörg D. Becker, and José A. Feijó. 2017. "GLUTAMATE RECEPTOR-LIKE Channels Are Essential for Chemotaxis and Reproduction in Mosses." *Nature* 549 (7670): 91–95. https://doi.org/10.1038/nature23478.

Park, Il Geun, Minsol Jeon, Hyunkyung Kim, and Ji Min Lee. 2022. "Coordinated Methyl Readers: Functional Communications in Cancer." *Seminars in Cancer Biology* 83 (August): 88–99. https://doi.org/10.1016/j.semcancer.2021.03.015.

Peng, Li, Zhen Kai Li, Xiao Li Ding, and Hui Qiao Tian. 2018. "Advances in the Study of Egg Activation of Higher Plants." *Zygote* 26 (6): 435–42. https://doi.org/10.1017/S0967199418000539.

Pereira, Ana Marta, Margarida Sofia Nobre, Sara Cristina Pinto, Ana Lúcia Lopes, Mário Luís Costa, Simona Masiero, and Sílvia Coimbra. 2016. "'love Is Strong, and You're so Sweet': JAGGER Is Essential for Persistent Synergid Degeneration and Polytubey Block in Arabidopsis Thaliana." *Molecular Plant* 9 (4): 601–14. https://doi.org/10.1016/j.molp.2016.01.002.

Peterson, Ross, Janet P. Slovin, and Changbin Chen. 2010. "A Simplified Method for Differential Staining of Aborted and Non-Aborted Pollen Grains." *International Journal of Plant Biology* 1 (2): 66–69. https://doi.org/10.4081/pb.2010.e13.

Pillot, Marion, Célia Baroux, Mario Arteaga Vazquez, Daphné Autran, Olivier Leblanc, Jean Philippe Vielle-Calzada, Ueli Grossniklaus, and Daniel Grimanelli. 2010. "Embryo and Endosperm Inherit Distinct Chromatin and Transcriptional States from the Female Gametes in Arabidopsis." *Plant Cell* 22 (2): 307–20. https://doi.org/10.1105/tpc.109.071647.

Pope, Benjamin D., Tyrone Ryba, Vishnu Dileep, Feng Yue, Weisheng Wu, Olgert Denas, Daniel L. Vera, et al. 2014. "Topologically Associating Domains Are Stable Units of Replication-Timing Regulation." *Nature* 515 (7527): 402–5. https://doi.org/10.1038/nature13986.

Portereiko, Michael F., Alan Lloyd, Joshua G. Steffen, Jayson A. Punwani, Denichiro Otsuga, and Gary N. Drews. 2006. "AGL80 Is Required for Central Cell and Endosperm Development in Arabidopsis." *Plant Cell* 18 (8): 1862–72. https://doi.org/10.1105/tpc.106.040824.

Punwani, Jayson A., David S. Rabiger, and Gary N. Drews. 2007. "MYB98 Positively Regulates a Battery of Synergid-Expressed Genes Encoding Filiform Apparatus-Localized Proteins." *Plant Cell* 19 (8): 2557–68. https://doi.org/10.1105/tpc.107.052076.

Rahman, Md Hassanur, Erika Toda, Masaaki Kobayashi, Toru Kudo, Shizuka Koshimizu, Mirei Takahara, Momoka Iwami, et al. 2019. "Expression of Genes from Paternal Alleles in Rice Zygotes and Involvement of OsASGR-BBML1 in Initiation of Zygotic

Development." *Plant and Cell Physiology* 60 (4): 725–37. https://doi.org/10.1093/pcp/pcz030.

Ravi, Maruthachalam, Fukashi Shibata, Joseph S. Ramahi, Kiyotaka Nagaki, Changbin Chen, Minoru Murata, and Simon W.L. Chan. 2011. "Meiosis-Specific Loading of the Centromere-Specific Histone CENH3 in Arabidopsis Thaliana." *PLoS Genetics* 7 (6). https://doi.org/10.1371/journal.pgen.1002121.

Ren, Wendan, Huitao Fan, Sara A. Grimm, Jae Jin Kim, Linhui Li, Yiran Guo, Christopher James Petell, et al. 2021. "DNMT1 Reads Heterochromatic H4K20me3 to Reinforce LINE-1 DNA Methylation." *Nature Communications* 12 (1): 1–16. https://doi.org/10.1038/s41467-021-22665-4.

Resh, Marilyn D. 1999. "Fatty Acylation of Proteins: New Insights into Membrane Targeting of Myristoylated and Palmitoylated Proteins." *Biochimica et Biophysica Acta - Molecular Cell Research* 1451 (1): 1–16. https://doi.org/10.1016/S0167-4889(99)00075-0.

Rocha, Pedro S.C.F., Mazhar Sheikh, Rosalba Melchiorre, Mathilde Fagard, Stéphanie Boutet, Rebecca Loach, Barbara Moffatt, Conrad Wagner, Hervé Vaucheret, and Ian Furner. 2005. "The Arabidopsis HOMOLOGY-DEPENDENT GENE SILENCING1 Gene Codes for an S-Adenosyl-L-Homocysteine Hydrolase Required for DNA Methylation-Dependent Gene Silencing." *Plant Cell* 17 (2): 404–17. https://doi.org/10.1105/tpc.104.028332.

Romeiro Motta, Mariana, Xin'Ai Zhao, Martine Pastuglia, Katia Belcram, Farshad Roodbarkelari, Maki Komaki, Hirofumi Harashima, et al. 2022. " B1-type Cyclins Control Microtubule Organization during Cell Division in Arabidopsis ." *EMBO Reports* 23 (1): e53995. https://doi.org/10.15252/embr.202153995.

Ronceret, Arnaud, Jose Gadea-Vacas, Jocelyne Guilleminot, Frédéric Lincker, Valérie Delorme, Sylvie Lahmy, Georges Pelletier, Marie Edith Chabouté, and Martine Devic. 2008. "The First Zygotic Division in Arabidopsis Requires de Novo Transcription of Thymidylate Kinase." *Plant Journal* 53 (5): 776–89. https://doi.org/10.1111/j.1365-313X.2007.03372.x.

Rosso, Mario G., Yong Li, Nicolai Strizhov, Bernd Reiss, Koen Dekker, and Bernd Weisshaar. 2003. "An Arabidopsis Thaliana T-DNA Mutagenized Population (GABI-Kat) for Flanking Sequence Tag-Based Reverse Genetics." *Plant Molecular Biology* 53 (1–2): 247–59. https://doi.org/10.1023/B:PLAN.0000009297.37235.4a.

Roszak, Pawel, and Claudia Köhler. 2011. "Polycomb Group Proteins Are Required to Couple Seed Coat Initiation to Fertilization." *Proceedings of the National Academy of Sciences of the United States of America* 108 (51): 20826–31. https://doi.org/10.1073/pnas.1117111108.

Sakakibara, Keiko, Sayuri Ando, Hoichong Karen Yip, Yosuke Tamada, Yuji Hiwatashi, Takashi Murata, Hironori Deguchi, Mitsuyasu Hasebe, and John L. Bowman. 2013. "KNOX2 Genes Regulate the Haploid-to-Diploid Morphological Transition in Land Plants." *Science* 339 (6123): 1067–70. https://doi.org/10.1126/science.1230082.

Samuel, Marcus A., Yolanda T. Chong, Katrina E. Haasen, May Grace Aldea-Brydges, Sophia L. Stone, and Daphne R. Goring. 2009. "Cellular Pathways Regulating Responses to Compatible and Self-Incompatible Pollen in Brassica and Arabidopsis

Stigmas Intersect at Exo70a1, a Putative Component of the Exocyst Complex." *Plant Cell* 21 (9): 2655–71. https://doi.org/10.1105/tpc.109.069740.

Sanchez, María De La Paz, and Crisanto Gutierrez. 2009. "Arabidopsis ORC1 Is a PHD-Containing H3K4me3 Effector That Regulates Transcription." *Proceedings of the National Academy of Sciences of the United States of America* 106 (6): 2065–70. https://doi.org/10.1073/pnas.0811093106.

Sanchez, Roberto, and Ming Ming Zhou. 2011. "The PHD Finger: A Versatile Epigenome Reader." *Trends in Biochemical Sciences* 36 (7): 364–72. https://doi.org/10.1016/j.tibs.2011.03.005.

Saredi, Giulia, Hongda Huang, Colin M. Hammond, Constance Alabert, Simon Bekker-Jensen, Ignasi Forne, Nazaret Reverón-Gómez, et al. 2016. "H4K20me0 Marks Post-Replicative Chromatin and Recruits the TONSL-MMS22L DNA Repair Complex." *Nature* 534 (7609): 714–18. https://doi.org/10.1038/nature18312.

Schier, Alexander F. 2007. "The Maternal-Zygotic Transition: Death and Birth of RNAs." *Science*. American Association for the Advancement of Science. https://doi.org/10.1126/science.1140693.

Schmidt, Jan Marten, and Franziska Bleichert. 2020. "Structural Mechanism for Replication Origin Binding and Remodeling by a Metazoan Origin Recognition Complex and Its Co-Loader Cdc6." *Nature Communications* 11 (1): 1–17. https://doi.org/10.1038/s41467-020-18067-7.

Schneeberger, Korbinian, Stephan Ossowski, Christa Lanz, Trine Juul, Annabeth Høgh Petersen, Kåre Lehmann Nielsen, Jan Elo Jørgensen, Detlef Weigel, and Stig Uggerhø Andersen. 2009. "SHOREmap: Simultaneous Mapping and Mutation Identification by Deep Sequencing." *Nature Methods* 6 (8): 550–51. https://doi.org/10.1038/nmeth0809-550.

Schneeberger, Korbinian, Stephan Ossowski, Felix Ott, Juliane D. Klein, Xi Wang, Christa Lanz, Lisa M. Smith, et al. 2011. "Reference-Guided Assembly of Four Diverse Arabidopsis Thaliana Genomes." *Proceedings of the National Academy of Sciences of the United States of America* 108 (25): 10249–54. https://doi.org/10.1073/pnas.1107739108.

Scholl, R. L., S. T. May, and D. H. Ware. 2000. "Seed and Molecular Resources for Arabidopsis." *Plant Physiology* 124 (4): 1477–80. https://doi.org/10.1104/pp.124.4.1477.

Sekimoto, Hiroyuki. 2017. "Sexual Reproduction and Sex Determination in Green Algae." *Journal of Plant Research* 130 (3): 423–31. https://doi.org/10.1007/s10265-017-0908-6.

Sha, Qian Qian, Jue Zhang, and Heng Yu Fan. 2019. "A Story of Birth and Death: MRNA Translation and Clearance at the Onset of Maternal-To-Zygotic Transition in Mammals." *Biology of Reproduction* 101 (3): 579–90. https://doi.org/10.1093/biolre/ioz012.

Shin, Jinwoo, Goowon Jeong, Jong Yoon Park, Hoyeun Kim, and Ilha Lee. 2018. "MUN (MERISTEM UNSTRUCTURED), Encoding a SPC24 Homolog of NDC80 Kinetochore Complex, Affects Development through Cell Division in Arabidopsis Thaliana." *Plant Journal* 93 (6): 977–91. https://doi.org/10.1111/tpj.13823.

Singer, S. D., and N. W. Ashton. 2007. "Revelation of Ancestral Roles of KNOX Genes by a Functional Analysis of Physcomitrella Homologues." *Plant Cell Reports* 26 (12): 2039–

54. https://doi.org/10.1007/s00299-007-0409-5.

Slane, Daniel, Jixiang Kong, Kenneth W. Berendzen, Joachim Kilian, Agnes Henschen, Martina Kolb, Markus Schmid, et al. 2014. “Cell Type-Specific Transcriptome Analysis in the Early Arabidopsis Thaliana Embryo.” *Development (Cambridge)* 141 (24): 4831–40. https://doi.org/10.1242/dev.116459.

Speck, Christian, Zhiqiang Chen, Huilin Li, and Bruce Stillman. 2005. “ATPase-Dependent Cooperative Binding of ORC and Cdc6 to Origin DNA.” *Nature Structural and Molecular Biology* 12 (11): 965–71. https://doi.org/10.1038/nsmb1002.

Stroud, Hume, Christopher J. Hale, Suhua Feng, Elena Caro, Yannick Jacob, Scott D. Michaels, and Steven E. Jacobsen. 2012. “DNA Methyltransferases Are Required to Induce Heterochromatic Re-Replication in Arabidopsis.” *PLoS Genetics* 8 (7): e1002808. https://doi.org/10.1371/journal.pgen.1002808.

Sukawa, Yumiko, and Takashi Okamoto. 2018. “Cell Cycle in Egg Cell and Its Progression during Zygotic Development in Rice.” *Plant Reproduction* 31 (1): 107–16. https://doi.org/10.1007/s00497-017-0318-x.

Tadros, Wael, and Howard D. Lipshitz. 2009. “The Maternal-to-Zygotic Transition: A Play in Two Acts.” *Development* 136 (18): 3033–42. https://doi.org/10.1242/dev.033183.

Takeda, Shin, Zerihun Tadele, Ingo Hofmann, Aline V. Probst, Karel J. Angelis, Hidetaka Kaya, Takashi Araki, et al. 2004. “BRU1, a Novel Link between Responses to DNA Damage and Epigenetic Gene Silencing in Arabidopsis.” *Genes and Development* 18 (7): 782–93. https://doi.org/10.1101/gad.295404.

Takeuchi, Hidenori, and Tetsuya Higashiyama. 2016. “Tip-Localized Receptors Control Pollen Tube Growth and LURE Sensing in Arabidopsis.” *Nature* 531 (7593): 245–48. https://doi.org/10.1038/nature17413.

Talbert, Paul B., Ricardo Masuelli, Anand P. Tyagi, Luca Comai, and Steven Henikoff. 2002. “Centromeric Localization and Adaptive Evolution of an Arabidopsis Histone H3 Variant.” *Plant Cell* 14 (5): 1053–66. https://doi.org/10.1105/tpc.010425.

Twell, David. 2011. “Male Gametogenesis and Germline Specification in Flowering Plants.” *Sexual Plant Reproduction* 24 (2): 149–60. https://doi.org/10.1007/s00497-010-0157-5.

Ueda, Minako, Ernst Aichinger, Wen Gong, Edwin Groot, Inge Verstraeten, Lam Dai Vu, Ive De Smet, Tetsuya Higashiyama, Masaaki Umeda, and Thomas Laux. 2017. “Transcriptional Integration of Paternal and Maternal Factors in the Arabidopsis Zygote.” *Genes & Development* 31 (6): 617–27. https://doi.org/10.1101/gad.292409.116.

Valansi, Clari, David Moi, Evgenia Leikina, Elena Matveev, Martín Graña, Leonid V. Chernomordik, Héctor Romero, Pablo S. Aguilar, and Benjamin Podbilewicz. 2017. “Arabidopsis HAP2/GCS1 Is a Gamete Fusion Protein Homologous to Somatic and Viral Fusogens.” *Journal of Cell Biology* 216 (3): 571–81. https://doi.org/10.1083/jcb.201610093.

Vogler, Frank, Christina Schmalzl, Maria Englhart, Martin Bircheneder, and Stefanie Sprunck. 2014. “Brassinosteroids Promote Arabidopsis Pollen Germination and Growth.” *Plant Reproduction* 27 (3): 153–67. https://doi.org/10.1007/s00497-014-0247-x.

Völz, Ronny, Juliane Heydlauff, Dagmar Ripper, Ludwig vonLyncker, and Rita Groß-Hardt.

2013. “Ethylene Signaling Is Required for Synergid Degeneration and the Establishment of a Pollen Tube Block.” *Developmental Cell* 25 (3): 310–16. https://doi.org/10.1016/j.devcel.2013.04.001.

Wang, Kai, Houming Chen, Marina Ortega-Perez, Yingjing Miao, Yanfei Ma, Agnes Henschen, Jan U. Lohmann, Sascha Laubinger, and Martin Bayer. 2021. “Independent Parental Contributions Initiate Zygote Polarization in Arabidopsis Thaliana.” *Current Biology* 31 (21): 4810-4816.e5. https://doi.org/10.1016/j.cub.2021.08.033.

Wang, Zhi Ping, Hui Li Xing, Li Dong, Hai Yan Zhang, Chun Yan Han, Xue Chen Wang, and Qi Jun Chen. 2015. “Egg Cell-Specific Promoter-Controlled CRISPR/Cas9 Efficiently Generates Homozygous Mutants for Multiple Target Genes in Arabidopsis in a Single Generation.” *Genome Biology* 16 (1): 1–12. https://doi.org/10.1186/s13059-015-0715-0.

Watanabe, Masao, Keita Suwabe, and Go Suzuki. 2012. “Molecular Genetics, Physiology and Biology of Self-Incompatibility: In Brassicaceae.” *Proceedings of the Japan Academy Series B: Physical and Biological Sciences* 88 (10): 519–35. https://doi.org/10.2183/pjab.88.519.

Weterings, Koen, and Scott D. Russell. 2004. “Experimental Analysis of the Fertilization Process.” *Plant Cell* 16 (SUPPL.): S107–18. https://doi.org/10.1105/tpc.016873.

Wheeler, Emily, Ashley M. Brooks, Lorenzo Concia, Daniel L. Vera, Emily E. Wear, Chantal LeBlanc, Umamaheswari Ramu, et al. 2020. “Arabidopsis DNA Replication Initiates in Intergenic, AT-Rich Open Chromatin.” *Plant Physiology* 183 (5): 206–20. https://doi.org/10.1104/pp.19.01520.

Wolff, Philip, Hua Jiang, Guifeng Wang, Juan Santos-González, and Claudia Köhler. 2015. “Paternally Expressed Imprinted Genes Establish Postzygotic Hybridization Barriers in Arabidopsis Thaliana.” *ELife* 4 (September 2015). https://doi.org/10.7554/eLife.10074.

Woodfine, Kathryn, Heike Fiegler, David M. Beare, John E. Collins, Owen T. McCann, Bryan D. Young, Silvana Debernardi, Richard Mott, Ian Dunham, and Nigel P. Carter. 2004. “Replication Timing of the Human Genome.” *Human Molecular Genetics* 13 (2): 191–202. https://doi.org/10.1093/hmg/ddh016.

Woody, Scott T., Sandra Austin-Phillips, Richard M. Amasino, and Patrick J. Krysan. 2007. “The WiscDsLox T-DNA Collection: An Arabidopsis Community Resource Generated by Using an Improved High-Throughput T-DNA Sequencing Pipeline.” *Journal of Plant Research* 120 (1): 157–65. https://doi.org/10.1007/s10265-006-0048-x.

Wu, Xianzhong, Fengling Li, Allan Kolenovsky, Allan Caplan, Yuhai Cui, Adrian Cutler, and Edward W.T. Tsang. 2009. “A Mutant Deficient in S-Adenosylhomocysteine Hydrolase in Arabidopsis Shows Defects in Roothair Development.” *Botany* 87 (6): 571–84. https://doi.org/10.1139/B08-124.

Xin, Hai Ping, Jing Zhao, and Meng Xiang Sun. 2012. “The Maternal-to-Zygotic Transition in Higher Plants.” *Journal of Integrative Plant Biology* 54 (9): 610–15. https://doi.org/10.1111/j.1744-7909.2012.01138.x.

Xiong, Hanxian, Wei Wang, and Meng Xiang Sun. 2021. “Endosperm Development Is an Autonomously Programmed Process Independent of Embryogenesis.” *Plant Cell* 33 (4): 1151–60. https://doi.org/10.1093/plcell/koab007.

Yadegari, Ramin, and Gary N. Drews. 2004. “Female Gametophyte Development.” *Plant Cell* 16 (SUPPL.): S133–41. https://doi.org/10.1105/tpc.018192.

Yaffe, Eitan, Shlomit Farkash-Amar, Andreas Polten, Zohar Yakhini, Amos Tanay, and Itamar Simon. 2010. “Comparative Analysis of DNA Replication Timing Reveals Conserved Large-Scale Chromosomal Architecture.” *PLoS Genetics* 6 (7): 1–12. https://doi.org/10.1371/journal.pgen.1001011.

Yamagishi, Kazutoshi, Noriko Nagata, Kelly Matsudaira Yee, Siobhan A. Braybrook, Julie Pelletier, Shozo Fujioka, Shigeo Yoshida, Robert L. Fischer, Robert B. Goldberg, and John J. Harada. 2005. “TANMEI/EMB2757 Encodes a WD Repeat Protein Required for Embryo Development in Arabidopsis.” *Plant Physiology* 139 (1): 163–73. https://doi.org/10.1104/pp.105.060467.

Yeeles, Joseph T.P., Tom D. Deegan, Agnieszka Janska, Anne Early, and John F.X. Diffley. 2015. “Regulated Eukaryotic DNA Replication Origin Firing with Purified Proteins.” *Nature* 519 (7544): 431–35. https://doi.org/10.1038/nature14285.

Yi, Peishan, and Gohta Goshima. 2018. “Microtubule Nucleation and Organization without Centrosomes.” *Current Opinion in Plant Biology* 46 (December): 1–7. https://doi.org/10.1016/j.pbi.2018.06.004.

Yu, Xiaobo, Xuecheng Zhang, Peng Zhao, Xiongbo Peng, Hong Chen, Andrea Bleckmann, Anastasiia Bazhenova, Ce Shi, Thomas Dresselhaus, and Meng xiang Sun. 2021. “Fertilized Egg Cells Secrete Endopeptidases to Avoid Polytubey.” *Nature* 592 (7854): 433–37. https://doi.org/10.1038/s41586-021-03387-5.

Zhang, Yan, and Sheila McCormick. 2007. “A Distinct Mechanism Regulating a Pollen-Specific Guanine Nucleotide Exchange Factor for the Small GTPase Rop in Arabidopsis Thaliana.” *Proceedings of the National Academy of Sciences of the United States of America* 104 (47): 18830–35. https://doi.org/10.1073/pnas.0705874104.

Zhao, Peng, Ce Shi, Ling Wang, and Meng xiang Sun. 2022. “The Parental Contributions to Early Plant Embryogenesis and the Concept of Maternal-to-Zygotic Transition in Plants.” *Current Opinion in Plant Biology* 65 (February): 102144. https://doi.org/10.1016/j.pbi.2021.102144.

Zhao, Peng, Xuemei Zhou, Kun Shen, Zhenzhen Liu, Tianhe Cheng, Danni Liu, Yanbing Cheng, Xiongbo Peng, and Meng xiang Sun. 2019. “Two-Step Maternal-to-Zygotic Transition with Two-Phase Parental Genome Contributions.” *Developmental Cell* 49 (6): 882-893.e5. https://doi.org/10.1016/j.devcel.2019.04.016.

Zhao, Peng, Xuemei Zhou, Yifan Zheng, Yanru Ren, and Meng xiang Sun. 2020. “Equal Parental Contribution to the Transcriptome Is Not Equal Control of Embryogenesis.” *Nature Plants* 6 (11): 1354–64. https://doi.org/10.1038/s41477-020-00793-x.

Zhao, Youshang, Songyun Wang, Wenye Wu, Lei Li, Ting Jiang, and Binglian Zheng. 2018. “Clearance of Maternal Barriers by Paternal MiR159 to Initiate Endosperm Nuclear Division in Arabidopsis.” *Nature Communications* 9 (1): 1–11. https://doi.org/10.1038/s41467-018-07429-x.

Zhong, Sheng, Ling Li, Zhijuan Wang, Zengxiang Ge, Qiyun Li, Andrea Bleckmann, Jizong Wang, et al. 2022. “RALF Peptide Signaling Controls the Polytubey Block in Arabidopsis.” *Science* 375 (6578): 290–96. https://doi.org/10.1126/science.abl4683.

Zhong, Sheng, Meiling Liu, Zhijuan Wang, Qingpei Huang, Saiying Hou, Yong Chao Xu, Zengxiang Ge, et al. 2019. “Cysteine-Rich Peptides Promote Interspecific Genetic Isolation in Arabidopsis.” *Science* 364 (6443). https://doi.org/10.1126/science.aau9564.

7 Appendix

Attached are the original manuscripts of the following publications:

1. Kai Wang, Houming Chen, Marina Ortega-Perez, **Yingjing Miao**, Yanfei Ma, Agnes Henschen, Jan U. Lohmann, Sascha Laubinger, and Martin Bayer. (2021). Independent parental contributions initiate zygote polarization in *Arabidopsis thaliana*. *Current Biology*, *31*(21), 4810-4816.e5. https://doi.org/10.1016/j.cub.2021.08.033
2. Houming Chen, **Yingjing Miao**, Kai Wang, and Martin Bayer. (2021). Zygotic Embryogenesis in Flowering Plants. *Methods in Molecular Biology*, *2288*, 73–88. https://doi.org/10.1007/978-1-0716-1335-1_4
3. Daniel Slane, Cameron H. Lee, Martina Kolb, Craig Dent, **Yingjing Miao**, Mirita Franz-Wachtel, Steffen Lau, Boris Maček, Sureshkumar Balasubramanian, Martin Bayer, and Gerd Jürgens. (2020). The integral spliceosomal component CWC15 is required for development in *Arabidopsis*. *Scientific Reports*, *10*(1). https://doi.org/10.1038/s41598-020-70324-3
4. Kai Wang, Houming Chen, **Yingjing Miao**, and Martin Bayer. (2020). Square one: zygote polarity and early embryogenesis in flowering plants. *Current Opinion in Plant Biology* (Vol. 53, pp. 128–133). https://doi.org/10.1016/j.pbi.2019.10.002

Report

Current Biology

Independent parental contributions initiate zygote polarization in *Arabidopsis thaliana*

Graphical abstract

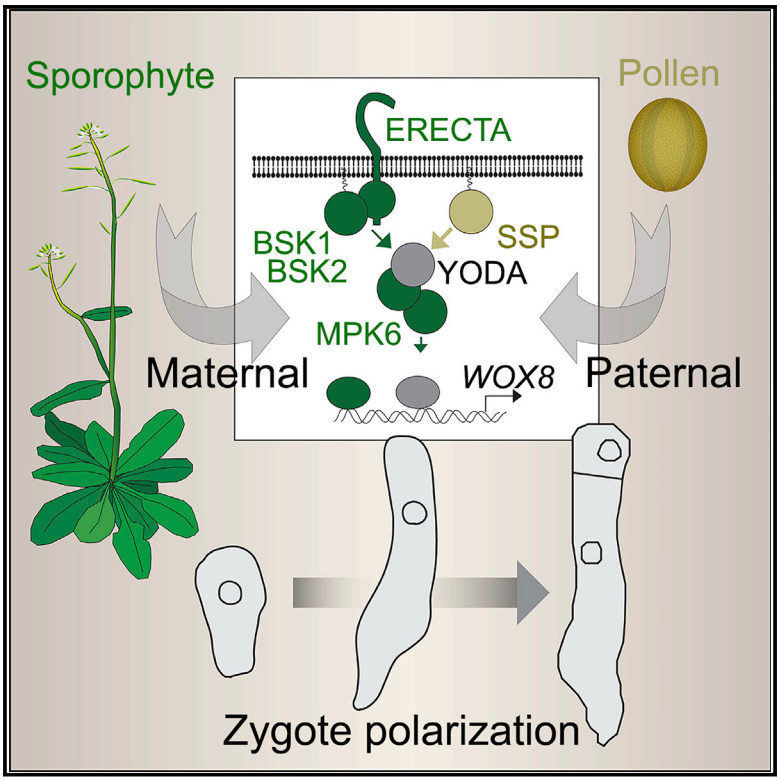

Authors

Kai Wang, Houming Chen, Marina Ortega-Perez, ..., Jan U. Lohmann, Sascha Laubinger, Martin Bayer

Correspondence

martin.bayer@tuebingen.mpg.de

In brief

Cell polarization and asymmetric division of the zygote initiate axis formation of the embryo in the model plant *Arabidopsis*. Wang et al. show in this context that a maternal receptor complex and a paternally provided constitutively active signaling protein independently contribute to MAP kinase signaling controlling zygote polarization.

Highlights

- Independent maternal and paternal factors influence *Arabidopsis* zygote polarity
- Maternal ERECTA family receptor kinases activate the MAP3K YODA in the zygote
- Paternal SHORT SUSPENSOR protein activates YODA independently of maternal ERECTA

Wang et al., 2021, Current Biology *31*, 4810–4816
November 8, 2021
https://doi.org/10.1016/j.cub.2021.08.033

CellPress

CellPress

Current Biology

Report

Independent parental contributions initiate zygote polarization in *Arabidopsis thaliana*

Kai Wang,[1] Houming Chen,[1] Marina Ortega-Perez,[1] Yingjing Miao,[1] Yanfei Ma,[2] Agnes Henschen,[1] Jan U. Lohmann,[2] Sascha Laubinger,[3] and Martin Bayer[1,4,*]

[1]Max Planck Institute for Developmental Biology, Department of Cell Biology, Max-Planck-Ring 5, 72076 Tübingen, Germany

[2]Centre for Organismal Studies, Heidelberg University, Department of Stem Cell Biology, Im Neuenheimer Feld 230, 69120 Heidelberg, Germany

[3]University of Oldenburg, Institute for Biology and Environmental Sciences, Carl-von-Ossietzky-Str. 9-11, 26111 Oldenburg, Germany

[4]Lead contact

*Correspondence: martin.bayer@tuebingen.mpg.de

https://doi.org/10.1016/j.cub.2021.08.033

SUMMARY

Embryogenesis of flowering plants is initiated by polarization of the zygote, a prerequisite for correct axis formation in the embryo. The daughter cells of the asymmetric zygote division form the pro-embryo and the mostly extra-embryonic suspensor.[1] The suspensor plays a pivotal role in nutrient and hormone transport and rapid growth of the embryo.[2,3] Zygote polarization is controlled by a MITOGEN-ACTIVATING PROTEIN (MAP) kinase signaling pathway including the MAPKK kinase (MAP3K) YODA (YDA)[4] and the upstream membrane-associated proteins BRASINOSTEROID SIGNALING KINASE 1 (BSK1) and BSK2.[5,6] Furthermore, suspensor development is controlled by cysteine-rich peptides of the EMBRYO SURROUNDING FACTOR 1 (ESF1) family.[7] While they act genetically upstream of YDA, the corresponding receptor to perceive these potential ligands is unknown. In other developmental processes, such as stomata development, YDA activity is controlled by receptor kinases of the ERECTA family (ERf).[8–12] While the receptor kinases upstream of BSK1/2 in the embryo have so far not been identified,[1] YDA is in part activated by the sperm cell-derived BSK family member SHORT SUSPENSOR (SSP) that represents a naturally occurring, constitutively active variant of BSK1.[5,13] It has been speculated that SSP might be a paternal component of a parental tug-of-war controlling resource allocation toward the embryo.[2,13] Here, we show that in addition to SSP, the receptor kinase ERECTA plays a crucial role in zygote polarization as a maternally contributed part of the embryonic YDA pathway. We conclude that two independent parental contributions initiate zygote polarization and control embryo development.

RESULTS AND DISCUSSION

Despite its central role in zygote polarization and controlling embryonic versus non-embryonic development, it is still unclear if the embryonic YDA pathway is activated in response to extracellular signals. In many aspects of *Arabidopsis* development, YDA activity is controlled by receptor kinases of the ERECTA family, including ERECTA (ER), ER-LIKE 1 (ERL1), and ERL2.[9,10,12] As transcripts of *ER* can be detected in the zygote (Table S1),[14] a critical function of *ER* in controlling zygote polarity seems plausible. Homozygous *er erl1 erl2* triple mutants are sterile and produce no embryos.[11] We therefore addressed a possible function of *ER* in early embryogenesis by examining homozygous single, double, and segregating triple mutants of *ERf* genes. As mutants in Ler background used in previous studies contain a non-functional *ER* gene, we performed all genetic experiments with alleles in Col-0 background.[4,13,15] When comparing *er* mutants with wild type, weak defects in zygote elongation, zygote polarization, and suspensor length became apparent (Figure 1) as well as aberrant division plane orientations in the suspensor (Figure S1). These defects are hallmarks of reduced YDA activity[4] and mimic the phenotypes of *ssp* or *bsk1 bsk2* double mutants.[5,13] Loss of *ERL1* and *ERL2* function only showed detectable defects in the absence of functional *ER* by enhancing the *er* phenotype, indicating that ERL1 and ERL2 play a minor role in early embryogenesis but can partially take over *ER* function in its absence (Figure 1), as previously described for *ERf* function during stomata development.[10,16–18] To test if ER acts upstream of YDA in the context of zygote polarization as it does in other developmental contexts,[10,18,19] we performed genetic rescue experiments with a constitutively active version of YDA (*yda-CA*;[4] Figure S1). Constitutive YDA activity rescued the *er erl2* double mutant phenotype and caused increased zygote elongation, suggesting that YDA acts downstream of ER in a common signaling cascade. As *yda-CA* was hemizygous in the parental plant and therefore segregated in the analyzed embryos, a quarter of the embryos did not carry the *yda-CA* transgene, resulting in slightly lower median values in the *er erl2* background compared to wild-type background. These results suggest that the ER/YDA pathways involved in embryogenesis and stomata development share a common overall architecture.[20] Triple *ERf* mutants with segregating *er* (*ER/er erl1 erl2*), however, did not show defects in zygote

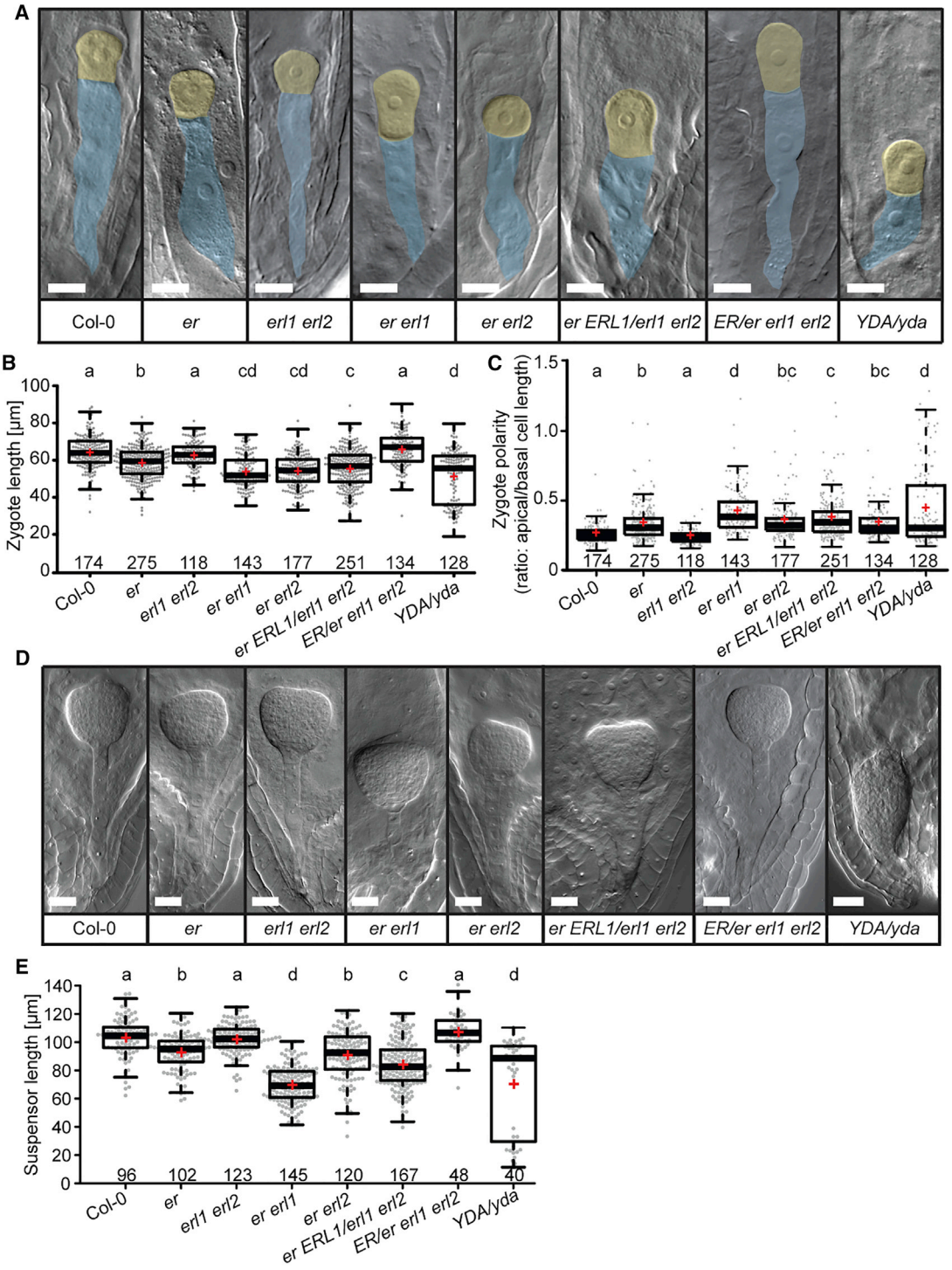

Figure 1. Zygote polarity and suspensor development

(A) DIC images of cleared ovules showing representative one-cell embryos (apical cell false-colored in yellow, basal cell in blue). Genotypes are given below images. Scale bar, 10 µm.

(B and C) Boxplot diagram of zygote length (B) and zygote polarity (C).

(D) DIC images of transition stage embryos. Genotypes are given below images. Scale bar, 20 µm.

(E) Boxplot diagram of suspensor length at transition stage.

(legend continued on next page)

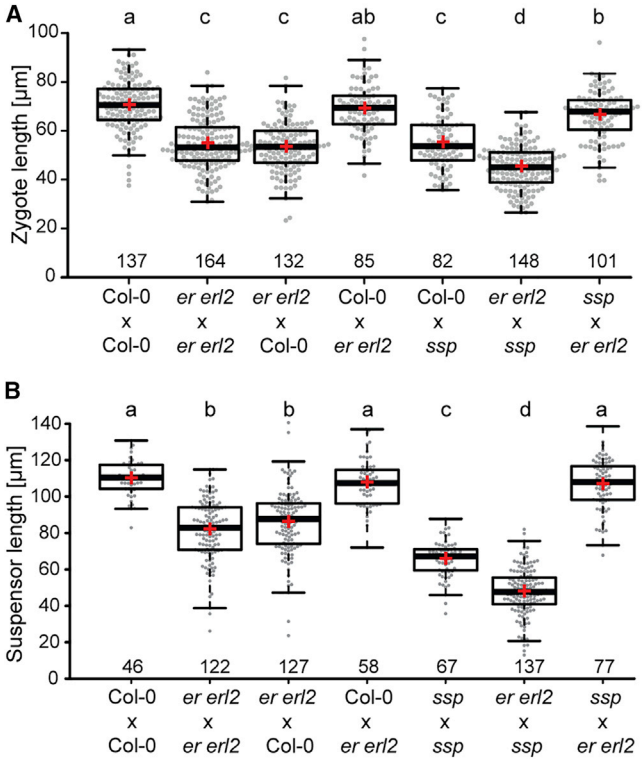

Figure 2. Parental effects in reciprocal crosses

Boxplot diagrams of zygote elongation (A) and suspensor length (B) in F1 embryos of reciprocal crosses. Genotypes are given as female × male. Boxplot data presentation as described in Figure 1. Different letters above boxes refer to individual groups in a one-way ANOVA with a post hoc Tukey test ($p < 0.05$). See also Figures S2 and S4 and Table S3.

elongation or suspensor formation despite normal transmission of the *er* mutant allele (Figure 1; Table S2). The fact that phenotypic defects in homozygous *er* embryos only became apparent if the parental plants were homozygous for *er*, but not in homozygous offspring of heterozygous *ER/er* parents, led us to test for possible parent-of-origin effects. In reciprocal crosses of *er erl* double mutants and wild type (Figures 2 and S2), we could only observe defects in F1 embryos if maternal plants carried the *er erl* mutations, but not if these alleles were transmitted by the pollen donors (Figures 2 and S2). Furthermore, zygote elongation defects could not be observed if maternal plants were heterozygous for the *er* mutation (Figure 1), although slightly altered zygote polarity can be observed in segregating triple *ER/er erl1 erl2* mutants (Figure 1). The phenotype of the embryo therefore seems to be predominantly determined by the genotype of the maternal sporophyte while loss of *ER* function in the haploid phase or the embryo in segregating plants did not have a major effect on the embryonic phenotype. This unusual parental effect may explain why a role of *ERECTA* in zygote polarization has so far been overlooked.

Two possible scenarios could explain the sporophytic maternal effect: zygote polarization could be affected by a non-cell-autonomous function of ER in sporophytic tissue. Such a scenario has, for example, been described for early auxin signaling in the embryo.[21] Alternatively, ER could function in the zygote but rely on *ER* transcripts and/or ER proteins inherited to the zygote via the pre-meiotic megaspore mother cell (MMC).

A transcriptional (ER_{pro}*:3xVenus-N7*) and a functional translational fusion (ER_{pro}*:ER-YPet*) reporter gene as well as RNA *in situ* hybridization revealed *ER* expression in the sporophytic seed coat as well as the female germline (Figure S3). As *ER* transcripts can be detected at low level in isolated zygotes[14] (Table S1) but are below detection limit in RNA *in situ* hybridization and very weak *ER-YPet* expression was sufficient to rescue the mutant phenotype in seedlings, we were not able to draw a definite conclusion about the location of ER function based on the observed expression pattern. However, *yda* has been reported as a zygotic recessive mutant,[4,15] and we confirmed this for the *yda-11* allele (Figures 1 and S1). On the other hand, *SSP* acts as sperm-derived activator.[5,13] Both genes would therefore argue for a function of the embryonic ERECTA/YDA pathway in the zygote. This is further supported by the function of WRKY2, a direct downstream target of MPK6 phosphorylation.[22] Consistently, loss-of-function *wrky2* null mutations are zygotic recessive without detectable parent-of-origin effects.[22] When looking at mRNA stability, *ER* transcripts showed a moderate half-life in seedlings at roughly the same level as typical housekeeping genes, such as *ACTIN 2*, for which rapid mRNA turnover does not appear necessary (Table S3).[23] *ER* transcripts can be detected in the egg cell, but transcript levels decline after fertilization, indicating that there is little or no *de novo* transcription of *ER* in the zygote (Table S1).[14] In order to address the question of where ER function is necessary for zygote polarization, we specifically reduced ER protein function in the zygote using the ER_{pro}*:ER-YPet* line in *er erl1 erl2* background. Genetically encoded anti-GFP nanobodies fused to ubiquitin ligases have been used as an elegant tool to specifically target GFP/YFP-tagged proteins for degradation.[24,25] To test its functionality, we expressed the NSlmb-vhhGFP4 nanobody under the *ER* promoter. The resulting seedlings mimicked the *er erl1 erl2* triple-mutant phenotype,[11] albeit with a slightly weaker phenotype (Figure 3), indicating that the nanobody is functional but does not completely abolish ER-YPet activity. In the next step, we expressed the nanobody under the strong egg cell-specific *EC1* promoter[26] to specifically reduce ER-YPet levels in the egg cell/zygote. This resulted in a significant reduction of zygote length in the ER_{pro}*:ER-YPet* rescue line (Figure 3), indicating that zygote polarization critically depends on functional *ER* protein in the zygote. Taken together, the available data suggest that the sporophytic maternal control of ER function can be explained by the inheritance of pre-meiotically produced *ER* transcripts/proteins to the zygote and that very low amounts of ER are sufficient to provide function in the zygote.

In (B)–(E), the sample size is given above the x axis. Center lines show the medians; box limits indicate the 25th and 75th percentiles; whiskers extend 1.5 times the interquartile range from the 25th and 75th percentiles; red crosses represent sample means; data points are plotted as gray dots. Letters above boxes refer to individual groups in a one-way ANOVA with a post hoc Tukey test ($p < 0.05$). In embryos of heterozygous *yda* plants, two distinct populations of data points can be observed, with approximately a quarter showing strong zygote elongation (B) and polarity defects (C), and reduced suspensor length (E) possibly representing the homozygous offspring. See also Figure S1 and Tables S1–S3.

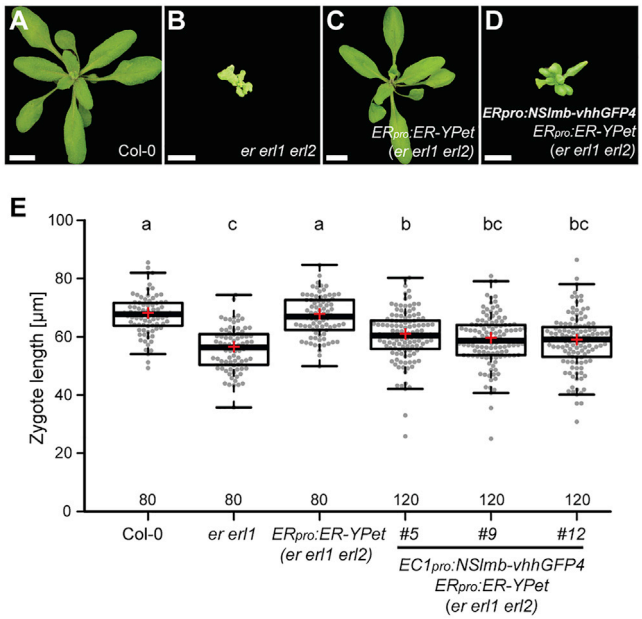

Figure 3. Cell-autonomous function of ER protein in the zygote

(A–D) Vegetative growth phenotype of wild-type Col-0 (A), *er erl1 erl2* triple homozygous (B), genetically rescued plants (ER_{pro}*:ER-YPet* in *er erl1 erl2*; C), and genetically recued plants expressing anti-GFP nanobody (ER_{pro}*:NSlmb-vhhGFP4* in ER_{pro}*:ER-YPet er erl1 erl2*; D). Scale bar, 1 cm. See also Figure S3. (E) Egg cell-specific expression of the anti-GFP nanobody ($EC1_{pro}$*:NSlmb-vhhGFP4*) in the ER_{pro}*:ER-YPet er erl1 erl2* plant leads to reduced zygote length. Boxplot diagram of zygote elongation. Boxplot data presentation as described in Figure 1. Different letters above boxes refer to individual groups in a one-way ANOVA with a post hoc Tukey test ($p < 0.05$).

Different mechanisms that cause maternal effects on plant embryogenesis including inheritance of cytoplasmic factors have been proposed more than two decades ago.[27] Furthermore, sporophytic maternal effects have previously been identified in the mutant *sin1-2* allele of the SHORT INTEGUMENTS 1 (SIN1)/DICER-LIKE 1 (DCL1) gene.[28,29] A comprehensive survey of essential genes in *Arabidopsis* showed that many mutations in essential genes can be transmitted through the female germline and only become deleterious in the early embryo.[30] This suggests that genetic compensation by premeiotic gene products prevents lethality in the female gametophyte for many essential genes and might therefore not be a rare event.[30]

BSK1 and BSK2 have been shown to act upstream of YDA, presumably linking ERECTA signaling with YDA activation.[5] Reciprocal crosses with *bsk1 bsk2* double mutants and wild type showed similar sporophytic maternal effects as observed for *er* (Figure S4). As maternal effects have been described for mutations in genes acting downstream of YDA,[31,32] not just *ER* but several components of this signaling pathway appear to be under maternal sporophytic control. This is quite intriguing, as the non-canonical BSK family member SSP activates YDA as paternal factor contributed by the sperm cell.[13] SSP has been shown to resemble a naturally occurring, constitutively active form of BSK that directly interacts with YDA via its TPR motif.[5] This raises the question of whether the two parental contributions to YDA activation can function independently. We tested this hypothesis in seedlings, where ectopic expression of *SSP* leads to constitutive activation of the YDA pathway[5,13] resulting in cotyledons lacking mature stomata. This was also observed for *SSP* expression in *er erl1 erl2* triple-mutant background, indicating that SSP can activate YDA in the absence of a functional receptor complex (Figure 4A). Overexpression of *BSK1* in *bsk1 bsk2* double-mutant background rescued the *bsk1 bsk2* phenotype, indicating that the construct is functional. In contrast to *SSP*, however, it failed to rescue the *er erl1 erl2* triple-mutant phenotype, despite having similar or higher transcript levels when compared to $35S_{pro}$*:SSP* (Figures 4B and 4C).

If SSP serves as an independent signal for YDA activation in the zygote, loss of *SSP* should have an additive effect to loss of *ER* function. The further loss of *SSP* in *er erl1* and *er erl2* mutants indeed led to further reduction in zygote length and an almost complete loss of zygote polarity (Figures 2 and S2), indicating that *SSP* provides additional YDA activation independently of *ER* function. If the embryonic YDA pathway indeed relies on two independent signaling inputs, additional SSP activity should compensate for the loss of ER function. To test this, we introduced an additional copy of *SSP* (SSP_{pro}*:SSP-YFP*) in the *er erl2* double mutant and found that additional *SSP* activity indeed partially rescued the loss-of-function phenotype of *er erl2* (Figure 4D).

Taken together, our data outline a signaling pathway (Figure 4E) with a maternally controlled receptor complex and a paternally provided activating protein that converge at the level of MAP3K activation. *SSP* is a *Brassicaceae*-specific gene while *ER*, *BSK1*, and *BSK2* are evolutionarily conserved in flowering plants.[33,34] *SSP* has been shown to be critical for correct suspensor development,[13] an organ that serves as a conduit for nutrients to the embryo,[3] and for rapid development of the embryo.[2] Therefore, suspensor development could be a possible target of a parental conflict over nutrient allocation to the embryo.[35] It has recently been observed that there are preferentially maternal expressed genes in the suspensor while there is mainly biparental expression in descendants of the apical cell.[36] This maternal bias in the suspensor could be interpreted in the context of the parental conflict theory enforcing equal nutrient distribution to all embryos by the maternal genome.[35] In this context, it might be significant that ER function is under sporophytic control as the sporophytic maternal effect would ensure uniform suspensor development of all embryos irrespective of segregating maternal alleles. In this scenario, *SSP* could be seen as a *Brassicaceae*-specific paternal contribution that circumvents the maternal control of suspensor development, bypassing ERECTA signaling as a strong independent activator of the YDA pathway.

This raises the question if suspensor development in other plant species is also under maternal control and whether the two independent inputs for YDA activation indeed are part of a parental tug-of-war over nutrient allocation to the embryo. Or are *Brassicaceae* shifting from ligand-/receptor-based zygote polarization to a sperm-based activation mechanism via SSP to fine-tune the timing of YDA activation as SSP naturally links fertilization with YDA activation?

The receptor kinase ER implies extra-cellular ligands in the control of zygote polarization, and the known ESF1 peptides are prime candidates. However, at present it is unclear if they have a function in zygote polarization or influence suspensor development after zygote polarization.[7] Future research will be needed to address the question of where the ligand for the ER

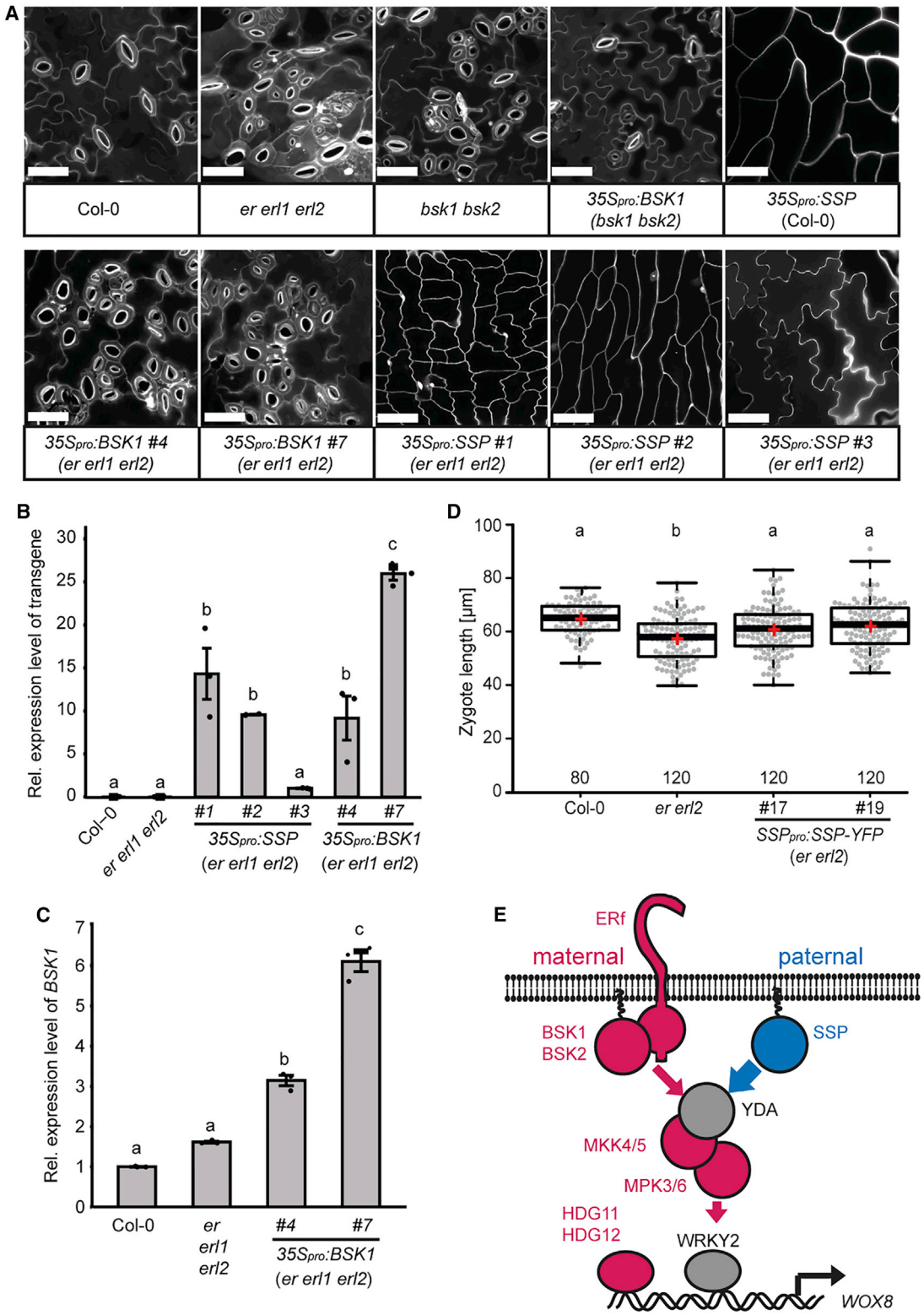

Figure 4. Independent parental contributions to YDA activation in the zygote

(A) Maximum projections of epidermal confocal images. Genotypes are given under each figure panel. Cell walls are stained with propidium iodide. Scale bar, 20 μm.

(B) Expression level of *35S$_{pro}$:SSP* and *35S$_{pro}$:BSK1* in *er erl1 erl2* seedlings shown in (A) as determined by qRT-PCR. Bar graph shows mean values of three technical replicates with standard error.

(legend continued on next page)

receptor kinase is originating and how conserved this mode of zygote polarization is in land plants.

STAR★METHODS

Detailed methods are provided in the online version of this paper and include the following:

- KEY RESOURCES TABLE
- RESOURCE AVAILABILITY
  - Lead contact
  - Materials availability
  - Data and code availability
- EXPERIMENTAL MODEL AND SUBJECT DETAILS
- METHOD DETAILS
  - Mutant lines
  - Genotyping
  - Plasmid construction
  - Transgenic plants
  - DIC and Confocal microscopy
  - RNA *in situ* hybridization
  - Quantitative RT-PCR analysis
  - Phenotypic analysis of rosette leaves
  - RNA stability
- QUANTIFICATION AND STATISTICAL ANALYSIS
  - Measurement of zygote/suspensor length
  - Statistical analysis

SUPPLEMENTAL INFORMATION

Supplemental information can be found online at https://doi.org/10.1016/j.cub.2021.08.033.

ACKNOWLEDGMENTS

We would like to thank Gerd Jürgens for helpful discussions and comments on the manuscript. We also thank the Salk Institute Genomic Analysis Laboratory as well as the Nottingham *Arabidopsis* Stock Centre (NASC) for providing the sequence-indexed *Arabidopsis* tDNA insertion mutants and the Light Microscopy Facility at the Max Planck Institute for Developmental Biology for support. Research in our groups is supported by the German Research Foundation (Deutsche Forschungsgemeinschaft - DFG SFB1101/B01 to M.B. and SFB1101/B07 to J.U.L.), the Chinese Scholarship Council (fellowship no. 201806320131 to Y. Miao), and the Max Planck Society.

AUTHOR CONTRIBUTIONS

K.W. and M.B. designed the study with critical comments and modifications by H.C., M.O.-P., Y. Miao, Y. Ma, J.U.L., and S.L. K.W., H.C., M.O.-P., Y. Miao, and A.H. performed the experiments. K.W., H.C., M.O.-P., Y. Miao, Y. Ma, A.H., J.U.L., S.L., and M.B. evaluated the data and interpreted the experimental results. K.W. and M.B. wrote the initial manuscript draft, and all authors commented on and edited the manuscript.

DECLARATION OF INTERESTS

The authors declare no competing interests.

Received: March 26, 2021
Revised: July 9, 2021
Accepted: August 11, 2021
Published: September 7, 2021

REFERENCES

1. Wang, K., Chen, H., Miao, Y., and Bayer, M. (2020). Square one: zygote polarity and early embryogenesis in flowering plants. Curr. Opin. Plant Biol. *53*, 128–133.
2. Babu, Y., Musielak, T., Henschen, A., and Bayer, M. (2013). Suspensor length determines developmental progression of the embryo in Arabidopsis. Plant Physiol. *162*, 1448–1458.
3. Kawashima, T., and Goldberg, R.B. (2010). The suspensor: not just suspending the embryo. Trends Plant Sci. *15*, 23–30.
4. Lukowitz, W., Roeder, A., Parmenter, D., and Somerville, C. (2004). A MAPKK kinase gene regulates extra-embryonic cell fate in Arabidopsis. Cell *116*, 109–119.
5. Neu, A., Eilbert, E., Asseck, L.Y., Slane, D., Henschen, A., Wang, K., Bürgel, P., Hildebrandt, M., Musielak, T.J., Kolb, M., et al. (2019). Constitutive signaling activity of a receptor-associated protein links fertilization with embryonic patterning in *Arabidopsis thaliana*. Proc. Natl. Acad. Sci. USA *116*, 5795–5804.
6. Kim, T.W., and Wang, Z.Y. (2010). Brassinosteroid signal transduction from receptor kinases to transcription factors. Annu. Rev. Plant Biol. *61*, 681–704.
7. Costa, L.M., Marshall, E., Tesfaye, M., Silverstein, K.A., Mori, M., Umetsu, Y., Otterbach, S.L., Papareddy, R., Dickinson, H.G., Boutiller, K., et al. (2014). Central cell-derived peptides regulate early embryo patterning in flowering plants. Science *344*, 168–172.
8. Torii, K.U., Mitsukawa, N., Oosumi, T., Matsuura, Y., Yokoyama, R., Whittier, R.F., and Komeda, Y. (1996). The Arabidopsis ERECTA gene encodes a putative receptor protein kinase with extracellular leucine-rich repeats. Plant Cell *8*, 735–746.
9. Bergmann, D.C., Lukowitz, W., and Somerville, C.R. (2004). Stomatal development and pattern controlled by a MAPKK kinase. Science *304*, 1494–1497.
10. Shpak, E.D., McAbee, J.M., Pillitteri, L.J., and Torii, K.U. (2005). Stomatal patterning and differentiation by synergistic interactions of receptor kinases. Science *309*, 290–293.
11. Shpak, E.D., Berthiaume, C.T., Hill, E.J., and Torii, K.U. (2004). Synergistic interaction of three ERECTA-family receptor-like kinases controls Arabidopsis organ growth and flower development by promoting cell proliferation. Development *131*, 1491–1501.
12. Meng, X., Wang, H., He, Y., Liu, Y., Walker, J.C., Torii, K.U., and Zhang, S. (2012). A MAPK cascade downstream of ERECTA receptor-like protein kinase regulates Arabidopsis inflorescence architecture by promoting localized cell proliferation. Plant Cell *24*, 4948–4960.
13. Bayer, M., Nawy, T., Giglione, C., Galli, M., Meinnel, T., and Lukowitz, W. (2009). Paternal control of embryonic patterning in Arabidopsis thaliana. Science *323*, 1485–1488.

(C) Expression level of *BSK1* in Col-0, *er erl1 erl2*, and $35S_{pro}$:*BSK1 er erl1 erl2* seedlings. Bar graph shows mean values of three technical replicates with standard error.
(D) An additional copy of *SSP* (SSP_{pro}:*SSP-YFP*) partially rescues the *er erl2* loss-of-function phenotype in the zygote. The boxplot diagram shows zygote length. Boxplot data presentation as described in Figure 1.
Different letters above bars and boxes in (B)–(D) refer to individual groups in a one-way ANOVA with a post hoc Tukey test ($p < 0.05$).
(E) Simplified schematic depiction of the embryonic YDA pathway. YDA is activated by the maternally supplied receptor complex consisting of ER and the membrane-associated proteins BSK1 and BSK2. YDA is also activated by the paternally contributed BSK family member SSP. Signaling components are colored according to genetic contribution: maternal effect (magenta), paternal effect (blue), and zygotic recessive (gray).

14. Zhao, P., Zhou, X., Shen, K., Liu, Z., Cheng, T., Liu, D., Cheng, Y., Peng, X., and Sun, M.X. (2019). Two-step maternal-to-zygotic transition with two-phase parental genome contributions. Dev. Cell *49*, 882–893.e5.

15. Del Toro-De León, G., García-Aguilar, M., and Gillmor, C.S. (2014). Non-equivalent contributions of maternal and paternal genomes to early plant embryogenesis. Nature *514*, 624–627.

16. Qi, X., Han, S.K., Dang, J.H., Garrick, J.M., Ito, M., Hofstetter, A.K., and Torii, K.U. (2017). Autocrine regulation of stomatal differentiation potential by EPF1 and ERECTA-LIKE1 ligand-receptor signaling. eLife *6*, e24102.

17. Ho, C.M., Paciorek, T., Abrash, E., and Bergmann, D.C. (2016). Modulators of stomatal lineage signal transduction alter membrane contact sites and reveal specialization among ERECTA kinases. Dev. Cell *38*, 345–357.

18. Shpak, E.D. (2013). Diverse roles of ERECTA family genes in plant development. J. Integr. Plant Biol. *55*, 1238–1250.

19. Hara, K., Kajita, R., Torii, K.U., Bergmann, D.C., and Kakimoto, T. (2007). The secretory peptide gene EPF1 enforces the stomatal one-cell-spacing rule. Genes Dev. *21*, 1720–1725.

20. Zoulias, N., Harrison, E.L., Casson, S.A., and Gray, J.E. (2018). Molecular control of stomatal development. Biochem. J. *475*, 441–454.

21. Robert, H.S., Park, C., Gutièrrez, C.L., Wójcikowska, B., Pěnčík, A., Novák, O., Chen, J., Grunewald, W., Dresselhaus, T., Friml, J., and Laux, T. (2018). Maternal auxin supply contributes to early embryo patterning in Arabidopsis. Nat. Plants *4*, 548–553.

22. Ueda, M., Zhang, Z., and Laux, T. (2011). Transcriptional activation of Arabidopsis axis patterning genes WOX8/9 links zygote polarity to embryo development. Dev. Cell *20*, 264–270.

23. Szabo, E.X., Reichert, P., Lehniger, M.K., Ohmer, M., de Francisco Amorim, M., Gowik, U., Schmitz-Linneweber, C., and Laubinger, S. (2020). Metabolic labeling of RNAs uncovers hidden features and dynamics of the Arabidopsis transcriptome. Plant Cell *32*, 871–887.

24. Caussinus, E., Kanca, O., and Affolter, M. (2011). Fluorescent fusion protein knockout mediated by anti-GFP nanobody. Nat. Struct. Mol. Biol. *19*, 117–121.

25. Ma, Y., Miotk, A., Šutiković, Z., Ermakova, O., Wenzl, C., Medzihradszky, A., Gaillochet, C., Forner, J., Utan, G., Brackmann, K., et al. (2019). WUSCHEL acts as an auxin response rheostat to maintain apical stem cells in Arabidopsis. Nat. Commun. *10*, 5093.

26. Sprunck, S., Rademacher, S., Vogler, F., Gheyselinck, J., Grossniklaus, U., and Dresselhaus, T. (2012). Egg cell-secreted EC1 triggers sperm cell activation during double fertilization. Science *338*, 1093–1097.

27. Grossniklaus, U., and Schneitz, K. (1998). The molecular and genetic basis of ovule and megagametophyte development. Semin. Cell Dev. Biol. *9*, 227–238.

28. Ray, S., Golden, T., and Ray, A. (1996). Maternal effects of the short integument mutation on embryo development in Arabidopsis. Dev. Biol. *180*, 365–369.

29. Golden, T.A., Schauer, S.E., Lang, J.D., Pien, S., Mushegian, A.R., Grossniklaus, U., Meinke, D.W., and Ray, A. (2002). SHORT INTEGUMENTS1/SUSPENSOR1/CARPEL FACTORY, a Dicer homolog, is a maternal effect gene required for embryo development in Arabidopsis. Plant Physiol. *130*, 808–822.

30. Muralla, R., Lloyd, J., and Meinke, D. (2011). Molecular foundations of reproductive lethality in Arabidopsis thaliana. PLoS ONE *6*, e28398.

31. Zhang, M., Wu, H., Su, J., Wang, H., Zhu, Q., Liu, Y., Xu, J., Lukowitz, W., and Zhang, S. (2017). Maternal control of embryogenesis by MPK6 and its upstream MKK4/MKK5 in Arabidopsis. Plant J. *92*, 1005–1019.

32. Ueda, M., Aichinger, E., Gong, W., Groot, E., Verstraeten, I., Vu, L.D., De Smet, I., Higashiyama, T., Umeda, M., and Laux, T. (2017). Transcriptional integration of paternal and maternal factors in the *Arabidopsis* zygote. Genes Dev. *31*, 617–627.

33. Liu, S.L., and Adams, K.L. (2010). Dramatic change in function and expression pattern of a gene duplicated by polyploidy created a paternal effect gene in the Brassicaceae. Mol. Biol. Evol. *27*, 2817–2828.

34. Caine, R.S., Chater, C.C., Kamisugi, Y., Cuming, A.C., Beerling, D.J., Gray, J.E., and Fleming, A.J. (2016). An ancestral stomatal patterning module revealed in the non-vascular land plant Physcomitrella patens. Development *143*, 3306–3314.

35. Haig, D. (1987). Kin conflict in seed plants. Trends Ecol. Evol. *2*, 337–340.

36. Zhao, P., Zhou, X., Zheng, Y., Ren, Y., and Sun, M.X. (2020). Equal parental contribution to the transcriptome is not equal control of embryogenesis. Nat. Plants *6*, 1354–1364.

37. Van Larebeke, N., Engler, G., Holsters, M., Van den Elsacker, S., Zaenen, I., Schilperoort, R.A., and Schell, J. (1974). Large plasmid in Agrobacterium tumefaciens essential for crown gall-inducing ability. Nature *252*, 169–170.

38. Scholl, R.L., May, S.T., and Ware, D.H. (2000). Seed and molecular resources for Arabidopsis. Plant Physiol. *124*, 1477–1480.

39. Mcelroy, D., Chamberlain, D.A., Moon, E., and Wilson, K.J. (1995). Development of gusa reporter gene constructs for cereal transformation - availability of plant transformation vectors from the Cambia Molecular-Genetic Resource Service. Mol. Breed. *1*, 27–37.

40. Hajdukiewicz, P., Svab, Z., and Maliga, P. (1994). The small, versatile pPZP family of Agrobacterium binary vectors for plant transformation. Plant Mol. Biol. *25*, 989–994.

41. Spitzer, M., Wildenhain, J., Rappsilber, J., and Tyers, M. (2014). BoxPlotR: a web tool for generation of box plots. Nat. Methods *11*, 121–122.

42. Schneider, C.A., Rasband, W.S., and Eliceiri, K.W. (2012). NIH Image to ImageJ: 25 years of image analysis. Nat. Methods *9*, 671–675.

43. Murashige, T., and Skoog, F. (1962). A revised medium for rapid growth and bio assays with tobacco tissue cultures. Physiol. Plant. *15*, 473–497.

44. Musielak, T.J., Schenkel, L., Kolb, M., Henschen, A., and Bayer, M. (2015). A simple and versatile cell wall staining protocol to study plant reproduction. Plant Reprod. *28*, 161–169.

45. Musielak, T.J., Bürgel, P., Kolb, M., and Bayer, M. (2016). Use of SCRI Renaissance 2200 (SR2200) as a versatile dye for imaging of developing embryos, whole ovules, pollen tubes and roots. Bio. Protoc. *6*, e1935.

46. Mayer, K.F., Schoof, H., Haecker, A., Lenhard, M., Jürgens, G., and Laux, T. (1998). Role of WUSCHEL in regulating stem cell fate in the Arabidopsis shoot meristem. Cell *95*, 805–815.

47. Pillitteri, L.J., Bemis, S.M., Shpak, E.D., and Torii, K.U. (2007). Haploinsufficiency after successive loss of signaling reveals a role for ERECTA-family genes in Arabidopsis ovule development. Development *134*, 3099–3109.

48. Slane, D., Kong, J., Berendzen, K.W., Kilian, J., Henschen, A., Kolb, M., Schmid, M., Harter, K., Mayer, U., De Smet, I., et al. (2014). Cell type-specific transcriptome analysis in the early Arabidopsis thaliana embryo. Development *141*, 4831–4840.

49. Czechowski, T., Stitt, M., Altmann, T., Udvardi, M.K., and Scheible, W.R. (2005). Genome-wide identification and testing of superior reference genes for transcript normalization in Arabidopsis. Plant Physiol. *139*, 5–17.

50. Livak, K.J., and Schmittgen, T.D. (2001). Analysis of relative gene expression data using real-time quantitative PCR and the 2(-Delta Delta C(T)) method. Methods *25*, 402–408.

STAR★METHODS

KEY RESOURCES TABLE

REAGENT or RESOURCE	SOURCE	IDENTIFIER
Bacterial and virus strains		
Stellar competent cells	Takara	Cat#636763
Agrobacterium tumefaciens GV3101	[37]	N/A
Chemicals, peptides, and recombinant proteins		
Murashige and Skoog Plant Salts	SERVA	Cat#47516.03
Propidium iodide	SIGMA-ALDRICH	Cat#P4170
SCRI Renaissance 2200	Renaissance Chemicals Ltd	N/A
Triton X-100	Carl Roth GmbH	Cat#3051.1
Glycerol	SIGMA-ALDRICH	Cat#G5516
Para-formaldehyde	SIGMA-ALDRICH	Cat#P6148
GUM arabic	SIGMA-ALDRICH	Cat#G9752
Chloral hydrat	Carl Roth GmbH	Cat#K318.1
Digoxigenin-11-UTP	Roche	Cat#11209256910
Anti-Digoxigenin-AP	Roche	Cat#11093274910; RRID: AB_514497
DIG-labeled Control	Roche	Cat#11585746910
Protease (Pronase)	SIGMA-ALDRICH	Cat#73702
T7 Polymerase	Thermo Scientific	Cat#EP0111
Q5 High-Fidelity DNA polymerase Kit	NEW ENGLAND BioLabs	Cat#M0491
In-Fusion HD Cloning Kit	TAKARA	Cat#639650
Dream Taq Green PCR Master Mix	Thermo Scientific	Cat#K1081
RNeasy Plant Mini Kit	QIAGEN	Cat#74904
RevertAid First Strand cDNA Synthesis Kit	Thermo Scientific	Cat#K1622
Luna Universal qPCR Master Mix	NEW ENGLAND BioLabs	Cat#M3003
Phosphinothricin	SIGMA-ALDRICH	Cat#45520
Hygromycin B	Carl Roth GmbH	Cat#CP13.1
Experimental models: Organisms/strains		
Arabidopsis thaliana: Col-0	N/A	N/A
Arabidopsis thaliana: er	[5]	SALK_066455
Arabidopsis thaliana: erl1	[5]	GK_109G04
Arabidopsis thaliana: erl2	[5]	GK_486E03
Arabidopsis thaliana: YDA/yda-11	NASC[38]	SALK_078777
Arabidopsis thaliana: bsk1-2	[5]	SALK_122120
Arabidopsis thaliana: bsk2-2	[5]	SALK_001600
Arabidopsis thaliana: BSK1/bsk1 bsk2	[5]	N/A
Arabidopsis thaliana: ssp-2	[13]	SALK_051462
Arabidopsis thaliana: er erl1	This paper	N/A
Arabidopsis thaliana: er erl2	This paper	N/A
Arabidopsis thaliana: erl1 erl2	This paper	N/A
Arabidopsis thaliana: er erl1 erl2	[5]	N/A
Arabidopsis thaliana: ER/er erl1	This paper	N/A
Arabidopsis thaliana: ER/er erl1 erl2	This paper	N/A
Arabidopsis thaliana: er ERL1/erl1 erl2	[5]	N/A
Arabidopsis thaliana: er erl1 ssp	This paper	N/A
Arabidopsis thaliana: ER_{pro}*:3xVenus-N7*	This paper	N/A
Arabidopsis thaliana: ER_{pro}*:ER-YPet; er erl1 erl2*	This paper	N/A
Arabidopsis thaliana: YDA_{pro}*:yda-CA*	This paper	N/A

(*Continued on next page*)

Continued		
REAGENT or RESOURCE	SOURCE	IDENTIFIER
Arabidopsis thaliana: YDA_{pro}:yda-CA; er erl2	This paper	N/A
Arabidopsis thaliana: ER_{pro}:NSlmb-vhhGFP4; ER_{pro}:ER-YPet; er erl1 erl2	This paper	N/A
Arabidopsis thaliana: $EC1_{pro}$:NSlmb-vhhGFP4; ER_{pro}:ER-YPet; er erl1 erl2	This paper	N/A
Arabidopsis thaliana: $35S_{pro}$:BSK1; bsk1 bsk2	This paper	N/A
Arabidopsis thaliana: $35S_{pro}$:BSK1; er erl1 erl2	This paper	N/A
Arabidopsis thaliana: $35S_{pro}$:SSP	This paper	N/A
Arabidopsis thaliana: $35S_{pro}$:SSP; er erl1 erl2	This paper	N/A
Arabidopsis thaliana: SSP_{pro}:SSP-YFP; er erl2	This paper	N/A
Oligonucleotides		
Listed in Table S4	This paper	N/A
Recombinant DNA		
pCambia 3300	[39,40]	N/A
pCambia 1300	[39,40]	N/A
pBay-bar	[5]	N/A
pBay-hyg	[5]	N/A
ER_{pro}:3xVenus-N7	This paper	N/A
ER_{pro}:ER-YPet	This paper	N/A
YDA_{pro}:yda-CA	[4]	N/A
ER_{pro}:NSlmb-vhhGFP4	This paper	N/A
$EC1_{pro}$:NSlmb-vhhGFP4	This paper	N/A
$35S_{pro}$:BSK1	This paper	N/A
$35S_{pro}$:SSP	This paper	N/A
SSP_{pro}:SSP-YFP	[5,13]	N/A
Software and algorithms		
R version 3.6.1	N/A	https://www.r-project.org/
R: multcompView package	N/A	https://cran.r-project.org/web/packages/multcompView/index.html
Adobe Illustrator CS6	Adobe	https://www.adobe.com/products/illustrator.html
Adobe Photoshop CS6	Adobe	https://www.adobe.com/products/photoshop.html
BoxPlotR	[41]	http://shiny.chemgrid.org/boxplotr/
ImageJ 1.52p	[42]	https://imagej.nih.gov/ij/
ZEN 2.0 blue edition	ZEISS	https://www.zeiss.de/messtechnik/produkte/software.html
AxioVision 4	ZEISS	https://www.micro-shop.zeiss.com/en/de/softwarefinder/

RESOURCE AVAILABILITY

Lead contact

Further information and requests for resources and reagents should be directed to and will be fulfilled by the lead contact, Martin Bayer (martin.bayer@tuebingen.mpg.de).

Materials availability

All plasmids and *Arabidopsis* lines generated in this study are available from the Lead Contact without restrictions.

Data and code availability

All data reported in this paper will be shared by the lead contact upon request. This paper does not report original code. Any additional information required to reanalyze the data reported in this paper is available from the lead contact upon request.

EXPERIMENTAL MODEL AND SUBJECT DETAILS

All *Arabidopsis thaliana* mutant and transgenic lines used in this study are in Col-0 background. Seeds were washed with 70% (v/v) ethanol for 5 min, followed by washing with 100% ethanol for 1 min. Then seeds were dried under clean bench. Surface-sterilized seeds were stratified at 4°C in dark for 2 days on half-strength Murashige and Skoog (½ MS) medium containing 1% (w/v) sucrose and 1% (w/v) agar (pH = 5.7)[43] then transferred to long-day conditions (16 h at 3000 photons per square meter per second, 8 h at dark) at 23°C for 1-2 weeks in custom-built walk-in growth chambers (Induplan, 8118140). Afterward, seedlings were transferred to soil and were grown under long-day conditions (16 h at 80 micromoles per square meter per second, 8 h at dark) at 23°C and 65% relative humidity as described before.[2] Mature seeds were harvested in seed bags and stored at room temperature.

METHOD DETAILS

Mutant lines

The *ssp-2* (SALK_051462), *bsk1-2* (SALK_122120), *bsk2-2* (SALK_001600), *er* (SALK_066455), *erl1* (GK_109G04), *erl2* (GK_486E03)[5,13] have been described previously. The *yda-11* (SALKseq_078777) allele in Col-0 background carries a T-DNA insertion in the second exon. As the truncated gene product lacks essential parts of the YDA coding region[4] and the mutant phenotype is similar to *yda-1*,[4] the *yda-11* presumably represents a null allele. Insertion lines were provided by the Nottingham *Arabidopsis* Stock Center (NASC).[38] *bsk1 bsk2* double mutant, *er ERL1/erl1 erl2* and *er erl1 erl2* triple mutants have been described before.[3] All other homozygous or heterozygous multiple mutant combinations were obtained by crossing. Crosses were performed by manual dissection of anthers before anthesis, followed by manual pollination approximately 24 h later.

Genotyping

For genotyping of mutant plants, PCR was performed with Dream Taq Green PCR Master Mix (Thermo Scientific). Gene-specific primers (LP and RP; Table S4) were used for the wild-type allele. Left border primers in combination with a gene-specific primer (RP) were used to detect the insertion allele. Segregation analysis of *ER/er erl1 erl2, er ERL1/erl1 erl2* and *BSK1/bsk1 bsk2* was based on counting the number of strong dwarfed mutant seedlings (phenotype of the *er erl1 erl2* triple homozygous and *bsk1 bsk2* double mutant seedlings) in the offspring.

Plasmid construction

Q5 High-Fidelity DNA polymerase Kit (NEW ENGLAND BioLabs) was used to clone DNA fragments from *Arabidopsis* Col-0. Plasmid construction was performed by in-fusion cloning using In-Fusion HD Cloning Kit (TAKARA) and transformed into Stellar competent cell (TAKARA). Oligonucleotide sequences for molecular cloning are summarized in Table S4. For plant transformation, transgenes were constructed in pCambia 3300[39] as well as pBay-bar and pBay-hyg binary vectors.[5] pBay-bar and pBay-hyg are modified versions of the pCambia binary vectors pCambia 3300 and pCambia 1300,[39] respectively. pCambia 3300 and pCambia 1300 (https://cambia.org) were modified from pPZP vectors.[40] In pBay-bar and pBay-hyg, the T-DNA has been replaced by a synthetic DNA fragment harboring unique restriction enzyme sites as well as plant codon-optimized selectable marker genes (conferring phosphinothricin and hygromycin resistance, respectively) under control of the *Arabidopsis RPL10A* promoter (−960 bp to +287 bp of At1g14320 including the first intron).[5] To generate ER_{pro}*:3xVenus-N7*, a 1934 bp genomic region immediately upstream of the start codon of *ER* was transcriptionally fused with the coding region of 3 copies of Venus *YFP* with a C-terminal N7 nuclear localization sequence and *UBQ10* terminator in pCambia 3300. ER_{pro}*:ER-YPet* contains a fragment of the *ER* locus including a 1934 bp region upstream of the start codon and the genomic sequence. The *ER* genomic sequence was fused in-frame at the 3′ end with the sequence of *YPet YFP* and *UBQ10* terminator. To generate ER_{pro}*:NSlmb-vhhGFP4,* the *ER-YPet* sequence in ER_{pro}*:ER-YPet* was replaced by the *NSlmb-vhhGFP4* coding sequence,[25] and the whole cassette was introduced into pBay-hyg. For $EC1_{pro}$*:NSlmb-vhhGFP4,* a 465 bp region of *EC1.1* was fused with *NSlmb-vhhGFP4* in pBay-hyg. To generate $35S_{pro}$*:BSK1* and $35S_{pro}$*:SSP*, *BSK1* CDS and *SSP* CDS, respectively, were fused with 2x 35S promoter and 35S terminator in pBay-bar backbone. SSP_{pro}*:SSP-YFP and* YDA_{pro}*:yda-CA* have been described previously.[4,13] In SSP_{pro}*:SSP-YFP*, 6630 bp *SSP* 5′ UTR, whole *SSP* genomic sequence and 153 bp *SSP* 3′ UTR of *SSP* were cloned to pCambia 3300. Citrine YFP sequence was fused in between the kinase domain sequence and TPR domain sequence of *SSP*. In YDA_{pro}*:yda-CA*, 3762 bp *YDA* 5′ UTR and 1217 *YDA* 3′ UTR were fused with truncated *YDA* genomic sequence in pCambia 3300. The truncated *YDA* genomic sequence contains a 447 bp deletion (+650 bp to +1096 bp) in the second exon.

Transgenic plants

All initial transgenic plants were transformed by floral dip using *Agrobacterium tumefaciens* GV3101.[37] ER_{pro}*:3xVenus-N7* was transformed into Col-0. ER_{pro}*:ER-YPet*, $35S_{pro}$*:BSK1* and $35S_{pro}$*:SSP* were transformed into *er erl1/ERL1 erl2* plants. $35S_{pro}$*:BSK1* and $35S_{pro}$*:SSP* were also transformed into *BSK1/bsk1 bsk2* and Col-0, respectively. YDA_{pro}*:yda-CA* and SSP_{pro}*:SSP-YFP* were transformed into *er erl2*. T_1 transgenic seedlings of these constructs were screened on $^3/_4$ $^3/_4$ $^3/_4$ MS plates containing 1% (w/v) sucrose and 50 mg/L phosphinothricin. ER_{pro}*:NSlmb-vhhGFP4* and $EC1_{pro}$*:NSlmb-vhhGFP4* in pBay-hyg were transformed into ER_{pro}*:ER-YPet #4* in *er erl1 erl2*, and T_1 seedlings were screened on $^3/_4$ $^3/_4$ $^3/_4$ MS plates containing 1% (w/v) sucrose, 50 mg/L phosphinothricin

and 20 mg/L hygromycin. T_3 plants were used for phenotypic analyses, except for *35S$_{pro}$:SSP, 35S$_{pro}$:SSP er erl1 erl2* and *35S$_{pro}$:BSK1 er erl1 erl2,* where T_1 seedlings were directly used because of sterility of the transgenic plants. Two independent transgenic lines of *YDA$_{pro}$:yda-CA* in *er erl2* (*#16* and *#19*) were crossed with Col-0 and offspring homozygous for the *ER ERL2* wild-type alleles were selected in the F2 generation. Transgene expression was determined by RT-PCR using M13rev and transgene-specific reverse primers (listed in Table S4).

DIC and Confocal microscopy

For differential interference contrast (DIC) imaging, ovules were dissected by hand and incubated overnight in Hoyeŕs solution (7.5g gum arabic, 5 mL glycerol, 100 g chloral hydrate and 30 mL water, diluted 2:1 with 10% (w/v) gum arabic solution). DIC images were taken with a Zeiss Axio Imager. Z1 microscope equipped with AxioCam HRc camera and AxioVision 4 software as described before.[5] Confocal microscopy was conducted with a Zeiss LSM 780 NLO microscope with ZEN 2.0 blue edition. SCRI Renaissance 2200 (SR2200) staining were performed according to published protocols[44,45] and confocal images were obtained with excitation at 405 nm and detection wavelength from 415 nm to 475 nm. For SR2200 staining of early ovules containing developing megaspore mother cell, early ovules were incubated in SR2200 solution (0.1% (v/v) SR2200, 1% (v/v) DMSO, 0.05% (w/v) Triton X-100, 5% (w/v) glycerol, 4% (w/v) para-formaldehyde in PBS buffer, pH 8.0) for 5 min. Then ovules were washed with water once and incubated in 5% (w/v) glycerol for imaging. For SR2200 staining of ovules containing megaspores or mature female gametes, both incubation and washing steps were performed with gentle vacuum to have a better staining. For YFP imaging, a 514 nm laser wavelength was used for excitation, a wavelength between 526 nm and 553 nm was recorded. For propidium iodide (PI) staining, cotyledons of seedlings (5 days after germination) were dissected and incubated in 10mg/L PI solution in water for 30 min, followed by brief washing with water. Afterward, cotyledons were transferred to microscopy slides and the abaxial side was imaged. PI fluorescence was detected from 571 nm to 656 nm with an excitation wavelength of 561 nm.

RNA *in situ* hybridization

RNA *in situ* hybridization were conducted according to Mayer et al.[46] with modifications (see below). The probes were amplified directly from cDNA from Col-0 seedlings using the primers ER-insitu-s: GTAAAGATCTCGGTGTGG and T7+ER-insitu-as: TAATACGACTCACTATAGGGCTGAAGACATATTCACA (T7 promoter sequence is the first 20bp) modified from Pillitteri et al.[47] They were transcribed and labeled with up to a 1:3 ratio of UTP: Digoxigenin-11-UTP (Roche) using the T7 Polymerase (Thermo Scientific). High specific labeling was by dot blot analysis using DIG-labeled Control RNA (Roche) as reference. For the plant material, unfertilized siliques were collected from Col-0, *ER/er*, and er plants. They were fixed and embedded as described previously,[48] shortening the ethanol series to 45 min and using 10 μm sections. Paraffin was removed by immersing twice in Histoclear (National Diagnostics) for 10 min. The samples were first rehydrated by ethanol series, then digested with 0.125 mg/mL Pronase (Sigma) for 10 min, treated shortly with Glycine 0.2% (w/v) in 1x PBS and 1x PBS before fixation in 4% (w/v) PFA for 10 min. Sections were dehydrated by ethanol series and 200 μl hybridization solution was applied per slide. After incubation in a humid box at 50°C overnight, the samples were shortly immersed in 2x SCC and washed three times in 0.2x SCC for 50 min at 50°C. The slides were incubated in 0.5% (w/v) blocking reagent (Boehringer) in TBS for 45 min. The Anti-Digoxigenin-alkaline-phosphatase-coupled antibody (Roche) was diluted 1:1250 in BXT (1% (w/v) BSA, 0.3% (w/v) Triton X-100 in TBS), 160 μl/slide applied and incubated for 1.5 h. Sections were washed 4 times in BXT for 20 min and incubated for 5 min in detection buffer (100 mM Tris (pH 9.5), 50 mM $MgCl_2$, 100 mM NaCl). Hundred twenty microliters of staining solution (450 μg/mL NBT, 175 μg/mL BCIP, 2% (w/v) Polyvinyl alcohol in detection buffer) were applied per slide and incubated overnight. They were immersed shortly in detection buffer, added 15% (w/v) glycerol to each slide and applied a coverslip for brightfield microscopy.

Quantitative RT-PCR analysis

RNA was extracted with the RNeasy Plant Mini Kit (QIAGEN) and quantified with a Nanodrop spectrophotometer. Col-0, *er erl1 erl2* and transgenic T_1 seedlings were grown on ½ MS media containing sucrose and agar for 14 days under long-day conditions. After 4 h in light, seedlings were collected and directly frozen in liquid nitrogen. 12 seedlings were collected for Col-0, *er erl1 erl2* and *35S$_{pro}$:BSK1 bsk1 bsk2* each. Single T_1 seedlings were collected for *35S$_{pro}$:SSP*, *35S$_{pro}$:SSP er erl1 erl2* and *35S$_{pro}$:BSK1 er erl1 erl2*. cDNA was synthesized with RevertAid First Strand cDNA Synthesis Kit (Thermo Scientific) from 1 μg total RNA of each sample, and was diluted 2-fold before quantitative PCR (qPCR) reaction. The qPCR was performed in a CFX Connect (Bio-Rad) with Luna Universal qPCR Master Mix (NEW ENGLAND Biolabs) in a total reaction volume of 20 μL (10 μL Luna Universal qPCR Master Mix, 0.5 μL 10 μM/L forward primers and reverse primers, 2 μL cDNA and 7 μL H_2O). The qPCR program was run as suggested by the qPCR Master Mix supplier (95°C for 60 s, 40 cycles: 95°C for 15 s and 60°C for 30 s). Melting curves were generated by increasing temperature from 65°C to 95°C with measurement every 0.5°C increment. Gene-specific primers were used for amplification (Table S4). *Actin2* (*At3g18780*) was used to normalize gene expression.[49] Relative gene expression level was shown as $2^{-\Delta\Delta Ct}$.[50] Three replicates per reaction were carried out. Biological replicates were not possible because T_1 lines of *35S$_{pro}$:SSP*, *35S$_{pro}$:SSP er erl1 erl2* and *35S$_{pro}$:BSK1 er erl1 erl2* were tiny and sterile.

Phenotypic analysis of rosette leaves

For Images of rosette leaves, three-week old plants were photographed with Canon EOS 1000D camera. To increase the visual contrast, images of rosette leaves were separated from background soil using Adobe Photoshop.

RNA stability

Arabidopsis RNA half-live (stability) was derived from published data by Szabo et al.[23] using an exponential decay model. All data, a detailed description of the analysis and a hands-on protocol have been previously published.[23]

QUANTIFICATION AND STATISTICAL ANALYSIS

Measurement of zygote/suspensor length

After DIC imaging, size measurements were performed using measurement tools of ImageJ software (version 1.52p).[42] The length of the fully elongated zygote was inferred from the sum of apical and basal daughter cell length of the 1-cell embryo. Zygote polarity was determined as ratio of apical and basal cell length. Suspensor length during transition stage was measured from the micropylar end of the basal suspensor cell to the center of uppermost suspensor cell. In crossing experiments, anthers were removed before anthesis, followed by manual pollination approximately 24 h later. Ovules were collected 24-30 h after pollination to image the 1-cell embryos and 4 days after pollination to image transition stage embryos.

Statistical analysis

Boxplot diagrams were made online with BoxPlotR.[41] For statistical analysis of phenotypic data and expression data, the one-way ANOVA analysis with post hoc Tukey test was performed in R (version 3.6.1) with multcompView package (https://cran.r-project.org/web/packages/multcompView/index.html). The number of data points in each group was listed at the bottom of each diagram. The segregation analysis was statistically analyzed with Chi-Square test.

Chapter 4

Zygotic Embryogenesis in Flowering Plants

Houming Chen, Yingjing Miao, Kai Wang, and Martin Bayer

Abstract

In the context of plant regeneration, in vitro systems to produce embryos are frequently used. In many of these protocols, nonzygotic embryos are initiated that will produce shoot-like structures but may lack a primary root. By increasing the auxin-to-cytokinin ratio in the growth medium, roots are then regenerated in a second step. Therefore, in vitro systems might not or only partially execute a similar developmental program as employed during zygotic embryogenesis. There are, however, in vitro systems that can remarkably mimic zygotic embryogenesis such as *Brassica* microspore-derived embryos. In this case, the patterning process of these haploid embryos closely follows zygotic embryogenesis and all fundamental tissue types are generated in a rather similar manner. In this review, we discuss the most fundamental molecular events during early zygotic embryogenesis and hope that this brief summary can serve as a reference for studying and developing in vitro embryogenesis systems in the context of doubled haploid production.

Key words Axis formation, Pattern formation, Radial patterning, Root formation, Shoot apical meristem, Zygote polarization, Zygotic embryogenesis

1 Introduction

Land plants form most of their body shape postembryonically in response to environmental cues [1, 2]. During embryogenesis, therefore, only a simple yet stereotypic manifestation of a small plant is set up. This seedling invariably consists of a few readily recognizable structures along its apical–basal axis, namely, the embryonic leave(s), the hypocotyl, and the embryonic root. Less obviously, the stem cell niches (meristems) for postembryonic development of the shoot and the root are also already established at the opposite ends of the apical–basal axis. The plant embryo is further partitioned along the radial axis into vasculature, ground tissue, and epidermis.

These different tissue types are generated by consecutive steps of patterning along the apical–basal as well as the radial axis [3]. Many of the molecular players orchestrating this development

Jose M. Seguí-Simarro (ed.), *Doubled Haploid Technology: Volume 2: Hot Topics, Apiaceae, Brassicaceae, Solanaceae*, Methods in Molecular Biology, vol. 2288, https://doi.org/10.1007/978-1-0716-1335-1_4,

have been identified in *Arabidopsis thaliana*, but other model species such as maize and rice have also significantly contributed to our understanding of embryonic patterning in plants. In this review, we mainly focus on *Brassicaceae* embryogenesis as the stereotypic patterning process in this plant family facilitates the identification of different cell types by position. The invariant patterning also makes it possible to trace the origin of cells back to decisive cell divisions without live imaging [4]. In order to keep this review concise, we limit our overview to key factors that seem to have a conserved function in flowering plants and will refer to more comprehensive or specialized reviews where necessary.

2 Early Steps of Axis Formation

2.1 Zygote Polarization

In Arabidopsis, the fertilized egg cell (zygote) seems to undergo a brief phase in which cell polarity is lost, before it repolarizes, elongates about threefold, and finally divides asymmetrically to form an apical and a basal cell [5, 6] (Fig. 1).

The apical cell will invariably develop into the embryo. Descendants of the basal cell will foremost contribute to an extraembryonic support structure, called suspensor. In *Brassicaceae*, the suspensor is a filamentous structure formed by a series of stereotypic horizontal divisions of the basal cell and its descendants. The early embryo and suspensor are clonally derived from the apical and basal cell, respectively. However, in other angiosperms, this boundary is less clear and cells originating from the apical cell can also contribute to the suspensor (i.e. in members of the *Caryophyllaceae*) or cells derived from the basal cell can form part of the embryo, as in members of the Asteraceae family [7, 8].

In Arabidopsis, the elongation of the zygote is accomplished by tip growth [9]. This rather specialized mechanism of cell elongation can also be seen during pollen tube growth and root hair growth. While zygote elongation is a common feature of many angiosperm species [7], it does not seem to be a necessity for zygote polarization. In some members of the grasses, such as maize and rice, the egg cell undergoes an asymmetric division right after fertilization without any apparent cell elongation [10, 11].

The correct positioning of the zygote nucleus during this repolarization phase depends on actin filaments and vacuolar dynamics [9, 12]. The intrinsic polarity of the zygote does not necessarily result in size differences of the daughter cells and there are quite a number of plant species in which the apical cell is equal in size or larger than the basal cell [10, 13]. Independently of their size, however, the apical cell pointing toward the central cell and the chalaza will always form (at least part of) the embryo proper. The basal cell that is positioned toward the micropyle and is in physical

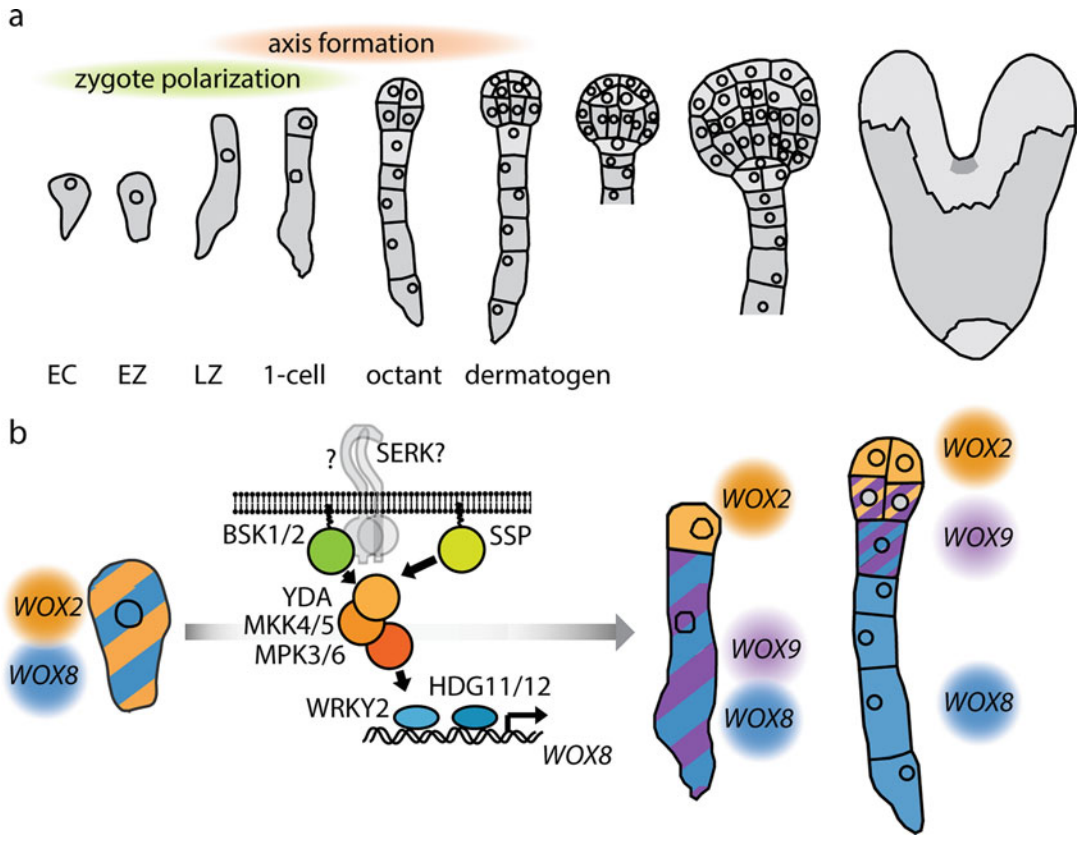

Fig. 1 Apical–basal axis formation. (**a**) Overview of early embryo morphology in Arabidopsis. Developmental stages are indicated below the graphic. *EC* egg cell, *EZ* early zygote, *LZ* late zygote. (**b**) Zygote polarization and patterning along the apical–basal axis. A simplified model of the embryonic YDA pathway is shown on the left. Differential expression of *WOX* gene family members along the apical–basal axis is depicted on the right

contact with sporophytic tissue of the seed coat will always contribute to the extraembryonic suspensor [14].

2.2 MAP Kinase Signaling

Zygote elongation and zygote polarization are at least in part regulated by a MITOGEN- ACTIVATED PROTEIN (MAP) kinase-dependent pathway (Fig. 1). This MAP kinase cascade includes the MAP2K kinase (MAP3K) YODA (YDA) [15], the MAPK kinases (MAP2K/MKK) MKK4 and MKK5, and the MAP kinases (MAPK/MPK) MPK3 and MPK6 [16, 17]. Upstream of YDA in this signaling cascade, two members of the BRASSINOSTEROID SIGNALING KINASE (BSK) family—BSK1 and BSK2—work in parallel [18]. These membrane-associated proteins typically function as signaling relay in SOMATIC EMBRYOGENESIS RECEPTOR-LIKE KINASE (SERK)-dependent receptor kinase pathways [19]. It is therefore a likely scenario that the YDA-dependent MAP kinase cascade is controlled by an extracellular signal received by a SERK-dependent receptor complex

[18]. Possible candidates for the extra-cellular signal include a family of small proteins termed EMBRYO SURROUNDING FACTOR [20] and the possible peptide ligand CLAVATA3/ESR-RELATED (CLE) 8 [21]. These extra-cellular molecules influence suspensor formation, but their direct involvement in activating the embryonic YDA pathway has not been shown and is therefore still hypothetical.

In *Brassicaceae*, an additional mechanism of YDA activation exists [22]. The atypical *BSK* family member *SHORT SUSPENSOR* (*SSP*) evolved as sister gene of *BSK1* [23]. In contrast to BSK1, which functions in a phosphorylation-dependent manner [24], the SSP protein seems to constitutively adopt an activated conformation [18]. *SSP* is tightly controlled at both transcriptional and translational levels. *SSP* transcripts accumulate at high level exclusively in sperm cells and seem to be paternally inherited to the zygote where the SSP protein transiently accumulates [25]. Since SSP directly interacts with YDA, the presence of SSP in the zygote links YDA activation with the fertilization event [18].

The rather mild defects in zygote polarization and suspensor development seen in *ssp* mutants are accompanied by strikingly slower embryo development possibly due to a malformed suspensor [26]. Therefore, the *Brassicaceae*-specific SSP protein might provide an additional, beneficial boost of early YDA activity in parallel to a BSK1/BSK2-dependent YDA activation [18].

One of the targets of this pathway is the transcription factor WRKY DNA-BINDING PROTEIN 2 (WRKY2) that is phosphorylated and activated by MPK6 [6, 27].

WRKY2 together with HOMEODOMAIN GLABROUS (HDG) HDG11 and HDG12 transcriptionally activates the homeodomain transcription factor gene *WUSCHEL RELATED HOMEOBOX 8* (*WOX8*) in the basal cell [6, 27, 28]. This possibly indicates that the embryonic YDA pathway is active at the basal pole of the zygote and/or in the basal daughter cell. Loss of *WOX8* and its close homolog *WOX9* leads to developmental defects in the suspensor. However, expression of the *WOX* gene family member *WOX2* as well as other genes that are normally confined to the apical daughter cell and its descendants is also lost in *wox8 wox9* double mutants, indicating a possible non–cell autonomous function [29].

Additional transcription factor complexes that include the RWP-RK domain–containing (RKD) protein GROUNDED (GRD)/RKD4 may be further targets of the embryonic YDA pathway as suggested by the genetic interaction of these mutants and the strikingly similar loss-of-function phenotype [30]. However, as members of this family seem to play a role in egg-to-zygote transition, a more general role in establishing a zygotic or embryonic transcriptional program and therefore setting the stage for

a functional embryonic YDA pathway might also be possible [30–32].

2.3 Auxin Taking the Stage

The two daughter cells shaped by the first zygotic cell division are characterized by differential gene expression [33]. Among the differentially expressed genes are members that control auxin transport and transcriptional auxin response [33, 34]. Consequently, with the formation of the embryogenic apical cell, auxin becomes one of the central players in the patterning process of the embryo. According to current data, sporophyte-derived auxin is transported by the auxin efflux facilitator PIN-FORMED 7 (PIN7) in the apical membrane of the basal cell to the terminal apical cell [34, 35]. Rising auxin levels in the apical cells lead to transcriptional auxin responses as well as a deviation of the stereotypic horizontal cell divisions by a 90° turn of the division plane [36]. If auxin responses are blocked in the early embryo, a stereotypic horizontal division plane following simple geometric rules of a local minimum in division plane size is formed [36, 37]. The initial apical transport of auxin and the corresponding differential auxin responses in the apical cell therefore seem to initiate the three-dimensional growth of the embryo.

It has been shown that auxin synthesis is coupled to auxin transport and response [38–40] and early in development of the embryo, the suspensor is a prominent source of auxin [39]. With rising auxin concentrations, the embryo proper itself will become the dominant source of auxin around globular stage, initiating a reversal of auxin transport in apical–basal direction [39, 41–43].

The differential auxin response in the apical cell vs. basal cell and their descendants is accomplished by directional auxin flow toward the apical cell and by different auxin response modules in the embryo vs. suspensor [44]. At this early stage, suspensor cells still possess embryogenic potential and cell proliferation seems to be repressed by a suspensor-specific auxin response module [44]. This is highlighted by laser ablation of the embryo or by suspensor-specific expression of certain embryo-specific factors initiating suspensor-derived secondary embryos [45, 46].

This raises the question how polar auxin transport and different auxin response modules are set up early in embryogenesis. As many factors in auxin synthesis, transport and response are expressed in an auxin-dependent manner, this could be in principle a self-organizing system [47]. However, since *wox8 wox9* double mutants show expanded auxin responses in the suspensor and lack the expression of some components of the embryo-specific auxin response module, a link between MAP kinase signaling in the zygote and differential auxin responses in the zygotic daughter cells seems to exist [6, 27, 29]. How direct this connection is, however, needs to be determined.

3 Patterning Along the Apical–Basal Axis

3.1 WOX Gene Expression

Three-dimensional growth of the embryo is initiated by two rounds of vertical divisions in the apical lineage of Arabidopsis. These four cells then divide each horizontally to form an upper and lower tier in the eight-cell preglobular embryo. The order of these cell divisions does not seem to be strictly necessary as other plant species (i.e., in the *Solanaceae* family) form a similar structure by an initial horizontal division of the apical cell followed by two rounds of vertical divisions in the upper and lower tier of the embryo, respectively [7].

At the eight-cell stage, the embryo can be functionally divided along its apical–basal axis. The four cells of the upper tier are the precursors of the embryonic leaves and the shoot apical meristem (SAM). Cells of the lower tier will form the hypocotyl, vasculature, and parts of the root meristem. The uppermost suspensor cell or hypophysis is the founder cell of the quiescent center (QC) of the root meristem as well as the columella. The rest of the suspensor remains extraembryonic. This organizational segmentation along the apical–basal axis is paralleled by overlapping expression domains of three *WOX* family genes [28] (Fig. 1).

The upper tier is characterized by *WOX2* expression, while in the lower tier, *WOX2* expression overlaps with the expression domain of *WOX9*. In the hypophysis, *WOX9* is coexpressed with *WOX8*. In the suspensor, *WOX8* is the only member of these three genes that is expressed [28] (Fig. 1). While the loss of *WOX2* or *WOX8* and *WOX9* lead to patterning defects in the embryo and the suspensor, respectively [29], their exact role during early embryogenesis is not fully understood. In the seedling, *WOX* family members control the proliferation of stem cells in various meristems (reviewed in [48]), a similar role in cell cycle regulation during early embryogenesis seems therefore possible [49].

3.2 Setting Boundaries

As the expression patterns of *WOX* genes illustrate, there seem to be clear boundaries between expression domains in the early Arabidopsis embryo that often are confined to single cell files. How this is achieved mechanistically is not clear. However, the GATA transcription factor HANABA TARANU (HAN) seems to play a critical role in setting up or maintaining the embryo–suspensor boundary [50]. In *han* mutants, genes typically expressed in the suspensor expand their expression domain to the lower tier. How *HAN* restricts the expression of these genes to the suspensor, however, and if/how this relates to the transcriptional network of *WOX* transcription factor genes, still needs to be investigated [50].

4 Radial Patterning

4.1 Protoderm Formation

Radial patterning is initiated with tangential divisions that form the 16-cell or dermatogen stage embryo [51]. This step depends on *WOX* gene function, as indicated by occasional anticlinal cell divisions in the upper tier in *wox2* mutants [29]. Similar incorrect orientation of cell divisions at this stage can be achieved by expression of a nondegradable version of the transcriptional repressor *BODENLOS* (*BDL*)*/ INDOLE-3-ACETIC ACID INDUCIBLE 12* (*IAA12*) [36], a critical component of the transcriptional auxin response module [37, 52]. This indirectly implies that asymmetric divisions forming the protoderm layer involve transcriptional auxin responses. Despite these early defects in division plane orientation, these embryos still form a functional epidermis [44], indicating that protoderm formation might be a rather robust process. Only a few molecular players involved in protoderm initiation are known (reviewed in [53]). However, the involvement of receptor kinases such as RECEPTOR-LIKE PROTEIN KINASE1 (RPK1) and RPK2 (TOADSTOOL2 (TOAD2) would suggest that protoderm formation relies on signaling at the outer cell surface [54, 55].

A key player in protoderm formation is the homeodomain leucine zipper class IV (HD-ZIP IV) transcription factor *A. thaliana* MERISTEM LAYER1 (AtML1) that is necessary and sufficient for epidermal cell identity [56–60]. Double mutants of *ATML1* and its closest homolog *PROTODERMAL FACTOR2 (PDF2)* show strong defects associated with misspecification of the protoderm while overexpression of *AtML1* can induce epidermal cell differentiation in nonepidermal cells [56, 58–60]. *AtML1* is initially expressed in all cells of the embryo but then confined to the outer cells (L1 layer) from the 16-cell stage onward [61].

How L1-specific expression of *AtML1* is controlled on a molecular level is not clear. However, this seems to involve posttranscriptional regulation [62, 63]. *AtML1* and *PDF2* activate the epidermis-specific expression of target genes by binding to a cis-regulatory element termed L1 box. As this element can be found in the *AtML1* and *PDF2* promoter region and is necessary for L1-specific expression of *PDF2*, a feedforward regulation seems to play a central role in controlling *AtML1* expression [56, 57, 61].

4.2 Patterning in the Lower Tier

Radial patterning in the lower tier establishes the initials for the vasculature, ground tissue and epidermis (Fig. 2; reviewed in [64]). By periclinal division, the ground tissue initials will then form endodermis and cortex. Many factors for differentiation and maintenance of different cell identities in the vasculature are known (reviewed in detail in [10, 65]). However, the initial setup in the embryo is less well understood. Radial patterning of the vasculature critically depends on auxin responses mediated by the auxin

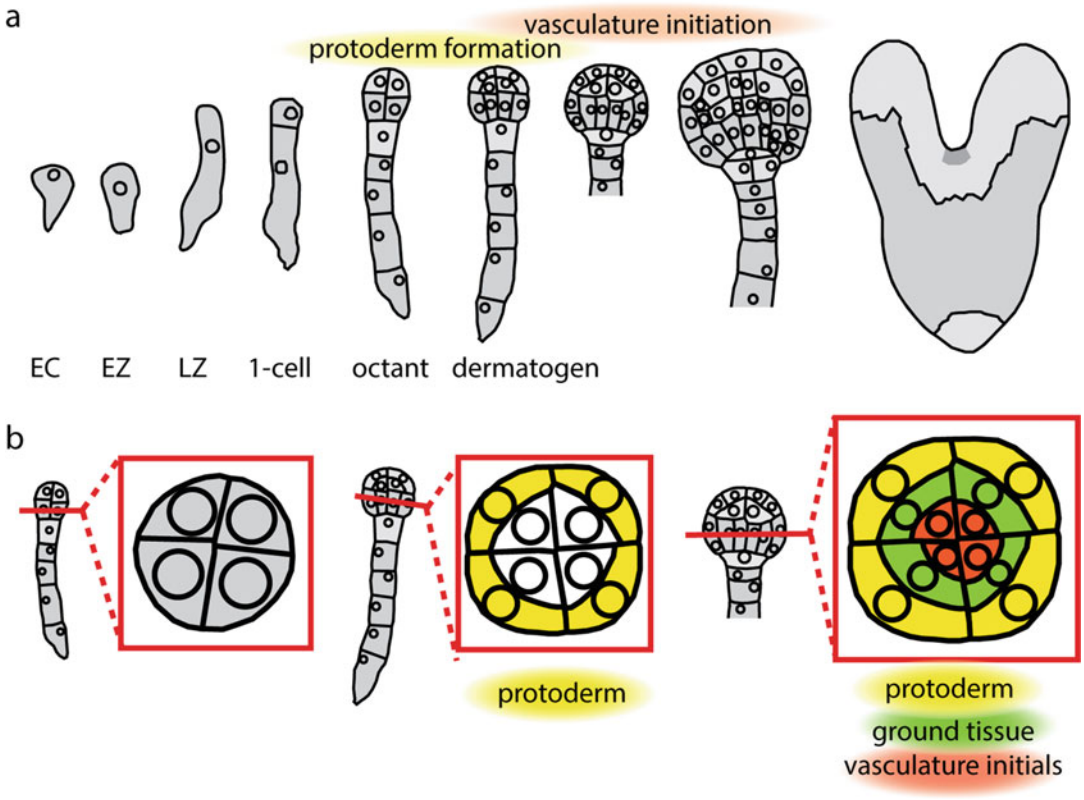

Fig. 2 Radial patterning in the Arabidopsis embryo. (**a**) Overview of early embryo morphology in Arabidopsis. Developmental stages are indicated below the graphic. *EC* egg cell, *EZ* early zygote, *LZ* late zygote. (**b**) Patterning along the radial axis in the lower tier of the embryo. Cross sections are illustrated in red squares. Yellow, protoderm; green, ground tissue; red, vasculature precursor cells

response factor (ARF) MONOPTEROS (MP) [66, 67] (Fig. 3). MP transcriptionally activates the bHLH transcription factor gene *TARGET OF MONOPTEROS 5* (*TMO5*) in the vasculature initials. TMO5 forms heterodimers with the bHLH transcription factor LONESOME HIGHWAY (LHW) and stimulates the expression of the cytokinin synthesis genes *LONELY GUY* (*LOG*) *3* and *LOG 4*. Together, this transcriptional complex controls periclinal divisions and therefore the number of cell files in the vasculature bundle (for comprehensive review, *see* ref. 68).

5 Establishing the Stem Cell Niches

5.1 Root Initiation

The first step of root meristem formation in Arabidopsis is the specification of the hypophysis [69]. This uppermost suspensor cell will form the QC that is responsible for stem cell maintenance [70]. The QC is characterized by expression of *WOX5* that maintains quiescence by controlling the cell cycle [28, 71, 72] (Fig. 3).

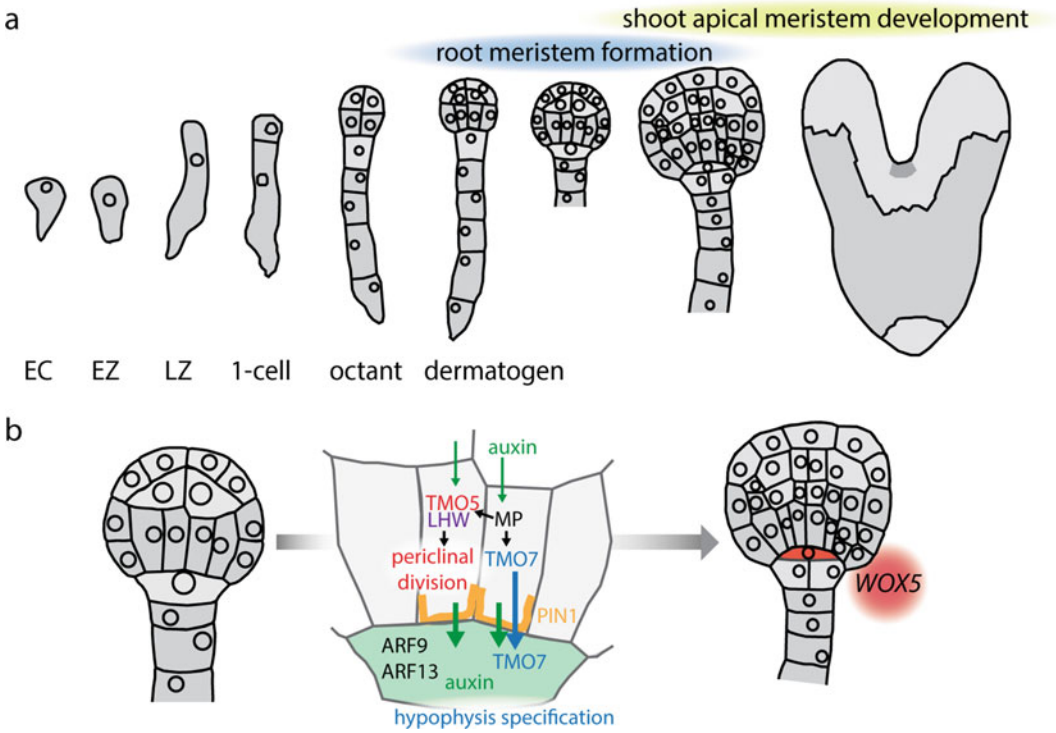

Fig. 3 Auxin signaling in vasculature formation and root meristem initiation. (**a**) Overview of early embryo morphology in Arabidopsis. Developmental stages are indicated below the graphic. *EC* egg cell, *EZ* early zygote, *LZ* late zygote. (**b**) A schematic overview of auxin responses leading to periclinal divisions in prevasculature cells and hypophysis specification. Auxin responses in the central cells of the lower tier and in the future hypophysis require cell-type specific auxin response machineries. After the asymmetric division of the hypophysis, expression of the *WOX* gene family member *WOX5* marks the quiescent center precursor cell

An intricate interaction of cells of the lower tier and the future hypophysis precedes the asymmetric division of the hypophysis that forms the QC. Auxin responses in the central cells of the lower tier lead to MP-dependent expression of *TMO7* [69]. This small bHLH transcription factor moves to the neighboring hypophysis where it plays a critical role in initiating QC formation [69]. This process also depends on the transcription factors NO TRANSMITTING TRACT (NTT)/WIP DOMAIN PROTEIN 2 (WIP2), WIP4, and WIP5 [73] that are expressed in the hypophysis, possibly in an auxin-dependent manner (reviewed in [64]).

Basal transport of auxin via PIN1 in the neighboring proembryo results in high auxin levels in the hypophysis as inferred from strong activity of synthetic auxin response reporters [34, 44, 69, 74]. Accumulation of auxin triggers transcriptional auxin responses mediated by a suspensor-specific auxin response machinery including ARF9, ARF13 and IAA10 [44] (Fig. 3).

Root initiation is also controlled by AP2 domain transcription factors of the PLETHORA (PLT) family [75]. *PLT1* and *PLT2* are expressed in the lower tier from the 8-cell embryo on and in the suspensor [50, 75]. PLT transcription factors can be considered to be master regulators of root identity. Loss of the four *PLT* gene family members *PLT1*, *PLT2*, *PLT3*, and *PLT4/BABY BOOM* (*BBM*) leads to misspecification of the hypophysis and rootless seedlings [76]. Ectopic expression of *PLT1* and *PLT2* in the shoot region or in the apical region of the embryo can induce ectopic root formation [75–77]. Expression of *PLT1* and *PLT2* depends on *MP*-dependent auxin signaling, emphasizing the importance of auxin in root formation [78].

5.2 The Shoot Apical Meristem

In tissue culture and in vitro plant regeneration, it has been known for a long time that the auxin-to-cytokinin ratio is crucial for the induction of shoots or roots, respectively. Under growth conditions where cytokinin is dominating, shoots can be regenerated, indicating an important role of cytokinin in formation of the SAM [79].

In the Arabidopsis embryo, this stem cell niche is first recognized at late heart stage as organized cell layers between the cotyledons [1, 80]. The organizing center of the SAM is characterized by the expression of the *WOX* gene family member *WUSCHEL* (*WUS*) [80, 81]. WUS moves to the neighboring stem cells where it suppresses differentiation [80–82]. The expression domain of *WUS* is negatively controlled by a receptor kinase pathway including the receptor kinase CLV1 [83–85]. WUS activates the expression of the corresponding peptide ligand CLV3 in the stem cells [86] and promotes its own expression in the organizing center by modulating cytokinin signaling [87, 88]. These (positive and negative) feedback loops restrict the size of the shoot meristem (reviewed in detail in [89]).

The position of stem cells underneath the shoot apex is controlled by L1-specific *miR394* [90]. This microRNA moves to the L2 and L3 layer and downregulates the expression of the F-box gene *LEAF CURLING RESPONSIVENESS* (*LCR*). LCR inhibits WUS activity. The *miR394/LCR* pathway therefore promotes WUS activity in the subepidermal region and ensures the correct position of the stem cell region in a growing shoot [90].

Although *WUS* expression starts at the 16-cell stage in the inner cells of the upper tier, it is dispensable for SAM formation. Instead, *WOX2* (together with *WOX1*, *WOX3*, and *WOX5*) is a key factor in meristem initiation [91]. In *wox1/2/3/5* quadruple mutant, a correct shoot meristem is not formed and the apical region of the embryo is characterized by increased auxin signaling [91]. Furthermore, the expression of the HD-ZIP III family members *PHABULOSA* (*PHB*), *PHAVOLUTA* (*PHV*), and *REVOLUTA* (*REV*) [92, 93] is strongly reduced or absent in the shoot meristem region of the embryo [91]. Therefore, *WOX2* seems to

promote HD-ZIP III expression in the shoot meristem initials. The HD-ZIPIII genes *PHB*, *PHV*, and *REV* are key players in shoot formation as ectopic accumulation in the basal part of the embryo leads to transformation of the root pole into shoot structures [77]. Since *PHB* and *PHV* control cytokinin production [94], *WOX2* regulates shoot meristem formation in part by promoting cytokinin levels in the upper tier of the embryo [91].

6 Outlook

While many molecular players in tissue differentiation and maintenance of cell types have emerged in recent years, our knowledge about the very first steps of initiating different identities in the early zygotic embryo is still fragmentary. What signals polarize the zygote and set up different auxin transport and response machineries in its daughter cells? How are different cell identities along the radial axis initiated? And how is the origin of the stem cell region for the shoot apical meristem controlled on a molecular level? Many fundamental questions about the early steps of zygotic embryogenesis are still waiting to be answered. Nevertheless, much less information is available about how microspore-derived embryos develop from dividing microspores, and about the genetic basis of some of the anatomical and functional abnormalities found in some cases. The knowledge summarized here may serve as a reference to compare with for the genetic dissection of microspore embryogenesis.

Acknowledgments

We would like to thank Gerd Jürgens for comments on the manuscript and apologize to our colleagues whose work we have not included in the chapter due to our focus on Brassicaceae embryogenesis. Research in our group is supported by the German Science Foundation (Deutsche Forschungsgemeinschaft—DFG: SFB1101/B01 to M.B.), the Chinese Scholarship Council (Fellowship No. 201806320131 to Y.M.), and the Max Planck Society.

References

1. Jurgens G (2003) Growing up green: cellular basis of plant development. Mech Dev 120 (11):1395–1406. https://doi.org/10.1016/j.mod.2003.03.001
2. Wang B, Smith SM, Li J (2018) Genetic regulation of shoot architecture. Annu Rev Plant Biol 69:437–468. https://doi.org/10.1146/annurev-arplant-042817-040422
3. Lau S, Slane D, Herud O, Kong JX, Jurgens G (2012) Early embryogenesis in flowering plants: setting up the basic body pattern. Annu Rev Plant Biol 63:483–506
4. ten Hove CA, Lu KJ, Weijers D (2015) Building a plant: cell fate specification in the early Arabidopsis embryo. Development 142

(3):420–430. https://doi.org/10.1242/dev.111500

5. Mansfield SG, Briarty LG (1991) Early embryogenesis in Arabidopsis-thaliana. 2. The developing embryo. Can J Bot 69(3):461–476
6. Ueda M, Zhang Z, Laux T (2011) Transcriptional activation of Arabidopsis axis patterning genes WOX8/9 links zygote polarity to embryo development. Dev Cell 20 (2):264–270. https://doi.org/10.1016/j.devcel.2011.01.009
7. Maheshwari P (1950) An introduction to the embryology of the angiosperms. McGraw-Hill, New York
8. Bayer M, Slane D, Jurgens G (2017) Early plant embryogenesis-dark ages or dark matter? Curr Opin Plant Biol 35:30–36. https://doi.org/10.1016/j.pbi.2016.10.004
9. Kimata Y, Higaki T, Kawashima T, Kurihara D, Sato Y, Yamada T, Hasezawa S, Berger F, Higashiyama T, Ueda M (2016) Cytoskeleton dynamics control the first asymmetric cell division in Arabidopsis zygote. Proc Natl Acad Sci U S A 113(49):14157–14162. https://doi.org/10.1073/pnas.1613979113
10. Johri BM, Ambegaokar KB, Srivastava PS (1992) Comparative embryology of angiosperms. Springer-Verlag, Berlin
11. Bommert P, Werr W (2001) Gene expression patterns in the maize caryopsis: clues to decisions in embryo and endosperm development. Gene 271(2):131–142. https://doi.org/10.1016/s0378-1119(01)00503-0
12. Kimata Y, Kato T, Higaki T, Kurihara D, Yamada T, Segami S, Morita MT, Maeshima M, Hasezawa S, Higashiyama T, Tasaka M, Ueda M (2019) Polar vacuolar distribution is essential for accurate asymmetric division of Arabidopsis zygotes. Proc Natl Acad Sci U S A 116(6):2338–2343. https://doi.org/10.1073/pnas.1814160116
13. Sivaramakrishna D (1978) Size relationships of apical cell and basal-cell in 2-celled embryos in angiosperms. Can J Bot 56(12):1434–1438. https://doi.org/10.1139/b78-166
14. Wang K, Chen H, Miao Y, Bayer M (2019) Square one: zygote polarity and early embryogenesis in flowering plants. Curr Opin Plant Biol. https://doi.org/10.1016/j.pbi.2019.10.002
15. Lukowitz W, Roeder A, Parmenter D, Somerville C (2004) A MAPKK kinase gene regulates extra-embryonic cell fate in Arabidopsis. Cell 116(1):109–119
16. Wang H, Ngwenyama N, Liu Y, Walker JC, Zhang S (2007) Stomatal development and patterning are regulated by environmentally responsive mitogen-activated protein kinases in Arabidopsis. Plant Cell 19(1):63–73. https://doi.org/10.1105/tpc.106.048298
17. Zhang M, Wu H, Su J, Wang H, Zhu Q, Liu Y, Xu J, Lukowitz W, Zhang S (2017) Maternal control of embryogenesis by MPK6 and its upstream MKK4/MKK5 in Arabidopsis. Plant J 92(6):1005–1019. https://doi.org/10.1111/tpj.13737
18. Neu A, Eilbert E, Asseck LY, Slane D, Henschen A, Wang K, Burgel P, Hildebrandt M, Musielak TJ, Kolb M, Lukowitz W, Grefen C, Bayer M (2019) Constitutive signaling activity of a receptor-associated protein links fertilization with embryonic patterning in Arabidopsis thaliana. Proc Natl Acad Sci U S A 116(12):5795–5804. https://doi.org/10.1073/pnas.1815866116
19. Shi H, Yan H, Li J, Tang D (2013) BSK1, a receptor-like cytoplasmic kinase, involved in both BR signaling and innate immunity in Arabidopsis. Plant Signal Behav 8(8). https://doi.org/10.4161/psb.24996
20. Costa LM, Marshall E, Tesfaye M, Silverstein KA, Mori M, Umetsu Y, Otterbach SL, Papareddy R, Dickinson HG, Boutiller K, VandenBosch KA, Ohki S, Gutierrez-Marcos JF (2014) Central cell-derived peptides regulate early embryo patterning in flowering plants. Science 344(6180):168–172. https://doi.org/10.1126/science.1243005
21. Fiume E, Fletcher JC (2012) Regulation of Arabidopsis embryo and endosperm development by the polypeptide signaling molecule CLE8. Plant Cell 24(3):1000–1012. https://doi.org/10.1105/tpc.111.094839
22. Musielak TJ, Bayer M (2014) YODA signalling in the early Arabidopsis embryo. Biochem Soc Trans 42(2):408–412
23. Liu SL, Adams KL (2010) Dramatic change in function and expression pattern of a gene duplicated by polyploidy created a paternal effect gene in the Brassicaceae. Mol Biol Evol 27(12):2817–2828. https://doi.org/10.1093/molbev/msq169
24. Tang W, Kim TW, Oses-Prieto JA, Sun Y, Deng Z, Zhu S, Wang R, Burlingame AL, Wang ZY (2008) BSKs mediate signal transduction from the receptor kinase BRI1 in Arabidopsis. Science 321(5888):557–560. https://doi.org/10.1126/science.1156973
25. Bayer M, Nawy T, Giglione C, Galli M, Meinnel T, Lukowitz W (2009) Paternal control of embryonic patterning in Arabidopsis thaliana. Science 323(5920):1485–1488. https://doi.org/10.1126/science.1167784

26. Babu Y, Musielak T, Henschen A, Bayer M (2013) Suspensor length determines developmental progression of the embryo in Arabidopsis. Plant Physiol 162(3):1448–1458. https://doi.org/10.1104/pp.113.217166
27. Ueda M, Aichinger E, Gong W, Groot E, Verstraeten I, Vu LD, De Smet I, Higashiyama T, Umeda M, Laux T (2017) Transcriptional integration of paternal and maternal factors in the Arabidopsis zygote. Genes Dev 31(6):617–627. https://doi.org/10.1101/gad.292409.116
28. Haecker A, Gross-Hardt R, Geiges B, Sarkar A, Breuninger H, Herrmann M, Laux T (2004) Expression dynamics of WOX genes mark cell fate decisions during early embryonic patterning in Arabidopsis thaliana. Development 131 (3):657–668. https://doi.org/10.1242/dev.00963
29. Breuninger H, Rikirsch E, Hermann M, Ueda M, Laux T (2008) Differential expression of WOX genes mediates apical-basal axis formation in the Arabidopsis embryo. Dev Cell 14 (6):867–876. https://doi.org/10.1016/j.devcel.2008.03.008
30. Jeong S, Palmer TM, Lukowitz W (2011) The RWP-RK factor GROUNDED promotes embryonic polarity by facilitating YODA MAP kinase signaling. Curr Biol 21 (15):1268–1276. https://doi.org/10.1016/j.cub.2011.06.049
31. Waki T, Hiki T, Watanabe R, Hashimoto T, Nakajima K (2011) The Arabidopsis RWP-RK protein RKD4 triggers gene expression and pattern formation in early embryogenesis. Curr Biol 21(15):1277–1281. https://doi.org/10.1016/j.cub.2011.07.001
32. Rovekamp M, Bowman JL, Grossniklaus U (2016) Marchantia MpRKD regulates the gametophyte-sporophyte transition by keeping egg cells quiescent in the absence of fertilization. Curr Biol 26(13):1782–1789. https://doi.org/10.1016/j.cub.2016.05.028
33. Zhou X, Liu Z, Shen K, Zhao P, Sun MX (2020) Cell lineage-specific transcriptome analysis for interpreting cell fate specification of proembryos. Nat Commun 11(1):1366. https://doi.org/10.1038/s41467-020-15189-w
34. Friml J, Vieten A, Sauer M, Weijers D, Schwarz H, Hamann T, Offringa R, Jurgens G (2003) Efflux-dependent auxin gradients establish the apical-basal axis of Arabidopsis. Nature 426(6963):147–153. https://doi.org/10.1038/nature02085
35. Robert HS, Park C, Gutierrez CL, Wojcikowska B, Pencik A, Novak O, Chen J, Grunewald W, Dresselhaus T, Friml J, Laux T (2018) Maternal auxin supply contributes to early embryo patterning in Arabidopsis. Nat Plants 4(8):548–553. https://doi.org/10.1038/s41477-018-0204-z
36. Yoshida S, Barbier de Reuille P, Lane B, Bassel GW, Prusinkiewicz P, Smith RS, Weijers D (2014) Genetic control of plant development by overriding a geometric division rule. Dev Cell 29(1):75–87. https://doi.org/10.1016/j.devcel.2014.02.002
37. Hamann T, Mayer U, Jurgens G (1999) The auxin-insensitive bodenlos mutation affects primary root formation and apical-basal patterning in the Arabidopsis embryo. Development 126(7):1387–1395
38. Robert HS, Crhak Khaitova L, Mroue S, Benkova E (2015) The importance of localized auxin production for morphogenesis of reproductive organs and embryos in Arabidopsis. J Exp Bot 66(16):5029–5042. https://doi.org/10.1093/jxb/erv256
39. Robert HS, Grones P, Stepanova AN, Robles LM, Lokerse AS, Alonso JM, Weijers D, Friml J (2013) Local auxin sources orient the apical-basal axis in Arabidopsis embryos. Curr Biol 23 (24):2506–2512. https://doi.org/10.1016/j.cub.2013.09.039
40. Wabnik K, Robert HS, Smith RS, Friml J (2013) Modeling framework for the establishment of the apical-basal embryonic axis in plants. Curr Biol 23(24):2513–2518. https://doi.org/10.1016/j.cub.2013.10.038
41. Stepanova AN, Robertson-Hoyt J, Yun J, Benavente LM, Xie DY, Dolezal K, Schlereth A, Jurgens G, Alonso JM (2008) TAA1-mediated auxin biosynthesis is essential for hormone crosstalk and plant development. Cell 133(1):177–191. https://doi.org/10.1016/j.cell.2008.01.047
42. Cheng Y, Dai X, Zhao Y (2007) Auxin synthesized by the YUCCA flavin monooxygenases is essential for embryogenesis and leaf formation in Arabidopsis. Plant Cell 19(8):2430–2439. https://doi.org/10.1105/tpc.107.053009
43. Brumos J, Alonso JM, Stepanova AN (2014) Genetic aspects of auxin biosynthesis and its regulation. Physiol Plant 151(1):3–12. https://doi.org/10.1111/ppl.12098
44. Rademacher EH, Lokerse AS, Schlereth A, Llavata-Peris CI, Bayer M, Kientz M, Freire Rios A, Borst JW, Lukowitz W, Jurgens G, Weijers D (2012) Different auxin response machineries control distinct cell fates in the early plant embryo. Dev Cell 22(1):211–222. https://doi.org/10.1016/j.devcel.2011.10.026

45. Liu Y, Li X, Zhao J, Tang X, Tian S, Chen J, Shi C, Wang W, Zhang L, Feng X, Sun MX (2015) Direct evidence that suspensor cells have embryogenic potential that is suppressed by the embryo proper during normal embryogenesis. Proc Natl Acad Sci U S A 112 (40):12432–12437. https://doi.org/10.1073/pnas.1508651112
46. Radoeva T, Albrecht C, Piepers M, de Vries S, Weijers D (2020) Suspensor-derived somatic embryogenesis in Arabidopsis. Development 147(13). https://doi.org/10.1242/dev.188912
47. Lau S, De Smet I, Kolb M, Meinhardt H, Jurgens G (2011) Auxin triggers a genetic switch. Nat Cell Biol 13(5):611–615. https://doi.org/10.1038/ncb2212
48. Jha P, Ochatt SJ, Kumar V (2020) WUSCHEL: a master regulator in plant growth signaling. Plant Cell Rep 39 (4):431–444. https://doi.org/10.1007/s00299-020-02511-5
49. Wu X, Chory J, Weigel D (2007) Combinations of WOX activities regulate tissue proliferation during Arabidopsis embryonic development. Dev Biol 309(2):306–316. https://doi.org/10.1016/j.ydbio.2007.07.019
50. Nawy T, Bayer M, Mravec J, Friml J, Birnbaum KD, Lukowitz W (2010) The GATA factor HANABA TARANU is required to position the proembryo boundary in the early Arabidopsis embryo. Dev Cell 19(1):103–113. https://doi.org/10.1016/j.devcel.2010.06.004
51. Jurgens G, Mayer U, Busch M, Lukowitz W, Laux T (1995) Pattern formation in the Arabidopsis embryo: a genetic perspective. Philos Trans R Soc Lond Ser B Biol Sci 350 (1331):19–25. https://doi.org/10.1098/rstb.1995.0132
52. Hamann T, Benkova E, Baurle I, Kientz M, Jurgens G (2002) The Arabidopsis BODENLOS gene encodes an auxin response protein inhibiting MONOPTEROS-mediated embryo patterning. Genes Dev 16(13):1610–1615. https://doi.org/10.1101/gad.229402
53. Takada S, Iida H (2014) Specification of epidermal cell fate in plant shoots. Front Plant Sci 5:49. https://doi.org/10.3389/fpls.2014.00049
54. Nodine MD, Yadegari R, Tax FE (2007) RPK1 and TOAD2 are two receptor-like kinases redundantly required for arabidopsis embryonic pattern formation. Dev Cell 12 (6):943–956. https://doi.org/10.1016/j.devcel.2007.04.003
55. Javelle M, Vernoud V, Rogowsky PM, Ingram GC (2011) Epidermis: the formation and functions of a fundamental plant tissue. New Phytol 189(1):17–39. https://doi.org/10.1111/j.1469-8137.2010.03514.x
56. Abe M, Katsumata H, Komeda Y, Takahashi T (2003) Regulation of shoot epidermal cell differentiation by a pair of homeodomain proteins in Arabidopsis. Development 130 (4):635–643. https://doi.org/10.1242/dev.00292
57. Abe M, Takahashi T, Komeda Y (2001) Identification of a cis-regulatory element for L1 layer-specific gene expression, which is targeted by an L1-specific homeodomain protein. Plant J 26(5):487–494. https://doi.org/10.1046/j.1365-313x.2001.01047.x
58. Peterson KM, Shyu C, Burr CA, Horst RJ, Kanaoka MM, Omae M, Sato Y, Torii KU (2013) Arabidopsis homeodomain-leucine zipper IV proteins promote stomatal development and ectopically induce stomata beyond the epidermis. Development 140(9):1924–1935. https://doi.org/10.1242/dev.090209
59. Takada S, Takada N, Yoshida A (2013) ATML1 promotes epidermal cell differentiation in Arabidopsis shoots. Development 140 (9):1919–1923. https://doi.org/10.1242/dev.094417
60. Ogawa E, Yamada Y, Sezaki N, Kosaka S, Kondo H, Kamata N, Abe M, Komeda Y, Takahashi T (2015) ATML1 and PDF2 play a redundant and essential role in arabidopsis embryo development. Plant Cell Physiol 56 (6):1183–1192. https://doi.org/10.1093/pcp/pcv045
61. Takada S, Jurgens G (2007) Transcriptional regulation of epidermal cell fate in the Arabidopsis embryo. Development 134 (6):1141–1150. https://doi.org/10.1242/dev.02803
62. Iida H, Yoshida A, Takada S (2019) ATML1 activity is restricted to the outermost cells of the embryo through post-transcriptional repressions. Development 146(4). https://doi.org/10.1242/dev.169300
63. Nodine MD, Bartel DP (2010) MicroRNAs prevent precocious gene expression and enable pattern formation during plant embryogenesis. Genes Dev 24(23):2678–2692. https://doi.org/10.1101/gad.1986710
64. Palovaara J, de Zeeuw T, Weijers D (2016) Tissue and organ initiation in the plant embryo: a first time for everything. Annu Rev Cell Dev Biol 32:47–75. https://doi.org/10.1146/annurev-cellbio-111315-124929

65. Ruonala R, Ko D, Helariutta Y (2017) Genetic Networks in Plant Vascular Development. Annual Review of Genetics, 51(51):335–359. https://doi.org/10.1146/annurev-genet-120116-024525
66. Hardtke CS, Berleth T (1998) The Arabidopsis gene MONOPTEROS encodes a transcription factor mediating embryo axis formation and vascular development. EMBO J 17 (5):1405–1411. https://doi.org/10.1093/emboj/17.5.1405
67. De Rybel B, Moller B, Yoshida S, Grabowicz I, Barbier de Reuille P, Boeren S, Smith RS, Borst JW, Weijers D (2013) A bHLH complex controls embryonic vascular tissue establishment and indeterminate growth in Arabidopsis. Dev Cell 24(4):426–437. https://doi.org/10.1016/j.devcel.2012.12.013
68. De Rybel B, Mahonen AP, Helariutta Y, Weijers D (2016) Plant vascular development: from early specification to differentiation. Nat Rev Mol Cell Biol 17(1):30–40. https://doi.org/10.1038/nrm.2015.6
69. Schlereth A, Moller B, Liu W, Kientz M, Flipse J, Rademacher EH, Schmid M, Jurgens G, Weijers D (2010) MONOPTEROS controls embryonic root initiation by regulating a mobile transcription factor. Nature 464 (7290):913–916. https://doi.org/10.1038/nature08836
70. Dolan L, Janmaat K, Willemsen V, Linstead P, Poethig S, Roberts K, Scheres B (1993) Cellular organisation of the Arabidopsis thaliana root. Development 119(1):71–84
71. Sarkar AK, Luijten M, Miyashima S, Lenhard M, Hashimoto T, Nakajima K, Scheres B, Heidstra R, Laux T (2007) Conserved factors regulate signalling in Arabidopsis thaliana shoot and root stem cell organizers. Nature 446(7137):811–814. https://doi.org/10.1038/nature05703
72. Forzani C, Aichinger E, Sornay E, Willemsen V, Laux T, Dewitte W, Murray JA (2014) WOX5 suppresses CYCLIN D activity to establish quiescence at the center of the root stem cell niche. Curr Biol 24(16):1939–1944. https://doi.org/10.1016/j.cub.2014.07.019
73. Crawford BC, Sewell J, Golembeski G, Roshan C, Long JA, Yanofsky MF (2015) Plant development. Genetic control of distal stem cell fate within root and embryonic meristems. Science 347(6222):655–659. https://doi.org/10.1126/science.aaa0196
74. Liao CY, Smet W, Brunoud G, Yoshida S, Vernoux T, Weijers D (2015) Reporters for sensitive and quantitative measurement of auxin response. Nat Methods 12(3):207–210. https://doi.org/10.1038/nmeth.3279
75. Aida M, Beis D, Heidstra R, Willemsen V, Blilou I, Galinha C, Nussaume L, Noh YS, Amasino R, Scheres B (2004) The PLETHORA genes mediate patterning of the Arabidopsis root stem cell niche. Cell 119 (1):109–120. https://doi.org/10.1016/j.cell.2004.09.018
76. Galinha C, Hofhuis H, Luijten M, Willemsen V, Blilou I, Heidstra R, Scheres B (2007) PLETHORA proteins as dose-dependent master regulators of Arabidopsis root development. Nature 449 (7165):1053–1057. https://doi.org/10.1038/nature06206
77. Smith ZR, Long JA (2010) Control of Arabidopsis apical-basal embryo polarity by antagonistic transcription factors. Nature 464 (7287):423–426. https://doi.org/10.1038/nature08843
78. Mahonen AP, Ten Tusscher K, Siligato R, Smetana O, Diaz-Trivino S, Salojarvi J, Wachsman G, Prasad K, Heidstra R, Scheres B (2014) PLETHORA gradient formation mechanism separates auxin responses. Nature 515(7525):125–129. https://doi.org/10.1038/nature13663
79. Miller LR, Murashige T (1976) Tissue culture propagation of tropical foliage plants. In Vitro 12(12):797–813. https://doi.org/10.1007/BF02796365
80. Laux T, Mayer KF, Berger J, Jurgens G (1996) The WUSCHEL gene is required for shoot and floral meristem integrity in Arabidopsis. Development 122(1):87–96
81. Mayer KF, Schoof H, Haecker A, Lenhard M, Jurgens G, Laux T (1998) Role of WUSCHEL in regulating stem cell fate in the Arabidopsis shoot meristem. Cell 95(6):805–815. https://doi.org/10.1016/s0092-8674(00)81703-1
82. Yadav RK, Perales M, Gruel J, Girke T, Jonsson H, Reddy GV (2011) WUSCHEL protein movement mediates stem cell homeostasis in the Arabidopsis shoot apex. Genes Dev 25(19):2025–2030. https://doi.org/10.1101/gad.17258511
83. Brand U, Fletcher JC, Hobe M, Meyerowitz EM, Simon R (2000) Dependence of stem cell fate in Arabidopsis on a feedback loop regulated by CLV3 activity. Science 289 (5479):617–619. https://doi.org/10.1126/science.289.5479.617
84. Schoof H, Lenhard M, Haecker A, Mayer KF, Jurgens G, Laux T (2000) The stem cell population of Arabidopsis shoot meristems in maintained by a regulatory loop between the CLAVATA and WUSCHEL genes. Cell 100 (6):635–644. https://doi.org/10.1016/s0092-8674(00)80700-x

85. Clark SE, Williams RW, Meyerowitz EM (1997) The CLAVATA1 gene encodes a putative receptor kinase that controls shoot and floral meristem size in Arabidopsis. Cell 89 (4):575–585. https://doi.org/10.1016/s0092-8674(00)80239-1
86. Perales M, Rodriguez K, Snipes S, Yadav RK, Diaz-Mendoza M, Reddy GV (2016) Threshold-dependent transcriptional discrimination underlies stem cell homeostasis. Proc Natl Acad Sci U S A 113(41):E6298–E6306. https://doi.org/10.1073/pnas.1607669113
87. Chickarmane VS, Gordon SP, Tarr PT, Heisler MG, Meyerowitz EM (2012) Cytokinin signaling as a positional cue for patterning the apical-basal axis of the growing Arabidopsis shoot meristem. Proc Natl Acad Sci U S A 109 (10):4002–4007. https://doi.org/10.1073/pnas.1200636109
88. Gordon SP, Chickarmane VS, Ohno C, Meyerowitz EM (2009) Multiple feedback loops through cytokinin signaling control stem cell number within the Arabidopsis shoot meristem. Proc Natl Acad Sci U S A 106 (38):16529–16534. https://doi.org/10.1073/pnas.0908122106
89. Kitagawa M, Jackson D (2019) Control of meristem size. Annu Rev Plant Biol 70:269–291. https://doi.org/10.1146/annurev-arplant-042817-040549
90. Knauer S, Holt AL, Rubio-Somoza I, Tucker EJ, Hinze A, Pisch M, Javelle M, Timmermans MC, Tucker MR, Laux T (2013) A protodermal miR394 signal defines a region of stem cell competence in the Arabidopsis shoot meristem. Dev Cell 24(2):125–132. https://doi.org/10.1016/j.devcel.2012.12.009
91. Zhang Z, Tucker E, Hermann M, Laux T (2017) A molecular framework for the embryonic initiation of shoot meristem stem cells. Dev Cell 40(3):264–277.e264. https://doi.org/10.1016/j.devcel.2017.01.002
92. McConnell JR, Emery J, Eshed Y, Bao N, Bowman J, Barton MK (2001) Role of PHABULOSA and PHAVOLUTA in determining radial patterning in shoots. Nature 411 (6838):709–713. https://doi.org/10.1038/35079635
93. Emery JF, Floyd SK, Alvarez J, Eshed Y, Hawker NP, Izhaki A, Baum SF, Bowman JL (2003) Radial patterning of Arabidopsis shoots by class III HD-ZIP and KANADI genes. Curr Biol 13(20):1768–1774. https://doi.org/10.1016/j.cub.2003.09.035
94. Dello Ioio R, Galinha C, Fletcher AG, Grigg SP, Molnar A, Willemsen V, Scheres B, Sabatini S, Baulcombe D, Maini PK, Tsiantis M (2012) A PHABULOSA/cytokinin feedback loop controls root growth in Arabidopsis. Curr Biol 22(18):1699–1704. https://doi.org/10.1016/j.cub.2012.07.005

SCIENTIFIC REPORTS
nature research

OPEN

The integral spliceosomal component CWC15 is required for development in Arabidopsis

Daniel Slane[1], Cameron H. Lee[2], Martina Kolb[1], Craig Dent[3], Yingjing Miao[1], Mirita Franz-Wachtel[4], Steffen Lau[1], Boris Maček[4], Sureshkumar Balasubramanian[3], Martin Bayer[1] & Gerd Jürgens[1]✉

Efficient mRNA splicing is a prerequisite for protein biosynthesis and the eukaryotic splicing machinery is evolutionarily conserved among species of various phyla. At its catalytic core resides the activated splicing complex Bact consisting of the three small nuclear ribonucleoprotein complexes (snRNPs) U2, U5 and U6 and the so-called NineTeen complex (NTC) which is important for spliceosomal activation. CWC15 is an integral part of the NTC in humans and it is associated with the NTC in other species. Here we show the ubiquitous expression and developmental importance of the Arabidopsis ortholog of yeast *CWC15*. CWC15 associates with core components of the Arabidopsis NTC and its loss leads to inefficient splicing. Consistent with the central role of CWC15 in RNA splicing, *cwc15* mutants are embryo lethal and additionally display strong defects in the female haploid phase. Interestingly, the haploid male gametophyte or pollen in Arabidopsis, on the other hand, can cope without functional *CWC15*, suggesting that developing pollen might be more tolerant to CWC15-mediated defects in splicing than either embryo or female gametophyte.

Angiosperms are the predominant group of land plants. A hallmark of this dominance in the course of evolution is the establishment of a reduced haploid phase (called gametophyte) in the life cycle of flowering plants. In free-living gametophytes of mosses, the gametophytic generation forms independently recognizable plants that can even be the dominant structure. In contrast, the gametophyte of flowering plants is reduced to a small dependent structure with an almost minimal number of cells and a short lifetime[1]. In Arabidopsis, the female gametophyte is deeply embedded in sporophytic tissue, whereas the male gametophyte or pollen has to be released from the sporophytic anther tissue for pollination to occur. Upon successful pollen-stigma interaction, the pollen tube grows inside the transmitting tract towards the ovule. Recent research has revealed that several signaling molecules including peptides play a role in the guidance of the pollen tube, attraction by the female gametophyte and burst of the pollen tube tip within one of the two synergid cells. If any of the aforementioned processes is disrupted, fertilization does not take place. Several mutants with disruptions in these processes have been isolated in the past[1–3]. Upon successful fertilization, the Arabidopsis zygote initiates a precise developmental program, which results in a heart-shaped embryo already comprising all major seedling organs: two primary leaves or cotyledons, a shoot meristem, a hypocotyl, and a primary root with a root meristem[4]. This invariant embryo patterning and development is impaired in mutants defective for various cellular response pathways e.g. responses to phytohormones, small RNA pathways, vesicular trafficking, cytoskeletal structure, and cell cycle control[5–9]. Furthermore, mutations in genes that are components of the RNA splicing machinery (spliceosome) affect gametophyte function and embryogenesis. For example, mutations such as *gfa1/clotho*, *rtf2*, *sus2/prp8*, or *bud13* cause severely reduced transmission of the mutant alleles via the female gametophyte and cause embryo lethality in Arabidopsis[10–14].

The pivotal step of splicing—intron removal—constitutes two *trans*-esterification reactions, mediated by the spliceosome, a dynamic protein complex containing more than 100 proteins and 5 small nuclear ribonucleoprotein particles (snRNP)[15], which is likely highly conserved among eukaryotes. The snRNPs consecutively interact

[1]Max Planck Institute for Developmental Biology, Cell Biology, 72076 Tübingen, Germany. [2]Howard Hughes Medical Institute, Division of Basic Sciences, Fred Hutchinson Cancer Research Center, Seattle, WA 98109, USA. [3]School of Biological Sciences, Monash University, Clayton Campus, Clayton, VIC 3800, Australia. [4]Proteome Center Tübingen, University of Tübingen, Auf der Morgenstelle 15, 72076 Tübingen, Germany. ✉email: gerd.juergens@tuebingen.mpg.de

with the pre-mRNA. First, U1 snRNP and U2 snRNP interact with the splice and the branch site, respectively. Then U4/U6-U5 snRNPs and the PRP19-CDCL5 complex (so-called NineTeen complex [NTC] in yeast) associate, thereby forming the pre-catalytic spliceosome[16]. After the dissociation of U4 snRNP, the Prp19 complex stabilizes the interaction of U5 snRNP and U6 snRNP with the spliceosome[17,18]. Recent studies using cryo-EM uncovered detailed spliceosomal structures during various steps of mRNA splicing. The NTC/PRP19 complex is highly conserved between yeast and human and contains six and seven core proteins, respectively[19–22]. Important for the function of the active spliceosome are also the so-called NTC-related (NTR) proteins, of which CWC15 is a member.

The developmental importance of Cwc15 was shown in yeast as a loss of function of Cwc15 confers lethality in *Schizosaccharomyces pombe* and it is synthetically lethal with *prp19-1* in *Saccharomyces cerevisiae*[23]. Furthermore, in *S. cerevisiae* it was shown that the core spliceosome components are not equally important for all pre-mRNAs, perhaps explaining why in Arabidopsis the absence of several components might affect tissues differently[24]. Regarding multicellular eukaryotes, *CWC15* was suggested to be important for bovine embryo development[25]. In *Arabidopsis thaliana,* CWC15 was not found in a proteomic approach as a member of the NTC[26]. Many genes coding for components of the core splicing machinery are duplicated in Arabidopsis although mutations in single-copy genes frequently result in gametophytic cell death[11,26]. Interestingly, the phenotypic consequences of mutations in spliceosomal genes are different between female and male gametophytes. Mutations in CLOTHO, which is a homolog of the yeast U5-associated Snu114, and ATROPOS, whose homolog has a demonstrated role in U2 assembly[27], result in defective female gametophytes, whereas male transmission is less severely affected[11].

In this work, we address the importance of the predicted splicing factor CWC15 in the model plant *Arabidopsis thaliana*. Our results show that CWC15 is associated with homologs of core yeast and human spliceosome components. Furthermore, CWC15 is essential for plant development including embryo development as splicing is affected on a whole-genome level. CWC15 also plays some role in the female gametophyte, however, pollen development proceeds normally in the absence of CWC15.

Results

***CWC15* encodes a highly conserved splicing factor with ubiquitous expression.** CWC15 was initially described as a spliceosome-associated protein in yeast and human cells. Subsequent cryoEM studies placed it within the core machinery of the spliceosome[15,28]. Our thorough phylogenetic analysis revealed the evolutionary conservation of CWC15 across all eukaryotes (Supplementary Fig. 1). CWC15 protein appears to have diverged between plants and animals, with specific amino acid sequences distinguishing the clades (Supplementary Fig. 1A and B). Nevertheless, major domains especially in the N- and C-terminal parts of the protein homologs appear to be conserved, which suggests the general importance of CWC15 during splicing in all eukaryotes.

To assess *CWC15* expression, we expressed a translational fusion of 3xGFP to a genomic rescue construct. The GFP signal was exclusively nuclear which is consistent with the potential role of CWC15 as a splicing factor. The fusion protein CWC15-3xGFP was ubiquitously expressed in all gametophyte, embryo, and seedling tissues and here too localized to the nucleus (Fig. 1). The integuments and all cells of the mature, unfertilized embryo sac showed GFP fluorescence, including central cell, synergids, and the egg cell (Fig. 1A). Likewise, the male gametophyte was marked by nuclear fluorescence during all developmental stages from unicellular microspore to tricellular, mature pollen (Fig. 1B, Supplementary Fig. 2A–C). Also, all cells of the embryo at the early globular (Supplementary Fig. 2D–F), globular and triangular (Fig. 1C, Supplementary Fig. 2G), late-heart or torpedo and bent-cotyledon stages (Supplementary Fig. 2H–J) showed clear nuclear fluorescent signals. We were also able to detect nuclear fluorescent signals in all cells of seedling tissues such as the cotyledon epidermis with stomata and pavement cells (Fig. 1D, Supplementary Fig. 2K), the primary root with all radially organized cell layers (Fig. 1E), the hypocotyl and the first rosette leaves including trichomes (Fig. 1F, Supplementary Fig. 2L). In summary, *CWC15* encodes a ubiquitously expressed, nuclear-localized protein.

CWC15 is closely associated with the Arabidopsis NTC. In yeast and human, CWC15 is an integral part of the core spliceosome[20,21]. To assess whether CWC15 is a component of the spliceosome in Arabidopsis, we performed immunoprecipitation experiments with GFP-tagged CWC15 and analyzed the precipitates by LC–MS/MS. As controls, we used GFP-tagged IMPORTIN-ALPHA 6 (IMPα6) and transcription factor AUXIN RESPONSE FACTOR 5 (ARF5) and carried out immunoprecipitation followed by liquid chromatography–mass spectrometry (LC–MS). Both IMPα6 and ARF5 are also localized to the nucleus, but functionally distinct from CWC15[29,30]. We looked for peptides that were specifically enriched in the CWC15 but absent in the two other immuno-precipitates. The most abundant peptides recovered were Arabidopsis counterparts of the human Prp19 complex (NTC), U5 snRNP, and NTC-related proteins (NTR) (Table 1). The majority of these mapped to Arabidopsis homologs of human spliceosomal proteins of the NTC such as Cdc5 and Prp19, two proteins that were well described in their function for NTC-related spliceosomal activation[31]. In addition to CWC15 itself (Ad-002 in human spliceosome), we found a homolog for the human NTC-related (NTR) protein Aquarius, which like CWC15 is required for embryo viability in Arabidopsis (*EMB2765*)[32]. Adding peptides with lower counts to our analysis, we detected a majority of all components of the U5 snRNP, NTC, NTR, and associated splicing factors (Supplementary Table 2) that were recently described in a multitude of structural cryo-EM reports for yeast and human spliceosomes[15,28]. These results suggest that CWC15 is potentially part of the NineTeen complex, which has an important general role in splicing in *Arabidopsis thaliana*[26,33].

Down-regulation of *CWC15* causes developmental defects. In an enhancer trap screen, we identified a T-DNA insertional mutant that displayed several phenotypic features reminiscent of auxin-related defects.

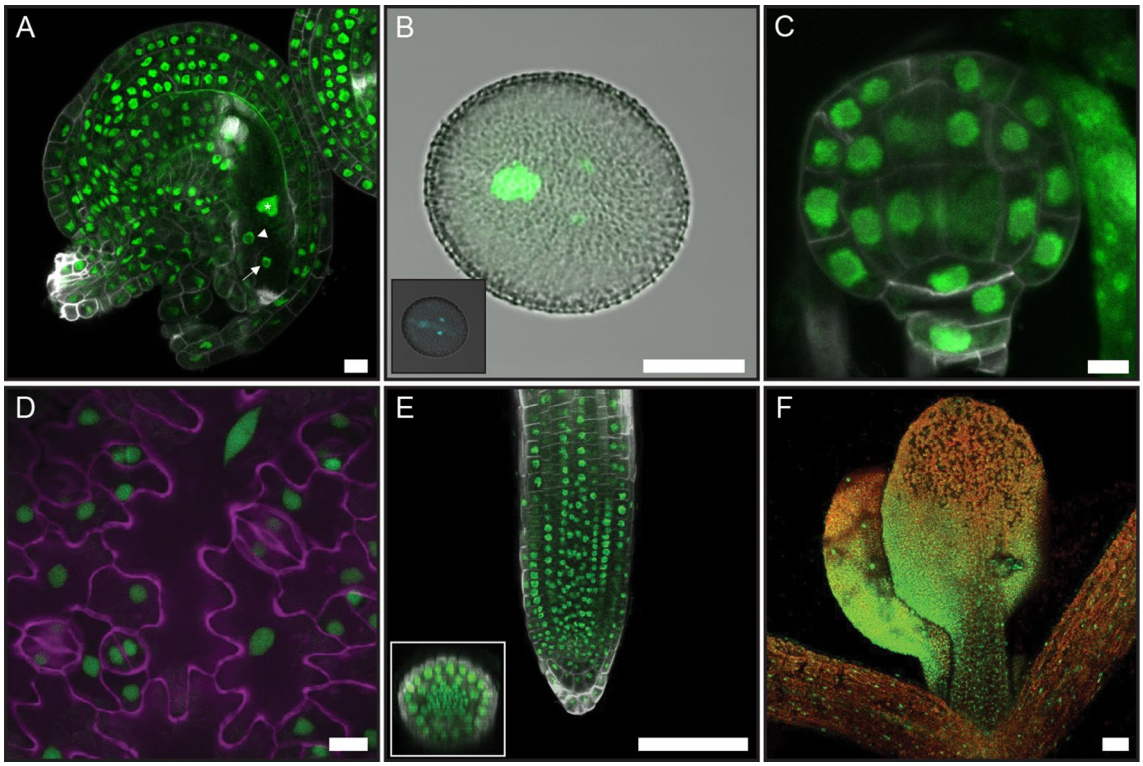

Figure 1. Expression pattern of genomic construct *gCWC15-3xGFP* during plant development. *CWC15* expression pattern monitored with a genomic fusion to GFP is visible in all nuclei of gametophytes, embryo, and seedling. (**A**) Mature female gametophyte with nuclear GFP signal in all tissue types including central cell (asterisk), synergid (arrowhead), and egg cell (arrow). (**B**) Both vegetative and generative nuclei show CWC15-3xGFP signals in mature pollen grain. Inset: DAPI-stained nuclei in the mature pollen grain. (**C**) CWC15-3xGFP is present in all nuclei at globular embryo stage. (**D**) *gCWC15-3xGFP* expression in epidermal cells. The image is a maximum projection of z-stacks across abaxial cotyledon epidermal cells. Nuclear-localized CWC15-3xGFP is shown in green, cell outlines are stained with propidium iodide (magenta). (**E**) *gCWC15-3xGFP* expression in seedling root. Nuclear-localized CWC15-3xGFP is shown in green, cell outlines are stained with Renaissance SR2200 dye (grey). Transverse root section is shown as inset. (**F**) *gCWC15-3xGFP* expression in seedling shoot. Nuclear-localized CWC15-3xGFP in primary leaves of a 7-day-old seedling is shown in green, autofluorescence is shown in red. Scale bar: (**A**–**D**) 5 µm, (**E**,**F**) 100 µm.

Homo sapiens	*Arabidopsis thaliana*	AGI locus	Peptides
U5 snRNP			
Prp8	PRP8B	*AT4G38780*	23
Snu114	GFA1/MEE5/CLO	*AT1G06220*	14
NTC			
Cdc5	CDC5/MAC1	*AT1G09770*	18
Prp19	MAC3A	*AT1G04510*	12
	MAC3B	*AT2G33340*	12
Syf1	MAC9	*AT5G28740*	14
Syf3	MAC10	*AT5G41770*	13
HSP73	HSP70	*AT3G09440*	21
NTR			
Ad-002	CWC15	*AT3G13200*	26
Aquarius	EMB2765	*AT2G38770*	12

Table 1. CWC15-associated proteins identified by mass spectrometry. Recovered unique peptides were compared to MS data for two other nuclear-localized proteins (IMPα6 and ARF5) and only peptides that were not present in the other two data sets are listed. Only loci with more than 10 unique peptide counts are depicted.

Compared to wild type, mutant seedlings and adult plants were strongly reduced in size (Fig. 2A–C). Adult plants were fertile despite stunted growth when compared to Col-0 wild-type plants (Fig. 2C). Mutant seedlings displayed stunted primary roots (Fig. 2B,D) and cotyledon defects ranging from monocots or asymmetrically positioned cotyledons to seedlings with three cotyledons (Fig. 2D). Phenotypic defects were visible in all offspring seedlings from homozygous mother plants when grown on agar plates while heterozygous plants did not show any obvious defects.

To determine the genomic insertion site of the transgene that caused the mutant phenotype, we sequenced the entire genome and aligned DNA sequencing reads both to the T-DNA used and the Arabidopsis genome as was previously described[34]. The insertion was located on the upper arm of chromosome 3 directly upstream of the genomic locus *CWC15/AT3G13200* (Fig. 2E). We tested the possible effects of the insertion on the expression of genes near the insertion site through semi-quantitative (sq) RT-PCR (Supplementary Fig. 3). We found that *CWC15/AT3G13200* was downregulated and confirmed the strong down-regulation also by quantitative (q) RT-PCR (Supplementary Fig. 4A). Among the other genes flanking the insertion site, we observed additional bands for *AT3G13190* and an up-regulation of *AT3G13210*. *AT3G13205* is a predicted pseudogene. Both *CWC15/AT3G13200* and *AT3G13210* code for putative splicing factors and the additional transcripts observed for *AT3G13190* suggested possible splicing defects in the mutant. Since multiple homozygous T-DNA insertion lines located in exons are available for *AT3G13210* and therefore its absence is not deleterious for development, we focused on *CWC15/AT3G13200*, the homolog of the yeast/human splicing factor *Cwc15/AD-002*. We termed the mutant therefore *cwc15-1*. A genomic construct expressing the *CWC15* gene from about 1 kb of the upstream sequence was able to fully complement the mutant seedling phenotypes (Fig. 2F). The same was observed when a strong ribosomal promoter *RPS5A* drove expression of *CWC15*. Interestingly, expression from a promoter only active during early embryogenesis[35] did not rescue the observed seedling defects, suggesting that continued protein activity during later embryo and seedling development might be necessary (Fig. 2F).

To elucidate the earliest deviation in development, we analyzed embryos from 2-cell to mid-globular stages comparing wild type to the *cwc15-1* mutant. In general, mutant embryos showed a variety of strongly pleiotropic embryo defects when compared to wild type. In Col-0 embryos, the division plane of the apical daughter cell of the zygote is vertical (Fig. 3A). In contrast, mutant embryos often showed a horizontal division plane (Fig. 3B). Also, we observed frequent erroneous divisions in the basal cell lineage of the embryo (Fig. 3C). These phenotypes are for example reminiscent of embryo phenotypes observed in *yda* or *wrky2* mutants[36,37]. When the wild-type embryos were at the 16-cell stage (Fig. 3D), mutant embryos displayed altered division planes, to varying degrees exhibiting raspberry-like phenotypes[38] (Fig. 3E,F). At mid-globular stage (Fig. 3G)—a time point when an asymmetric division of the so-called hypophysis establishes the root—apical and basal domains appeared strongly misshapen, resembling *fass* mutant phenotypes[39] (Fig. 3H,I). In conclusion, mutant embryos displayed a range of phenotypic alterations, which are similar to already described embryo mutants and this suggested that there is potentially mis-regulation of multiple genes during early embryogenesis in the *cwc15-1* mutant.

CWC15 is important for efficient splicing. To determine the extent of potential splicing defects in *cwc15* mutants, we performed RNA sequencing on total RNA extracted from tissues representing the early and late stages of development. First, we analyzed RNA from wild-type and hypomorphic *cwc15-1* seedlings, where we observed a clear phenotypic difference. Second, we did RNA-seq profiling on total RNA extracted from mature pollen tissue from wild-type and *cwc15-1* mutants. To assess the comparability of biological replicates we used principal component analysis. Tissue/developmental difference was the major component of variation (accounting for ~81%) in expression levels (Supplementary Figure 5A).

To analyze whether specific splice sites across the genome are affected in *cwc15-1* mutants, we utilized SpliSER[40], which enables the quantification of splicing at the level of individual splice sites. We first compared the variation in splice-site strength of the splice-sites across both tissues through PCA analysis. The PCA analysis revealed that the within tissue/replicate variation is much lower in pollen compared to seedlings, which suggested that our ability to detect differential splicing would be higher in pollen compared to seedlings (Supplementary Figure 5B–D).

The analysis of differential splicing through diffSpliSE in SpliSER (Supplementary Dataset File 1) showed 620 splice sites to be differentially utilized in seedlings, corresponding to 564 genes. Most of the splice sites were canonical, consistent with the notion that CWC15 is an integral component of the core splicing machinery. We saw no clear bias in the prevalence of 5′ or 3′ splice site, 58%, and 42% respectively. SpliSER uses competition between splice sites as a parameter in assessing splice-site strength. The majority of differentially spliced sites (75%) had no competing splice sites observed in any sample, which indicates that they are constitutive splice sites undergoing intron retention (Supplementary Figure 4B). In pollen, we detected 3,997 splice sites to be differentially spliced, across 2,380 genes. 88 of these genes were common to both seedlings and pollen (Fig. 4A). Unlike in seedlings, where a vast majority of differentially-spliced sites showed a decrease in splice-site strength (99.7%), we saw an even distribution of up- and down-regulated splice sites in pollen, with no apparent bias towards a particular splicing event. Together these results suggest that the splicing defect observed in *cwc15-1* mutant seedlings is primarily a reduced capacity for the splicing of some introns (i.e. intron retention), rather than a change in splice-site preference (i.e. alternative usage of 3′ and 5′ splice sites, exon skipping, etc.).

Since differences in splicing can indeed lead to changes in expression levels[41,42], we compared transcripts that were differentially up- or down-regulated (Supplementary Dataset File 1). 324 genes were differentially expressed more than twofold in seedlings, and 3,864 in pollen. We saw a significant overlap between differentially spliced and differentially expressed genes in pollen (Fig. 4B), but not in seedlings (Fig. 4C), suggesting that the *cwc15-1* splicing defects observed in seedlings may not be directly correlated with changes in gene expression. However, given that these results are derived from two RNA-seq replicates, we cannot rule out the tissue-specific differences

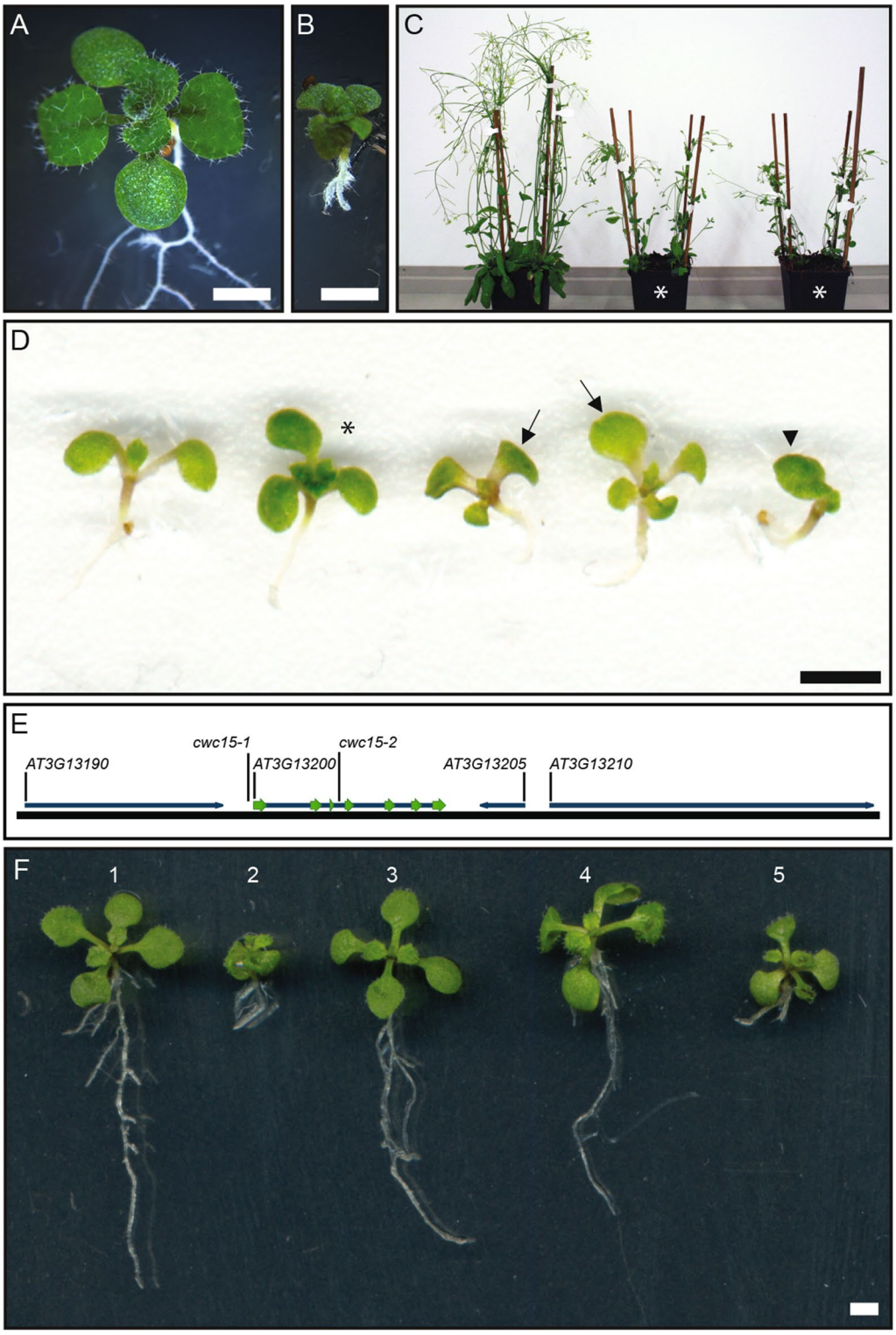

Figure 2. Mis-regulation of *CWC15* is causative for embryo and seedling phenotypes. (**A**,**B**) Normal wild-type (**A**) and *cwc15-1* mutant seedling (**B**) with short primary root and three cotyledons. (**C**) Adult *cwc15-1* mutant plants (marked by asterisks) grow smaller compared to wild type. (**D**) Range of *cwc15-1* mutant seedling phenotypes with wild-type seedling on the left. Asterisk marks tricot seedling with normal root, arrows point to seedlings with asymmetrically positioned cotyledons, and arrowhead marks seedling with only one fully developed cotyledon. (**E**) The insertion site of the transgene is in the vicinity of 4 gene loci, among them *CWC15* (*At3g13200*). Mutant alleles with corresponding insertion sites are depicted as *cwc15-1* (promoter) and *cwc15-2* (SALK insertion line, 3rd intron). Exons are shown as green arrows. Image of gene loci was exported from CLC Genomics Workbench software version 10.1.1 (https://digitalinsights.qiagen.com/products-overview/discovery-insights-portfolio/analysis-and-visualization/qiagen-clc-genomics-workbench/). (**F**) *cwc15-1* rescue lines (at least 6 independent transgenic lines tested for each construct) with seedling phenotypes from left to right: (1) Wild type, (2) *cwc15-1* mutant, (3) genomic rescue, (4) rescue with constitutive expression from ribosomal *RPS5A* promoter, (5) no rescue if expressed from putative promoter of gene *At3g10100* which is only active during early embryogenesis. Scale bar: 2 mm.

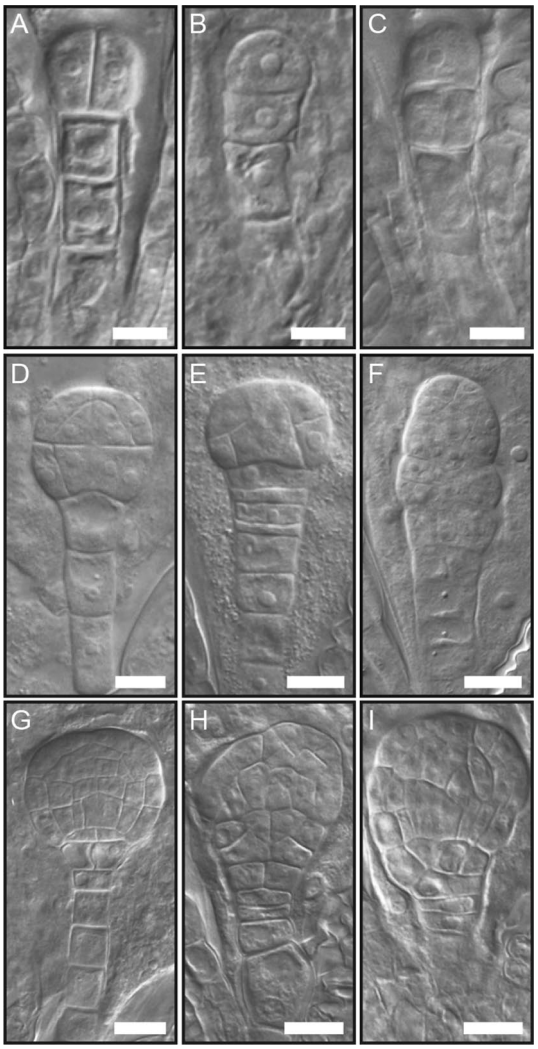

Figure 3. Embryo phenotypes at early stages of development. (**A**–**I**) Corresponding embryos are shown for 2-cell (**A**–**C**), 16-cell (**D**–**F**), and globular stages (**G**–**I**). Wild-type embryos are depicted in (**A**,**D**,**G**) and mutant embryos in (**B**,**C**,**E**,**F**,**H**,**I**). Scale bar: 10 µm.

observed in splicing and gene expression are due to differences in statistical power. To corroborate these results, we performed gene ontology (GO) enrichment analysis for differentially spliced and expressed genes in pollen and seedlings (Supplementary Dataset File 2). For differentially spliced genes in both seedlings and pollen we found enrichment for a wide range of processes including numerous GO terms involving metabolism and response to various stimuli with functions in both protein and nucleotide binding. This was also the case for differentially expressed genes in pollen. The number of enriched GO terms for differentially expressed genes in seedlings was considerably lower and we saw enrichment of response terms, the top three hits being related to iron homeostasis which do not appear in any of the other lists.

Taken together, these findings reveal three aspects of *CWC15* function. First, even a hypomorphic allele of *CWC15* leads to changes in splicing patterns. Second, compromising *CWC15* function has a direct and/or indirect effect on gene expression. Third, the effect of CWC15 differs between tissue types and/or stages of development.

Loss of CWC15 function is female gametophytic and embryo lethal. The pleiotropic phenotypes in *cwc15-1* are caused by the downregulation of *CWC15* transcript levels, indicating that *cwc15-1* might be a hypomorphic allele. Therefore, we analyzed a T-DNA insertion allele, with the T-DNA residing in the third intron, termed *cwc15-2*. For this allele, we never recovered homozygous mutant progeny from heterozygous plants (*cwc15-2*$^{+/+}$ n = 114, 48.3% vs. *cwc15-2*$^{+/-}$ n = 122, 51.7%). When we opened siliques of selfed *cwc15-2*$^{+/-}$ plants we found missing and shriveled ovules compared to WT, corresponding to aborted ovules (Supplementary Fig. 6). Reciprocal crosses of heterozygous *cwc15-2*$^{+/-}$ and wild-type plants showed that transmission of the mutant allele via the female gametophyte was reduced from the expected 50% to 29% whereas the male gametophyte seemed not affected at all (Supplementary Table 3).

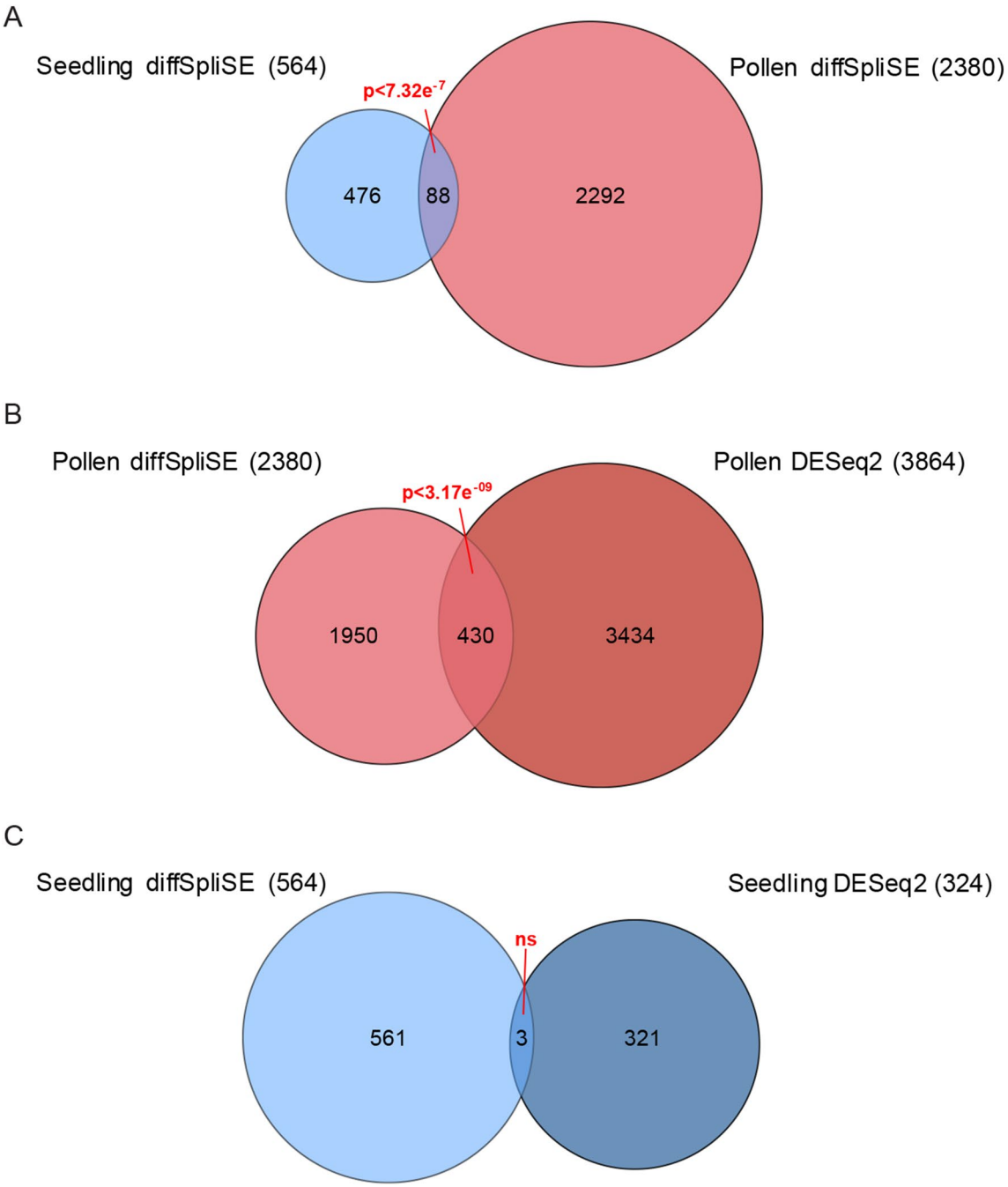

Figure 4. Down-regulation of *CWC15* in *cwc15-1* leads to global splicing defects and transcriptional differences. (**A**) Venn diagram showing number of genes differentially spliced in seedling and pollen tissue, between wild type and mutant. (**B**) Venn diagram comparing genes detected as differentially spliced and differentially expressed in pollen. (**C**) Venn diagram comparing genes detected as differentially spliced and differentially expressed in seedlings. Venn Diagram Plotter v1.5.5228 (https://omics.pnl.gov/software/venn-diagram-plotter) was used to generate Venn diagrams.

Next, we analyzed cell type-specific fluorescent marker lines for the female gametophyte expressed in the central cell, the synergid cells, or the egg cell. However, we could not detect any differences in *cwc15-2*$^{+/-}$ compared to wild type in any of the marker crosses analyzed ($n > 100$), which suggested that cell identity was not affected in these lines (Supplementary Fig. 6, Supplementary Videos 1–3). This also suggests that the altered function of the female gametophyte rather than aborted development causes the observed decreased female transmission of *cwc15-2*$^{+/-}$. To detect defects during pollen tube attraction and fertilization, we used a pollen multiple marker line. Sperm cell nuclei were labeled with a male gamete-specific Histone H3.3-YFP fusion protein (HTR10-YFP) and a centromeric CenH3-mCherry fusion protein (HTR12-mCherry). Upon fertilization, the HTR10-YFP protein is turned over while zygote and endosperm show mCherry fluorescence at the centromeric chromatin, resulting in distinct foci in the zygote and endosperm nuclei[43]. *CWC15* loss of function resulted in a range of

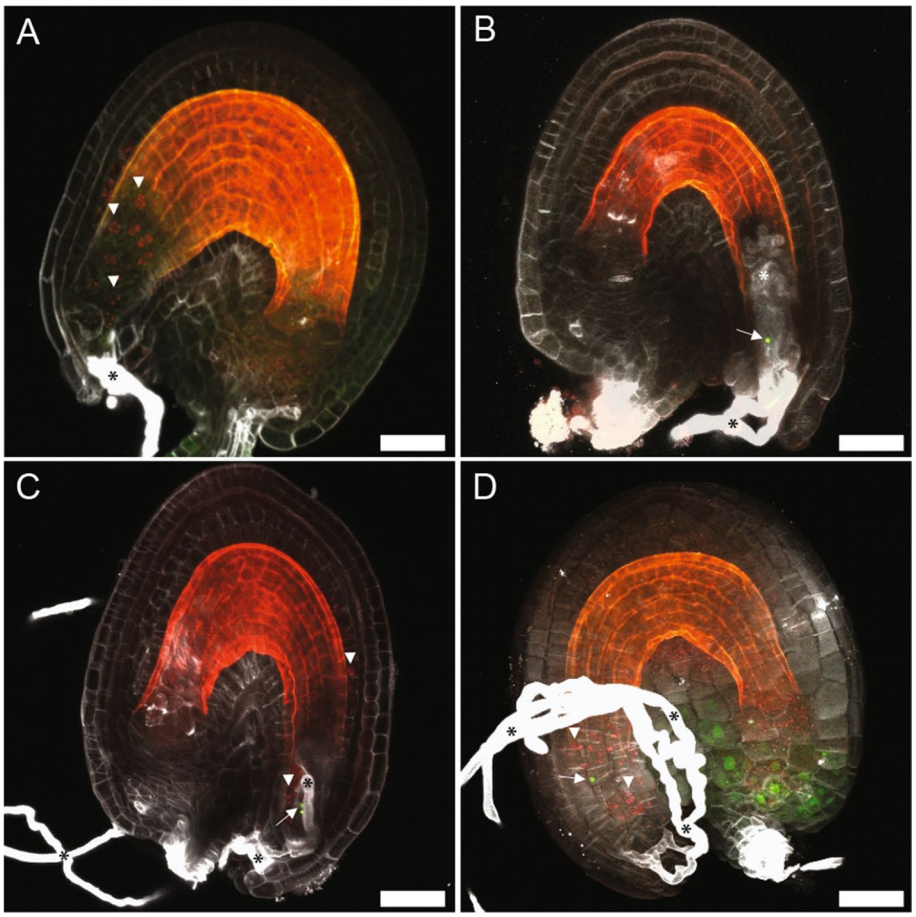

Figure 5. Loss of CWC15 function in *cwc15-2* leads to defects in double fertilization. (**A**–**D**) Overlay images of wild-type control (**A**) or CWC15 deficient ovules (**B**–**D**) 20 h after pollination expressing pollen double marker visualizing histones of fertilized endosperm nuclei in red (**A**,**C**,**D**), sperm nuclei in green (**B**,**C**,**D**), and SR2200 counter-staining of pollen tube cell walls in white (**A**–**D**). Arrowheads mark endosperm nuclei (red), arrows point to sperm nuclei (green), and asterisks indicate pollen tubes (white). Scale bar: 20 µm.

phenotypic consequences in pollen tube perception and fertilization (Fig. 5). After successful double fertilization, endosperm nuclei in wild-type plants showed 15 spots of nuclear-localized mCherry signal and no YFP signal could be detected (Fig. 5A). In ovules of *cwc15-2*$^{+/-}$ plants, however, we frequently observed pollen tubes without double fertilization as indicated by the absence of mCherry signal and the presence of nuclear YFP signal of unfused, persisting sperm cells (Fig. 5B). Also, we observed pollen tube overgrowth inside the ovule (Fig. 5B and C) as well as polytubey (Fig. 5D). Taken together, these observations suggest that CWC15 is required for efficient pollen tube reception and gamete interaction leading to successful double fertilization.

The ratio of aborted ovules from crosses of *cwc15-2*$^{+/-}$ gynoecia pollinated with pollen from Col-0 anthers (13.6%, n = 132) indicated, as well as the aforementioned reciprocal crosses, that a low percentage of ovules in *cwc15-2*$^{+/-}$ plants and their egg cells within can be fertilized. To investigate at which stage cwc15-2$^{-/-}$ zygote/embryo development might be arrested, we looked at ovules in *cwc15-2*$^{+/-}$ plants in self-pollinated flowers 72 h after pollination. We were able to identify seemingly aborted or delayed embryos at zygote and the earliest embryo stages of development (Fig. 6A-D). These results show that CWC15 function is important for female gametophyte development and fertilization and essential for embryogenesis, whereas the male gametophyte is not affected.

Discussion

Although the eukaryotic spliceosome machinery is evolutionarily conserved, there are species-specific differences. The spliceosome and the activating NineTeen complex show differences in both the number and nature of proteins involved between yeast, human and Arabidopsis[26,44,45]. In Arabidopsis, for example, there seems to be a duplication and likely redundancy of factors playing major roles during splicing (e.g., Prp8 or Prp19)[33]. One of the single-copy genes previously associated with the splicing machinery is CWC15. Our thorough phylogenetic analysis indicated that CWC15 is present and conserved in virtually all eukaryotic genomes. Until recently, knowledge about the exact function of CWC15 has been scarce. Protein–protein interaction data revealed CWC15 as a protein associated with yeast and human spliceosomes[23,46]. CWC15 was later considered an integral part of the Prp19 complex/NTC through its direct interaction with CDC5[47,48]. In Arabidopsis, however, co-precipitation with Prp19 could not be demonstrated and CWC15 was therefore deemed not being part of the

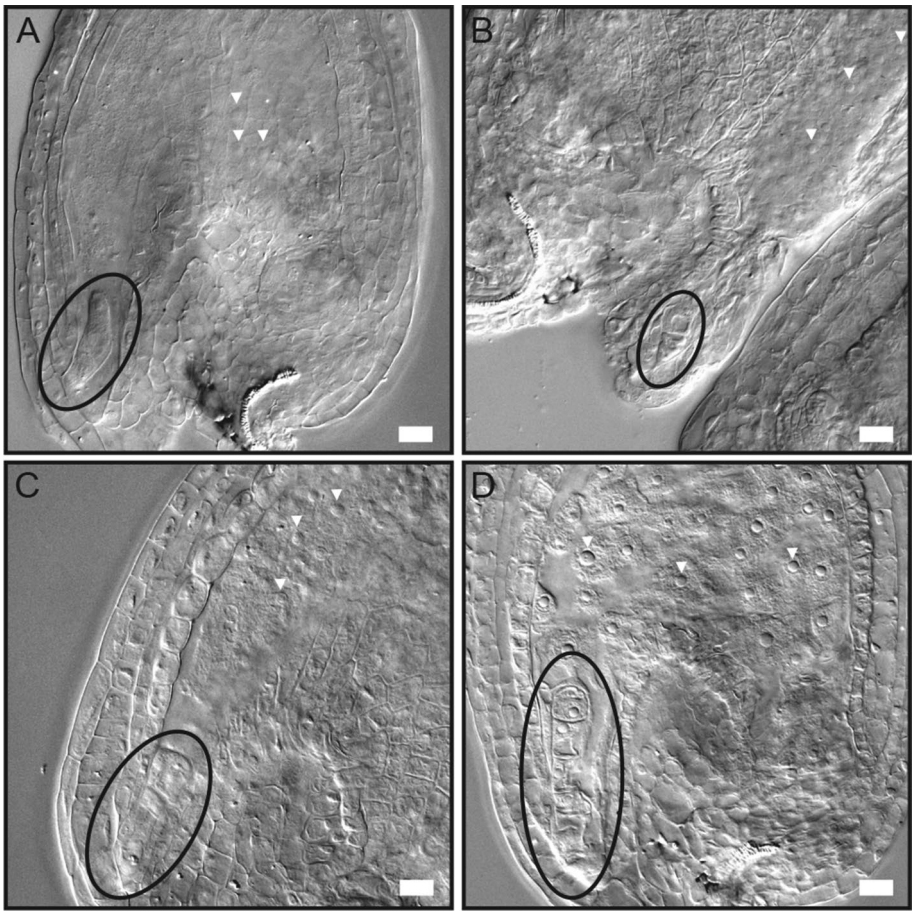

Figure 6. Zygote and embryo-arrest phenotypes in *cwc15-2*$^{+/-}$ mutant embryos. (**A**) Embryo arrested at zygote stage. (**B**, **C**) Embryos arrested at 1-cell stage. (**D**) Embryo arrested at 2-cell stage. Zygote and embryos are encircled by ellipses. Arrowheads indicate nuclei of fertilized endosperm. Scale bar: 10 µm.

NTC[26,49]. In contrast, our mass spectrometry-based analysis showed co-precipitation of most Arabidopsis NTC components with CWC15, indicating that there is a close interaction of CWC15 with the NTC in Arabidopsis. We also detected other components of the core spliceosomal machinery, which is in line with recent structural data gained from yeast and human spliceosomes. The yeast homolog Cwf15/Cwc15 interacts with several U5 snRNA components and together with Prp45 is thought to be important for the stability of the spliceosomal core or main body[20,45,50,51,52]. Like the yeast multi-protein complex, the human CWC15 counterpart Ad-002 is also present at the core region of the human spliceosome[21,44,53] and might be modified by human spliceosome-specific peptidyl-prolyl isomerases for functional catalytic activity[54]. Structures of plant spliceosomes have yet to be determined, but Arabidopsis CWC15 possibly has a similarly central role in the spliceosomal multi-protein complex as do the homologous proteins in yeast and human.

Alternative splicing (AS) is very common in humans, where essentially 100% of the transcripts have at least two isoforms[55]. The prevalent form of AS in animals is exon skipping[56]. We have utilized an approach that allows the detection of specific splice-sites that show aberrant usage between samples[40]. It has been estimated that 61% of Arabidopsis genes undergo AS, with the majority of AS events being intron retention[57] which in turn leads to nonsense-mediated decay (NMD) of the affected transcript[56]. However, in plants retained introns do not always trigger NMD[58]. In Arabidopsis, AS can be achieved by cell type-specific expression patterns of splicing factors[59,60] and this has been studied mainly during flowering time[61]. In our work, RNA sequencing analysis in a hypomorphic mutant background with seedling and adult growth defects showed that a decrease in CWC15 protein abundance causes clear splicing defects. While differences in splicing can lead to expression differences, in *cwc15* mutants, the observed differences in gene expression cannot be solely attributed to splicing defects. Additional changes in expression may be secondary effects resulting from splicing abnormalities. The phenotypic severity increased strongly in a putative knock-out mutant of CWC15 which showed pleiotropic fertilization defects and was embryo lethal. It has been previously shown that mutations in splicing factors primarily affect the viability of the female gametophyte[11,12,62,63]. Likewise, loss of the splicing factor CWC15 caused strongly decreased transmission via the female gametophyte while the pollen was entirely unaffected. Several studies detected new transcripts, differential splicing and even alternative transcriptional start sites in pollen when compared to leaf tissues[64,65]. However, transcripts enriched in pollen appear to have roles in splicing which could contribute to

increased robustness of the pollen when compared to the egg cell. It has been shown that so-called housekeeping genes can be linked to specific mutant phenotypes as is the case for various splicing factors that affect the development of the female gametophyte[66]. This could explain why the loss of CWC15, and other splicing factors causes different phenotypes between male and female gametophytes. Curiously, recent research showed that a pair of splicing factors specifically affects the male gametophyte in double mutants but not the female gametophyte[67]. Future research will show if the composition of the splicing machinery in plants is indeed tissue-specific and is possibly involved in the different needs of various tissue types during development.

Material and methods

Plant material and in silico analysis. The wild-type plant line used was the Col-0 accession and plants were grown as previously described[35]. The T-DNA insertion line *cwc15-2*$^{+/-}$ (SALK_010555, Col-0) was provided by the Nottingham Arabidopsis Stock Centre (NASC). The transgenic marker lines for specific cell types in the female gametophyte *pEC1:HTA6-3xeGFP*, *pNTA>>ntdTomato*, and *pMEA:3xGFP* as well as the multi-color marker were previously described[43,68].

Acquisition of protein sequences, sequence alignment, and generation of the phylogenetic tree was performed as shown before[69]. Representation of protein sequence alignment in RasMol color and sequence conservation was done with CLC Genomics Workbench software version 10.1.1.

Molecular cloning. The sequences of primers used in this study are listed in Supplementary Table 4. Both the CWC15 genomic rescue construct and the translational GFP fusion construct were generated by PCR amplifying a 2,825 bp fragment including 1,087 bp upstream of the CWC15 start codon and cloned into *GIIK-tNOS* (*CWC15* genomic start and stop primers) and *GIIK-3xeGFP-tNOS* (*CWC15* genomic start and -TAG stop primers), respectively, using restriction enzymes SalI/BclI. *GIIK-pRPS5A:CWC15-tNOS* was cloned by PCR amplifying the 693 bp CWC15 coding sequence (CDS) with CWC15 CDS start and stop primers and inserting the CDS into *GIIK-pRPS5A-tNOS*[70] using restriction site BclI. The construct for early embryo expression was cloned by amplifying a 2 kb promoter element upstream of the *AT3G10100* start codon[35] with *AT3G10100* start and stop primers and inserting the amplicon into *GIIK-tNOS*, using restriction enzymes XhoI/SmaI. The *CWC15* CDS was subsequently amplified with CWC15 CDS start and stop primers, and restriction enzyme BclI was used for cloning into *GIIK-pAT3G10100-tNOS*.

Whole-genome sequencing. Genomic DNA was extracted from pooled *cwc15-1* seedlings 6 days after germination (6 dag), using the Qiagen DNeasy Plant Mini Kit. Libraries for DNA Next Generation Sequencing (NGS) were prepared with 1 µg DNA, using the Illumina TruSeq DNA PCR-free Low Throughput Library Prep Kit and Single Indexes Set A, and sequenced on an Illumina HiSeq 2000 machine. The transgenic insertion site in *cwc15-1* was initially determined by aligning sequencing reads to the Arabidopsis genome (https://www.araport.org/data/araport11) and the border region of the transgenic construct, using CLC Genomics Workbench software version 10.1.1. The insertion site was confirmed by PCR genotyping of border regions, using transgenic and genomic primers (LB and *cwc15-1* genotyping start primers, 341 bp; RB and *cwc15-1* genotyping stop primers, 323 bp), and subsequently by Sanger sequencing of PCR products.

PCR genotyping. The *cwc15-2* T-DNA allele was genotyped with primers *cwc15-2* RP, *cwc15-2* LP, and T-DNA-specific primer LBa1 (wild-type allele RP + LP 824 bp, T-DNA containing allele RP + LBa1 approximately 450 bp). The *cwc15-2*$^{-}$ insertion site was determined by sequencing the T-DNA allele PCR product, using primer LBb1.3.

sqRT-PCR and qRT-PCR. Total RNA was extracted from Col-0 and *cwc15-1* mature pollen or pooled seedlings 6 dag, using the Qiagen RNeasy Plant Mini Kit and on-column DNase digest (Qiagen RNase-free DNase Set). Reverse transcription was carried out with 1 µg total RNA using the RevertAid RT Reverse Transcription Kit (Thermo Scientific). For sqRT-PCR analysis, the following PCR conditions were used: 94° for 5 min followed by 30 or 35 cycles of 94° for 10 s, 58° for 30 s, and 72° for 1 min with a final extension step 72° for 5 min. For qRT-PCR analysis, we used the intronless and ubiquitously expressed control gene *UBQ10* for normalization and the following PCR program: 95° for 3 min followed by 40 cycles of 95° for 10 s, 60° for 10 s, and 72° for 20 s. Gene *AT3G08950* as an example for splice-site usage was randomly chosen from among the top sites from Supplementary Dataset 1. Example gene *AT2G34060* was among the not statistically significant sites. All primers used can be found in Supplementary Table 4.

RNA sequencing, splicing, and GO enrichment analysis. Gene lists for differential expression and splicing analysis as well as GO terms can be found in the Supplementary Dataset Files 1 and 2. As described above, total RNA was extracted from two biological replicates for both pollen and seedlings and libraries for RNA NGS were prepared with 1 µg total RNA, using Illumina TruSeq RNA Library Prep Kit v2 and sequenced on an Illumina HiSeq 2000 machine. RNA-seq data were mapped using STAR v2.5.2[71], taking only uniquely mapping reads, with minimum intron size 20, and maximum intron size 6,000. A splice junction BED file was generated using RegTools v0.5.2[72] with the same intron limits. Each mapped RNA-seq sample was processed with SpliSER v0.1.1 and analyzed using the diffSpliSE pipeline[40]. To maintain the accuracy of the quantification, a splice site would be filtered out unless each replicate being assessed had at least 10 reads showing evidence of its utilization, or non-utilization. When comparing RNA from wild-type and *cwc15-1* seedlings, SpliSER detected

247,741 splice sites with sufficient read coverage in all samples; in pollen 66,191 splice sites were detected with sufficient read coverage in all samples.

For differential gene expression analysis, read counts were extracted from RNA-seq alignments using featureCounts v1.5.1[73]. Differential gene expression was called using DESeq2 v1.22.2[74] with read counts normalized using the sizeFactors() function. Genes with a corrected p-value < 0.05 and log2FoldChange > ± 2 were taken as differentially expressed. Differential gene expression PCA plots used DESeq2 regularized-log transformation read counts (rlog() function). Overlaps between gene lists were tested through hypergeometric probabilities. Venn diagrams were generated with Venn Diagram Plotter Software v1.5.5228 (https://omics.pnl.gov/software/venn-diagram-plotter). For gene ontology (GO) enrichment analysis, we took lists of genes that showed differential expression or that contained differentially spliced sites. Gene lists were uploaded to the AgriGO web portal (v2.0)[75], and we performed singular enrichment analysis using the TAIR10_2017 background gene set. A corrected p-value less than 0.05 was considered to be significant.

Microscopy. Images of seedlings and plants were taken with a Canon EOS 1000D camera. Clearing of ovules or embryos and staining with SR2200 were done as previously described[35,43]. Images of embryos were taken with a Zeiss Axio Imager. Fluorescent proteins were imaged using Leica TCS SP8, Olympus FV1000, or Zeiss LSM780 NLO confocal laser scanning microscopes and LAS X, FLUOVIEW, or ZEN software respectively. Images were processed using ImageJ version 1.52i and Adobe Photoshop and Illustrator CS6.

Immunoprecipitation and LC–MS/MS analysis. Precipitation of GFP-tagged proteins from seedlings 6 dag and subsequent mass spectrometry analysis was in essence the exact same procedure as was described previously[76,77]. Briefly, 1–2 g fresh weight seedling material was ground in liquid nitrogen, using mortar and pestle. The resultant seedling powder was suspended in 2–3 ml lysis buffer (150 mM NaCl, 50 mM Tris pH 7.5, 2 mM EDTA, 0.5% Triton X-100) containing 20–30 µl Protease Inhibitor Cocktail (P9599, Sigma-Aldrich). After centrifugation, the supernatant was filtered with Miracloth (Calbiochem) and 2 ml of the supernatant was incubated with 20 µl GFP-Trap beads (Chromotek) for 3 h at 4 °C, using a tube rotator. The magnetic beads were washed three times with wash buffer (150 mM NaCl, 50 mM Tris pH 7.5, 0.1% Triton X-100) on a magnetic stand. Bead-bound proteins were eluted by boiling in 1 × Laemmli buffer and purified by SDS-PAGE followed by in-gel Trypsin digest. The digested peptides were subjected to LC–MS/MS analysis and MS spectra were processed with MaxQuant package software version 1.5.2.8 with integrated Andromeda search engine[78].

Received: 31 August 2019; Accepted: 27 July 2020
Published online: 07 August 2020

References

1. Dresselhaus, T., Sprunck, S. & Wessel, G. M. Fertilization mechanisms in flowering plants. *Curr. Biol.* **26**, R125–R139 (2016).
2. Huck, N., Moore, J. M., Federer, M. & Grossniklaus, U. The *Arabidopsis* mutant *feronia* disrupts the female gametophytic control of pollen tube receptor. *Development* **130**, 2149–2159 (2003).
3. Takeuchi, H. & Higashiyama, T. Tip-localized receptors control pollen tube growth and LURE sensing in *Arabidopsis*. *Nature* **531**, 245–248 (2016).
4. Lau, S., Slane, D., Herud, O., Kong, J. & Jürgens, G. Early embryogenesis in flowering plants: setting up the basic body pattern. *Annu. Rev. Plant Biol.* **63**, 483–506 (2012).
5. Lukowitz, W., Mayer, U. & Jürgens, G. Cytokinesis in the Arabidopsis embryo involves the syntaxin-related KNOLLE gene product. *Cell* **84**, 61–71 (1996).
6. Hamann, T., Mayer, U. & Jürgens, G. The auxin-insensitive *bodenlos* mutation affects primary root formation and apical-basal patterning in the *Arabidopsis* embryo. *Development* **126**, 1387–1395 (1999).
7. Hemerly, A. S., Ferreira, P. C. G., Van Montagu, M., Engler, G. & Inzé, D. Cell division events are essential for embryo patterning and morphogenesis: Studies on dominant-negative *cdc2aAt* mutants of *Arabidopsis*. *Plant J.* **1**, 123–130 (2000).
8. Steinborn, K. *et al.* The *Arabidopsis PILZ* group genes encode tubulin-folding cofactor orthologs required for cell division but not cell growth. *Genes Dev.* **16**, 959–971 (2002).
9. Nodine, M. D. & Bartel, D. P. MicroRNAs prevent precocious gene expression and enable pattern formation during plant embryogenesis. *Genes Dev.* **24**, 2678–2692 (2010).
10. Schwartz, B. W., Yeung, E. C. & Meinke, D. W. Disruption of morphogenesis and transformation of the suspensor in abnormal *sus*pensor mutants of *Arabidopsis*. *Development* **120**, 3235–3245 (1994).
11. Moll, C. *et al. CLO/GFA1* and *ATO* are novel regulators of gametic cell fate in plants. *Plant J.* **56**, 913–921 (2008).
12. Liu, M. *et al. GAMETOPHYTIC FACTOR 1*, Involved in Pre-mRNA Splicing, Is Essential for Megagametogenesis and Embryogenesis in *Arabidopsis*. *J. Integr. Plant Biol.* **51**, 261–271 (2009).
13. Sasaki, T. *et al.* An Rtf2 Domain-containing protein influences pre-mRNA splicing and is essential for embryonic development in *Arabidopsis thaliana*. *Genetics* **200**, 523–535 (2015).
14. Xiong, F. *et al. AtBUD13* affects pre-mRNA splicing and is essential for embryo development in Arabidopsis. *Plant J.* **98**, 714–726 (2019).
15. Shi, Y. Mechanistic insights into precursor messenger RNA splicing by the spliceosome. *Nat. Rev. Mol. Cell Biol.* **18**, 655–670 (2017).
16. Will, C. L. & Lührmann, R. Spliceosome structure and function. *Cold Spring Harb. Perspect. Biol.* **3**, a003707 (2011).
17. Chan, S. P. & Cheng, S. C. The Prp19-associated complex is required for specifying interactions of U5 and U6 with pre-mRNA during spliceosome activation. *J. Biol. Chem.* **280**, 31190–31199 (2005).
18. Chan, S. P., Kao, D. I., Tsai, W. Y. & Cheng, S. C. The Prp19p-associated complex in spliceosome activation. *Science* **302**, 279–282 (2003).
19. Yan, C., Wan, R., Bai, R., Huang, G. & Shi, Y. Structure of a yeast activated spliceosome at 3.5 Å resolution. *Science* **353**, 904–911 (2016).
20. Wan, R., Yan, C., Bai, R., Huang, G. & Shi, Y. Structure of a yeast catalytic step I spliceosome at 3.4 Å resolution. *Science* **353**, 895–904 (2016).

21. Zhang, X. *et al.* An atomic structure of the human spliceosome. *Cell* **169**, 918-929.e14 (2017).
22. Fica, S. M., Oubridge, C., Wilkinson, M. E., Newman, A. J. & Nagai, K. A human postcatalytic spliceosome structure reveals essential roles of metazoan factors for exon ligation. *Science* **363**, 710–714 (2019).
23. Ohi, M. D. & Gould, K. L. Characterization of interactions among the Cef1p-Prp19p-associated splicing complex. *RNA* **8**, 798–815 (2002).
24. Pleiss, J. A., Whitworth, G. B., Bergkessel, M. & Guthrie, C. Transcript specificity in yeast pre-mRNA splicing revealed by mutations in core spliceosomal components. *PLoS Biol.* **5**, 745–757 (2007).
25. Sonstegard, T. S. *et al.* Identification of a nonsense mutation in CWC15 associated with decreased reproductive efficiency in Jersey cattle. *PLoS ONE* **8**, e54872 (2013).
26. Koncz, C., deJong, F., Villacorta, N., Szakonyi, D. & Koncz, Z. The spliceosome-activating complex: molecular mechanisms underlying the function of a pleiotropic regulator. *Front. Plant Sci.* **3**, 9 (2012).
27. Nesic, D. & Kramer, A. Domains in human splicing factors SF3a60 and SF3a66 required for binding to SF3a120, assembly of the 17S U2 snRNP, and prespliceosome formation. *Mol. Cell. Biol.* **21**, 6406–6417 (2001).
28. Nguyen, T. H. D. *et al.* CryoEM structures of two spliceosomal complexes: starter and dessert at the spliceosome feast. *Curr. Opin. Struct. Biol.* **36**, 48–57 (2016).
29. Schlereth, A. *et al.* MONOPTEROS controls embryonic root initiation by regulating a mobile transcription factor. *Nature* **464**, 913–916 (2010).
30. Herud, O., Weijers, D., Lau, S. & Jürgens, G. Auxin responsiveness of the MONOPTEROS-BODENLOS module in primary root initiation critically depends on the nuclear import kinetics of the Aux/IAA inhibitor BODENLOS. *Plant J.* **85**, 269–277 (2016).
31. Chanarat, S. & Sträßer, K. Splicing and beyond: the many faces of the Prp19 complex. *Biochim. Biophys. Acta Mol. Cell Res.* **1833**, 2126–2134 (2013).
32. Jia, T. *et al.* The Arabidopsis MOS4-associated complex promotes microRNA biogenesis and precursor messenger RNA splicing. *Plant Cell* **29**, 2626–2643 (2017).
33. Meyer, K., Koester, T. & Staiger, D. Pre-mRNA splicing in plants: in vivo functions of RNA-binding proteins implicated in the splicing process. *Biomolecules* **5**, 1717–1740 (2015).
34. Polkoa, J. K. *et al.* Illumina sequencing technology as a method of identifying T-DNA insertion loci in activation-tagged *Arabidopsis thaliana* plants. *Mol. Plant* **5**, 948–950 (2012).
35. Slane, D. *et al.* Cell type-specific transcriptome analysis in the early *Arabidopsis thaliana* embryo. *Development* **141**, 4831–4840 (2014).
36. Lukowitz, W., Roeder, A., Parmenter, D. & Somerville, C. A MAPKK kinase gene regulates extra-embryonic cell fate in Arabidopsis. *Cell* **116**, 109–119 (2004).
37. Ueda, M., Zhang, Z. & Laux, T. Transcriptional activation of *Arabidopsis* axis patterning genes *WOX8/9* links zygote polarity to embryo development. *Dev. Cell* **20**, 264–270 (2011).
38. Yadegari, R. *et al.* Cell differentiation and morphogenesis are uncoupled in Arabidopsis *raspberry* embryos. *Plant Cell* **6**, 1713–1729 (1994).
39. Torres-Ruiz, R. A. & Jürgens, G. Mutations in the *FASS* gene uncouple pattern formation and morphogenesis in *Arabidopsis* development. *Development* **120**, 2967–2978 (1994).
40. Dent, C. *et al.* Splice-site strength estimation: a simple yet powerful approach to analyse RNA splicing https://doi.org/10.1101/2020.02.12.946756 (2020).
41. Sureshkumar, S., Dent, C., Seleznev, A., Tasset, C. & Balasubramanian, S. Nonsense-mediated mRNA decay modulates FLM-dependent thermosensory flowering response in *Arabidopsis*. *Nat. Plants* **2**, 16055 (2016).
42. Hartmann, L. *et al.* Alternative splicing substantially diversifies the transcriptome during early photomorphogenesis and correlates with the energy availability in Arabidopsis. *Plant Cell* **28**, 2715–2734 (2016).
43. Musielak, T. J., Schenkel, L., Kolb, M., Henschen, A. & Bayer, M. A simple and versatile cell wall staining protocol to study plant reproduction. *Plant Reprod.* **28**, 161–169 (2015).
44. Haselbach, D. *et al.* Structure and conformational dynamics of the human spliceosomal Bact complex. *Cell* **172**, 454-464.e11 (2018).
45. Yan, C., Wan, R., Bai, R., Huang, G. & Shi, Y. Structure of a yeast step II catalytically activated spliceosome. *Science* **355**, 149–155 (2017).
46. Makarova, O. V. *et al.* A subset of human 35S U5 proteins, including Prp19, function prior to catalytic step 1 of splicing. *EMBO J.* **23**, 2381–2391 (2004).
47. Grote, M. *et al.* Molecular architecture of the human Prp19/CDC5L complex. *Mol. Cell. Biol.* **30**, 2105–2119 (2010).
48. Van Maldegem, F. *et al.* CTNNBL1 facilitates the association of CWC15 with CDC5L and is required to maintain the abundance of the Prp19 spliceosomal complex. *Nucleic Acids Res.* **43**, 7058–7069 (2015).
49. Monaghan, J. *et al.* Two Prp19-like U-box proteins in the MOS4-associated complex play redundant roles in plant innate immunity. *PLoS Pathog.* **5**, e1000526 (2009).
50. Yan, C. *et al.* Structure of a yeast spliceosome at 3.6-angstrom resolution. *Science* **349**, 1182–1191 (2015).
51. Bai, R., Yan, C., Wan, R., Lei, J. & Shi, Y. Structure of the post-catalytic spliceosome from *Saccharomyces cerevisiae*. *Cell* **171**, 1589–1598 (2017).
52. Galej, W. P. *et al.* Cryo-EM structure of the spliceosome immediately after branching. *Nature* **537**, 197–201 (2016).
53. Bertram, K. *et al.* Cryo-EM structure of a human spliceosome activated for step 2 of splicing. *Nature* **542**, 318–323 (2017).
54. Zhang, X. *et al.* Structure of the human activated spliceosome in three conformational states. *Cell Res.* **28**, 307–322 (2018).
55. Lee, Y. & Rio, D. C. Mechanisms and regulation of alternative pre-mRNA splicing. *Annu. Rev. Biochem.* **84**, 291–323 (2015).
56. Kornblihtt, A. R. *et al.* Alternative splicing: a pivotal step between eukaryotic transcription and translation. *Nat. Rev. Mol. Cell Biol.* **14**, 153–165 (2013).
57. Staiger, D. & Simpson, G. G. Enter exitrons. *Genome Biol.* **16**, 136 (2015).
58. Shaul, O. Unique aspects of plant nonsense-mediated mRNA decay. *Trends Plant Sci.* **20**, 767–779 (2015).
59. Fang, Y., Hearn, S. & Spector, D. L. Tissue-specific expression and dynamic organization of SR splicing factors in *Arabidopsis*. *Mol. Biol. Cell* **15**, 2664–2673 (2004).
60. Li, S., Yamada, M., Han, X., Ohler, U. & Benfey, P. N. High-resolution expression map of the Arabidopsis root reveals alternative splicing and lincRNA regulation. *Dev. Cell* **39**, 508–522 (2016).
61. Park, Y. J., Lee, J. H., Kim, J. Y. & Park, C. M. Alternative RNA splicing expands the developmental plasticity of flowering transition. *Front. Plant Sci.* **10**, 1–7 (2019).
62. Groß-Hardt, R. *et al. LACHESIS* restricts gametic cell fate in the female gametophyte of *Arabidopsis*. *PLoS Biol.* **5**, e47 (2007).
63. Ohtani, M., Demura, T. & Sugiyama, M. *Arabidopsis* root initiation defective1, a DEAH-box RNA helicase involved in pre-mRNA splicing, is essential for plant development. *Plant Cell* **25**, 2056–2069 (2013).
64. Loraine, A. E., McCormick, S., Estrada, A., Patel, K. & Qin, P. RNA-seq of Arabidopsis pollen uncovers novel transcription and alternative splicing. *Plant Physiol.* **162**, 1092–1109 (2013).
65. Estrada, A. D., Freese, N. H., Blakley, I. C. & Loraine, A. E. Analysis of pollen-specific alternative splicing in *Arabidopsis thaliana* via semi-quantitative PCR. *PeerJ* **3**, e919 (2015).
66. Tsukaya, H. *et al.* How do 'housekeeping' genes control organogenesis? Unexpected new findings on the role of housekeeping genes in cell and organ differentiation. *J. Plant Res.* **126**, 3–15 (2013).

67. Park, H. Y., Lee, H. T., Lee, J. H. & Kim, J. K. *Arabidopsis U2AF65* regulates flowering time and the growth of pollen tubes. *Front. Plant Sci.* **10**, 569 (2019).
68. Kong, J., Lau, S. & Jürgens, G. Twin plants from supernumerary egg cells in *Arabidopsis*. *Curr. Biol.* **25**, 225–230 (2015).
69. Slane, D., Reichardt, I., El Kasmi, F., Bayer, M. & Jürgens, G. Evolutionarily diverse SYP1 Qa-SNAREs jointly sustain pollen tube growth in Arabidopsis. *Plant J.* **92**, 375–385 (2017).
70. Weijers, D., Geldner, N., Offringa, R. & Jürgens, G. Seed development: early paternal gene activity in *Arabidopsis*. *Nature* **414**, 709–710 (2001).
71. Dobin, A. *et al.* STAR: ultrafast universal RNA-seq aligner. *Bioinformatics* **29**, 15–21 (2013).
72. Feng, Y.-Y. *et al.* RegTools: integrated analysis of genomic and transcriptomic data for discovery of splicing variants in cancer (2018).
73. Yang, L., Smyth, G. K. & Wei, S. featureCounts: an efficient general purpose program for assigning sequence reads to genomic features. *Bioinformatics* **30**, 923–930 (2014).
74. Anders, S. & Huber, W. DEseq2: differential gene expression analysis based on the negative binomial distribution. *Genome Biol.* **11**, R106 (2010).
75. Tian, T. *et al.* agriGO v2.0: a GO analysis toolkit for the agricultural community, 2017 update. *Nucleic Acids Res.* **45**, 122–129 (2017).
76. Singh, M. K. *et al.* A single class of ARF GTPase activated by several pathway-specific ARF-GEFs regulates essential membrane traffic in *Arabidopsis*. *PLoS Genet.* **14**, e1007795 (2018).
77. Speth, C. *et al.* Arabidopsis RNA processing factor SERRATE regulates the transcription of intronless genes. *Elife* **7**, e37078 (2018).
78. Cox, J. *et al.* Andromeda: a peptide search engine integrated into the MaxQuant environment. *J Proteome Res.* **10**, 1794–1805 (2011).

Acknowledgements

We thank the Nottingham Arabidopsis Stock Centre for providing T-DNA insertion lines, Martin Vogt for his assistance, and the Genome Center of the Max Plank Institute for Developmental Biology for their support. Research in our lab was supported by the German Science Foundation (Deutsche Forschungsgemeinschaft – DFG: SFB 1101/B01 to MB) and the Max Planck Society. Portions of this research (Venn Diagram Plotter Software) were supported by the W.R. Wiley Environmental Molecular Science Laboratory, a national scientific user facility sponsored by the U.S. Department of Energy's Office of Biological and Environmental Research and located at PNNL. PNNL is operated by Battelle Memorial Institute for the U.S. Department of Energy under contract DE-AC05-76RL0 1830. Research on splicing in SB group is supported by Australian Research Council Discovery Project DP190101479. Open access funding provided by Projekt DEAL.

Author contributions

D.S., C.H.L., S.L., M.B., and G.J. designed the study. D.S., C.H.L., M.K., C.D., Y.M., M.F.W., and M.B. performed the experiments and evaluated the data. S.B. and B.M. analyzed and interpreted the experimental results. D.S. wrote the manuscript. All authors commented on the manuscript.

Competing interests

The authors declare no competing interests.

Additional information

Supplementary information is available for this paper at https://doi.org/10.1038/s41598-020-70324-3.

Correspondence and requests for materials should be addressed to G.J.

Reprints and permissions information is available at www.nature.com/reprints.

Publisher's note Springer Nature remains neutral with regard to jurisdictional claims in published maps and institutional affiliations.

Available online at www.sciencedirect.com

ScienceDirect

Current Opinion in Plant Biology

Square one: zygote polarity and early embryogenesis in flowering plants

Kai Wang, Houming Chen, Yingjing Miao and Martin Bayer

In the last two decades, work on auxin signaling has helped to understand many aspects of the fundamental process underlying the specification of tissue types in the plant embryo. However, the immediate steps after fertilization including the polarization of the zygote and the initial body axis formation remained poorly understood. Valuable insight into these enigmatic processes has been gained by studying fertilization in grasses. Recent technical advances in transcriptomics of developing embryos with high spatial and temporal resolution give an emerging picture of the rapid changes of the zygotic developmental program. Together with the use of live imaging of novel fluorescent marker lines, these data are now the basis of unraveling the very first steps of the embryonic patterning process.

Address
Max Planck Institute for Developmental Biology, Department of Cell Biology, Max-Planck-Ring 5, 72076 Tübingen, Germany

Corresponding author: Bayer, Martin (martin.bayer@tuebingen.mpg.de)

Current Opinion in Plant Biology 2020, **53**:128–133

This review comes from a themed issue on **Growth and development**

Edited by **Marcus Heisler** and **Alexis Maizel**

For a complete overview see the Issue and the Editorial

Available online 11th November 2019

https://doi.org/10.1016/j.pbi.2019.10.002

Introduction

In embryogenesis, a single cell generally develops into a miniature version of the adult organism. In plants, however, the final body architecture is determined post-embryonically, likely as adaption to their sessile life. Plant embryos represent primitive versions of seedlings and only a few basic cell types are established during embryogenesis [1] (Figure 1).

Fertilization of the egg cell marks the beginning of a new sporophytic generation, starting with the zygote. In many angiosperm species, the zygote divides asymmetrically, often after an initial phase of cell elongation [2]. The apical daughter cell will always form at least part of the embryo. The basal daughter cell contains a large central vacuole and its descendants will mainly contribute extra-embryonic tissue [3]. In *Brassicaceae*, embryogenesis follows an invariable series of cell divisions, in which the apical cell forms a spherical proembryo (Figure 1a). The basal daughter cell undergoes a series of transverse mitotic divisions to form the filamentous suspensor. Except the uppermost cell, the suspensor is extra-embryonic, connects the embryo with maternal seed tissue, and does not contribute to the later plant seedling. Therefore, in *Brassicaceae*, the first zygotic division already marks the boundary between embryonic and extra-embryonic development [4]. In other flowering plants, however, the patterning process can be less stereotypic and in some cases there is no clear boundary between embryonic and suspensor tissue (Figure 2). Cells derived from the first apical cell can also differentiate into suspensor cells, as seen in some members of the *Caryophyllaceae*. In a similar manner, descendants of the basal cell might also contribute to large portions of the proembryo as in some *Asteraceae* family members [3]. Therefore, patterning seems to be mainly influenced by position-dependent cues and the concept of cell lineages apparently does not apply in the early plant embryo. Nonetheless, a universal feature of embryogenesis in seed plants is the polarity of the first zygotic division with the apical daughter cell always contributing to the embryo. This division seems to be an essential step in axis formation of the angiosperm embryo and it is therefore a fundamental question how the zygote is polarized.

Early morphological changes

In flowering plants, already the egg cell is a polar structure with the nucleus at the apex and a large central vacuole at the basal pole [5] (Figure 1b). Microtubules are preferentially oriented in a longitudinal direction [6•]. Directly after fertilization, however, this polarity seems to be lost as the large vacuole is broken up into smaller, evenly distributed vacuoles and the nucleus moves to a central position [5,7]. After this transient apolar phase, polarity is reestablished and the zygote starts to elongate in a similar fashion as tip-growing cells such as pollen tubes or root hair cells [6•,7]. In Arabidopsis, the zygote grows threefold in size whereas in many grasses there is barely any noticeable growth at this stage [3]. The first hallmark of polarity reestablishment happens at this stage as the nucleus moves out of the center to an apical position, followed by an asymmetric division. What kind of positional information determines the direction of cell elongation and the position of the cell division plane?

In many animals, the sperm entry site can function as positional cue [8,9]. In a similar fashion, the brown alga *Fucus* relies on the position of sperm entry in the absence

Figure 1

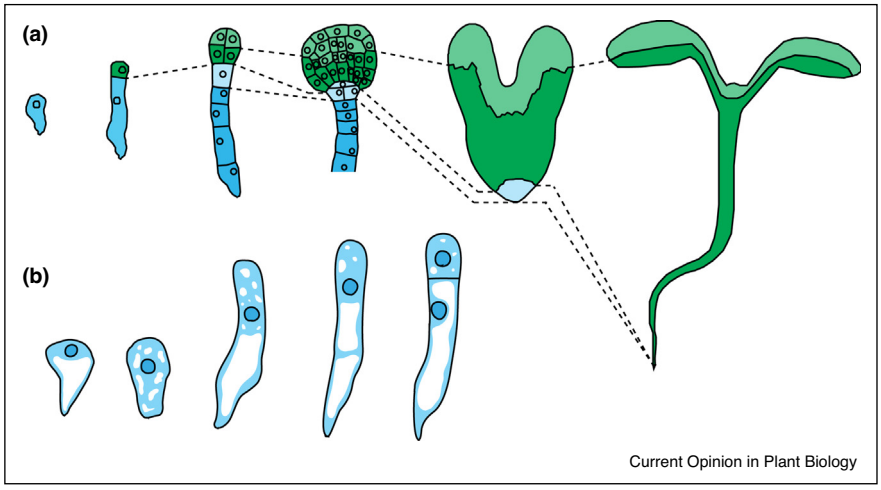

Embryogenesis in Arabidopsis.
(a) After the first zygotic division, the apical cell forms the spherical embryo (green) while the basal cell forms the mostly extra-embryonic suspensor (blue). The final seedling is mainly formed by the upper tier (light green) and lower tier (dark green) of the embryo proper. Only the upper-most suspensor cell (light blue) in direct contact with the embryo proper contributes to the embryonic root. The rest of the suspensor (dark blue) remains extra-embryonic. **(b)** In accordance with morphological criteria, egg cell polarity is lost in the early zygote. The large central vacuole (white) at the basal pole of the egg cell is partitioned into smaller evenly distributed vacuoles. During cell elongation, the zygote repolarized and the nucleus moves to the apex before the first asymmetric division. During zygotic cell elongation, a large central vacuole is reformed at the basal pole.

of other polarizing cues [10]. In flowering plants, however, *in vitro* experiments with rice gametes would argue against positional information provided by the sperm entry site as there was no correlation between its position and polarity of the zygote [11]. Fusion with the sperm, on the other hand, seems to be a necessary trigger for egg activation as it causes Calcium influx and initiates karyogamy and the activation of a zygotic transcriptional program [12] which cannot be achieved by artificial fusion of two egg cells.

In rice, egg activation possibly involves the paternally provided AP2 transcription factor OsASGR-BBML1 [13••]. Overexpression of BBML1 in the egg cell leads to proliferation without fertilization. Dominant negative versions of BBML1 lead to developmental arrest if expressed in the zygote. As ectopic overexpression of BBM induces embryogenesis in somatic cells in Arabidopsis [14], this family of transcription factors could be part of a two-component system of maternal and paternal factors that initiate a zygotic transcriptional program similar to the BELL/KNOX transcriptional regulators in the unicellular alga *Chlamydomonas reinhardtii* [15]

Zygotic gene expression

There have been conflicting reports about the timing of the maternal-to-zygotic transition and the degree of maternal and paternal contribution to early embryogenesis of flowering plants [16–21,22•]. Recent advances in manual isolation of single cells made it possible to generate transcriptional profiles of gametic cells and early embryos with much higher temporal and spatial resolution and lower contamination by surrounding maternal tissue [13••,23••,24••]. With these latest transcriptomic data from grasses and Arabidopsis, a clear picture is emerging.

In animals, the maternal-to-zygotic transition follows two phases. At the beginning, development is regulated purely post-transcriptionally by maternal mRNAs and proteins stored in the oocyte. Later, as the zygotic genome is activated, maternal RNAs are depleted and zygotic mRNAs take over functionally [25]. In flowering plants, there seems to be in principle a similar progressive activation of zygotic bi-parental transcripts [13••,23••,24••]. However, this transition seems to happen rapidly in the zygote. In Arabidopsis, sperm-specific transcripts can be detected in zygotes at 14 hours after pollination (hap) but are dramatically reduced or absent in zygotes at 24 hap. At the same time, egg cell-specific transcripts are rapidly eliminated and several thousand genes are upregulated in the zygote compared to the egg cell [24••]. In Arabidospsis, it has been shown that already the first zygotic cell division relies on *de novo* transcription [24••]. The onset of zygotic transcription is accompanied by rapid turn-over of gametic histones and replacement by zygotic histones [26]. These new data therefore further support the view that zygotic genome activation happens very rapidly in flowering plants as previously proposed by Nodine and Bartel [20]. However,

Figure 2

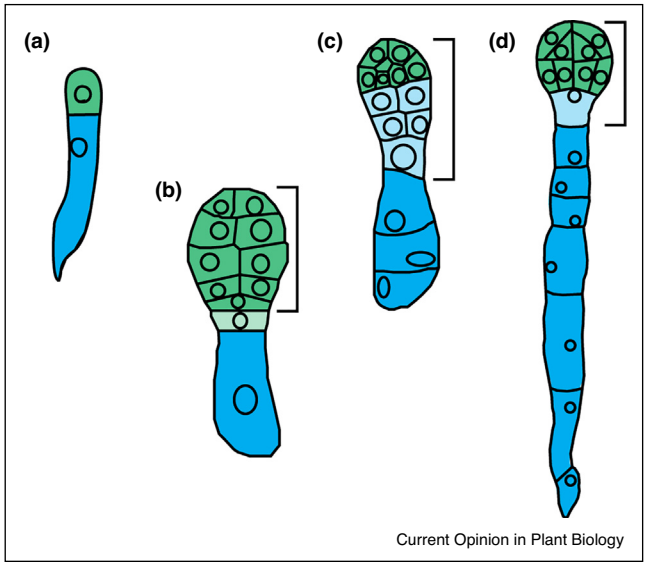

Clonal origin of embryonic structures (after [3], modified). **(a)** The first cell division gives rise to an apical (green) and basal (blue) daughter cell. **(b)** Suspensor cells derived from the apical cell in *Sagina procumbens* (*Caryophyllaceae*); shown in light green. **(c)** Cells originating from the basal cell contribute substantially to the embryo proper in *Geum urbanum* (*Asteraceae*); depicted in light blue. **(d)** In *Brassicaceae*, only the upper-most descendent of the basal cell (light blue) contributes to the embryo. Cells contributing to the later seedling are marked by brackets.

these rapid transcriptome changes and the observed intracellular reorganization of the zygote raise the question if polarization of this cell relies on pre-existing parental factors or if polarity establishment is an intrinsic zygotic process.

MAP kinase signaling

Polarity of the zygote and differentiation of the first daughter cells seem to be at least in part controlled by a MAP kinase-dependent signaling pathway. This pathway includes the MAP kinases MPK3 and MPK6, the MAPK kinases MKK4 and MKK5 as well as the MAPKK kinase YODA (YDA) [27–29] (Figure 3). Loss of YDA impairs zygote elongation and results in symmetric cell division. Furthermore, both daughter cells adopt embryo-like division patterns, resulting in embryos lacking a recognizable suspensor. Constitutive activation of the YDA pathway leads to structures entirely consisting of suspensor-like cells [27]. This pathway therefore seems to promote zygote elongation and polarity and suppresses embryonic development in the basal daughter cell [30].

One of the direct phosphorylation targets of this signaling cascade is the transcription factor WRKY2. Together with the HOMEODOMAIN GLABROUS (HDG) transcription factors HDG11/12, WRKY2 activates expression of *WUSCHEL-RELATED HOMEOBOX 8* (*WOX8*) [31,32]. *WOX8* and *WOX9* are necessary for correct suspensor development and expression of several developmentally important genes in the embryo [33]. *WOX* genes generally play important roles as transcriptional repressor in stem cell niches. However, these members of the evolutionarily more ancient *WOX9* clade rather seem to act as transcriptional activators [34].

As the *wrky2* mutant recapitulates certain aspects of the *yda* phenotype but lacks others, there are likely additional targets of the YDA-dependent signaling cascade in the zygote. Potential targets could be transcription factor complexes including the RWP-RK protein GRD/RKD4, although GRD itself does not seem to be a direct target [35,36]. Mutant *grd* embryos in principle resemble *yda* embryos albeit the phenotype is less pronounced. Some members of the *RKD* family play a pivotal role in the egg-to-zygote transition [37,38]. It is therefore tempting to speculate that YDA might be involved in setting up a zygotic genome program via GRD regulation. As the overexpression of RKD4 can induce somatic embryogenesis [36], a role of RKD4 in activating a zygotic transcriptome seems at least plausible.

YDA is activated in the zygote by the BRASSINOSTEROID SIGNALING KINASE family members BSK1 and BSK2 [39••]. These membrane-associated proteins directly interact with the YDA kinase domain, possibly in a phosphorylation-dependent manner. BSK family proteins have been described as integral part of SOMATIC EMBRYOGENESIS RECEPTOR KINASE (SERK)-dependent receptor complexes in various signaling pathways [40–42]. These leucine-rich repeat containing co-receptors are involved in YDA-dependent developmental processes [43]. However, the receptor teaming up with the SERK co-receptors upstream of YDA in the embryo as well as possible ligands are still unknown.

Possible candidates include peptides of the EMBRYO SURROUNDING FACTOR (ESF) family. Downregulation by RNAi causes mild suspensor defects that can be rescued by expression of a constitutively active variant of *YDA* [44]. The spatial and temporal information provided by these possible ligands is, however, presently unclear.

In *Brassicaceae*, an additional way of YDA activation exists in the zygote. The unusual BSK family member SHORT SUSPENSOR (SSP/BSK12) accumulates specifically in the zygote, apparently translated from paternally inherited transcripts [45]. The SSP protein lacks a regulatory intra-molecular interaction typically seen in BSK proteins [39••]. Resembling a constitutively active version of BSK1, SSP can activate YDA directly after fertilization possibly without involving canonical receptor activation (Figure 3). As *ssp* mutants show slower embryonic development and a less defined boundary between embryo and suspensor, much like many species outside the

Figure 3

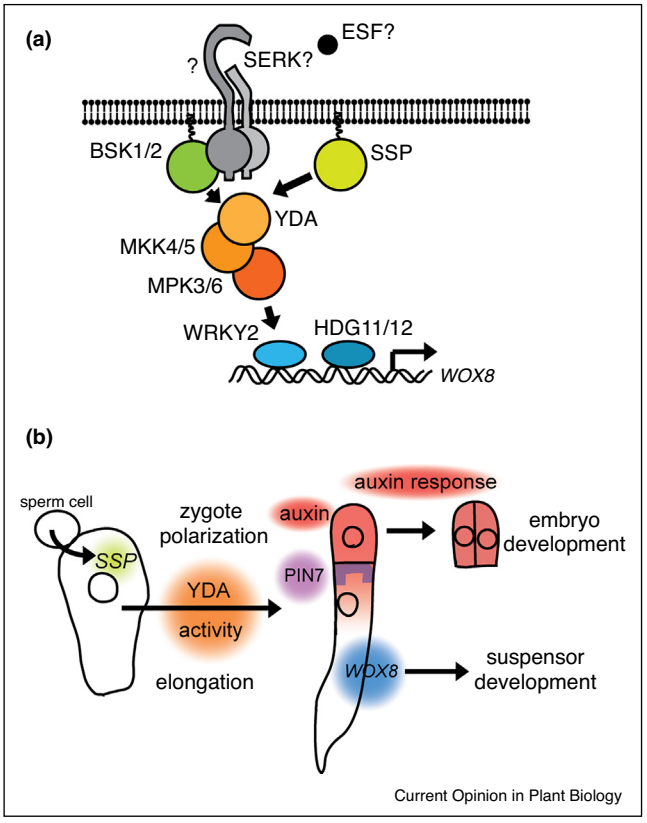

Signaling events in the early embryo.
(a) Schematic depiction of the embryonic YDA signaling pathways. The MAPKKK YDA can be activated by a possible receptor kinase complex including the membrane-associated proteins BSK1/2. In addition, paternally provided SSP directly activates YDA in *Brassicaceae*. **(b)** Consecutive signaling events in the early embryo. YDA activity contributes to zygote elongation, asymmetric cell division, and differential *WOX8* expression. A local, PIN7-mediated auxin maximum in the apical daughter cell initiates 3-dimensional growth of the embryo proper.

Brassicaceae family, this paternal input might provide a beneficial boost of YDA activity contributing to the rapid life cycle of *Brassicaceae* family members [45,46].

Auxin signaling

Many developmental processes in plants start with an asymmetric division and almost universally seem to involve the plant hormone auxin [47–49]. In the zygote, however, direct evidence for a role of auxin in regulating the first asymmetric division is lacking [30]. As the zygote seems to elongate in a tip-growing manner similar to pollen tubes or root hair cells, there is the possibility that this division actually resembles a rather specialized case independent of auxin signaling. The resulting daughter cells, however, show differential expression of genes involved in auxin response and transport. PIN7 in the basal cell is thought to initiate basal-to-apical auxin transport [50]. According to this model, three-dimensional growth of the embryo is then initiated by an auxin response maximum in the apical cell, re-orienting the cell division plane [48]. Auxin responses in the apical cell, therefore, seem to be an essential part of initiating embryonic development. Since the differential auxin response in the two zygotic daughter cells relies on already differentially expressed genes of auxin transport and response [50,51], this raises the question if auxin signaling in this context mainly amplifies and firmly establishes already pre-existing, transient differences.

Auxin transport is intimately linked to auxin synthesis and recent seemingly conflicting reports indicate possibly several sources [52–54,55••]. Consistent with PIN7-mediated transport from the basal cell, auxin might initially be synthesized in maternal cells in the micropylar region that are in direct contact with the basal daughter cell [55••]. However, once suspensor differentiation is initiated in the basal cell, the suspensor itself seems to become an auxin source [54].

Conclusions

Recent advances in live imaging and novel fluorescent markers [6•,7,56] as well as transcriptomic approaches [13••,23••,24••] have yielded new insights into the enigmatic processes that lead to symmetry breaking in the zygote. Polarity information seems to be ubiquitous in plant cells and interpreted at least in part by the recently discovered SOSEKI proteins [57••]. Their role in zygote polarization, however, has to be investigated in detail. It is still an open question if cell polarity in the zygote is inherited from the parental generation or established *de novo*. Does this process rely on external cues or is it directed by an intrinsic mechanism possibly including mechanical forces? How does the MAP kinase-WRKY-WOX pathway integrate with auxin signaling in establishing different cell identities? Recently described MPK-dependent phosphorylation of PIN proteins might suggest that this interaction could be rather direct [58•,59•]. With the recently developed and refined methods, future research will help to answer these fundamental questions at the very first step of plant development.

Conflict of interest statement

Nothing declared.

Acknowledgements

We apologize to our colleagues whose work we have not included in this manuscript due to space restrictions. We would like to thank Daniel Slane and Gerd Jürgens for critical reading of the manuscript and helpful discussions. Research in our group is supported by the German Science Foundation (Deutsche Forschungsgemeinschaft – DFG: SFB1101/B01 to M.B.), the Chinese Scholarship Council (Fellowship No. 201806320131 to Y.M.), and the Max Planck Society. The authors declare no conflict of interest.

References and recommended reading

Papers of particular interest, published within the period of review, have been highlighted as:

- • of special interest
- •• of outstanding interest

1. Lau S, Slane D, Herud O, Kong JX, Jurgens G: **Early embryogenesis in flowering plants: setting up the basic body pattern**. *Annu Rev Plant Biol* 2012, **63**:483-506.

2. Johri BM, Ambegaokar KB, Srivastava PS: *Comparative Embryology of Angiosperms*. Berlin: Springer-Verlag; 1992.

3. Maheshwari P: *An Introduction to the Embryology of the Angiosperms*. New York: McGraw-Hill; 1950.

4. Bayer M, Slane D, Jurgens G: **Early plant embryogenesis-dark ages or dark matter?** *Curr Opin Plant Biol* 2017, **35**:30-36.

5. Faure JE, Rotman N, Fortune P, Dumas C: **Fertilization in *Arabidopsis thaliana* wild type: developmental stages and time course**. *Plant J* 2002, **30**:481-488.

6. • Kimata Y, Higaki T, Kawashima T, Kurihara D, Sato Y, Yamada T, Hasezawa S, Berger F, Higashiyama T, Ueda M: **Cytoskeleton dynamics control the first asymmetric cell division in Arabidopsis zygote**. *Proc Natl Acad Sci U S A* 2016, **113**:14157-14162.

This study uses novel fluorescent marker lines and sophisticated live imaging to describe the dynamics of the cytoskeleton during zygote elongation and the first mitotic division.

7. Kimata Y, Kato T, Higaki T, Kurihara D, Yamada T, Segami S, Morita MT, Maeshima M, Hasezawa S, Higashiyama T *et al.*: **Polar vacuolar distribution is essential for accurate asymmetric division of Arabidopsis zygotes**. *Proc Natl Acad Sci U S A* 2019, **116**:2338-2343.

8. Piotrowska K, Zernicka-Goetz M: **Role for sperm in spatial patterning of the early mouse embryo**. *Nature* 2001, **409**:517-521.

9. Marston DJ, Goldstein B: **Symmetry breaking in *C. elegans*: another gift from the sperm**. *Dev Cell* 2006, **11**:273-274.

10. Hable WE, Kropf DL: **Sperm entry induces polarity in fucoid zygotes**. *Development* 2000, **127**:493-501.

11. Nakajima K, Uchiumi T, Okamoto T: **Positional relationship between the gamete fusion site and the first division plane in the rice zygote**. *J Exp Bot* 2010, **61**:3101-3105.

12. Antoine AF, Faure JE, Cordeiro S, Dumas C, Rougier M, Feijo JA: **A calcium influx is triggered and propagates in the zygote as a wavefront during in vitro fertilization of flowering plants**. *Proc Natl Acad Sci U S A* 2000, **97**:10643-10648.

13. •• Rahman MH, Toda E, Kobayashi M, Kudo T, Koshimizu S, Takahara M, Iwami M, Watanabe Y, Sekimoto H, Yano K, Okamoto T: **Expression of genes from paternal alleles in rice zygotes and involvement of OsASGR-BBML1 in initiation of zygotic development**. *Plant Cell Physiol* 2019, **60**:725-737.

By SNP-based transcriptome analysis of hybrid zygotes, this study identified 23 genes expressed from the paternal allele. Among those genes, OsASGR-BBML1 plays a crucial role in egg cell activation and initiating a zygotic genome program.

14. Horstman A, Li M, Heidmann I, Weemen M, Chen B, Muino JM, Angenent GC, Boutilier K: **The BABY BOOM transcription factor activates the LEC1-ABI3-FUS3-LEC2 network to induce somatic embryogenesis**. *Plant Physiol* 2017, **175**:848-857.

15. Goodenough U, Lin H, Lee JH: **Sex determination in *Chlamydomonas***. *Semin Cell Dev Biol* 2007, **18**:350-361.

16. Meyer S, Scholten S: **Equivalent parental contribution to early plant zygotic development**. *Curr Biol* 2007, **17**:1686-1691.

17. Pillot M, Baroux C, Vazquez MA, Autran D, Leblanc O, Vielle-Calzada JP, Grossniklaus U, Grimanelli D: **Embryo and endosperm inherit distinct chromatin and transcriptional states from the female gametes in Arabidopsis**. *Plant Cell* 2010, **22**:307-320.

18. Autran D, Baroux C, Raissig MT, Lenormand T, Wittig M, Grob S, Steimer A, Barann M, Klostermeier UC, Leblanc O *et al.*: **Maternal epigenetic pathways control parental contributions to Arabidopsis early embryogenesis**. *Cell* 2011, **145**:707-719.

19. Zhao J, Xin H, Qu L, Ning J, Peng X, Yan T, Ma L, Li S, Sun MX: **Dynamic changes of transcript profiles after fertilization are associated with de novo transcription and maternal elimination in tobacco zygote, and mark the onset of the maternal-to-zygotic transition**. *Plant J* 2011, **65**:131-145.

20. Nodine MD, Bartel DP: **Maternal and paternal genomes contribute equally to the transcriptome of early plant embryos**. *Nature* 2012, **482**:94-97.

21. Del Toro-De Leon G, Lepe-Soltero D, Gillmor CS: **Zygotic genome activation in isogenic and hybrid plant embryos**. *Curr Opin Plant Biol* 2016, **29**:148-153.

22. • Schon MA, Nodine MD: **Widespread contamination of Arabidopsis embryo and endosperm transcriptome data sets**. *Plant Cell* 2017, **29**:608-617.

Using an *in silico* approach, the authors assessed the contamination of embryonic transcriptome data by RNA derived from surrounding maternal and endosperm tissue. They conclude that previous data universally included maternal contamination leading to possible misinterpretations.

23. •• Chen J, Strieder N, Krohn NG, Cyprys P, Sprunck S, Engelmann JC, Dresselhaus T: **Zygotic genome activation occurs shortly after fertilization in maize**. *Plant Cell* 2017, **29**:2106-2125.

This work provides transcriptome data of gametes and zygotes as well as apical and basal cells of maize embryos. This study therefore provides a complete set of transcriptome data prefertilization and post-fertilization with high temporal resolution. The data clearly demonstrate that zygotic genome activation happens shortly after fertilization in the zygote.

24. •• Zhao P, Zhou X, Shen K, Liu Z, Cheng T, Liu D, Cheng Y, Peng X, Sun MX: **Two-step maternal-to-zygotic transition with two-phase parental genome contributions**. *Dev Cell* 2019, **49**:882-893 e885.

In this work, the authors present transcriptome data of Arabidopsis egg cells, zygotes, and embryos after the first division. The transcriptome data include SNP-based analysis of parental origin of the transcripts. Zygote were analyzed before (14 hour after pollination) and during elongation (24 hour after pollination). This work therefore provides very high temporal resolution and identifies a two-phased zygotic genome activation.

25. Vastenhouw NL, Cao WX, Lipshitz HD: **The maternal-to-zygotic transition revisited**. *Development* 2019, **146**.

26. Ingouff M, Rademacher S, Holec S, Soljic L, Xin N, Readshaw A, Foo SH, Lahouze B, Sprunck S, Berger F: **Zygotic resetting of the HISTONE 3 variant repertoire participates in epigenetic reprogramming in Arabidopsis**. *Curr Biol* 2010, **20**:2137-2143.

27. Lukowitz W, Roeder A, Parmenter D, Somerville C: **A MAPKK kinase gene regulates extra-embryonic cell fate in Arabidopsis**. *Cell* 2004, **116**:109-119.

28. Wang H, Ngwenyama N, Liu Y, Walker JC, Zhang S: **Stomatal development and patterning are regulated by environmentally responsive mitogen-activated protein kinases in Arabidopsis**. *Plant Cell* 2007, **19**:63-73.

29. Zhang M, Wu H, Su J, Wang H, Zhu Q, Liu Y, Xu J, Lukowitz W, Zhang S: **Maternal control of embryogenesis by MPK6 and its upstream MKK4/MKK5 in Arabidopsis**. *Plant J* 2017, **92**:1005-1019.

30. Musielak TJ, Bayer M: **YODA signalling in the early Arabidopsis embryo**. *Biochem Soc Trans* 2014, **42**:408-412.

31. Ueda M, Zhang Z, Laux T: **Transcriptional activation of Arabidopsis axis patterning genes WOX8/9 links zygote polarity to embryo development**. *Dev Cell* 2011, **20**:264-270.

32. Ueda M, Aichinger E, Gong W, Groot E, Verstraeten I, Vu LD, De Smet I, Higashiyama T, Umeda M, Laux T: **Transcriptional integration of paternal and maternal factors in the Arabidopsis zygote**. *Genes Dev* 2017, **31**:617-627.

33. Breuninger H, Rikirsch E, Hermann M, Ueda M, Laux T: **Differential expression of WOX genes mediates apical-basal axis formation in the Arabidopsis embryo**. *Dev Cell* 2008, **14**:867-876.

34. Dolzblasz A, Nardmann J, Clerici E, Causier B, van der Graaff E, Chen J, Davies B, Werr W, Laux T: **Stem cell regulation by Arabidopsis WOX genes**. *Mol Plant* 2016, **9**:1028-1039.

35. Jeong S, Palmer TM, Lukowitz W: **The RWP-RK factor GROUNDED promotes embryonic polarity by facilitating YODA MAP kinase signaling**. *Curr Biol* 2011, **21**:1268-1276.

36. Waki T, Hiki T, Watanabe R, Hashimoto T, Nakajima K: **The Arabidopsis RWP-RK protein RKD4 triggers gene expression and pattern formation in early embryogenesis**. *Curr Biol* 2011, **21**:1277-1281.

37. Koi S, Hisanaga T, Sato K, Shimamura M, Yamato KT, Ishizaki K, Kohchi T, Nakajima K: **An evolutionarily conserved plant RKD Factor controls germ cell differentiation**. *Curr Biol* 2016, **26**:1775-1781.

38. Rovekamp M, Bowman JL, Grossniklaus U: **Marchantia MpRKD regulates the gametophyte-sporophyte transition by keeping egg cells quiescent in the absence of fertilization**. *Curr Biol* 2016, **26**:1782-1789.

39. •• Neu A, Eilbert E, Asseck LY, Slane D, Henschen A, Wang K, Burgel P, Hildebrandt M, Musielak TJ, Kolb M *et al.*: **Constitutive signaling activity of a receptor-associated protein links fertilization with embryonic patterning in Arabidopsis thaliana**. *Proc Natl Acad Sci U S A* 2019, **116**:5795-5804.
The BRASSINOSTEROID SIGNALING KINASES BSK1 and BSK2 act in parallel upstream of YDA in various signaling pathways. As these proteins are universal components of SERK-dependent signaling pathways, this study suggests that the embryonic YDA pathway is activated by a SERK-dependent receptor complex. Furthermore, the authors show that the unusual BSK family member SSP/BSK12 mimics a constitutively active form of BSK1 and can activate YDA possibly without involving canonical receptor activation.

40. Shi H, Yan H, Li J, Tang D: **BSK1, a receptor-like cytoplasmic kinase, involved in both BR signaling and innate immunity in Arabidopsis**. *Plant Signal Behav* 2013, **8**.

41. Majhi BB, Sreeramulu S, Sessa G: **BRASSINOSTEROID-SIGNALING KINASE5 associates with immune receptors and is required for immune responses**. *Plant Physiol* 2019, **180**:1166-1184.

42. Zhao Y, Wu G, Shi H, Tang D: **RECEPTOR-LIKE KINASE 902 associates with and phosphorylates BRASSINOSTEROID-SIGNALING KINASE1 to regulate plant immunity**. *Mol Plant* 2019, **12**:59-70.

43. Meng X, Chen X, Mang H, Liu C, Yu X, Gao X, Torii KU, He P, Shan L: **Differential function of Arabidopsis SERK family receptor-like kinases in stomatal patterning**. *Curr Biol* 2015, **25**:2361-2372.

44. Costa LM, Marshall E, Tesfaye M, Silverstein KA, Mori M, Umetsu Y, Otterbach SL, Papareddy R, Dickinson HG, Boutiller K *et al.*: **Central cell-derived peptides regulate early embryo patterning in flowering plants**. *Science* 2014, **344**:168-172.

45. Bayer M, Nawy T, Giglione C, Galli M, Meinnel T, Lukowitz W: **Paternal control of embryonic patterning in *Arabidopsis thaliana***. *Science* 2009, **323**:1485-1488.

46. Babu Y, Musielak T, Henschen A, Bayer M: **Suspensor length determines developmental progression of the embryo in Arabidopsis**. *Plant Physiol* 2013, **162**:1448-1458.

47. De Smet I, Beeckman T: **Asymmetric cell division in land plants and algae: the driving force for differentiation**. *Nat Rev Mol Cell Biol* 2011, **12**:177-188.

48. Yoshida S, Barbier de Reuille P, Lane B, Bassel GW, Prusinkiewicz P, Smith RS, Weijers D: **Genetic control of plant development by overriding a geometric division rule**. *Dev Cell* 2014, **29**:75-87.

49. Shao W, Dong J: **Polarity in plant asymmetric cell division: division orientation and cell fate differentiation**. *Dev Biol* 2016, **419**:121-131.

50. Friml J, Vieten A, Sauer M, Weijers D, Schwarz H, Hamann T, Offringa R, Jurgens G: **Efflux-dependent auxin gradients establish the apical-basal axis of Arabidopsis**. *Nature* 2003, **426**:147-153.

51. Rademacher EH, Lokerse AS, Schlereth A, Llavata-Peris CI, Bayer M, Kientz M, Freire Rios A, Borst JW, Lukowitz W, Jurgens G, Weijers D: **Different auxin response machineries control distinct cell fates in the early plant embryo**. *Dev Cell* 2012, **22**:211-222.

52. Cheng Y, Dai X, Zhao Y: **Auxin synthesized by the YUCCA flavin monooxygenases is essential for embryogenesis and leaf formation in Arabidopsis**. *Plant Cell* 2007, **19**:2430-2439.

53. Robert HS, Grones P, Stepanova AN, Robles LM, Lokerse AS, Alonso JM, Weijers D, Friml J: **Local auxin sources orient the apical-basal axis in Arabidopsis embryos**. *Curr Biol* 2013, **23**:2506-2512.

54. Robert HS, Crhak Khaitova L, Mroue S, Benkova E: **The importance of localized auxin production for morphogenesis of reproductive organs and embryos in Arabidopsis**. *J Exp Bot* 2015, **66**:5029-5042.

55. •• Robert HS, Park C, Gutierrez CL, Wojcikowska B, Pencik A, Novak O, Chen J, Grunewald W, Dresselhaus T, Friml J, Laux T: **Maternal auxin supply contributes to early embryo patterning in Arabidopsis**. *Nat Plants* 2018, **4**:548-553.
This study identifies the maternal integument tissue at the micropolar end as source of auxin during early phases of embryogenesis.

56. Liao CY, Weijers D: **A toolkit for studying cellular reorganization during early embryogenesis in *Arabidopsis thaliana***. *Plant J* 2018, **93**:963-976.

57. •• Yoshida S, van der Schuren A, van Dop M, van Galen L, Saiga S, Adibi M, Moller B, Ten Hove CA, Marhavy P, Smith R *et al.*: **A SOSEKI-based coordinate system interprets global polarity cues in Arabidopsis**. *Nat Plants* 2019, **5**:160-166.
On the basis of conserved domain structure, the authors identified an apparently evolutionarily conserved family of proteins. The SOSEKI proteins show specific intra-cellular localization according to intrinsic polarity cues and seem to be involved in their interpretation.

58. • Jia W, Li B, Li S, Liang Y, Wu X, Ma M, Wang J, Gao J, Cai Y, Zhang Y *et al.*: **Mitogen-activated protein kinase cascade MKK7-MPK6 plays important roles in plant development and regulates shoot branching by phosphorylating PIN1 in Arabidopsis**. *PLoS Biol* 2016, **14**:e1002550.
Phosphorylation of PIN1 by MPK6 was demonstrated *in vivo* and therefore indicates a direct link between MAP kinase signaling and regulation of auxin transport.

59. • Dory M, Hatzimasoura E, Kallai BM, Nagy SK, Jager K, Darula Z, Nadai TV, Meszaros T, Lopez-Juez E, Barnabas B *et al.*: **Coevolving MAPK and PID phosphosites indicate an ancient environmental control of PIN auxin transporters in land plants**. *FEBS Lett* 2018, **592**:89-102.
This study describes conserved MAP kinase phosphorylation sites in PIN proteins. These data suggest a direct link between receptor kinase signaling and auxin transport.